nagra.

Technical Report 03-03

Grimsel Test Site Investigation Phase V

The CRR Final Project Report Series III:

Results of the Supporting Modelling Programme

June 2006

P. A. Smith, J. Guimerà, G. Kosakowski,
A. Pudewills and M. Ibaraki (editors)

National Cooperative
for the Disposal of
Radioactive Waste

Hardstrasse 73
CH-5430 Wettingen
Switzerland
Tel. +41 56 437 11 11

www.nagra.ch

nagra.

Technical Report 03-03

Grimsel Test Site Investigation Phase V

The CRR Final Project Report Series III:

Results of the Supporting Modelling Programme

June 2006

P. A. Smith [1], J. Guimerà [2], G. Kosakowski [3], A. Pudewills [4] and M. Ibaraki [5] (editors)

[1] SAM (Safety Assessment Management), North Berwick, UK
[2] Enviros, Barcelona, Spain
[3] PSI (Paul Scherrer Institute), Villigen, Switzerland
[4] FZK-INE (Forschungszentrum Karlsruhe), Karlsruhe, Germany
[5] OSU (Ohio State University), Ohio, USA

National Cooperative
for the Disposal of
Radioactive Waste

Hardstrasse 73
CH-5430 Wettingen
Switzerland
Tel. +41 56 437 11 11

www.nagra.ch

This report was prepared on behalf of Nagra. The viewpoints presented and conclusions reached are those of the author(s) and do not necessarily represent those of Nagra.

ISSN 1015-2636

Foreword

Concepts for the disposal of radioactive waste in geological formations depend crucially on a thorough knowledge of relevant processes in the host rock and on an understanding of the whole repository system, comprising both engineered and geological barriers. The Grimsel Test Site (GTS) is a first-generation underground rock laboratory which is used to investigate many of these processes in hard, fractured rocks. It has been operated since 1984 by the Swiss National Cooperative for the Disposal of Radioactive Waste (NAGRA).

The laboratory is located in the crystalline rock of the Central Aar Massif, 450 m below the eastern flank of the Juchlistock at an altitude of 1730 m. It is reached via a 1200 m horizontal access tunnel, operated by the hydropower plant KWO. The layout of the tunnels that comprise the GTS allowed the establishment of a radiation controlled zone (IAEA type B/C) in 1990 in which experiments with radioactive tracers are carried out. With increasing experience in the implementation of in-situ experiments, improved process understanding and more advanced repository concepts, the experimental programmes at the GTS have gradually become more complex and more directly related to open questions defined by performance assessors or by regulatory bodies. Demonstration of disposal concepts by performing large- or full-scale, long-term experiments has also become a key aspect of investigations in the rock laboratory.

The investigation phase V of the Grimsel Rock Laboratory was initiated in 1997 in close co-operation with international partner organisations. Seven experimental programmes and projects are included in this Phase, covering a broad spectrum of investigations.

This report documents the results of the modelling investigations of the 'Colloid and Radionuclide Retardation' (CRR) project. The aims of the CRR project are to examine the migration of bentonite colloids in fractured rocks, to investigate the interaction between safety relevant radionuclides and bentonite colloids and to test the applicability of numerical codes for colloid-mediated radionuclide transport.

In addition to the modelling programme, the project partners, namely ANDRA (F), ENRESA (E), FZK-INE (D), JNC (now JAEA, J), Nagra (CH) and the USDoE/Sandia (USA), funded a series of *in situ* dipole tracer experiments carried out at the Grimsel Test Site (GTS) and laboratory investigations, the results of which are reported elsewhere in the CRR final report series (NTB 03-01 and 03-02).

Vorwort

Bei der Entsorgung radioaktiver Abfälle wird aus Sicherheitsüberlegungen die Endlagerung in geologischen Formationen vorgesehen. Dafür sind Kenntnis über das Wirtgestein sowie ein vertieftes Verständnis der technischen Sicherheitsbarrieren von entscheidender Bedeutung.

Seit 1984 betreibt die Nagra (Nationale Genossenschaft für die Lagerung radioaktiver Abfälle) ein standortunabhängiges Felslabor im Grimselgebiet (FLG), in den granitischen Gesteinen des Zentralen Aar Massivs.

Das FLG liegt 450 m unter der Ostflanke des Juchlistocks auf einer Höhe von 1730 m ü.M. und kann durch einen 1200 m langen horizontalen Zugangsstollen der Kraftwerke Oberhasli AG (KWO) erreicht werden. Im Jahr 1990 wurde in einem der Stollenabschnitte des FLG's eine kontrollierte Zone (IAEA Typ B/C) für Versuche mit radioaktiven Tracern eingerichtet.

Mit zunehmender Erfahrung in der Durchführung von Feldversuchen, verbessertem Systemverständnis der geologischen und technischen Barrieren sowie der weiterentwickelten Lagerkonzepte, verlagerten sich die Programm-Schwerpunkte zu komplexen, direkt auf die Anforderungen der Sicherheitsanalyse ausgerichteten Versuche. Langzeitdemonstrationsversuche gewannen in den letzten Jahren immer mehr an Bedeutung.

Die Untersuchungsphase V des FLG wurde 1997 in enger Zusammenarbeit mit den Partnerorganisationen geplant. Sie beteiligen sich wesentlich bei der Durchführung der insgesamt 7 Versuchsprogramme, die ein breites Spektrum wissenschaftlicher und technischer Fragestellungen abdecken.

Der vorliegende Bericht präsentiert die Resultate der Modellierungsstudien, welche im Rahmen des Projekts 'Kolloid- und Radionuklid-Retardierung' (CRR) durchgeführt wurden. Die Hauptzielsetzungen des CRR-Experiments waren die Untersuchung des Transportverhaltens von Bentonitkolloiden in einer Scherzone, die Wechselwirkung von sicherheitsrelevanten Radionukliden mit Bentonitkolloiden sowie die Überprüfung und Weiterentwicklung von Transportmodellen zur Vorhersage von kolloidalem Radionuklidtransport.

Zusätzlich zu den umfangreichen Transportmodellierungen ermöglichten die beteiligten Projektpartner ANDRA (F), ENRESA (E), FZK-INE (D), JNC (heute JAEA, J), USDoE/Sandia (USA) und Nagra (CH) die Durchführung einer Vielzahl von *in situ* Dipol-Tracer-Experimenten, welche im Felslabor Grimsel (FLG) durchgeführt wurden, und des Laborprogramms, welche ebenfalls in der Serie der Schlussberichte zum CRR-Projekt dokumentiert sind (NTB 03-01 und 03-02).

Préface

Le stockage définitif des déchets radioactifs est prévu, pour des questions de sûreté, dans des formations géologiques. La connaissance détaillée des roches d'accueil et une compréhension approfondie des processus se déroulant dans la roche et dans les barrières techniques de sûreté sont d'une importance décisive.

Le laboratoire souterrain du Grimsel (LSG) est un laboratoire de première génération en fonction depuis 1984, exploité par la Société coopérative nationale pour l'entreposage de déchets radioactifs (NAGRA).

Le laboratoire est situé à une altitude de 1730 m dans les roches granitiques du Massif Central de l'Aar, à 450 m de profondeur sous le flanc est du Juchlistock. On l'atteint par un tunnel d'accès horizontal exploité par la centrale électrique Oberhasli AG de la société KWO. En 1990, on a aménagé dans le LSG une zone de radiation contrôlée (type B/C de l'AIEA) pour des essais avec traceurs radioactifs.

Avec l'expérience croissante dans la conduite d'essais in-situ, une meilleure compréhension des barrières géologiques et techniques, le programme de recherche s'est orienté vers des essais toujours plus complexes liés aux exigences des analyses de sûreté. La démonstration de faisabilité de concepts de dépôt à grande échelle et sur de longues durées est devenue l'un des points forts des recherches dans le laboratoire souterrain.

La phase de recherche actuelle du LSG, qui a débuté en 1997, a été planifiée en concertation étroite avec les partenaires internationaux. Elle comprend sept projets et programmes d'essais couvrant un large spectre de questions scientifiques et techniques.

Ce rapport présente les résultats des études de modélisation réalisées dans le cadre du projet 'Retard des colloïdes et des radionucléides' (CRR). Les objectifs principaux de l'expérience CRR étaient les suivants: observer la migration des colloïdes de la bentonite dans une zone de cisaillement, étudier les interactions entre les colloïdes de la bentonite et les radionucléides importants pour la sûreté du dépôt, et enfin tester les codes numériques visant à modéliser le transport des radionucléides qui s'effectue par le biais des colloïdes.

En marge du programme d'essais de modélisation du transport des radionucléides, les partenaires du projet – à savoir l'ANDRA (F), ENRESA (E), FZK-INE (D), JNC (aujourd'hui JAEA, J), la Nagra (CH) et USDoE/Sandia (USA) – ont rendu possible une série de tests de traçage en dipôle *in situ*, réalisés au Laboratoire souterrain du Grimsel (LSG), ainsi que des expériences en laboratoire, dont les résultats ont également été publiés dans la série des rapports finals du projet CRR (NTB 03-01 et 03-02).

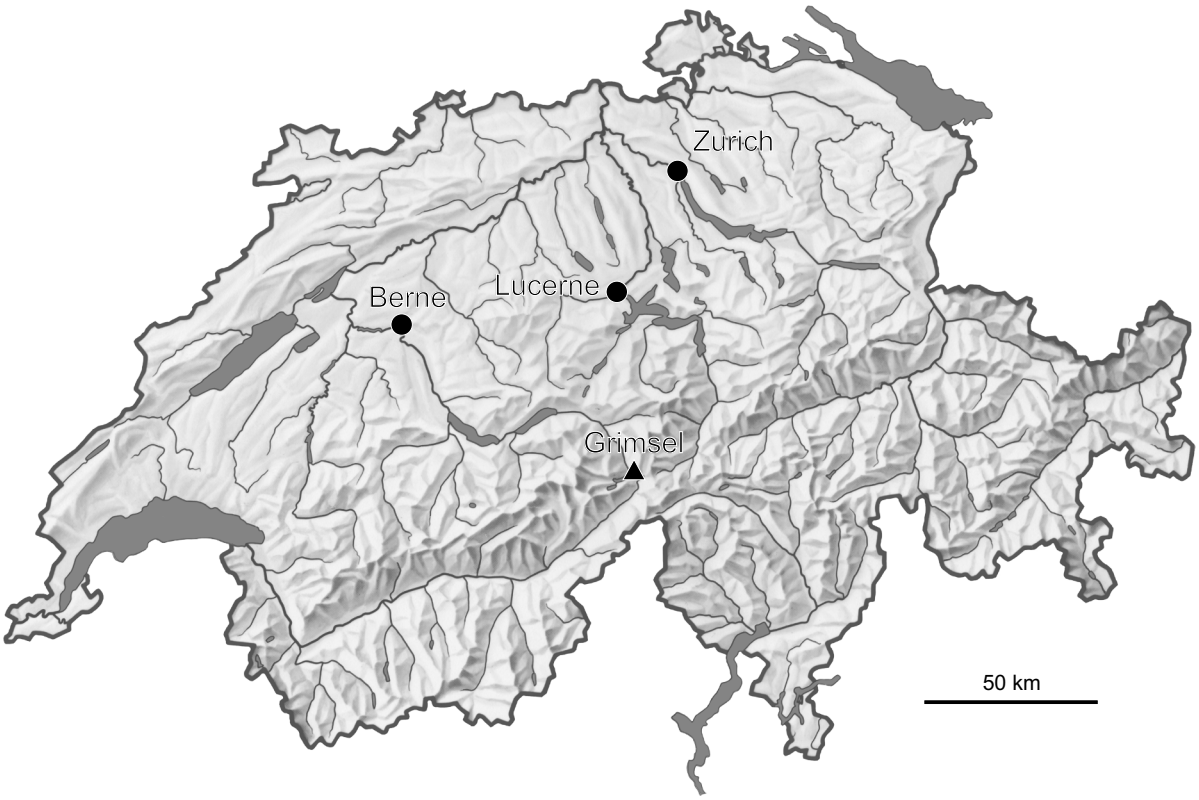

Location of Nagra's underground test facility at the Grimsel Pass in the Central Alps (Bernese Alps) of Switzerland

Grimsel area (view to the west)

1 Grimsel Test Site 2 Lake Raeterichsboden 3 Lake Grimsel 4 Juchlistock

Grimsel Test Site (GTS)

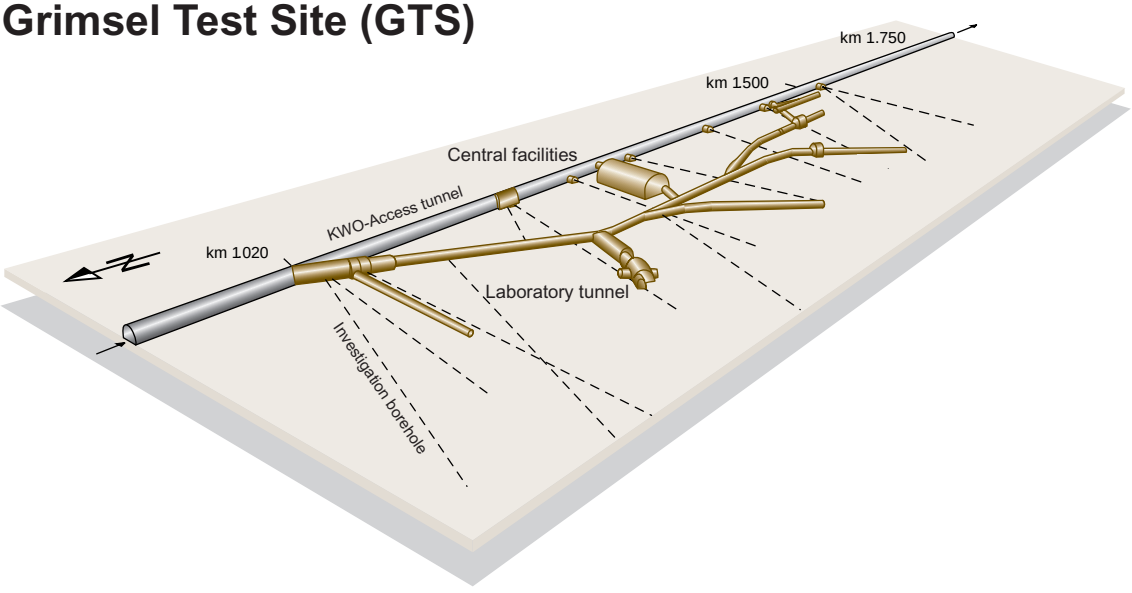

Grimsel Test Site
GTS

KWO-Access tunnel

Laboratory tunnel

Central Aaregranite (CAGR)
High biotite content CAGR

Grimsel-Granodiorite

Shear zone

Lamprophyre

SB — Investigation borehole

ZB — Central facilities

GTS Phase V 1997-2002

HPF — Hyperalkaline Plume

CRR — Colloid and Radionuclide Retardation

GAM — Gastransport in the Geosphere

FEBEX — 1:1 EBS – Demonstration (HLW)

GMT — Gas Migration Test in the EBS

GMB — Geophysical Methods in Boreholes

EFP — Effective Parameters

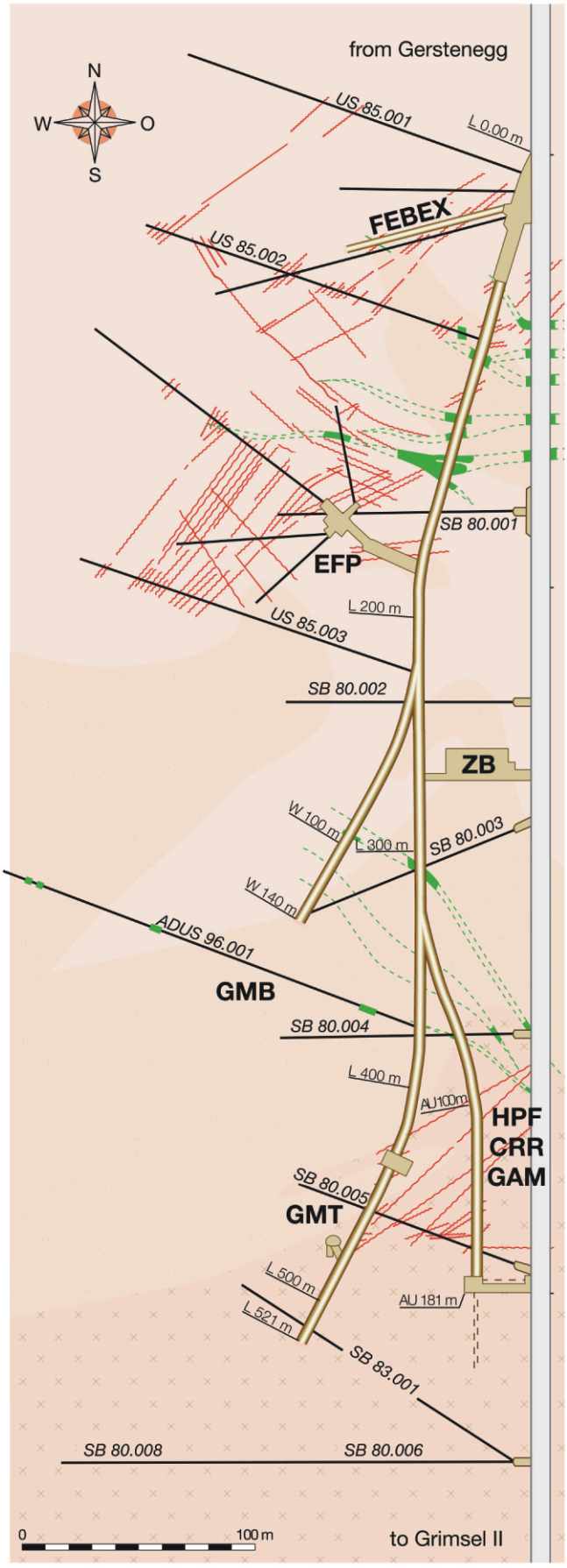

Abstract

The Colloid and Radionuclide Retardation Experiment (CRR) is dedicated to improving the understanding of the *in situ* retardation of safety-relevant actinides and fission products associated with bentonite colloids in the vicinity of the Engineered Barrier System (EBS)/host rock interface. In addition to a series of *in situ* dipole experiments that were carried out at the Grimsel Test Site (GTS), the project partners, namely ANDRA (F), ENRESA (E), FZK-INE (D), JNC[1] (J), USDoE/Sandia (USA) and Nagra (CH), funded an extensive programme of laboratory and modelling investigations. The aims of CRR were: examination of the *in situ* migration of bentonite colloids in fractured rocks, investigation of the interactions between safety-relevant radionuclides and bentonite colloids in the laboratory and *in situ* and, in addition, the testing of the applicability of numerical codes for representing colloid-mediated radionuclide transport.

The present report is one of three final project reports that summarise the findings of the CRR project. In addition to this modelling report, the series includes reports on the field and laboratory work. This report summarises and discusses the results of the modelling investigations that were carried out by four teams (Enviros, FZK-INE, JNC and PSI) working largely independently with the aim of developing understanding of the structures and processes affecting tracer transport in the *in situ* field tests.

The modelling teams had access to the same set of field observations and supporting laboratory work and the models developed by the teams had many similarities. All of the models considered that radionuclide tracers could be transported either in solution or in association with colloids and all considered:

- advection and hydrodynamic dispersion of solutes and colloids in a fracture or fractures within the shear zone,
- retardation of solutes by sorption and / or matrix diffusion, and
- exclusion of colloids from rock matrix pores.

The most significant difference was probably the treatment of the interaction between solutes and colloids; the assumptions employed included equilibrium sorption, non-equilibrium sorption with first-order kinetics and irreversible sorption of radioactive tracers on colloids. A similar range of assumptions has been used in modelling colloid-facilitated radionuclide transport in recent repository safety assessments. There were also significant differences in the treatment of hydrodynamic dispersion, including its treatment as a diffusion-like process described by Fick's Laws and as a non-Fickian process, as well as a model that explicitly modelled the dispersion arising from a network of multiple orthogonal fractures.

The Enviros and PSI teams carried out some predictive modelling in advance of the main experimental runs in order to test their approaches and to aid in the planning of the experiments. Most of the modelling was, however, carried out after the main runs and involved a degree of inverse modelling. The success of some modelling approaches (and, equally importantly, the difficulties of others) in predicting or reproducing the experimental results enabled a number of conclusions to be drawn.

[1] Now JAEA, Japan Atomic Energy Agency

The CRR experiment and the modelling work discussed in this report indicate that, in the main experimental run #32 with bentonite colloids added to the injection cocktail:

- Am, Pu and Th were transported principally in association with colloids, and
- Cs was also transported in part in association with colloids, although the main part of the injected inventory was transported in solution.

Some radionuclides, including Am, Pu and Th, were also transported in colloidal form even when no colloids were added to the injection cocktail (run #31). The addition of bentonite colloids, however, increased recovery of these tracers. The role of colloids in the transport of Np and U in the two main runs was not unambiguously determined. Laboratory experiments, however, demonstrated that colloidal species are of minor relevance for Np(V) and U(VI).

Regarding processes:

- The narrowness of the experimental dipole flow field was such that tracer transport and breakthrough could be adequately treated with advection and dispersion modelled as 1-D processes along a direct line between the injection and withdrawal wells.
- Advection-dispersion models with matrix diffusion were adequate for modelling the breakthrough of conservative tracers and several sorbing tracers, confirming the findings of modelling studies in support of the earlier Migration Experiment (MI).
- Colloids (and tracers associated with them) were advected with little or no retardation and with a breakthrough peak that occurs slightly earlier than that of a conservative solute tracer, consistent with the assumption that colloids do not undergo significant matrix diffusion in the shear zone. The absence of matrix diffusion for colloids is also confirmed by unsuccessful attempts to reproduce the shapes of the tails of colloid breakthrough curves with physically plausible diffusion parameters, and by the fact that the shape of this tailing is independent of colloid size.
- The shapes of the tails of the colloid breakthrough curves suggest that Fick's Laws do not adequately describe dispersion in the shear zone and that a high degree of heterogeneity exists along the transport paths. For solutes, it has not been possible to distinguish the effects of possible non-Fickian dispersion from those of matrix diffusion.
- An equilibrium sorption approach for the association of sorbing tracers with colloids, where sorption parameters are taken from laboratory experiments, did not successfully reproduce the experimental breakthrough curves. It is possible that the association of tracers with colloids is effectively irreversible, or only partly reversible, on the timescale of the experiments.

Although the models used in support of CRR may only be applicable over the spatial and temporal scales of the CRR experiments, the results suggest that the issue of slow sorption / desorption kinetics and the possibility of effectively irreversible sorption of tracers on colloids, which have significant implications for repository safety assessment, deserve further study in longer-term experiments.

Zusammenfassung

Das Experiment 'Kolloid- und Radionuklid-Retardierung' (Colloid and Radionuclide Retardation CRR) verbessert das Verständnis der *in situ* Retardierung sicherheitsrelevanter Aktinide und Spaltprodukte in Anwesenheit von Kolloiden im Bereich der Kontaktzone System der technischen Barrieren (EBS) / Wirtgestein. Neben einer Vielzahl von *in situ* Dipol-Tracer-Experimenten, die im Felslabor Grimsel (FLG) durchgeführt wurden, haben die beteiligten CRR-Partnerorganisationen ANDRA (F), ENRESA (E), FZK-INE (D), JNC[2] (J), USDoE/Sandia (USA) und Nagra (CH) umfangreiche Laborexperimente und numerische Transportmodellierungen unterstützt. Die Hauptzielsetzungen des CRR-Versuchs waren die Untersuchung der *in situ* Migration von Bentonitkolloiden im geklüfteten Gestein und der Wechselwirkungen zwischen sicherheitsrelevanten Radionukliden und Bentonitkolloiden im Labor und *in situ* sowie eine Überprüfung der Anwendbarkeit von numerischen Modellen, welche den Transport von Radionukliden an Kolloiden beschreiben.

Der vorliegende Bericht ist einer von drei Schlussberichten, welche die Erkenntnisse aus dem CRR-Projekt zusammenfassen. Neben diesem Bericht über die durchgeführten Modellierungen, enthält die Berichtsreihe zwei Berichte über die Feld- resp. Laborexperimente. Der vorliegende Bericht präsentiert und diskutiert die Resultate der Modellierungsstudien. Ziel dieser Studien, die von vier weitgehend unabhängigen Gruppen (Enviros, FZK-INE, JNC und PSI) durchgeführt wurden, war ein verbessertes Verständnis der Strukturen und Prozesse, die den Tracertransport in den *in situ* Feldversuchen beeinflussen.

Den Modellierungsgruppen wurden identische Datensätze bestehend aus Feldbeobachtungen und ergänzenden Laborarbeiten zur Verfügung gestellt. Die unabhängig entwickelten Modelle zeigen viele Ähnlichkeiten. Bei allen Modellen werden die Radionuklidtracer entweder in gelöster Form oder kolloidal transportiert. Weiter wurden die folgenden Randbedingungen in Betracht gezogen:

- Advektion und hydrodynamische Dispersion von gelösten Stoffen und Kolloiden in einer Kluft/Klüften in der Scherzone,
- Retardierung von gelösten Stoffen durch Sorption und/oder Matrixdiffusion und
- Ausschluss von Kolloiden vom Porenraum der Gesteinsmatrix.

Der wichtigste Unterschied lag in der Behandlung der Wechselwirkung zwischen gelösten Stoffen und Kolloiden; die Annahmen berücksichtigten Gleichgewichtssorption, Nichtgleichgewichtssorption mit Kinetik erster Ordnung sowie irreversible Sorption von radioaktiven Tracern an Kolloiden. Für die Modellierung des Kolloid-gebundenen Radionuklidtransports in den aktuellen Sicherheitsanalysen für das geologische Tiefenlagersystem wurden ähnliche Annahmen getroffen. Bedeutende Unterschiede gab es auch bei der Behandlung der hydrodynamischen Dispersion einschliesslich deren Behandlung als diffusionsähnlicher Prozess (beschrieben mit Fickschen Gesetzen) und als Nicht-Fickscher Prozess sowie ein Modell, welches die Dispersion explizit modelliert, die durch ein Netzwerk von mehreren rechtwinklig zueinander stehenden Klüften verursacht wird.

Um ihre Ansätze zu testen und die Planung der Hauptexperimente zu unterstützen, haben die Gruppen von Enviros und PSI eine Prognosemodellierung durchgeführt; zum grössten Teil fand aber die Modellierung nach den Hauptexperimenten statt und umfasste auch inverse Modellierung. Der Erfolg einiger Modellierungsansätze bei der Abbildung oder Vorhersage von experi-

[2] Jetzt: JAEA, Japan Atomic Energy Agency.

mentellen Resultaten (und, genauso wichtig, die Schwierigkeiten bei anderen Ansätzen) ermöglichten eine Reihe von Schlussfolgerungen.

Der CRR-Versuch sowie die in diesem Bericht diskutierten Modellierungsarbeiten weisen darauf hin, dass im Hauptexperiment # 32 mit Bentonitkolloiden im Injektionscocktail:

- Am, Pu und Th vorwiegend kolloidal transportiert wurden, und
- Cs auch zum Teil kolloidal transportiert; der Hauptteil des injizierten Inventars aber in gelöster Form transportiert wurde.

Einige Radionuklide, darunter Am, Pu und Th, wurden ebenfalls in kolloidaler Form transportiert, auch wenn keine Kolloide im Injektionscocktail vorhanden waren (Experiment # 31). Allerdings erhöhte die Zugabe von Bentonitkolloiden zum Injektionscocktail die Rückgewinnung dieser Tracer. Die Rolle der Kolloide beim Transport von Np und U in den beiden Hauptexperimenten konnte nicht eindeutig bestimmt werden. Laborexperimente haben aber gezeigt, dass Kolloide nur wenig relevant für den Transport von Np(V) and U(VI) sind.

Hinsichtlich der Prozesse wurden folgende Schlussfolgerungen getroffen:

- Wegen der beschränkten Dimensionen des Dipol-Fliessfelds konnten der Transport und der Durchbruch von Tracern ausreichend behandelt werden mit der Modellierung von Advektion und Dispersion als 1D-Prozesse entlang einer direkten Linie zwischen den Injektions- und Extraktionsbohrlöchern.
- Advektions-Dispersions-Modelle mit Matrixdiffusion waren für die Modellierung des Durchbruchs von konservativen und einigen sorbierenden Tracern geeignet und bestätigen damit die Ergebnisse der Modellierungsarbeiten im Rahmen des früheren Migrationsexperiments (MI).
- Kolloide (und assoziierte Tracer) wurden durch Advektion transportiert ohne (bedeutende) Retardierung. Der "Peak" des Durchbruchs tritt etwas früher auf als für konservative gelöste Tracer. Dies ist konsistent mit der Annahme, dass Kolloide keiner bedeutenden Matrixdiffusion in der Scherzone ausgesetzt sind. Das Fehlen von Matrixdiffusion für Kolloide wird auch durch die erfolglosen Versuche bestätigt, die Tailings der Kolloid-Durchbruchskurven mit physikalisch plausiblen Diffusionsparametern wiederzugeben, sowie durch die Tatsache, dass die Form der Tailings unabhängig von der Kolloidgrösse ist.
- Die Form der Tailings der Durchbruchskurven deutet darauf hin, dass die Fickschen Gesetze die Dispersion in der Scherzone nicht ausreichend beschreiben können und dass eine grosse Heterogenität entlang der Transportpfade besteht. Für gelöste Stoffe konnten die Effekte einer möglichen Nicht-Fickschen Dispersion nicht von denen der Matrixdiffusion unterschieden werden.
- Die Annahme eines Gleichgewichtssorptions-Ansatzes für die Assoziation von sorbierenden Tracern mit Kolloiden (wobei die Sorptionsparameter aus Laborexperimenten stammen) konnte die experimentellen Durchbruchskurven nicht adäquat wiedergeben. Es ist möglich, dass für die Dauer der Experimente die Assoziation von Tracern mit Kolloiden tatsächlich irreversibel oder nur teilweise reversibel ist.

Obwohl die für den CRR-Versuch eingesetzten Modelle nur über die zeitlichen und räumlichen Dimensionen der CRR-Experimente anwendbar sind, deuten die Resultate darauf hin, dass die langsame Sorptions-/Desorptionskinetik und die Möglichkeit einer tatsächlich irreversiblen Sorption von Tracern an Kolloiden weitere Untersuchungen im Rahmen von Langzeitexperimenten notwendig machen. Diese Faktoren haben wichtige Auswirkungen für die Sicherheitsanalyse eines geologischen Tiefenlagers.

Résumé

L'expérience "Retard des colloïdes et des radionucléides" (CRR) avait pour but d'améliorer la compréhension des mécanismes qui gouvernent, *in situ,* le retard des actinides et des produits de fission pertinents pour la sûreté lorsqu'ils sont associés aux colloïdes de la bentonite, à l'interface entre barrières ouvragées et roche d'accueil. En sus des essais en dipôle effectués en grandeur réelle au Laboratoire souterrain du Grimsel (LSG), les partenaires du projet – à savoir ANDRA (F), ENRESA (E), FZK-INE (D), JNC [3] (J), USDoE/Sandia (USA) et Nagra (CH) – ont financé un vaste programme d'études en laboratoire et de modélisation. Le projet CRR avait pour principaux objectifs: observer la migration *in situ* des colloïdes de la bentonite dans une zone de cisaillement, étudier les interactions entre les colloïdes de la bentonite et les radionucléides importants pour la sûreté du dépôt, en laboratoire et sur le terrain, et enfin tester l'applicabilité des codes numériques utilisés pour représenter le transport des radionucléides qui s'effectue par le biais des colloïdes.

Le présent document est l'un des quatre rapports finals résumant les résultats du projet CRR. Il est consacré à la modélisation; deux autres traitent des travaux respectivement sur le terrain et en laboratoire, le dernier étant le rapport de synthèse. Il résume et évalue les résultats des essais de modélisation réalisés par quatre équipes (Enviros, FZK-INE, JNC et IPS), qui ont travaillé pour une grande part de manière indépendante, le but étant de comprendre les structures et les processus influant sur le transport de traceurs dans les essais sur site en grandeur réelle.

Les quatre équipes avaient accès aux mêmes données (observations sur le terrain et travaux de laboratoire associés) et les modèles mis au point présentent de grandes similitudes. Tous partent du principe que les traceurs radioactifs peuvent être transportés en solution ou en association avec des colloïdes et prennent en compte les aspects suivants:

- advection et dispersion hydrodynamique des solutés et des colloïdes dans la ou les fractures d'une zone de cisaillement,
- effets retardateurs sur les solutés dus à l'adsorption et / ou la diffusion matricielle, et
- exclusion des colloïdes de la matrice poreuse.

Les plus grandes différences concernent probablement le traitement des interactions entre solutés et colloïdes. Ici, les hypothèses à la base des modèles vont d'une situation d'équilibre de l'adsorption à l'adsorption irréversible de traceurs radioactifs sur les colloïdes, en passant par un non-équilibre de l'adsorption avec cinétique de premier ordre. Une série d'hypothèses similaires a été récemment utilisée dans des analyses de sûreté pour modéliser le transport de radionucléides par le biais des colloïdes. On recense également d'importantes différences dans les considérations sur la dispersion hydrodynamique. Les uns sont partis d'un processus proche de la diffusion décrite dans la loi de Fick, les autres ont tablé sur un comportement non-fickien, d'autres encore ont explicitement modélisé une dispersion résultant d'un réseau de fractures orthogonales multiples.

Les équipes Enviros et IPS ont procédé à une modélisation prédictive avant d'entamer les essais principaux afin de tester leurs hypothèses et de faciliter la planification des expériences. L'essentiel de la modélisation s'est toutefois déroulé à la suite des essais principaux, y compris une part de modélisation inverse. Le succès de certaines approches de modélisation (et, inversement, les difficultés rencontrées par d'autres) dans la prédiction ou la reproduction des résultats expérimentaux a permis de tirer un certain nombre de conclusions.

[3] Aujourd'hui JAEA, Japan Atomic Energy Agency

L'expérience CRR et le travail de modélisation décrits dans le présent rapport indiquent que durant la série d'essais principaux n° 32, où des colloïdes de la bentonite ont été ajoutés au mélange injecté :

- Am, Pu et Th ont migré principalement en association avec des colloïdes, et
- le transport de Cs s'est effectué en partie en association avec des colloïdes, mais la majeure partie de la quantité injectée a été transportée en solution.

Certains radionucléides, dont Am, Pu et Th, ont été transportés sous forme colloïdale même quand il n'y avait aucun colloïde dans le mélange injecté (série n° 31). L'adjonction de colloïdes de la bentonite a toutefois augmenté la récupération de ces traceurs. Le rôle joué par les colloïdes dans le transport de Np et de U n'a pas pu être déterminé clairement dans les deux principales séries d'essais. Les expériences en laboratoire ont cependant montré que les colloïdes revêtent une importance secondaire pour Np(V) et U(VI).

A propos des processus :

- Le champ d'écoulement dipolaire expérimental était suffisamment étroit pour que le transport et la restitution des traceurs soient traités de manière adéquate en modélisant l'advection et la dispersion comme des processus unidimensionnels le long d'une ligne droite entre les puits d'injection et de récupération.
- Les modèles d'advection/dispersion avec diffusion matricielle se sont révélés appropriés pour modéliser la restitution de traceurs conservatifs et de traceurs adsorbants, confirmant les résultats d'études de modélisation effectuées pour la précédente expérience de migration (MI).
- L'advection des colloïdes (et des traceurs associés) a eu lieu avec très peu ou aucun retard, la restitution atteignant son point culminant peu avant celle des traceurs conservatifs dissous, ce qui confirme l'hypothèse que la diffusion matricielle des colloïdes est faible dans la zone de cisaillement. L'absence de diffusion matricielle est corroborée par des tentatives infructueuses de reproduire les formes des extrémités de courbes de restitution colloïdale en utilisant des paramètres de diffusion physiquement plausibles et par le fait que la forme de ces extrémités est indépendante de la taille des colloïdes.
- La forme des extrémités des courbes de restitution colloïdale suggère que les lois de Fick ne se prêtent pas à la description de la dispersion dans la zone de cisaillement et qu'il y a une forte hétérogénéité le long des voies d'écoulement. Pour les solutés, il n'a pas été possible de faire la distinction entre les effets d'une éventuelle dispersion non-fickienne et ceux de la diffusion matricielle.
- L'approche posant comme hypothèse une situation d'équilibre pour l'association de traceurs adsorbants et de colloïdes – les paramètres d'adsorption étant repris d'expériences en laboratoire – n'a pas permis de reproduire les courbes de restitution expérimentales. Il est possible que l'association de traceurs avec des colloïdes soit véritablement irréversible, ou partiellement réversible seulement, à l'échelle temporelle des essais.

Si les modèles utilisés pour le projet CRR ne sont peut-être applicables qu'aux échelles spatiale et temporelle des essais effectués, les résultats suggèrent néanmoins qu'il est indiqué d'approfondir dans des expériences à plus long terme la question des cinétiques de sorption / désorption lente ainsi que la probabilité d'une irréversibilité effective de la sorption de traceurs sur des colloïdes, questions qui revêtent une importance considérable pour évaluer la sûreté des dépôts (comme il ressort du rapport de synthèse CRR).

Table of Contents

List of Tables

List of Figures

1 Introduction

The Colloid and Radionuclide Retardation Project (CRR) comprises a series of field tracer tests in a water-conducting feature (the Migration or MI shear zone) at Nagra's Grimsel Test Site (GTS) in southern Switzerland, supported by an intensive programme of laboratory studies and modelling at various institutions around the world. This report focuses on transport modelling of the field tracer tests with only a short introduction to the experiment as a whole in the next section.

1.1 Background and aims of the CRR project

Colloids (suspended particles in the size range 1nm to 1μm) are natural and ubiquitous in groundwater, and may also be generated by physical and chemical processes resulting from the presence of a deep geological repository for radioactive waste. In most repository designs for vitrified high-level waste (HLW) and spent fuel (SF), the waste is packaged in canisters that are separated from the host rock by a layer of bentonite clay or bentonite/sand. Repository designs for other waste types also sometimes involve the use of bentonite. Although the canisters are designed to provide long-term containment of the waste and its associated radionuclides, complete containment cannot be guaranteed indefinitely, and some radionuclides may eventually be released. Subsequent transport through the bentonite is expected to be slow. This is due to its fine pore structure, which filters any radionuclides associated with colloids, its low permeability, and the operation of geochemical retention processes, collectively termed retardation.

Although bentonite is expected to act as a colloid filter, the outer surface of the bentonite may itself act as a source of colloids due, for example, to erosion by flowing water in host rock fractures. For these colloids to have any effect on radionuclide transport in the host rock, the radionuclides in question must be able (i), to migrate to the bentonite/host rock interface before they decay, and (ii) subsequently sorb to the bentonite colloids that are generated there (the colloids themselves must also fulfil a number of criteria, as discussed in Section 1.2). If the bentonite layer operates as expected, transport of any sorbing radionuclides will be slow and these conditions are unlikely to be met for most safety-relevant radionuclides. There are, however, conceivable scenarios that would allow more rapid transport of some sorbing radionuclides through the bentonite layer, including, for example, the creation of temporary flow paths through the layer by repository-induced gas (see Fig. 1.1). The impact of natural groundwater colloids on transport is also a concern in the case of fractured hard rocks.

As discussed later in Appendices 1 and 2 of this report, due largely to deficiencies in process understanding and a lack of relevant *in situ* data on colloid transport and colloid-mediated radionuclide transport in the geosphere, those safety assessment studies that consider colloids treat their impact on radionuclide transport in a highly simplified manner. This led HSK (the Swiss Federal Nuclear Safety Inspectorate) to note in 1998 that "...the generation of colloids at the bentonite surface cannot be excluded" and that "...possible colloid associated transport of radionuclides remains an important open question."

CRR was started in 1998 in order to address these deficiencies. The overall aim of the project is to improve understanding of radionuclide transport in fractured geological media and, in particular, the impact of the presence of colloids on the transport of selected actinides and fission products. Improved understanding of the impact of colloids on transport should provide a firmer basis for the treatment of geosphere transport in safety assessments for such repositories. CRR is concerned primarily with the impact of bentonite colloids (released to a

host rock fracture at the bentonite/host rock interface) on radionuclide transport. The findings of CRR, however, have implications for the understanding of colloid-facilitated transport in general, including the impact of natural groundwater colloids.

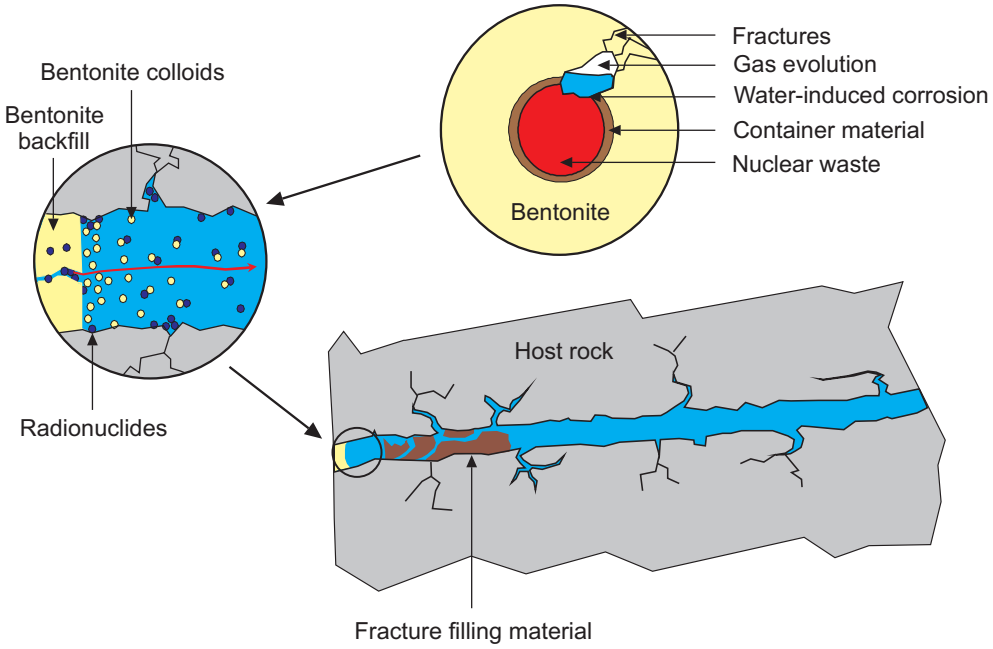

Fig. 1.1: Possible scenario for radionuclide release and bentonite colloid formation.

1.2 Key safety-relevant issues related to colloids

Although there has been little or no unambiguous evidence from field observations of natural and artificially perturbed systems for colloid facilitated transport of radionuclides over long distances under relevant conditions (Hadermann 2001), there remains concern that colloids may have an impact on the transport of radionuclides released from a repository. This remains, in part, due to observations such as those at the Nevada Test Site, in which Pu, which is generally fairly immobile in groundwater systems, was found to migrate over a distance of 1.3 km in only 30 years (Kersting et al. 1999)[4]. *In situ* experiments such as CRR are attempting to deal with this concern.

CRR addresses the transport of radionuclide-bearing colloids in a fractured hard rock. In general, there exist good arguments for assuming efficient filtration of any colloids in unfractured sedimentary rocks with fine pore structures (e.g. Baeyens et al. 1985). It should be noted, however, that even in the Boom Clay, which is being studied in Belgium as a potential repository host rock, field experiments have demonstrated the diffusion-dominated transport of ^{14}C-labelled natural organic matter (NOM) colloids over distances in the order of 0.5 m (Dierckx et al. 2000).

Several recent safety assessments have considered the possibility that radionuclides released from a repository become sorbed to colloids or incorporated within them, and subsequently

[4] Conditions in this case are unrepresentative of repository systems, most obviously because of the transient flow and fracturing when the radioactive source material was explosively emplaced.

transported by advection/dispersion in flowing groundwater in fractured hard rocks. Colloids may not be subject to some of the processes that retard the transport of radionuclides in solution. Indeed, they may move faster than the average groundwater flow velocity, because both their physical size and electrostatic effects can keep them away from solid surfaces where friction slows the flow of groundwater. This phenomenon is exploited in hydrodynamic chromatography, as discussed, for example, in Prieve & Hoysan (1978) and Dodds (1982). There are, however, retardation and immobilisation processes that could affect radionuclides associated with colloids. In fractured media, they could conceivably diffuse into stagnant water in the rock matrix. Their diffusion coefficient would be lower than that of un-complexed ions and the extent to which they penetrated into the matrix (if at all) would depend on the sizes of matrix pores with respect to the size of the colloids, as well as charge effects. The investigations of James & Chrysikopoulos (1999), for example, which considered the influence of matrix diffusion on the breakthrough of polydispersed colloids in rough fractures, showed that larger particles are the least retarded and smaller particles are more slowly transported. Colloids may, in some circumstances, become unstable through aggregation or dissolution. They may also come into contact with fixed solid surfaces, such as fracture walls and the pore surfaces of fracture infill material, to which they can become attached (although the negative charge often found on the surfaces of both colloids and solid phase surfaces acts against this process), or become trapped at constrictions in fractures or in the pore space of the rock matrix because they are too large to pass through. These processes are termed filtration: mechanical filtration, where large colloids become trapped in small pores or narrow channels, and chemical filtration, where colloids become chemically attached to fracture or pore surfaces.

Colloids may have either beneficial or detrimental effects on repository performance. A beneficial effect would be if radionuclides became irreversibly bound to colloids that are later immobilised, e.g. by filtration. A detrimental effect would be if radionuclide-bearing colloids were mobile, and excluded from matrix pores. In general, it can be stated that colloid facilitated transport may be important and detrimental to performance if the following conditions are met (e.g. Gardiner et al. 2001).

1. There is a large population of colloids occurring naturally in groundwater or arising from the presence of the repository.
2. Fracture apertures and other pore spaces conducting flowing groundwater are sufficiently large to allow colloids to pass without significant physical or chemical filtration.
3. The groundwater chemistry is conducive to colloid stability.
4. Radionuclide sorption on colloids is favoured by electrostatic attraction and groundwater chemistry, and desorption processes are irreversible, or at least slow relative to transport times through the geosphere.

This combination of conditions is illustrated schematically in Figure 1.2. As pointed out in Gardiner et al. (2001), no chemical process, such as the sorption of radionuclides by colloids, is strictly speaking irreversible. The key issue here is whether the process is reversible over the timescales of interest to repository safety assessments.

It should also be noted that the presence of gas bubbles in the geosphere has been suggested as potentially important with respect to colloid facilitated radionuclide transport, since radionuclide-bearing colloids may accumulate at gas-water interfaces (see, for example, Wan & Wilson 1994a, b and Neretnieks & Ernstsson 1997), but this possibility is not addressed in CRR.

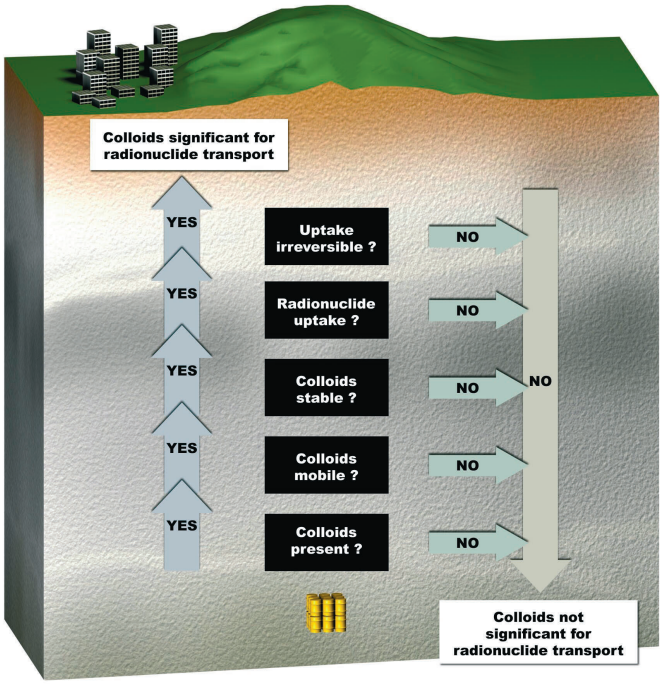

Fig. 1.2: The "colloid ladder"

This indicates when colloid facilitated radionuclide transport is likely to become relevant to the long-term safety of a deep geological repository (Miller et al. 2000)

1.3 Overview of the CRR project

1.3.1 General concept

The central component of the CRR project was a series of *in situ* tracer tests in the experimental shear zone at the GTS. The injection into the shear zone of a cocktail of tracers including, in some tests, bentonite colloids was intended to shed light on the impact of colloids released to a host rock fracture at the bentonite/host rock interface of a radioactive waste repository on radionuclide transport in fracture or shear zone (Fig. 1.3).

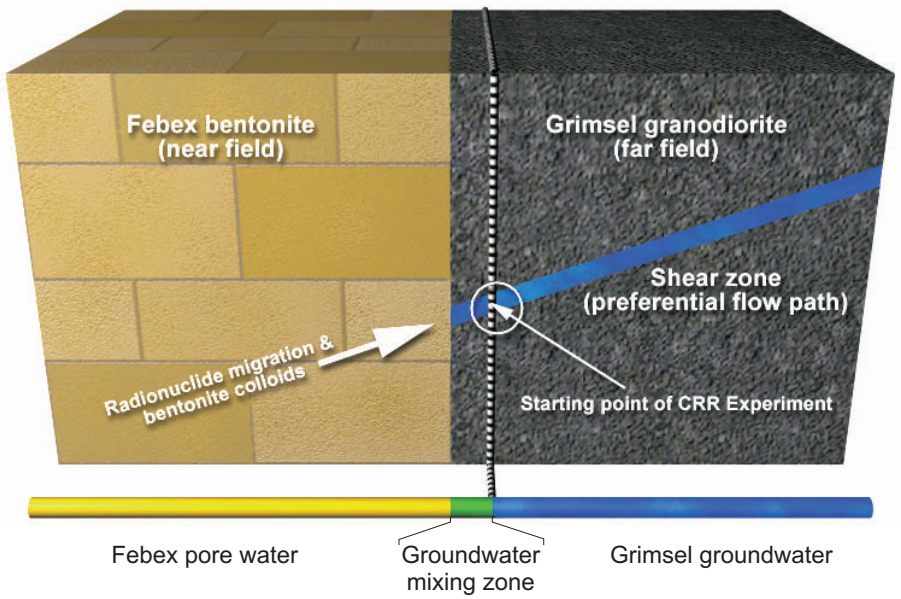

Fig. 1.3: The situation addressed by CRR

The impact of bentonite colloids released to a host rock (geosphere) fracture at the bentonite/host rock on radionuclide transport.

There are of course some key differences between the experimental situation and the bentonite/host rock interface of an actual repository, including the far higher water velocities that were used in the experiments in order to achieve manageable experimental timescales. These differences are important to keep in mind when evaluating the implications of the results for repository safety assessment (see comments in Alexander et al. 2003).

1.3.2 CRR tasks and time schedule

In addition to the CRR *in situ* tracer tests themselves, an intensive programme of supporting field and laboratory studies and modelling work was also carried out in order to plan, implement and interpret the results of the tests, The work was divided into two main phases:

- Phase 1, in which the feasibility of conducting *in situ* tracer tests was examined (and the tests themselves planned with the aid of site characterisation), preliminary calculations, a preparatory laboratory programme and predictive transport modelling, and
- Phase 2, which consisted of the tests themselves, various supporting field and laboratory studies, further transport modelling and final reporting.

The time schedules for these various tasks are summarised in Table 1.1.

Tab. 1.1: Major tasks and time schedule of the CRR project.

Phase	Task	1998		1999		2000		2001		2002		2003	
Phase 1 Feasibility	Site characterisation												
	Preliminary calculations												
	Preparatory laboratory programme												
	Predictive transport modelling												
Phase 2 In situ experiment	Preparatory colloid and homologue tests												
	Field experiment												
	Natural colloid background study												
	Supporting laboratory programme												
	Transport modelling												
	Final reporting												

A key consideration in designing the *in situ* tests, as well as the supporting laboratory experiments, was to minimise experimental artefacts as far as possible. Moreover, in such a highly complex experiment, where actinides and bentonite colloids are used in combination with the natural Grimsel groundwater, the chemical and hydraulic experimental conditions had to be optimised as far as possible. The final layout for the tests nevertheless inevitably involved a degree of compromise that has to be taken into account in the final discussion and interpretation of the results.

1.3.3 The *in situ* tracer tests

The *in situ* tracer tests are reported in detail in Möri (2004). The tests were conducted in four different artificial asymmetric dipole flow fields in the shear zone, established by pumping water into one borehole (the injection borehole) and withdrawing water at a higher rate at a second borehole (the extraction borehole); for details see Fierz et al. (2001), Möri (2004) and Missana & Geckeis (2006).

In preparation for CRR, three new 86 mm boreholes (BOCR 99.001, 99.002 and 00.003) were drilled from the AU gallery of the GTS almost perpendicular to the shear zone and equipped with triple packer systems. Other boreholes (BOMI 86.004, 86.005, 87.007, 87.008, 87.010 and 87.011) were already available from the earlier GTS Migration Experiment (MI) conducted in the same shear zone (see Frick et al. 1992, Smith et al 2001, for details). Figure 1.5 provides an overview of the boreholes and the different flow fields that were established between the packed-off intervals (black arrows). In each dipole, the direction of water flow was towards the gallery, thus coinciding with the unperturbed groundwater flow direction.

In the tracer tests, once the flow field had been established, individual tracers or tracer cocktails were injected at the injection borehole, and the resulting breakthrough curves measured at the withdrawal borehole. An overview of the tracer tests is given in Table 1.1.

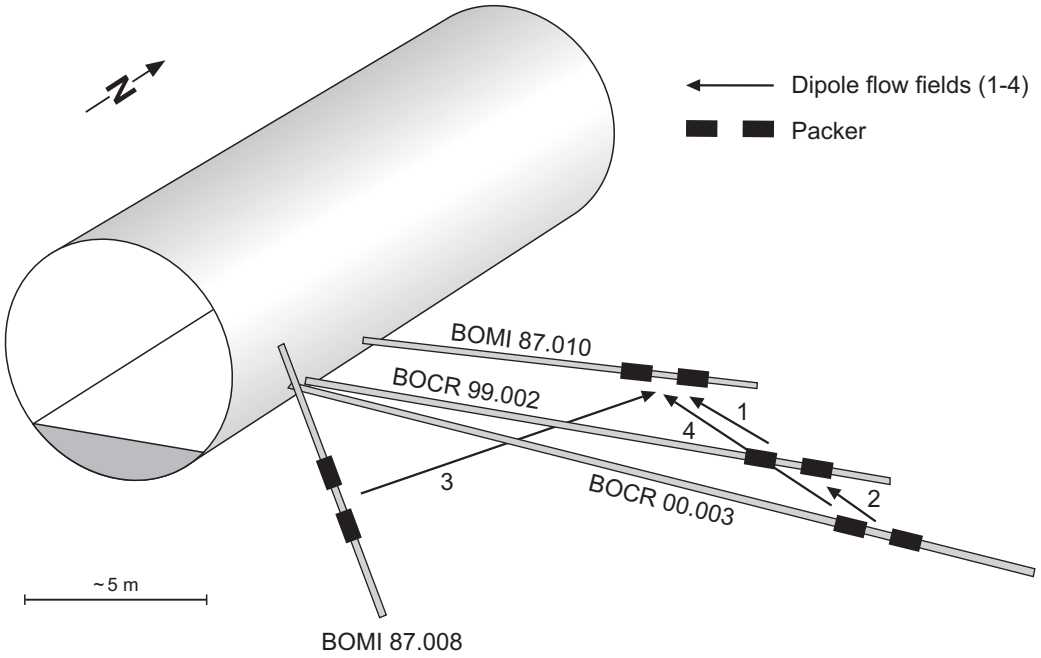

Fig. 1.4: 3D view of the CRR test site

The view direction is perpendicular to the experimental shear zone

Tests using the conservative (i.e. non-interacting) tracer uranine were performed in order to calibrate hydraulic models of flow within the dipoles and to optimise the flow conditions so that a recovery close to 100 % was achieved. Iodine was then added as iodide $^{131}I^-$ to the uranine tracer cocktails in order to confirm that it was still suitable to use as a conservative tracer in later, more complex tests (see also Frick et al. 1992). Preparatory tests were also carried out with bentonite colloids and with the trivalent ^{159}Tb and the tetravalent Hf[5] and ^{232}Th, which provide homologues for the behaviour of a range of actinides.

Two main tracer tests were carried out in dipole D-1 with a suite of different radionuclides. These were:

- run #31, in which ^{243}Am, ^{237}Np, ^{242}Pu, ^{238}Pu, ^{238}U, ^{85}Sr, ^{131}I and ^{232}Th were injected in the absence of bentonite colloids and
- run #32, in which ^{241}Am, ^{237}Np, ^{244}Pu, ^{238}Pu, ^{233}U, ^{99}Tc, ^{137}Cs, ^{85}Sr, ^{131}I and ^{232}Th were injected in the presence of 20 mg L^{-1} of bentonite colloids.

[5] Natural Hf was used, which includes 5 stable isotopes

Tab. 1.2: List of dipoles with corresponding boreholes, experimental runs and tracers used

Dipole	**Length** [m]	**Injection/extraction borehole**	**Flow rates (in/out)** [mL min^{-1}]	**Number of run where this dipole was tested and type of tracer composition**
D-1	2.23	CRR 99.002 /BOMI 87.010	08/120	run #1, uranine
			06/160	run #2, uranine
			08/213	run #3, uranine
			10/150	run #13, uranine
			10/150	run #14, homologues[1]
			10/150	run #21, uranine, ^{85}Sr & ^{82}Br
			10/150	run #28 to 30, uranine, ^{131}I
			10/150	run #31, RN cocktail
			10/150	run #32, RN cocktail & colloids
			10/150	run #33 to 35 uranine, ^{131}I
D-2	1.71	CRR 00.003 /CRR 99.002	10/150	run #4, uranine
			05/075	run #5, uranine
			10/150	run #9, uranine
			10/150	run #10, homologues
			10/150	run #11, uranine
D-3	5.25	BOMI 87.008 /BOMI 87.010	10/150	run #6 & 7, uranine
			10/150	run #6a, bentonite colloid injection
			10/150	run #7a, bentonite colloid injection with homologues
			10/150	run #8, uranine
			10/150	run #15, homologues
			10/150	run #16, uranine
D-4	3.94	CRR 00.003 /BOMI 87.010	10/150	run #12, uranine

[1] The homologues are trivalent ^{159}Tb and tetravalent Hf and ^{232}Th, the natural Hf used being a mix of 5 stable isotopes

1.3.4 Supporting field and laboratory studies

In addition to the *in situ* experiment, a series of supporting field and laboratory experiments and theoretical studies was carried out, addressing, most notably:

- the hydraulic characteristics of the test shear zone,
- a study of natural background colloids,
- tracer solubilities in Grimsel groundwater, and
- sorption on shear zone materials and on colloids.

Findings relevant to model development are discussed in Chapter 2.

1.3.5 Modelling

The aim of the modelling work carried out in support of CRR was to develop understanding of the structures and processes affecting tracer breakthrough by constructing numerical models, and comparing their output with the results of the *in situ* tests. This work is the focus of the present report and is described in detail in later chapters and in Appendix 1.

The models and parameter values used were, to some extent, constrained by field observations and supporting laboratory work conducted as part of CRR (see Chapter 2), as well as wider experience from the earlier MI and Excavation Experiment (EP) at GTS, and other relevant work conducted internationally. Uncertainties were, however, such that various alternative conceptualisations were possible, some of which were explored in the CRR modelling work.

Models were developed and applied by four modelling teams:

- the Enviros QuantiSci team,
- the Paul Scherrer Institute (PSI) team,
- the Forschungszentrum Karlsruhe - Institut für Nukleare Entsorgung (FZK-INE) team, and
- the Japan Nuclear Cycle Development Institute (JNC[6]) team.

The Enviros and FKZ-INE teams were involved with the project from an early stage. The PSI team joined later, followed by the JNC team. Each modelling team worked largely independently, but all had access to the same information from the laboratory and field studies, and progress was reviewed and experience shared periodically in project meetings. The teams developed and applied their models iteratively.

Some predictive modelling was carried out in advance of the main experimental runs #31 and #32 in order to test the model being applied and to aid in the planning of the experiments. Most of the modelling was, however, carried out after the main runs and, as described in Chapter 3, involved a degree of inverse modelling, whereby parameter values are adjusted until the closest possible fit is obtained to the measured breakthrough curves.

1.3.6 Reporting

The raw data are reported in a series of unpublished Nagra internal reports and are referenced in the corresponding sections below. Publications which have been produced as part of the CRR project are:

Biggin C., Möri A., Alexander W.R., Ota K., Frieg B., Kickmaier W. & McKinley I.G. (2002). *In situ* radionuclide retardation in groundwater conducting systems: overview of the research carried out at Nagra's Grimsel Test site, central Switzerland pp 207-228 *in* Environmental Radiochemical Analysis II (ed. P.Warwick) RSC, London, UK.

Geckeis H., Schäfer T., Hauser W., Rabung Th., Missana T., Degueldre C., Möri A., Eikenberg J., Fierz Th. & Alexander W. R. (2004). Results of the Colloid and Radionuclide Retention experiment (CRR) at the Grimsel Test Site (GTS), Switzerland - Impact of Reaction Kinetics and Speciation on Radionuclide Migration -, Radiochimica Acta, 92, 765–774.

[6] Now JAEA, Japan Atomic Energy Agency

Guimerà J., Duro L. & Bruno J. (2000). Radionuclide field tests in a single fracture. Proc. Int. Conf. on tracers and modelling in hydrogeology; Liège, Belgium (Dassargues, Ed); IAHS Pub. 262, 309-314.

Hauser W., Geckeis H., Kim J.I. & Fierz Th. (2002). A mobile laser-induced breakdown detection system and its application for the *in situ*-monitoring of colloid migration. Colloids and Surfaces A: Physicochem. and Eng. Aspects; 203, 37-45.

Kosakowski G. & Smith P. A. (2004). Modelling the transport of solutes and colloids in a water-conducting shear zone in the Grimsel Test Site. Nagra Technical Report NTB 04-01. Nagra, Wettingen, Switzerland.

Kosakowski G. (2004). Anomalous transport of colloids and solutes in a shear zone, J. Contam. Hydrol. 72, 23– 46.

Missana T. & Adel A. (2000). On the Applicability of DLVO Theory to the Prediction of Clay Colloids Stability. J. Coll. Interface Sci., 230, pp. 150-156.

Missana T., Alonso U. & Turrero M.J. (2003a). Generation and Stability of Bentonite Colloids at the Bentonite/Granite Interface of a Deep Geological Radioactive Waste Repository. Journal of Contaminant Hydrology 61 (1-4), 17-31.

Missana T., Garcia-Gutierrez M. & Alonso U. (2003b). Kinetics and Irreversibility of Caesium and Uranium Sorption onto Bentonite Colloids. Applied Clay Science, 26 (2004) pp. 137-150.

Möri A., Alexander W. R., Geckeis H., Hauser W., Schäfer Th., Eikenberg J., Fierz Th., Degueldre C. & Missana T. (2002). The Colloid and Radionuclide Retardation experiment (CRR) at the Grimsel Test Site (GTS): influence of bentonite colloids on radionuclide migration in a fractured rock. Colloids and Surfaces A: Physicochem. and Eng. Aspects; 217, 33-47.

Pudewills A., Hauser W. & Geckeis H. (2002). Numerical modelling of flow and transport phenomena in fractured crystalline rock. Proc. 2nd Biot Conf. on Poromechanics, (Auriault et al., Eds), Balkema; 527-532.

Pudewills A. (2003). Modelling of flow and transport phenomena in a granitic fracture, in O. Natau, E. Fecker, E. Pimentel, Geotechnical Measurements and Modelling, Proc. of the international symposium on geotechnical measurements and modeling, 23-24 September, 2003, Karlsruhe, Germany, A.A. Balkema, Lisse, 155-160.

Schäfer Th., Bauer A., Bundschuh T., Rabung Th., Geckeis H. & Kim J.I. (2000). Colloidal stability of inorganic colloids in natural and synthetic groundwater, Applied Mineralogy in Research, Economy, Technology and Culture, Proc. of the 6th Internat. Congress ICAM 2000, Göttingen, July 13-21, A.A. Balkema, Rotterdam, Vol. 2, 675-678.

Schäfer Th., Geckeis H., Bouby M. &Fanghänel Th. (2004). U, Th, Eu and colloid mobility in a granite fracture under near-natural flow conditions, Radiochimica Acta, 92, 731–737.

A set of 3 final project reports summarise the findings of the CRR project:

Möri A. (ed.) (2004). The CRR final project report series I: Description of the Field Phase - Methodologies and Raw Data. Nagra Technical Report NTB 03-01.

Missana T. & Geckeis H. (eds.) (2006). The CRR final project report series II: Results of the Supporting Laboratory Programme. Nagra Technical Report NTB 03-02.

and the present one.

1.4 Overview of the present report

The present report describes the CRR modelling work. The models and results of the four different modelling teams are described in detail in Appendix 1. The main chapters of the report describe the common background to the modelling work, provide a synthesis of the work carried out and draw conclusions from the modelling.

Chapter 2 describes the empirical information from field and laboratory studies that provided constraints on the representation of features and processes in the models and allowed the models to be tested. The information includes not only the breakthrough curves from the *in situ* tests, but also information about the geological setting in which the tests were performed and the results of supporting hydraulic studies, solubility calculations and batch sorption experiments.

Chapter 3 describes the key similarities and differences between the models, the strategies for applying them and the results obtained by the different modelling teams. The reader is referred to Appendix 1 for a comprehensive description of the individual models and modelling results.

Chapter 4 provides a discussion of transport modelling issues, a summary of key findings and conclusions.

2 Empirical basis for model development and testing

This chapter describes the empirical information from field and laboratory studies that provided constraints on the representation of features and processes in the models and allowed the models to be tested. The information includes not only the breakthrough curves from the *in situ* tests, but also information about the geological setting in which the tests were performed and the results of supporting hydraulic studies, solubility calculations and batch sorption experiments.

2.1 Geological setting

The GTS, where the *in situ* tests were performed, is located at about 1730 m above sea level under a ~450 m thick overburden of crystalline rock (Grimsel granodiorite). The test shear zone has been well characterised in work carried out in connection with the MI and EP projects (see Frick et al. 1992, Alexander et al. 1996, Smith et al. 2001 and Möri et al. 2006, for details).

The granodiorite at the GTS is a medium to coarse grained rock, transected by a series of shear zones and lamprophyre and aplitic dykes. The granodiorite consists mainly of 28 vol% quartz, 29 vol% plagioclase, 24 vol% potassium feldspar and 18 vol% sheet silicates (biotite, muscovite and chlorite).

Ductile structures (mylonites) have been overprinted by brittle deformation. The brittle deformation is characterised by destruction of the mylonitic fabric followed by brecciation of the material. The thickness of fault breccia horizons range from a few mm to 1 cm. Brittle deformation led to the formation of fault gouge within the shear zones and preferential flow paths were created within these horizons. Fault gouge porosity of the test shear zone is in the range of 10 to 40 %. Fault gouge mineral composition does not differ significantly from the mylonitic composition (albite ca. 28 vol%), although biotite content is increased compared to the mylonite (41 vol%) and the clay content in the fault gouge ranges from 0 to 1 vol%.

The MI shear zone used for the CRR experiment is largely described in Bossart & Mazurek (1991) and in Möri et al. (2006) and is characterised as a WSW-ENE striking, steeply dipping (to the SSE) cleavage parallel plane. The original shear direction was sub-vertical, parallel to the mineral stretching lineation with a minimum value for shear displacement of 3 m. The thickness of the shear zone varies between 0.15 and 0.90 m.

2.2 Hydraulic characteristics

Hydraulic tests were performed in the different test dipoles prior to starting the tracer tests (for details see Fisch 2002 and Möri 2004). The observed interference pressure reactions demonstrated good hydraulic interconnectivity between boreholes BOCR 99.002 and BOCR 00.003 (dipole D-2) as well as between the shear-zone intervals of boreholes BOMI 86.004 and BOMI 86.005 and the two CRR boreholes mentioned above. Table 2.1 shows that transmissivity estimates for the shear zone lie within the range 3.0×10^{-7} to 4×10^{-6} m^2 s^{-1}. A low transmissivity zone was, however, inferred to exist between BOMI 86.008 and BOMI 87.010 and between BOCR 99.002 and BOMI 87.010 (dipole D-1). It was not determined from the hydraulic tests whether tracers injected in dipole D-1 would travel through this low transmissivity zone at reduced velocities or whether they would be diverted around this zone along more conducting paths before reaching the extraction borehole.

Tab. 2.1: Shear zone transmissivity estimates

Transmissivity [$m^2\ s^{-1}$]	**Location**	**Source**
~3.0×10^{-7} to 2.4×10^{-6}	Boreholes BOCR 99.002 and BOCR 00.003	Direct measurement (single hole testing and crosshole tests)
~2×10^{-6} $m^2\ s^{-1}$	BOCR 99.002	Early-time breakthrough curve matches and early time straight-line fits
1.4×10^{-6} to 4×10^{-6}	BOCR 00.003	
3×10^{-7} $m^2\ s^{-1}$ to 7×10^{-7}	Boreholes BOCR 99.002 and BOCR 00.003	Middle/late time straight-line fitting

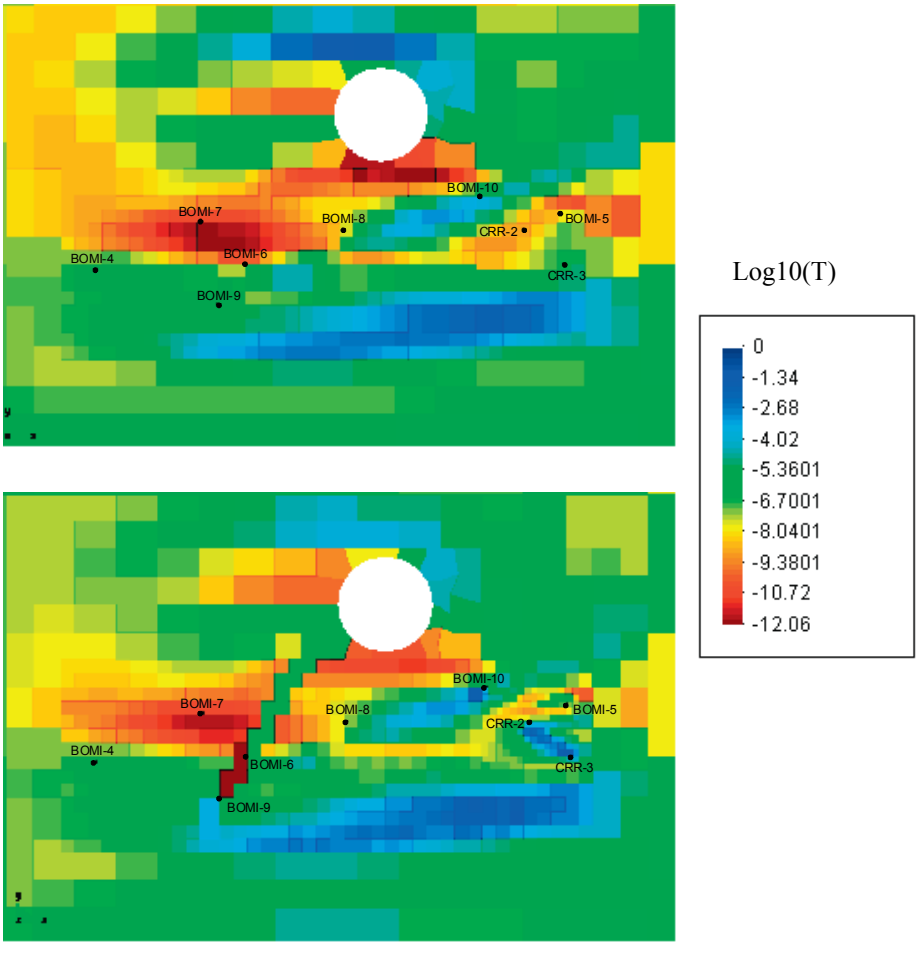

Fig. 2.1: Outcome of a geostatistical inverse modelling exercise performed in support of CRR by UPC

Upper part: $\log_{10}(T)$ field based on investigations carried out in support of the earlier migration experiment (MI); lower part: $\log_{10}(T)$ field modified to account for new information obtained in the course of CRR; T = transmissivity and has units of $m^2\ s^{-1}$

The test shear zone is highly planar and is located in a region of largely intact rock. For the purposes of hydrogeological modelling, it can therefore be idealised as a two-dimensional system at scales of metres to tens of metres. Figure 2.1 shows the outcome of a geostatistical inverse modelling exercise that was performed in support of CRR by the Technical University of Catalonia (UPC). The work was based on an existing model of the transmissivity field of the test shear zone developed as part of MI (see Meier 1999), and extended to incorporate new data from the CRR hydraulic tests. The model suggests the existence of channels with enhanced transmissivities mainly between the boreholes BOMI 86.005, BOCR 99.002 and 00.003 respectively (dipole D-2) and transmissivity barriers in the region of the CRR boreholes are mainly located between boreholes BOMI 87.010 and BOCR 99.002 (dipole D-1) and "behind" dipole D-2.

Dipole D-1 was selected for the final tracer injections as it provided a longer transport time compared to dipole D-2. This residence time (about 80 minutes) is still, however, fairly short, and, as discussed in the following chapter, some of the models developed in support of CRR considered the possibility that association of radionuclides with bentonite colloids may not be appropriately represented as equilibrium sorption during transport through the shear zone, but rather that kinetic effects are potentially important or even that association is effectively irreversible over the timescale of the experiment.

Hydraulic head and transmissivity information on the shear zone is in principle relevant to transport modelling in that it indicates the transport paths to be considered. In the transport modelling for CRR, however, because the dipole flow fields were highly asymmetric, with an extraction flow rate greatly exceeding the injection flow rate, transport paths between the injection and extraction wells were assumed by all the transport modelling teams not to deviate greatly (on a scale of metres) from a straight line connecting the two wells (Section 3.2.2). The transmissivity of the shear zone (and the pressure difference between the injection and withdrawal wells) is determined by its small-scale structure. It was not, however, possible to use transmissivity or head data to constrain the representation of small-scale structure in the transport models. PSI, for example, considered alternative models in which flow and transport occurred either in a single fracture in the shear zone plane or in multiple parallel fractures. Use of transmissivity or head data to discriminate between these models would require a reliable theoretical relationship between transmissivity and aperture. For flow between parallel plates, the so-called "cubic law" can be used (Witherspoon et al. 1980), but this relationship generally fails to hold for the heterogeneous fractures found in geological systems.

2.3 Natural background colloids

Information on the natural background colloid population in the GTS groundwater was required in order to separate the breakthrough of bentonite colloids from the overall colloid concentrations measured at the withdrawal borehole and in order to understand the potential for colloid formation in the injection cocktails. The colloid background was therefore studied before the main tracer tests in dipole D-1 were performed in parallel to the preparatory homologue and colloid tests, as well as in a separate colloid background study which took place after the main tests (see Hauser et al. 2003). The colloid concentration and the average size distribution of the colloids in the GTS groundwater of the CRR test site was determined at different extraction flow rates from 4 to 150 mL min^{-1} and at different times.

These studies revealed that the background concentration of colloids is rather stable. It does not depend significantly on stabilised extraction flow rates up to 150 mL min^{-1}, and does not show significant temporal fluctuations during the sampling period. The average colloid diameter was found to be around 200 nm and the colloid concentration around 5 µg L^{-1}. Increased colloid

concentrations were observed temporarily at the beginning of the experiments and are most likely due to transient mechanical stresses induced by pressure pulses before steady flow conditions were established.

2.4 Input concentrations of tracer cocktails

Table 2.2 shows the input concentrations (M_0) for some of the main tracers in the cocktails used in the two main runs #31 and #32. The chosen concentrations of Th, Tc, U, Np and Pu in the tracer cocktails were limited by the solubility of these elements in Grimsel groundwater. Concentrations were selected such that precipitation due to oversaturation was not expected, based on laboratory experiments[7] and guided by calculated solubility values (Missana & Geckeis 2006). In the case of Am, Sr and Cs, on the other hand, the concentrations utilised were defined by the maximum permitted activity of these radionuclides at the site. Higher activities (and therefore concentrations) would have been permissable, but only by re-licensing the site as a IAEA Level B laboratory once again (as was the case during the EP experiment; see Alexander et al. 1996, Möri et al. 2006 for details).

Tab. 2.2: Oxidation states and injected concentrations in the *in situ* test

Tracer	**Oxidation state**	**Run #31: input concentration M_0** [mol l^{-1}]	**Run #32: input concentration M_0** [mol l^{-1}]
Tc	IV	---	^{99}Tc: 1.0×10^{-8}
Am	III	^{243}Am: 5.9×10^{-9}	^{241}Am: 6.6×10^{-10}
Th	IV	^{232}Th: 1.1×10^{-8}	^{232}Th: 1.1×10^{-8}
U	VI	^{238}U: 9.5×10^{-7}	^{233}U: 8.7×10^{-7}
Np	V	^{237}Np: 9.4×10^{-7}	^{237}Np: 1.1×10^{-6}
Pu	IV	^{238}Pu: 4.4×10^{-11} ^{242}Pu: 9.9×10^{-9}	^{238}Pu: 4.8×10^{-11} ^{244}Pu: 6.7×10^{-9}

2.5 Sorption

The partitioning of different tracer elements dissolved in Grimsel groundwater between aqueous and sorbed phases was measured in the laboratory in presence of different solids and for different "contact times"; see Table 2.3.

[7] It was, however, found in laboratory experiments that, for some of the radionuclides, radiocolloids formed spontaneously (see Missana & Geckeis 2006, for details)

Tab. 2.3: The partitioning of different tracer elements dissolved in Grimsel groundwater

Between aqueous and sorbed phases measured in the laboratory in presence of different solids for different "contact times" (from Missana & Geckeis 2006)

Element (Contact time) [Units]	**Granite (2 h)** [mL g^{-1}]	**Fracture filling material (2 h)** [mL g^{-1}]*	**Bentonite colloids (1 week)** [mL g^{-1}]
Cs (I)[c]	167 ± 15	596 ± 25[a]	8746 ± 900
U (VI)[c]	12.18 ± 0.2	5.6 ± 0.5[a]	824 ± 50
Tc (VII)[c]	0.18 ± 0.09	0.4 ± 0.1[a]	0
Tc (IV)[c]	no data yet	11.5 ± 0.5[a]	361 ± 50
Se (IV)[c]	0.28 ± 0.05	1.6 ± 0.2[a]	7 ± 3
Np (V)[c]	<1[b]	<1[b]	$<5 \cdot 10^3$
Am (III)[d]	12±4[b]	46±5[b]	$2.1 \pm 0.1 \cdot 10^6$
Pu (IV)[d]	4.8±2.5[b]	8±0.8[b]	$1.3 \pm 0.04 \cdot 10^5$

[a] Size fraction: < 300 µm

[b] Size fraction: 250-800 µm

[c] Errors correspond to one standard deviation, based on the results of multiple experiments

[d] Errors correspond to triplicate or duplicate experiments, except for measurements of actinides on fracture infill, which were taken from experiments performed only once and the errors correspond to the analytical error

2.6 Other findings from the laboratory programme

Other findings of the laboratory programme that are potentially relevant to model development and testing are reported in more detail in Missana & Geckeis (2006), and can be summarised as follows:

- relatively large colloid concentrations (up to 1000 mg L^{-1}) have been shown to remain stable over several weeks in the alkaline Grimsel groundwater,
- bentonite colloids significantly influence the uptake of Am, Pu, U and Cs on granodiorite and fracture filling material,
- sorption reactions of U, Pu, Am and Cs on granodiorite and fracture filling material show relatively slow kinetics (compared to the timescale of the experiments),
- there is no evidence for the interaction of bentonite colloids with the matrix of the granodiorite and the fracture filling material, and
- sorption of both Cs and U onto bentonite colloids in Grimsel groundwater is not completely reversible (over the timescales of the experiments).

The following additional observations, though not directly relevant to the modelling of the CRR *in situ* tests, are presented here because of their potential relevance to repository safety studies:

- increasing the groundwater salinity or reducing pH to below 6 increases the agglomeration of colloids and therefore reduces colloid stability, and
- experiments simulating groundwater flow at the host-rock/bentonite interface indicate colloid generation, even under chemical conditions which would normally physically stabilise the bentonite.

2.7 General observations from the shapes of the breakthrough curves

Some constraints on the modelling approaches that can reasonably be considered can be deduced from the shapes of the breakthrough curves.

The breakthrough curves of the radionuclide tracers in the main experimental runs #31 and #32 are shown in Figures 2.2 and 2.3, Figure 2.4 shows the breakthrough curves for bentonite colloids in run #32 and Figure 2.5 compares the breakthrough curves of radionuclide tracers and bentonite colloids in run #32. Table 2.4 summarises the peak times and recoveries of the radionuclide tracers. Note that observations based on these curves were not available to constrain predictive modelling carried out by Enviros and PSI in advance of these runs and referred to in Chapter 1, but were available for most of the other modelling work carried out in support of CRR.

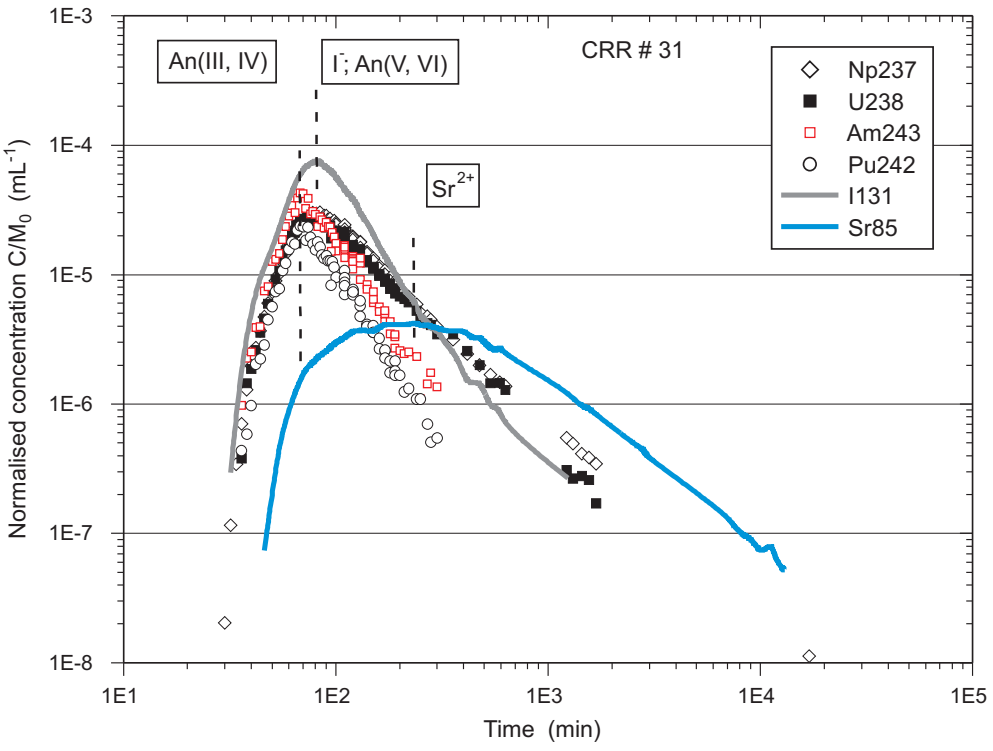

Fig. 2.2: Breakthrough curves measured in run #31 (normalised concentrations)

Peak maxima for the different breakthrough curves are marked with vertical dashed lines

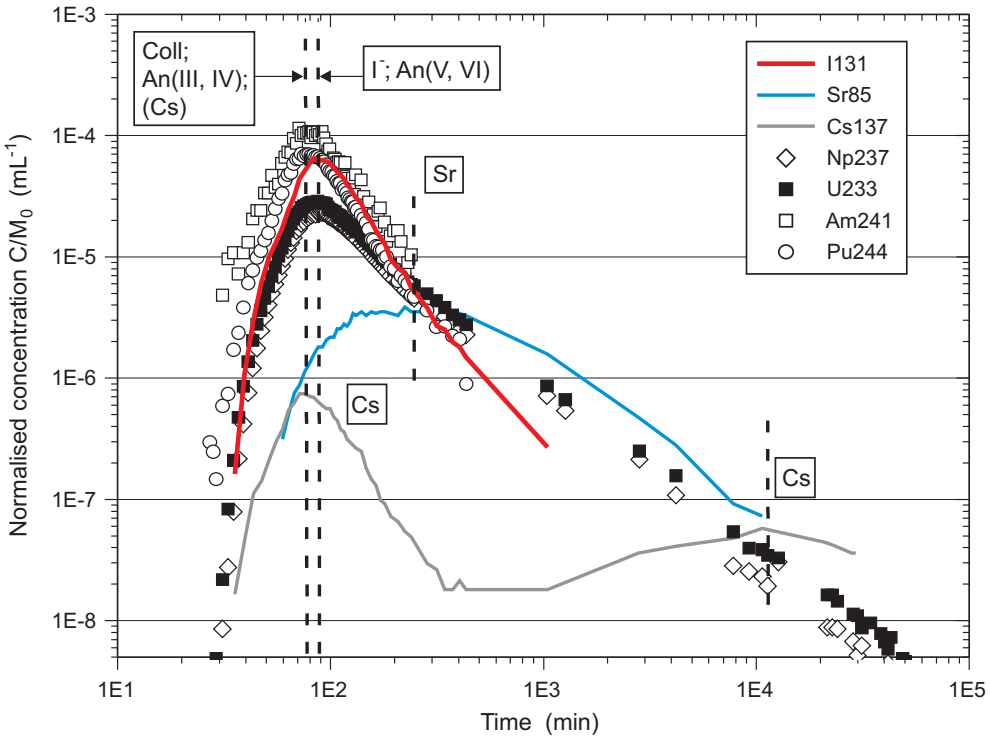

Fig. 2.3: Breakthrough curves measured in run #32 (normalised concentrations)
Peak maxima for the different breakthrough curves are marked with vertical dashed lines

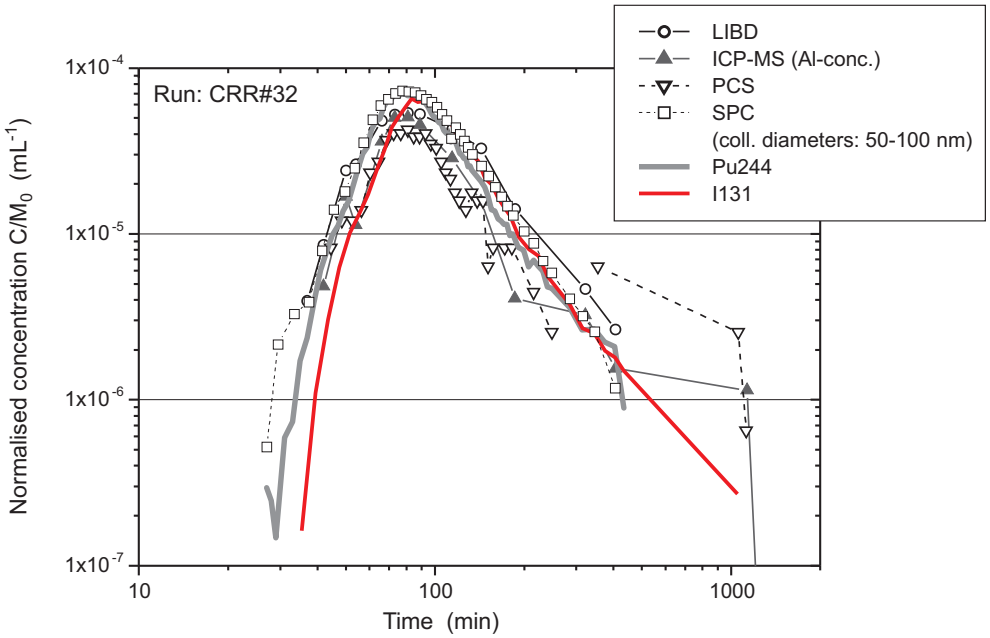

Fig. 2.4: Colloid breakthrough curves detected by LIBD, PCS and ICP-MS

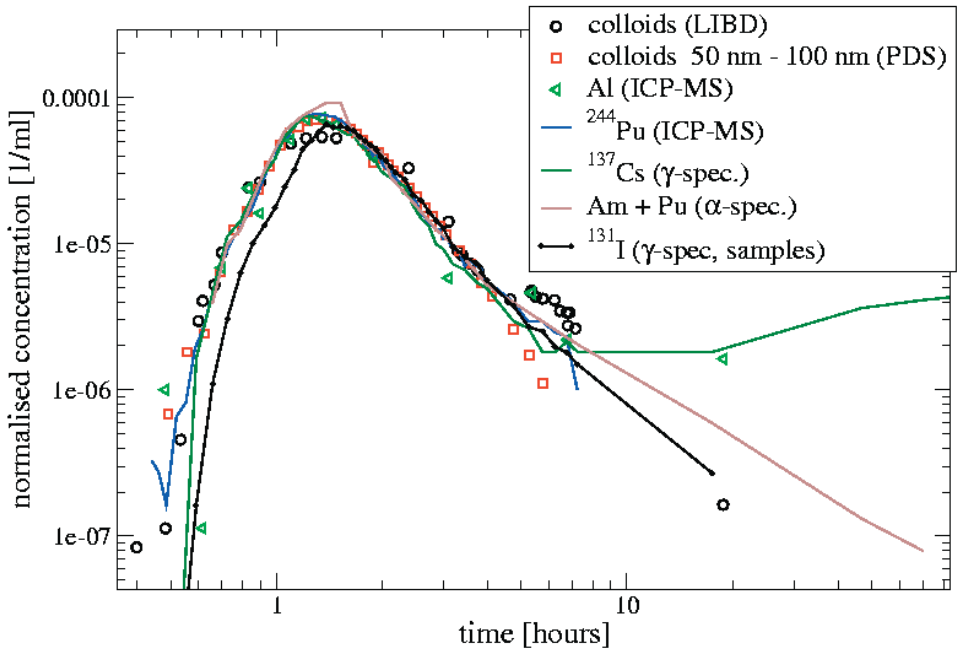

Fig. 2.5: The breakthrough data for colloids and selected tracers in main run #32

Figure 2.5 shows that, when normalised to 100 % recovery, the breakthrough curve for colloids measured in run #32 coincides closely with those of Am, Pu and Cs (and Th, though not shown in the figure), and also with that of the conservative tracer I, although the conservative tracer peak appears slightly later and, as discussed in Chapter 3, Cs displays a second peak at a much later time. This supports the assumption made by all the modelling teams that part of the inventory of these tracers in run #32 was transported in association with colloids.

In planning run #31, it was initially assumed, partly on the basis of calculated solubilities (Section 2.3), that all radionuclides would be transported only in solution; i.e. there would be no production of colloids due, for example, to oversaturation or precipitation, and the effects of natural groundwater colloids would be negligible. This assumption had to be revised when the breakthrough curves of sorbing tracers such as Am, Pu and Th were found to peak at similar times to a conservative tracer, in spite of the fact that these elements have been found to sorb significantly on fault gouge material in laboratory sorption experiments. Furthermore, the shapes of the breakthrough curves for Am and Pu are almost identical in runs #31 and #32, although the recovery is less in run #31.

It appears that a part of the injected inventory of Am, Pu and Th in run #31 was transported in colloidal form, even though no bentonite colloids were present in the injection cocktail. The addition of bentonite colloids increases the amount of these tracers transported in association with colloids. A similar suggestion had also been made earlier on the basis of preliminary runs using Th, Tb and Hf. Characterisation of the run#31 injection cocktail using both ultracentrifugation and laser induced breakdown detection (LIBD) technique confirmed the presence of colloids.

Other relevant observations are:

- more than 80 % of the injected bentonite colloids passed through the flow field without retardation or filtration of larger colloids,

- bentonite colloid, Am, Pu and Th peaks occur approximately 10 minutes earlier than those of U, Np and I, and
- recovery of Am and Pu increased from 20-30 % in the absence of bentonite colloids to 60 – 80 % in the presence of bentonite colloids.

Finally, a general observation made in the preliminary experiments was that recovery was highest in case of the smallest colloids, and decreased with increasing size. Nevertheless, when normalised to 100 % recovery, the breakthrough curves for colloids of different sizes coincide closely with each other. This observation supports the model assumptions made by all the teams that colloids are excluded from rock matrix pores (see Chapter 3).

Tab. 2.4: Recoveries and the peak times in runs #31 and #32

Tracer	**Run**	**Peak time breakthrough** [min]	**Recovery** [%]	**Analysis technique**
^{131}I	31	82	102	γ-spec
^{85}Sr		236	87	γ-spec
^{232}Th		68	<LLD	ICP-MS
^{238}U		78	62	ICP-MS
^{237}Np		84	70	ICP-MS
		82	67	α-spec
^{238}Pu		82	33	α-spec
^{242}Pu		68	21	ICP-MS
^{243}Am		68	34	ICP-MS
		72	43	α-spec
^{131}I	32	83	92	γ-spec
^{85}Sr		223	88	γ-spec
^{137}Cs		72 / 10’680	70	γ-spec
^{99}Tc		85	<LLD	ICP-MS
^{232}Th		69	63	ICP-MS
^{233}U		87	103	ICP-MS
		90	80	α-spec*
^{237}Np		93	82	ICP-MS
		90	80	α-spec*
^{238}Pu		84	70	α-spec*
^{244}Pu		73	86	ICP-MS
^{241}Am		71	<LLD	ICP-MS
		84	70	α-spec*

* Note that U/Np and Am/Pu respectively were analysed in pair

3 Overview of CRR modelling

This chapter describes the key similarities and differences between the models, the strategies for applying them and the results obtained by the different modelling teams. The reader is referred to Appendix 1 for a comprehensive description of the individual models and modelling results.

3.1 The modelling teams and the models

As described in Chapter 1, four modelling teams were set up to analyse the results of the CRR *in situ* experiments. The ways in which the structure of the shear zone, the flow field and the various transport processes are treated in the models developed by the teams are summarised in Table 3.1, highlighting the similarities and differences.

A key similarity between all the models is that colloids are assumed not to be retarded by reversible interactions with solid surfaces and are excluded from pores in the rock matrix adjacent to water-conducting fractures in the shear zone. This assumption is supported by the observation that the shapes of the breakthrough curves and the time of the breakthrough peak are not dependent on colloid size (Section 2.7). These processes can, however, significantly retard the transport of tracers not associated with colloids and conveyed as aqueous solutes.

The most significant difference between the models affecting colloid facilitated transport of radionuclide tracers is probably the treatment of the interaction of tracers with colloids, which is treated using a range of assumptions, including equilibrium sorption in the JNC STAMMT-L and Enviros models, non-equilibrium sorption with first-order sorption kinetics in the JNC COLFRAC model and irreversible sorption in the FZK-INE and PSI models. The assumption of irreversible sorption here means that the distribution of a tracer between the aqueous phase and any colloids at the time of injection remains constant during transport within the shear zone - i.e. there is no further sorption onto, or desorption from, colloids *on the timescale of the experiment*. Sorption may, of course, be reversible over longer timescales. It should be noted that a similar range of assumptions has been made in models used in recent safety assessments (Appendix 2).

Some of the modelling teams describe more than one modelling approach. In particular:

- JNC considered two modelling approaches, which will be referred to here as the STAMMT-L and COLFRAC models after the codes that were used to solve the respective governing equations. The STAMMT-L model does not include the effects of colloids on transport and was applied only to main run #31, under the assumption that no colloids were present in this run. COLFRAC was applied to both run #31 and run #32.
- PSI considered approaches that will be referred to as 1-D and 2-D variants of the PSI advection-dispersion model, and a non-Fickian dispersion model. The non-Fickian dispersion model does not currently include matrix diffusion, and so was applied only to the breakthrough of colloids and tracers that are assumed to be (irreversibly) attached to colloids, since colloids are assumed to be excluded for rock matrix pores.

Tab. 3.1: Overview of the treatment of flow and transport processes in the various models applied in CRR

	FZK-INE	JNC		Enviros	PSI		
		STAMMT-L	COLFRAC		1-D advection-dispersion	2-D advection-dispersion	Non-Fickian dispersion
Flow / advection	2-D flow / advection in porous medium in shear-zone plane with anisotropic transmissivity	1-D flow / advection in "mobile zone"	2-D fracture network, with 1-D flow in fractures and 2-D flow in matrix	2-D flow / advection in porous medium in shear-zone plane	1-D flow / advection in single or multiple parallel fractures	2-D flow / advection in single or multiple parallel fractures	1-D flow / advection in single fracture
Dispersion	Diffusion-like processes, described by Fick's Laws ("Fickian dispersion")						Non-Fickian dispersion
Matrix diffusion	Not included	Included		Not included	Included		Not included
Solute sorption on solid surfaces	Equilibrium		Eqm. on matrix pore surfaces; non-eqm. 1st order kinetics on fracture surfaces	Equilibrium			Not included
Solute association with colloids	Irreversible	Not included	Non-eqm., 1st order kinetics	Equilibrium	Irreversible		Not included
Colloid interactions with solid surfaces	Not included		Irreversible filtration included via first order rate equation	Not included			

The PSI modelling team applied the 1-D and 2-D advection dispersion models to preliminary CRR experiments carried out in advance of the main runs #31 and #32. Results were found to be similar, and so only the 1-D advection dispersion model was used to model the breakthrough of tracers transported as aqueous solutes in the main runs. Both FZK-INE and PSI modelling of bentonite colloid transport in preliminary experimental runs in dipole D-3 showed that colloid breakthrough can be reasonably well fitted using a model with a Fickian representation of dispersion. In the case of the preliminary run in dipole D-1 (run #14), however, PSI found that a non-Fickian dispersion model was required in order to reproduce accurately the late-time tailing of homologue tracers that appear to be transported in colloidal form (Section 2.7). This model was also used by PSI to model the breakthrough of tracers assumed to be irreversibly associated with colloids in the main runs.

3.2 Treatment of structures and processes

3.2.1 The structure of the shear zone

In order to derive tractable equations for flow and tracer transport, the geological structure of the shear zone has to be simplified. In all the models, the complex and highly connected network of open and partially filled fractures observed in the actual shear zone is replaced by one or more planar fractures separated by porous rock matrix, or, in the case of the JNC STAMMT-L model, a mobile (water-conducting) zone and an immobile zone.

The Enviros and FZK-INE models both consider a single fracture filled with porous fault gouge. The PSI models consider either a single fracture or multiple parallel fractures in the shear zone plane, with adjoining rock matrix (Fig. 3.1). The JNC COLFRAC model considers a network of orthogonal fractures, which are either parallel to the shear zone plane, or normal to it (Fig. 3.2).

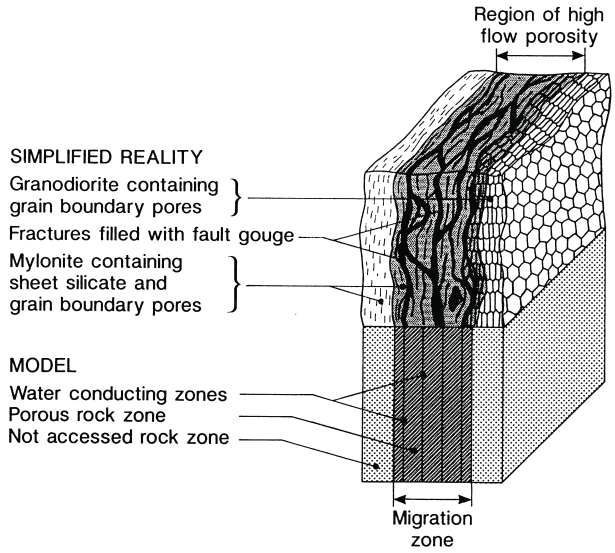

Fig. 3.1: Sketch of the geological structure of the shear zone (upper part) and its simplification in the PSI models

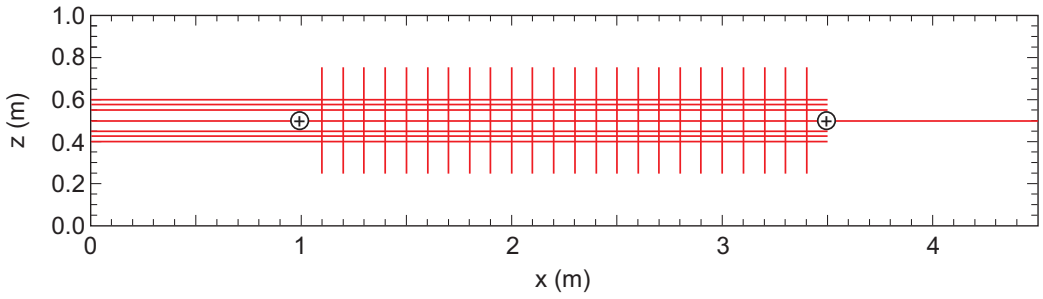

Fig. 3.2: Geometry of the model fracture system used in the JNC COLFRAC model; the injection and withdrawal wells are shown as small circles

All the modelling teams considered both the fractures and rock matrix to be spatially uniform (homogeneous) and to have properties that are constant in time.

3.2.2 The flow field

The dipole flow fields in CRR were highly asymmetric, with an extraction flow rate greatly exceeding the injection flow rate. Transport paths between the injection and extraction wells are therefore assumed by all the transport teams not to deviate greatly (on a scale of metres) from a straight line connecting the two wells. The transmissivity of the shear zone is, however, highly heterogeneous (Fig. 2.1). Multiple paths with different mean flow rates and transport times could, in principle, exist between injection and extraction, although there is no evidence for this, at least on the scale of metres, in the form, for example, of multiple peaks in the breakthrough curves. Any increase in the mean transport path length due to the smaller-scale tortuosity of the transport paths was assumed by the modelling teams to be minimal. The spreading due to smaller-scale heterogeneity is, however, taken into account either as a Fickian or non-Fickian dispersion term in the governing equations of the transport models, or explicitly by means of a stylised fracture network in the case of the JNC COLFRAC model (Fig. 3.2).

All the modelling teams considered only steady flow. Small variations in the flow field due, for example, to fluctuations in the pumping rates at the injection and withdrawal wells were neglected. The FZK-INE, PSI and Enviros teams assumed that flow was confined entirely to a discrete water-conducting feature or features within the shear zone. In the Enviros and FZK-INE models, a planar porous zone is considered. In the PSI models, the discrete features are one or more open fractures running parallel to the shear-zone plane. The JNC STAMMT-L model assumes that flow was confined to a mobile zone that can be thought of as either an open or partly infilled fracture or set of fractures. The JNC COLFRAC model, on the other hand, considers the possibility of flow within the rock matrix between fractures, as well as in the fractures themselves.

Both 1-D and 2-D models of flow along the transport paths in the shear zone were considered. The JNC STAMMT-L model, the PSI 1-D advection-dispersion model and the PSI non-Fickian dispersion model are all one-dimensional in their treatment of flow and advective transport. The Enviros model, the FZK-INE model and the PSI 2-D advection-dispersion model consider 2-D flow in the plane of the feature, with anisotropy considered in the FZK-INE model. The JNC COLFRAC model considers 1-D flow in a 2-D network of orthogonal fractures (see Fig. 3.2), with 2-D flow in the rock matrix between the fractures. In all the other models, the rock matrix is considered to be impermeable, but accessible by matrix diffusion in the JNC models and in the PSI advection-dispersion models (see Section A1.1).

A process that needs special attention in the case of the 1-D models is the dilution of tracer concentrations due to mixing water drawn into the dipole flow field from more distant parts of the shear zone. This reduces tracer concentration at the withdrawal well by a factor Q_p/Q_i, where Q_p [m^3 s^{-1}] and Q_i [m^3 s^{-1}] are the pumping rates at the withdrawal well and the injection well, respectively. The calculated 1-D model concentrations are thus multiplied by a factor

$$\frac{1}{RF}\frac{Q_p}{Q_i}$$

in order to take account of the effects of dilution. *RF* is a scaling factor used for tracers (including colloids) that showed a less than 100 % recovery.

Additional dilution or scaling factors were required to match calculational results to experimental observations in the case of the JNC STAMMT-L runs and some JNC COLFRAC runs.

In most of the modelling approaches, the flow field is fully specified by the injection and withdrawal flow rates and the assumptions regarding the structure of the shear zone. In the JNC COLFRAC model, on the other hand, the hydraulic properties of the fractures and rock matrix also have to be specified, in order to define how flow is partitioned between the two.

3.3 Transport processes

3.3.1 Overview of processes

The transport processes discussed by the different modelling teams are broadly the same, and are illustrated in Figure 3.3, although not all processes are included in all the models considered (see Table 3.1).

The processes thought to operate on the injected solutes and colloids are:

1. advection and hydrodynamic dispersion of solutes and colloids in a fracture or fractures within the shear zone (advection and hydrodynamic dispersion of solutes in the matrix are only considered in the JNC COLFRAC model)
2. matrix diffusion of solutes into the rock matrix adjacent to the fracture or fractures
3. sorption of solutes onto solid surfaces (either fracture surfaces or matrix pore surfaces)
4. interaction of solutes with colloids
5. interaction of colloids with the fracture walls, which is termed filtration if the interaction is irreversible over the timescales of concern.

The differences in the ways in which these processes are treated in the various modelling approaches are discussed in the following sections.

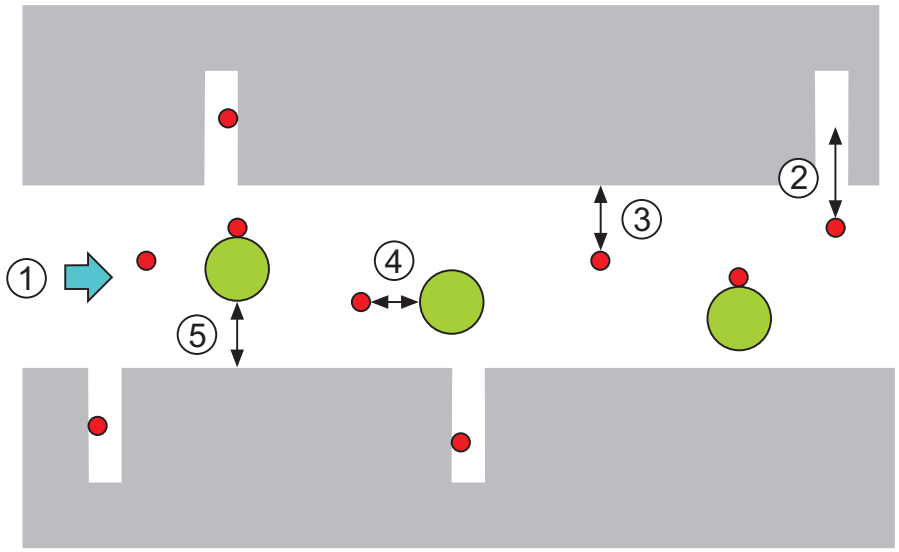

Fig. 3.3: Schematic illustration of the broad processes considered by the different modelling teams

All the models assume that colloids may be described by a single set of parameter values, irrespective of their size, even though, in reality, bentonite colloids in the injection cocktail were polydispersed (i.e. varied in size). The FZK-INE, JNC and PSI models also assume that the transport of the various tracers that were injected as aqueous solutes can be calculated independently of each other. This implies the following additional assumptions:

- tracers in aqueous solution do not interact (chemically) with each other
- there is no competition between tracers for sorption sites, e.g. on the surfaces of colloids or on pore surfaces of the rock matrix.

The Enviros model is based on a reactive transport approach that, in principle, allows for competition for sorption sites among species.

The models also neglect decay during transport of radioactive tracers in the injection cocktails. This assumption is readily justified for all tracers apart from ^{85}Sr and ^{131}I, which have half lives of about 1560 and 190 hours, respectively. Even for these tracers, however, the concentration changes due to decay are small.

3.3.2 Advection and hydrodynamic dispersion

The velocity profile across an ideal, open fracture is parabolic in shape, with the highest velocity occurring along the centre streamline, and with the groundwater velocity falling to zero at the fracture walls. Diffusion across the fracture aperture means that both solute particles and colloids sample a range of velocities as they migrate along the fractures. This gives rise to a form of dispersion termed "Taylor dispersion".

The diffusion coefficient is inversely proportional to particle size, and thus is much smaller for colloids than for solutes. It has been suggested in a detailed report of the PSI modelling (Kosakowski & Smith 2004) that diffusion of colloids across the fracture aperture may be insufficient to ensure that colloids sample the full parabolic velocity profile during the transport across the dipole flow field (due to the short transport times), and this might affect the form of the Taylor dispersion undergone by colloids. In addition, the size of the colloids, as well as charge effects, means that colloids may not sample the lowest velocities near the fracture walls. Thus, colloids may have an average velocity that exceeds the mean fluid velocity in a fracture (see Section 1.2). Nevertheless, in all the models applied in CRR it is assumed that these effects are small and can be neglected. Colloids and solutes are both advected at the mean fluid velocity in a fracture, and undergo hydrodynamic dispersion, which includes the effects of Taylor dispersion.

Hydrodynamic dispersion in a water-conducting fracture arises as a result of heterogeneity (mechanical dispersion) and molecular diffusion in the fracture plane, as well as Taylor dispersion described above. All of the modelling teams considered models in which hydrodynamic dispersion is modelled as a diffusion-like process, described by Fick's laws. PSI considered an additional model variant (Kosakowski 2004) in which the dispersion of colloids was treated using the continuous time random walk (CTRW) approach (Berkowitz & Scher 1995). This is referred to as the non-Fickian dispersion model, although it includes Fickian dispersion as a special case. The network of multiple orthogonal fractures in the JNC COLFRAC model also gives rise to dispersion, which is not necessarily described by Fick's laws.

Longitudinal dispersion (i.e. dispersion in the flow direction) in fractures is considered in all the models. In addition:

- the JNC COLFRAC model, in which solutes are advected in the rock matrix as well as in fractures, considers both longitudinal dispersion and dispersion normal to the fracture plane in the rock matrix, and
- the Enviros, FZK-INE and PSI 2-D advection-dispersion models consider transverse as well as longitudinal dispersion in the fracture plane.

3.3.3 Matrix diffusion

Matrix diffusion of solutes

The JNC models and the PSI advection-dispersion[8] models allow tracers to be transferred between the fractures and the adjacent rock matrix. This transfer takes place by diffusion, and, for any given solute, matrix diffusion is defined by a single set of parameters for, say, the pore diffusion coefficient, matrix porosity, and maximum depth of the diffusion-accessible matrix[9]. The JNC COLFRAC model, allows for advection / dispersion as well as diffusion in the rock matrix, and these processes may also contribute to the transfer of tracers between fractures and rock matrix.

Matrix diffusion of colloids

All the modelling teams assumed that colloids are excluded for rock matrix pores due to their size and charge, and thus migrate only within fractures or, in the case of the Enviros and FZK-INE models, within a porous shear zone filled with fault gouge.

3.3.4 Sorption of solutes to solid surfaces

All of the models assume that sorption of solutes on matrix pore surfaces is a reversible, equilibrium process, described by a sorption coefficient K_d [m^3 kg^{-1}]. Solutes may also sorb onto the fracture walls. This is included as a reversible, equilibrium process in the JNC STAMMT_L model. In the JNC COLFRAC model, the possibility of non-equilibrium sorption on fracture walls is considered, described by first-order sorption kinetics in a similar way to the interaction of solutes with colloids (see below).

3.3.5 Interaction of solutes with colloids

All of the models consider that solutes may become associated with colloids. The most general representation of the interaction of an individual solute with colloids is that of the JNC COLFRAC model, in which first order linear reactions[10] are assumed to describe interaction kinetics:

---

[8] The PSI non-Fickian dispersion model does not include matrix diffusion, and was applied only to the transport of colloids

[9] The STAMMT-L code allows matrix diffusion to be described as a multirate process to account for matrix heterogeneity, although this capability was not used for the CRR modelling studies

[10] The COLFRAC code allows other forms for these interactions, and also allows interactions between mobile and immobile (filtered) colloids to be treated differently to each other, although these capabilities were not used for the CRR modelling exercise

$$\frac{d\widetilde{c}_n^*}{dt} = \beta_n \left(K_n c_m - \widetilde{c}_n^* \right) , \tag{3-1}$$

and

$$\frac{d\widetilde{c}_{\tilde{n}}^*}{dt} = \beta_n \left(K_n c_m - \widetilde{c}_{\tilde{n}}^* \right) \tag{3-2}$$

where:

- c_m [kg m^{-3}] is the concentration of a solute in solution,
- $\widetilde{c}_n^*$ [-] is the mass of the same substance sorbed onto unit mass of colloids migrating with flowing water,
- $\widetilde{c}_{\tilde{n}}^*$ [-] is the mass per unit area of the same substance sorbed onto unit mass of colloids irreversibly attached to fracture walls (see below),
- K_n [m^3 kg^{-1}] is an equilibrium sorption coefficient for sorption of solutes on colloids , and
- β_n [s^{-1}] is a kinetic constant.

In the Enviros model, sorption of a solute on colloids migrating with flowing water is assumed to be rapid with respect to the timescale of the field experiments, so that $\beta_n \to \infty$ and, from Eq. 3-1:

$$\frac{\widetilde{c}_n^*}{c_m} \approx K_n \text{ for the Enviros model.} \tag{3-3}$$

In the FZK-INE and PSI models, on the other hand, interaction kinetics for sorption on colloids are assumed to be slow with respect to the timescale of the field experiments, so that, again from Eq. 3-1:

$$\frac{\partial\widetilde{c}_n^*}{\partial t} \approx 0 \text{ for the FZK-INE and PSI models.} \tag{3-4}$$

Only the JNC models consider sorption of solutes on colloids attached to fracture walls.

Although the FZK-INE and PSI models allow for the interaction of solutes with colloids, this interaction is considered to occur at or before the time of tracer injection. Once tracers are injected into the dipole flow field, any that are associated with colloids remain associated with colloids. There is no further sorption of tracers in solution onto colloids or desorption from colloids, i.e. the colloid-bound fraction of each tracers remains constant during transport. In this sense, the FZK-INE and PSI models assume irreversible solute sorption on colloids.

3.3.6 Interaction of colloids with fracture walls

Irreversible attachment of colloids to a fracture wall, i.e. colloid filtration, is considered explicitly only in the JNC COLFRAC model via the equation:

$$\frac{d\tilde{n}}{dt} = \lambda q_n n \,, \tag{3-5}$$

where $\tilde{n}$ [kg m^{-2}] is the concentration of colloids attached to the fracture walls, n [kg m^{-3}] is the concentration of colloids in flowing water in the fracture, q_n [m s^{-1}] is the colloid velocity and λ [-] is an empirical parameter termed the "filter coefficient".

The colloid breakthrough curves and breakthrough curves of tracers associated with colloids generated by the FZK-INE and PSI models may simply be scaled to account for filtration, since the association of tracers with colloids is assumed irreversible and colloid breakthrough is calculated independently of solute breakthrough.

3.4 Computer codes

The computer codes used to solve the governing equations of the transport models developed by the different modelling teams are listed in Table 3.2, with references to detailed documentation of the codes. In many cases, the codes used were not specifically developed for CRR modelling, but rather for a broad range of applications, including in some cases repository safety assessment. Often, only a subset of the capabilities of a code was used when applying it in CRR.

Tab. 3.2: The computer codes used to solve the governing equations of the transport models developed by the different modelling teams

Modelling team	Code	Application	References
ENVIROS	PHAST	All modelling by ENVIROS modelling team	Parkhurst et al. (2000)
FZK-INE	ADINA-F	All modelling by FZK-INE modelling team	Bathe (1996); ADINA R&D (2001)
JNC	STAMMT-L	JNC STAMMT-L preliminary modelling of solute tracer breakthrough	Haggerty & Gorelick (1995)
	COLFRAC	JNC COLFRAC modelling, including sorption kinetics for solutes on colloids	Ibaraki & Sudicky (1995a,b)
	PEST	Used in conjunction with COLFRAC to fit model results to experimental data	Doherty (2002)
PSI	PICNIC	The PSI 1-D advection-dispersion model	Barten (1996); Barten & Robinson (2001).
	RockFlow	The PSI 2-D advection-dispersion model	Kolditz et al. (1999)
	GRACE[1] CTRW implemented as external routines	The non-Fickian dispersion model	Berkowitz et al. (2001)

[1] GRACE is a graphical analysis package that can access external functions. The library functions for non-Fickian dispersion (CTRW) modelling are described in Berkowitz et al. (2001)

3.5 Strategy for applying the models

3.5.1 General strategy

Ideally, modelling would have proceeded by setting parameters values based on independent measurements of the shear zone and laboratory results, such as those of batch sorption experiments, predicting breakthrough curves in advance of the field tests being carried out, and comparing the predictions with the measured breakthrough curves (see the discussion in Alexander et al. 2003).

In practice, however, although some parameters could be set in this way, others had to be obtained by inverse modelling - i.e. by adjusting parameter values until the closest possible fit to the measured breakthrough curves.

Some predictive modelling was carried out in advance of the main experimental runs #31 and #32 in order not only to test the model being applied, but also to aid in the planning of the experiments (see, e.g. the description of the PSI work in Appendix 1). For these predictions, parameters that could not be fixed from independent measurements were obtained by inverse modelling of the results of preliminary experiments conducted mainly in the same dipole as the main runs (dipole D-1). In all other cases, the strategies adopted involved some inverse modelling of the main experimental runs themselves.

Where inverse modelling is used, the success of a model is judged not only by the closeness of the best fit to the measured curves, but also, and equally importantly, by the plausibility and self-consistency of the fitted parameters. Plausibility in this context means that the values are physically and chemically possible, and are at least broadly consistent with values obtained from comparable systems elsewhere. Self-consistency means, for example, that a parameter that is expected to be tracer-independent does indeed take the same value (within the uncertainty range) when derived from the breakthrough curves of different tracers. Plausible and self-consistent parameter values were obtained in some but not all of the inverse modelling carried out in support of CRR, as discussed later in this chapter.

3.5.2 Methods for setting parameters

The methods adopted by the modelling teams for setting parameters for the main experimental runs were broadly similar, and are summarised in Table 3.3. Although there were differences in detail, the idea in all cases was:

- To apply inverse modelling to the breakthrough curves of tracers that are thought to be relatively simple - i.e. to be affected during transport by a small number of processes.
- To use the fitted parameters derived in this way in conjunction with parameters (e.g. for sorption) derived from laboratory experiments in modelling the breakthrough curves of more complex tracers.

Enviros fitted parameters related to advection and dispersion by inverse modelling of the breakthrough curves of the conservative tracer uranine and of bentonite colloids. Laboratory data were then used to set parameters for sorption reactions on bentonite colloids and on fault gouge. On the basis of these reactions, and using the advection and dispersion parameters from the inverse modelling, the breakthrough of sorbing tracers in runs #31 and #32 was then modelled and the results compared to the experimental breakthrough curves. Sensitivity analyses were carried out on sorption-relevant parameters, namely the specific surface area available for sorption and the surface complexation constants for the sorption reactions, in order to investigate whether an improved match could be obtained.

Tab. 3.3: Summary of methods applied to set parameters for modelling the main CRR experimental runs #31 and #32

Parameters	**Enviros**	**FZK-INE**	**JNC**	**PSI**
Advection/dispersion	Values obtained from inverse modelling of runs #31, #32 for uranine and bentonite colloid tracers	Values obtained from inverse modelling of runs #29, #34 for uranine tracer	Values obtained from inverse modelling of runs #31 for iodine tracer	Values obtained from inverse modelling of run #14 for Th, Tb, Hf tracers (assumed transported as colloids)
Matrix diffusion	Process not included in chosen model			Values obtained from inverse modelling of runs #13, #21 for uranine tracer
Solute sorption on rock surfaces	Values inferred from laboratory data	Values obtained from inverse modelling of run #32 for U, Np tracers	Values obtained from inverse modelling of run #31 for Am, Np tracers (assumed transported as solutes) and run #32 for U	Values inferred from laboratory data; value for Sr also obtained from inverse modelling of run #21
Partitioning colloids/solution		Np and U assumed 50 % unretarded and 50 % retarded. It is not explicitly assumed that the unretarded fraction is associated with colloids.	Values obtained from inverse modelling of run #32 for Am, Np, U tracers	Values inferred from laboratory data; also direct measurement of colloid-bound fractions in injection cocktails
Filtration	Process not included in chosen model			Process not included in chosen model

FZK-INE fitted parameters related to advection and dispersion by inverse modelling of the breakthrough curves of the conservative tracer uranine in preliminary runs #29 and #34 in dipole D-3. These parameters had to be modified in order to simulate the transport of bentonite colloids in other preliminary runs in the same dipole (runs #6a and #7a). Finally, in order to model the transport of Np and U in the presence of bentonite colloids in main run #32 (and strontium, although this case was not discussed in detail), FZK-INE assumed that these tracers are transported 50 % unretarded (like uranine) and 50 % as retarded. Advection and dispersion parameters determined from inverse modelling of the conservative tracer I in run #31, and a retardation factor fitted to account for sorption on matrix pore surfaces. It is not explicitly stated in Appendix A1.2 that the unretarded fraction is associated with colloids. Although this is one possible interpretation of the assumption of an unretarded fraction, the assumed distribution

between solutes and colloids would be inconsistent with laboratory measurements, which indicate 9 % and 2 % colloid bound fractions for Np and U, respectively - see the discussion of Np and U transport, below.

JNC fitted parameters related to advection, dispersion and matrix diffusion by inverse modelling of the breakthrough curves of the conservative tracer I, and used these parameters when modelling the breakthrough curves of the sorbing tracers Am and Np in run #31, assuming no colloids to be present (in spite of the observations described in Section 2.6 that this assumption is probably not valid). In this case, sorption parameters for Am and Np were extracted by fitting. This procedure was carried out using both the STAMMT-L and COLFRAC models. Finally, the breakthrough curves of the sorbing tracers Am, Np and U in the presence of bentonite colloids in run #32 were modelled using COLFRAC. In this case, parameters related to advection, dispersion, matrix diffusion and sorption of solutes on solid surfaces were taken from the results of the previous fits, and parameters for the sorption of radionuclides on colloids and for colloid filtration were extracted by inverse modelling.

The PSI modelling team applied the 1-D and 2-D advection-dispersion models to perform inverse modelling of the breakthrough of Th, Tb and Hf in preliminary experimental runs in dipole D-1 (run #14)[11]. These tracers were assumed to be transported as colloids (see Section 2.6), and as such, in the models at least, subject only to the transport processes of advection and dispersion, but not matrix diffusion. These fitted advection and dispersion parameters were then set at fixed values when applying inverse modelling to the breakthrough of the conservative tracer uranine in preliminary runs #13 and #21 in order to obtain matrix diffusion parameters. Finally, the breakthrough curves of sorbing tracers both in the assumed absence of colloids (run #31) and with bentonite colloids present (run #32) were predicted in advance of the experiments, with parameters related to advection, dispersion and matrix diffusion taken from the results of the previous fits, and parameters for the sorption of tracers on solid surfaces obtained from laboratory batch sorption measurements. In the case of the run #32 predictions, the partitioning of radionuclides between the aqueous phase and colloids was also based on the results of laboratory batch sorption measurements. The predictions were improved upon subsequent to the main runs being carried out, when direct measurements of the colloid bound fractions in the injection cocktails became available.

The PSI team also obtained the sorption coefficient for Sr by inverse modelling of the Sr breakthrough curve in the preliminary run #21 (no colloids added), and showed it to be within the range obtained in earlier MI modelling studies reported in Heer & Hadermann (1996).

[11] It was not possible to obtain unique parameters for the non-Fickian dispersion model used to predict transport of tracers associated with bentonite colloids in run #32 on the basis of Th, Tb and Hf breakthrough in dipole D-1, and additional inverse modelling of bentonite colloid breakthrough in dipole D-3 (runs #6a and #7a) had to be performed to fix one of the model parameters. Once run #32 had been carried out, it was found that a small adjustment to this parameter was required to obtain good agreement between experimental results and predictions.

3.6 Findings from applying the models

3.6.1 Conservative tracer transport

All the modelling teams obtained close fits to the measured breakthrough curves for the conservative tracer I, although the calculated breakthrough curves by Enviros and FZK-INE lacked the long-time tailing associated with matrix diffusion that was observed in the measured breakthrough curves. Furthermore, the matrix diffusion parameters fitted using the JNC models differ substantially from those fitted using the PSI models. The differences probably arise, at least in part, because some of the breakthrough curve tailing attributed to matrix diffusion in the PSI model is attributed to dispersion in the fracture network that represents the shear zone in the JNC COLFRAC model (see Fig. 3.2). The pore diffusion coefficient derived from JNC COLFRAC inverse modelling is in fact unrealistically large (two orders of magnitude greater than the diffusion coefficient in free water). A high diffusion rate means the rock matrix in the model rapidly saturates with migrating tracers, and this contributes to a delay but not to tailing in tracer breakthrough. It should also be noted that JNC found it necessary to apply an unexplained scaling factor of 100 to the calculated breakthrough curve for I in order to obtain a satisfactory match to the experimental curve. Overall, the difference in the fitted parameters obtained by the different teams illustrates the difficulties that can arise in unambiguously separating the effects of dispersion and matrix diffusion on the spreading of tracer breakthrough.

Another point that distinguishes the JNC COLFRAC model from other models applied in CRR is that it allows for advection and dispersion in the rock matrix between fractures, as well as in the fractures themselves. The values for matrix advection and dispersion parameters obtained by the inverse modelling of I breakthrough show a very large uncertainty. For the best fit, however, both the total rate of water flow and the advection velocity within the rock matrix are small compared to those within the fractures and probably do not contribute significantly to the shape of the breakthrough curves. The large uncertainties are thus unsurprising, and the COLFRAC modelling provides some support for the assumption made in the other models that advective and dispersive transport processes in the rock matrix can be neglected.

3.6.2 Sorbing tracer transport

Table 3.4 gives an overview of the main observations and findings from applying the different models to the breakthrough of sorbing tracers in the main runs #31 and #32. More detailed discussions of the findings are given in the following sections.

Tab. 3.4: Overview of main observations and findings from modelling the breakthrough of sorbing tracers in main runs #31 and #32

Tracers	Run	Models applied (key features)	Observations	Conclusions
Am, Pu, Th	#31	**Enviros; PSI:** No colloid-facilitated transport; retardation of solutes by sorption based on laboratory measurements	Predicted breakthrough curves more retarded and broadened compared to measured breakthrough; predictions by Enviros (corresponding to solute transport) do not reach experimental detection limits	Solute transport of Am, Pu, Th does not contribute significantly to the breakthrough curves, in spite of the absence of bentonite colloids
		JNC: No colloid-facilitated transport; retardation of solutes by sorption calibrated by fitting	Fitted sorption parameter values significantly smaller than in laboratory tests	
	#32	**Enviros; JNC:** Reversible association of tracers with colloids	Reasonable fit obtained by Enviros only by individual calibration of sorption parameters for tracers on colloids	Solute transport of Am, Pu, Th does not contribute significantly to the breakthrough curves, except possibly the late-time tails
			Very large uncertainties (non-uniqueness) in fitted parameter values obtained by JNC, and inconsistency with filtration parameter value fitted for Am with those for Np and U.	
		PSI: Irreversible association of tracers with colloids, (high) colloid-bound fraction measured in advance of the run	Am, Pu breakthrough well predicted; some indication of a change in slope of breakthrough curves after 3 - 4 hours reflecting a possible change from colloid-facilitated transport to solute transport as the dominant mechanism	
Np; U	#31	**Enviros; PSI:** No colloid-facilitated transport; retardation of solutes by sorption based on laboratory measurements	Np breakthrough well predicted (PSI only)	Np transported mostly in aqueous solution, retarded by matrix diffusion and sorption; sorption of U (and possibly Np) on matrix pore surfaces less than expected from laboratory measurements
			Significant discrepancy between predictions and measured breakthrough for U	
		JNC: No colloid-facilitated transport; retardation of Np by sorption calibrated by fitting	Fitted sorption parameter values significantly smaller than in laboratory tests	
Np; U	#32	**Enviros; JNC:** Reversible association with colloids	Reasonable fit obtained by Enviros only by individual calibration of sorption parameters for tracers on colloids	As for run #31, but possibly with some contribution of colloids to the shapes of the breakthrough curve tails
			Best fit breakthrough curves produced by JNC poorly match experimental breakthrough	
		FZK-INE: Irreversible association of tracers with colloids; 50 % colloid-bound fraction assumed; retardation factor for solute transport calibrated by fitting	Reasonable fit obtained, but 50 % colloid-bound fraction is inconsistent with laboratory measurements	

Tracers	Run	Models applied (key features)	Observations	Conclusions
		PSI: Irreversible association of tracers with colloids, (low) colloid-bound fraction measured in advance of the run	Np breakthrough well predicted	
			Significant discrepancy between predictions and measured breakthrough for U	
Cs	#32	**PSI**: Irreversible association of Cs with colloids, colloid-bound fraction measured in advance of the run	Qualitately successful predictions of douple-peak breakthrough	Cs transported in part as colloid-bound fraction and in part in aqueous solution; association of Cs with colloids irreversible or only slowly reversible on experimental timescale

Transport of Am, Pu and Th

Laboratory sorption studies suggest high association of Am, Pu and Th with bentonite colloids in run #32 (98 %, 72 % and 98 % colloid bound fractions, respectively, on the basis of sorption measurements made in advance of the main runs). Large colloid-bound fractions were later confirmed by the direct analysis of the injection cocktails. Furthermore, in the case of run #31 (as mentioned above) the breakthrough curves, which are almost identical in shape to those of run #32, but with lower recoveries, suggest that Am, Pu and Th were transported partly in colloidal form, even though no bentonite colloids were present in the injection cocktail (referring to Fig. 2.2, it can be seen that the breakthrough curve maxima for Am and Pu occur slightly in advance of that for the conservative tracer iodine, consistent with colloid-facilitated transport).

The nature of the colloids in run #31 is not completely clear; at the time of the modelling work, it was an open issue whether they were heterogeneous (radionuclides associated with natural groundwater colloids) or homogeneous (formed, e.g. by precipitation at or before the time of injection). This uncertainty affected the modelling strategies adopted by the teams. The Enviros team opted to consider only the fraction of Am and Th that is transported in solution in their modelling of run#31 (they did not model Pu). Enviros did, however, model bentonite colloid facilitated transport in run #32. The FKZ-INE team chose not to model the transport of sorbing tracers in run #31 at all, and concentrated their efforts on run #32. PSI made predictions of Am and Pu breakthrough assuming these tracers would be conveyed as aqueous solutes (these predictions were made in advance of run #31, before it was suggested that these tracers may be conveyed partly as colloids). JNC, however, chose to disregard the possibility of colloid-facilitated tracer transport in their modelling of run #31.

The Enviros model results indicated that Am and Th transported in solution in run #31 does not attain the detection limits. In the case of run #32, their predictions, made on the basis of laboratory data for tracer sorption on colloids and on fault gouge, showed significantly differences to the measured breakthrough curves, with more retarded and broadened break-through. This suggests that, in the model, there is too much sorption of the tracers with fault gouge, and too little on colloids. An improved match to the experimental breakthrough of Am and Th could be obtained by arbitrarily reducing the assumed specific surface area available for sorption on fault gouge (this is a particularly uncertain model parameter). Am and Th were then transported almost entirely in association with colloids, consistent with the shape of the breakthrough curves. The problem then is that U is also predicted to be transported almost entirely in

association with colloids, and this is not consistent with observations. The problem can be avoided by individually calibrating (and in so doing increasing) the surface complexation constants for the sorption reactions of tracers on colloids instead of specific surface area available for sorption, but it is acknowledged that there is no theoretical justification for so doing, especially if at the same time the corresponding constants for sorption in infill are left unchanged.

The JNC modelling team fitted the Am breakthrough curve for run #31 using both the STAMMT-L and COLFRAC models, assuming this tracer to be transported entirely as a solute. They were able to obtain a good fit by adjusting the sorption parameters for Am in the STAMMT_L model, but the sorption coefficient obtained (1.4×10^{-3} m^3 kg^{-1}) was more than an order of magnitude smaller than that obtained from laboratory tests (4.6×10^{-2} m^3 kg^{-1}; Möri 2001). JNC suggested that this inconsistency might be due to non-equilibrium sorption, as accounted for in the COLFRAC model. Inverse modelling using COLFRAC, however, suggested timescale for sorption onto fracture surfaces[12] of more than 10^7 s (the experimental duration was less than 10^5 seconds) and no sorption on matrix pore surfaces, suggesting that, if the model assumptions are correct, Am in solution effectively does not sorb onto solid surfaces over the timescale of the experiment. This is, however, inconsistent with the findings of laboratory sorption tests.

The JNC modelling team also fitted the Am breakthrough curve for run #32 using the COLFRAC model by adjusting the parameters for sorption of Am on colloids and for colloid filtration until a best fit was found, with parameters for matrix diffusion and Am sorption taken from the modelling of run #31, in spite of the inconsistencies noted above. Very large uncertainties were identified in the best fit value for the filtration coefficient λ (Eq. 3-5), and the value of this parameter extracted from Am breakthrough was inconsistent with the values obtained for Np and U breakthrough in the same experimental run (although these were also subject to very large uncertainties, possibly because of the small Np and U colloid bound fractions - see the discussion of Np and U transport, below), once again suggesting a problem with the underlying model assumptions.

The PSI modelling team predicted Am and Pu breakthrough in advance of runs #31 and #32 based on the colloid bound fractions derived from sorption measurements made in advance of the main runs. PSI used the 1-D advection-dispersion model for the fraction of the Am and Pu assumed to be transported in solution, and the non-Fickian dispersion model for the fraction assumed to be transported in association with colloids. Predictions and measured data for Am are shown in Figure 3.4.

In the case of run #32, the breakthrough curves were predicted well. Both predictions and measurements show a change in slope of the curves between 3 and 4 hours after injection, reflecting a change from colloid facilitated transport as the dominant mechanism at earlier times to transport in solution, retarded by matrix diffusion and sorption on matrix pore surfaces. The slope of the breakthrough curve at later times is proportional to $t^{-3/2}$, which is a signature of matrix diffusion. By contrast, the predictions for run #31, made on the basis that Am and Pu were transported as solutes and retarded by matrix diffusion and sorption on matrix pore surfaces, were significantly different to the measured breakthrough curves, and show a far more retarded and broadened breakthrough than that actually observed.

---

[12] This timescale is $1/(\beta_a K_a \rho_g)$ in the notation of the report of the JNC model. The fitted timescale for Am desorption ($1/\beta_a$) is even longer - about 10^{10} seconds, but with very large uncertainty.

These model findings are consistent with the suggestion that Am and Pu and Th were transported in colloidal form even in the absence of bentonite colloids in the injection cocktail, and not in aqueous solution as assumed in the JNC and PSI models. The difficultly in predicting breakthrough in run #32 using an equilibrium model suggests that sorption on colloids may be effectively irreversible over the timescale of the experiments.

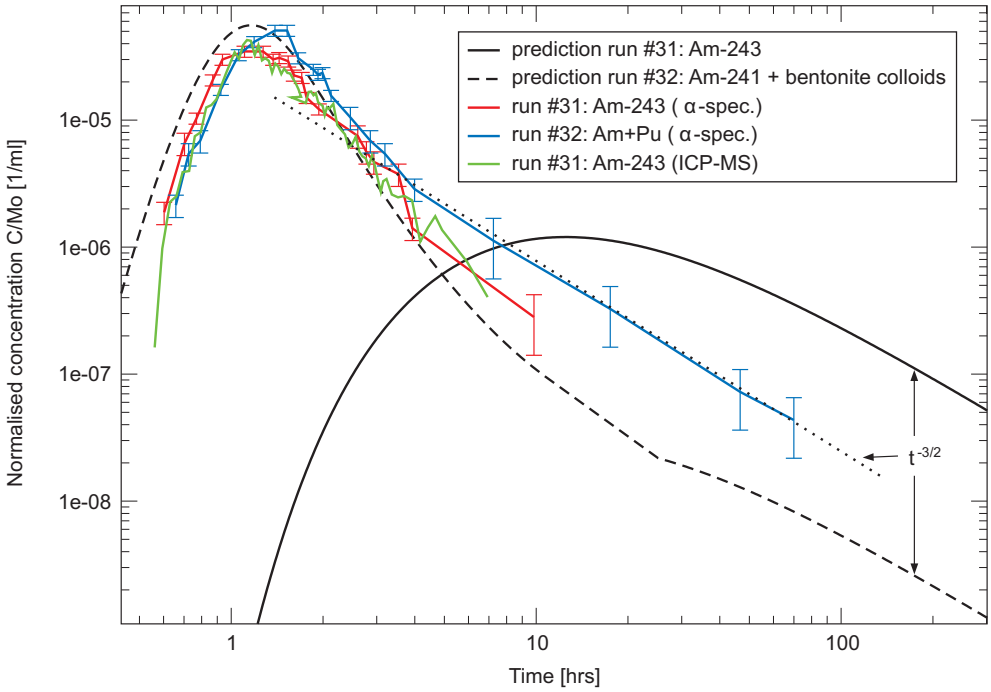

Fig. 3.4: PSI predictions (black full and dashed lines) and measured data (coloured lines) for Am breakthrough in runs #31 and #32

Transport of Np and U

Laboratory sorption studies suggest much lower association of Np and U with bentonite colloids in run #32 than is the case for Am, Pu and Th. Np and U were calculated to have - 9 % and 2 % colloid bound fractions, respectively, on the basis of sorption measurements made in advance of the main runs. Somewhat different, but still low values, of 0-1 % and 6 % were obtained from the direct analysis of the injection cocktails. Like Am, Pu and Th, the shapes of the breakthrough curves for Np and U are almost identical in shape in runs #31 and #32, when normalised to 100 % recovery. Np and U breakthrough, however, displays a more prolonged tailing than that displayed by Am, suggesting that additional retardation processes affect Np and U (Fig. 3.5). If a part at least of the injected Np and U is transported as an aqueous solute, then this addition process is likely to be matrix diffusion with sorption on matrix pore surfaces. The influence of matrix diffusion is suggested by the characteristic $t^{-3/2}$ long-term tailing of the breakthrough curves (Tsang 1995; Heer & Hadermann 1996). All of the teams that modelled run #31 considered only aqueous phase transport of these tracers. Colloid facilitated transport of Np and U[13] was considered only in run #32.

[13] Enviros also considered the breakthrough of Tc in run #32, which laboratory studies also indicate to have a low colloid bound fraction

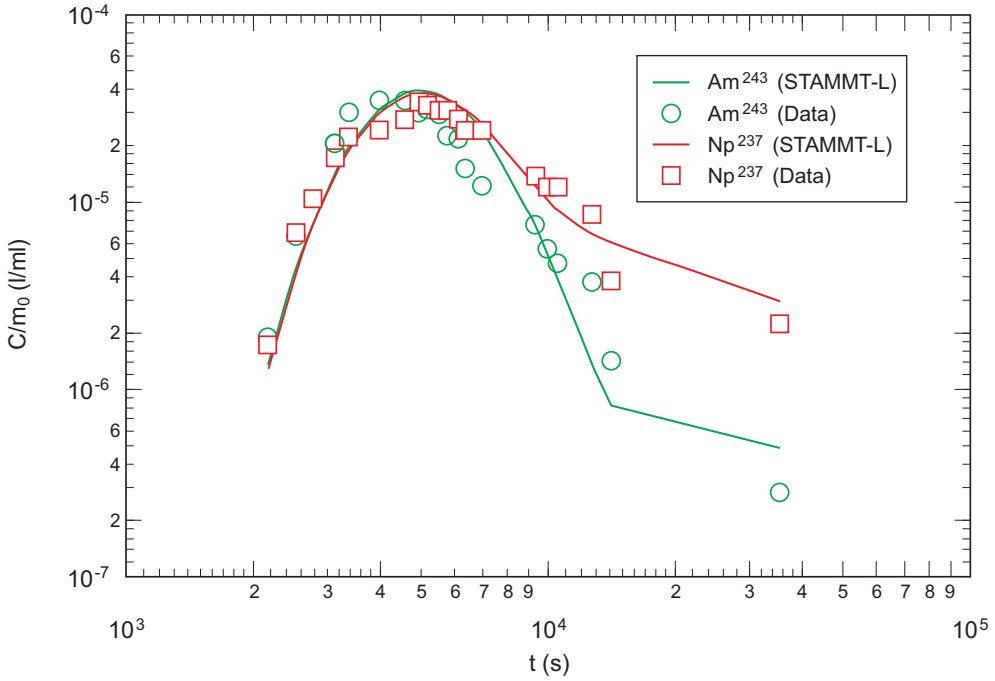

Fig. 3.5: Am and Np breakthrough in run #31, with the best fits obtained using the JNC STAMML-T model

Modelling results from Enviros indicated that the breakthrough of U transported in solution in run #31, assuming laboratory determined sorption parameters, only approaches the detection limit at the latest times measured, and so does not account for the major part of the breakthrough curve. The Enviros team did not model Np. For run #32, as mentioned previously, the breakthrough curve for U can be approximately reproduced using the Enviros model, but only by individually calibrating the surface complexation constants for the sorption reactions of tracers on colloids.

The FKZ-INE team again concentrated their efforts on run #32. They modelled the breakthrough of Np and U in run #32 assuming them to be transported 50 % unretarded and 50 % retarded, and obtained a reasonable fit of the breakthrough curves of these tracers by fitting a retardation factor for solute transport to account for sorption on fault gouge. It is not explicitly stated in Appendix A1.2 that the unretarded fraction is associated with colloids. Although this is one possible interpretation of the assumption of an unretarded fraction, the assumed distribution between solutes and colloids would be inconsistent with the laboratory measurements mentioned above.

The JNC modelling team fitted the Np breakthrough curve for run #31 using both the STAMMT-L and COLFRAC models. They were able to obtain a good fit by adjusting the sorption parameters for Np in the STAMMT_L model (Fig. 3.5), but the sorption coefficient obtained (8×10^{-5} m^3 kg^{-1}) was, as in their modelling of Am, more than an order of magnitude smaller than that obtained from laboratory tests (10^{-3} m^3 kg^{-1}; Möri 2001). Again, COLFRAC modelling suggested that sorption on fracture surfaces and on matrix pore surfaces is effectively absent, at least over the timescale of the experiment.

The JNC modelling team fitted the Np and U breakthrough curves for run #32 using the COLFRAC model by adjusting the parameters for sorption of U on solid surfaces (U breakthrough in run #31 was not modelled), for sorption of Np and U on colloids and for colloid

filtration, until a best fit was found. Unfortunately, these best-fit breakthrough curves poorly matched the experimental breakthrough. The disparity between modelled and experimental breakthrough curves was such that uncertainties in the fitted parameters for U could not be estimated. Large uncertainties were identified in the best fit value for the filtration coefficient extracted from Np breakthrough, and, as mentioned in the discussion of COLFRAC modelling in the previous section, values of this parameter obtained for Am, Np and U breakthrough were inconsistent.

The PSI modelling team predicted Np and U breakthrough in advance of runs #31 and #32 based on laboratory determined sorption parameters and, in the case of run #32, colloid bound fractions. Np breakthrough was predicted well for both runs (Fig. 3.6), but a greater discrepancy was found between predictions and measurements for U (Fig. 3.7), which was attributed by PSI to the overestimation of U sorption on matrix pore surfaces.

Overall, the breakthrough of Np and U in runs #31 and #32 can be fitted well on the assumption that these tracers are transported mainly as solutes in both runs, with retardation by sorption and matrix diffusion, although there are indications that, if these are the main transport mechanisms, the sorption of U and possibly Np is less than expected on the basis of laboratory measurements. Alternatively, the results of Enviros (and a possible interpretation of the FZK-INE model and results if the unretarded fraction is taken to be associated with colloids) suggest that colloid facilitated transport might contribute to shapes of the curves in run #32, but in this case a degree of association of solutes with colloids is higher than expected on the basis of laboratory studies. The similarity between runs #31 and #32 is also difficult to explain in this case, since colloid-facilitated transport would not be expected to play role in run #31, where bentonite colloids are absent (but see the comments on the recent laboratory results above).

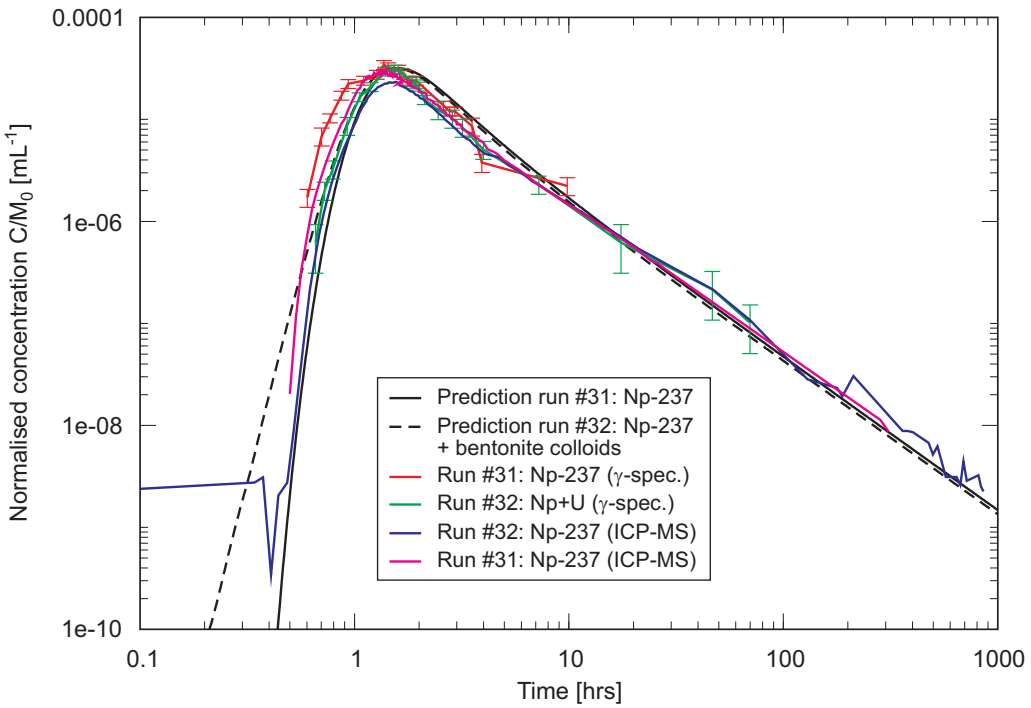

Fig. 3.6: PSI predictions (black full and dashed lines) and measured data (coloured lines) for Np breakthrough in runs #31 and #32

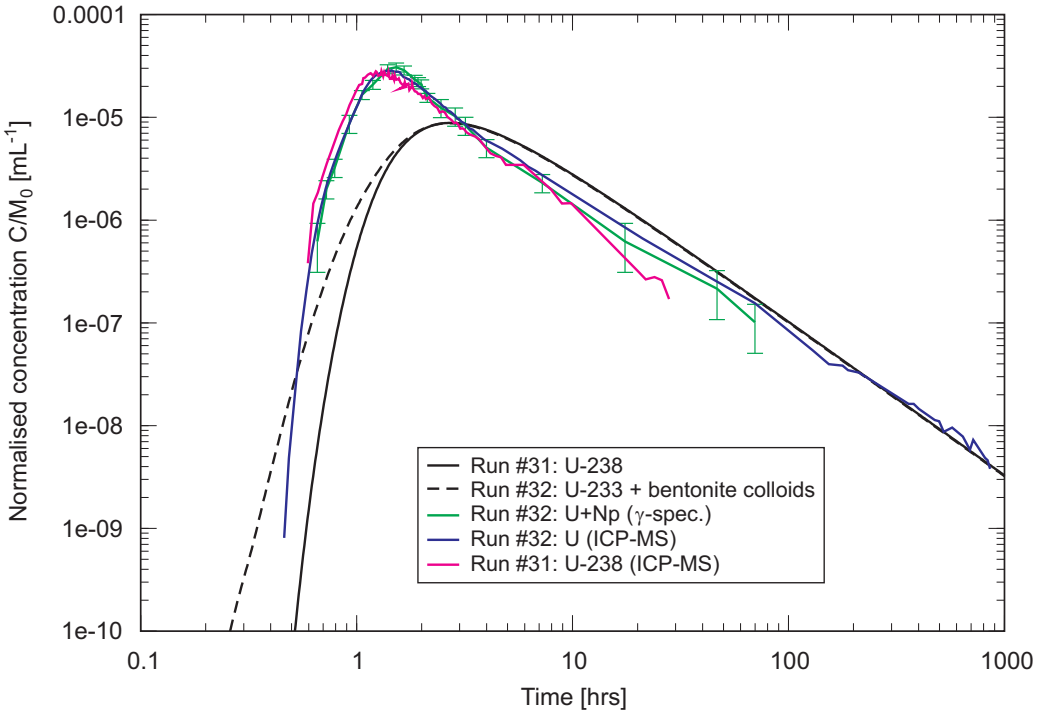

Fig. 3.7: PSI predictions (black full and dashed lines) and measured data (coloured lines) for U breakthrough in runs #31 and #32

Transport of Cs

The PSI modelling team predicted Cs breakthrough in advance of run #32 (Cs was not used in the injection cocktail for run #31) based on a colloid bound fraction for Cs measured in advance of the run, which was found to be intermediate between the high values for Am, Pu and Th and the low values for Np and U. The predictions showed two peaks, the first corresponding to colloid-bound Cs, and the second to Cs in aqueous solution, retarded by matrix diffusion and sorption on matrix pore surfaces. The predictions were qualitatively successful. Quantitative discrepancies were attributed by PSI to possible desorption of Cs from colloids during transport, to inaccuracy in the assumed initial colloid-bound fraction, and to the non-linearity of Cs sorption, which was neglected in the model.

4 Discussion and conclusions

This chapter provides a discussion of transport modelling issues, a summary of key findings and conclusions.

4.1 Modelling strategy

The strategy applied by the modelling teams was, in all cases, to use inverse modelling to obtain some or all of the parameter values required to model the main runs, complemented in some cases with laboratory data. The strategy employed by the PSI team was perhaps the most systematic and successful in terms of the information it yielded (though not in all cases in terms of the accuracy of the fits or predictions). It consisted of:

(i) employing inverse modelling to the breakthrough curves from preliminary experiments carried out prior to the main runs

(ii) using fitted parameters describing the material and transport properties of the dipole, together with laboratory sorption data and data on injection concentrations, to make predictions of the breakthrough curves for the main runs, in advance of the runs being carried out

(iii) modifying the models or their parameter values as necessary in the light of the comparison between model predictions and experimental predictions.

In addition to providing parameters for step (ii), step (i) provided a first test of the applicability of the chosen models by an assessment of the quality of the fits and of the plausibility of the parameters values obtained by the fitting procedure. Step (ii) assisted in the planning of the main runs by indicating whether it would be possible to detect the breakthrough of the different radionuclides with the combination of planned input concentrations and given detection limits. It also provided a rigorous test of the hypotheses built into the models by comparing the actual breakthrough data from the main runs with the predicted curves.

4.2 Transport and retention processes

The four modelling teams worked largely independently and each developed one or more alternative conceptual models that differ from each other in some fundamental aspects - particularly in their treatment of radionuclide association with colloids. The modelling studies thus addressed issues of conceptual model uncertainty. On some occasions at least, the modelling groups made predictions in advance of experiments being carried out. These both assisted in the planning of the experiments and allowed the predictive capability of the model to be tested without the danger of bias from foreknowledge of the experimental results (cf. Pate et al. 1994). The success of some modelling approaches (and, equally importantly, the difficulties of others) in predicting the experimental results enabled a number of conclusions to be drawn regarding the radionuclide transport in the CRR *in situ* tests.

4.2.1 The flow field

The success of the 1-D JNC STAMMT-L model in reproducing conservative tracer breakthrough in run #31 model, and the similarity in the results obtained with the PSI 1-D and 2-D advection-dispersion models suggest that tracer transport and breakthrough can be adequately treated with advection and dispersion modelled as one-dimensional processes along

line between the injection and withdrawal wells. This is consistent with the expected narrowness of the dipole flow field, given the asymmetric injection and withdrawal rates. The assumption that this line is a direct one, as assumed by all the modelling teams, is more difficult to support. Given the highly heterogeneous transmissivity distribution in the shear zone (Fig. 2.1), the transport paths from the injection borehole to the withdrawal borehole may well be tortuous and significantly longer on average than assumed in the models. The form of the transport paths cannot, however, be inferred on the basis of the breakthrough curves, and any increase in mean transport path length due to the hydraulic heterogeneity of the shear zone may well be compensated for by variations in other model parameters.

4.2.2 Dispersion and matrix diffusion

As tracers migrate through the shear zone, spreading of the injected pulse occurs, giving rise to relatively broad breakthrough curves with long tails. In the case of tracers transported as solutes, the JNC and PSI models attribute this tailing to a combination of matrix diffusion, retarded, in the case of sorbing tracers, by sorption on matrix pore surfaces, and hydrodynamic dispersion. For conservative tracer transport, there was some difficultly in distinguishing the effects of these two processes; the JNC COLFRAC model in particular attributes much of the spreading to dispersion resulting from the fracture network, whereas matrix diffusion is important in the other models. For the transport of sorbing tracers, such as Np and U (and also Sr), the influence of matrix diffusion is suggested by the characteristic $t^{-3/2}$ long-time tailing of the breakthrough curves. The Enviros and FZK-INE models do not include matrix diffusion, and do not reproduce this long-term tailing accurately.

The fact that advection-dispersion models with matrix diffusion are adequate for modelling the breakthrough of conservative tracers and several sorbing tracers confirms the findings of the earlier MI modelling studies (see Smith et al. 2001, for an overview).

Colloids (and tracers associated with then) are advected with little or no retardation during transport in the CRR runs - there is a marked similarity between the breakthrough of colloids and that of a conservative tracer, although the peak breakthrough for colloids occurs slightly earlier. This difference may be attributed, at least in part, to the absence of matrix diffusion in the case of colloids. The assumption that colloids do not undergo matrix diffusion is supported by the observation that, when normalised to 100 % recovery, the breakthrough curves for colloids of different sizes coincide closely with each other (Section 2.6). Diffusion coefficients are sensitive to colloid size, and thus any tailing due to matrix diffusion would also be expected to show a variation with colloid size. The PSI modelling team attempted to model colloid breakthrough curves using a Fickian dispersion model with matrix diffusion (the 1-D advection-dispersion model), but were unable to do so unless an unrealistically large value for colloid diffusivity in the matrix was used (see Kosakowski 2004, for details).

Although colloid breakthrough (or the breakthrough of tracers associated with colloids) can be modelled approximately using advection-dispersion models based on a Fickian representation of dispersion, a good fit between model and experiment appears to require a non-Fickian model of dispersion (Kosakowski 2004). Non-Fickian dispersion generally reflects a high degree of heterogeneity in the transport paths, although the effects of the parabolic velocity profiles across individual fractures, which may be different for colloids compared to solutes, may also give rise to non-Fickian spreading. In particular, individual colloids, unlike solutes, may not diffuse across, and thus sample, the entire velocity profile during transport because of their lower diffusion coefficients. In addition, the physical size of colloids and charge effects may prevent them from approaching close to the fracture walls, although this would be expected to result in earlier breakthrough for the largest colloids, which was not observed in CRR. Both the PSI non-

Fickian dispersion model and the JNC COLFRAC model, which models the shear zone as a network of orthogonal fractures, can account for dispersion that is not necessarily described by Fick's laws.

The possibility of non-Fickian dispersion due to heterogeneity also applies to tracers transported as solutes, although the $t^{-3/2}$ tailing mentioned above indicates that, if it occurs, it does so in addition to matrix diffusion. In CRR it has not been possible to distinguish non-Fickian dispersion effects from the effects of matrix diffusion for the transport of solutes.

The identification of non-Fickian dispersion resulting from heterogeneity within the shear zone as a significant process affecting colloid transport also has implications for the modelling of transport of the aqueous phase. At least some of the tailing of breakthrough curves of conservative tracers that had, for example in the MI experiment, been attributed to matrix diffusion could in fact be the result of non-Fickian dispersion. This has implications for the derivation of matrix diffusion parameters for safety assessment from the results of *in situ* radionuclide migration experiments, as discussed in Section 4.4.

4.2.3 Association of radionuclides with colloids

Even though Am, Pu and Th appear to be transported in colloidal form, even when no colloids were added to the injection cocktail, an examination of tracer recovery in run #32 compared to run #31 shows that the addition of bentonite colloids does increase the *recovery* of these tracers. This suggests that the colloid-bound fraction increases with the addition of bentonite colloids. Because of the strong sorption of these tracers on fault gouge, any fraction not bound to colloids is highly retarded during transport, and is apparent only in the latest parts of the tails of the breakthrough curves.

The short groundwater travel time between the injection and withdrawal wells of the dipole flow field suggests that assumptions other than equilibrium sorption may be appropriate for modelling sorption of tracers on solid surfaces and the association of tracers with colloids. This is further indicated by the apparent inapplicability of an equilibrium sorption approach in modelling the association of sorbing tracers with colloids, with sorption parameters taken from laboratory experiments.

4.2.4 Colloid filtration

Colloids are mobile in the fluid phase, but they can be immobilised as a result of processes that include mechanical filtration, sedimentation (gravitational settling), and electrochemical filtration. Filtration is included explicitly only in JNC's COLFRAC model, but the modelling team were unable to obtain a consistent value for the filtration coefficient. Some inferences can, however, be tentatively made on the basis of the observed breakthrough curves. In particular, unlike electrochemical filtration, gravitational settling and mechanical filtration have a greater effect on larger colloids, and their occurrence in CRR would be consistent with the observation that colloid recovery decreases with increasing colloid size. There is also no evidence from batch sorption experiments for any chemical interaction between bentonite colloids and fracture infill or wallrock materials. In addition, the fact that the peak of the breakthrough curves of tracers associated with colloids are not retarded with respect to a conservative tracer suggests that immobilisation is irreversible over the timescale of the CRR experiments.

Colloid filtration could only be observed in run # 6a and #7a and there only for the larger sized colloid fraction. Clay colloids injected during run #32 were smaller and colloid mass recoveries were significantly higher pointing to the absence of significant colloid filtration in this experiment.

4.3 Impact of experimental artefacts

In applying the models, it has been generally assumed that measured breakthrough data is a faithful record of shear zone response and that any artefacts associated with the testing procedure are negligible. In reality, during the tracer tests, the tracer was not injected as an ideal step function, but was rather introduced with significant tailing. In such a case, the observed breakthrough will be influenced by this experimental artefact. The injection device used for the CRR tracer tests was equipped with a sensor for measuring the uranine concentration in the injection borehole. A typical injection function (uranine input) is shown in Figure 4.1. The duration of the injection tail is much less than the breakthrough tails of the tracers (see the examples of uranine and Sr in Figure 4.1, noting the logarithmic time scale). Furthermore, a sensitivity study carried out by PSI with the non-Fickian dispersion and with the advection-dispersion models revealed that the tailing of the measured injection function has a negligible impact on the tailing of the breakthrough of conservative and sorbing tracers.

A potentially greater problem is the production of homogenous radiocolloids during tracer preparation and the full implications of this are still under study in the CRR follow-on study at the GTS, the CFM (Colloid Formation and Migration; see www.grimsel.com) experiment.

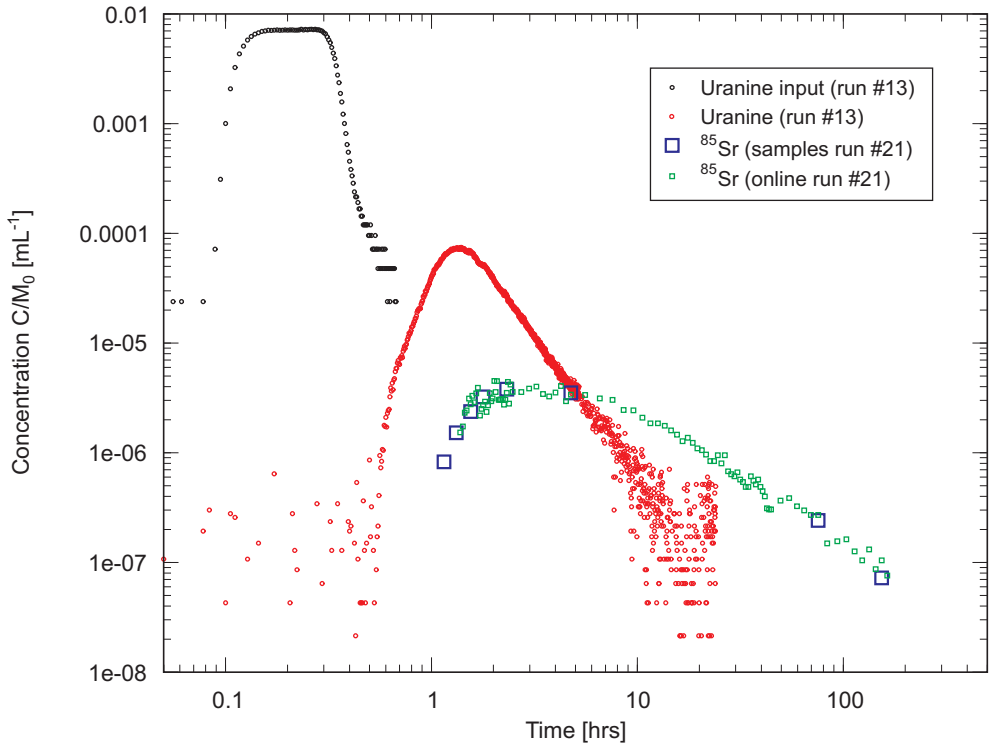

Fig. 4.1: A typical injection function for uranine, as well as uranine and Sr breakthrough in dipole 1

4.4 Summary of key findings and conclusions

The models investigated by different teams incorporated a range of alternative model assumptions, the most significant perhaps being treatment of the interaction of solutes with colloids, which is treated alternatively as being an equilibrium processes, a non-equilibrium process with first-order sorption kinetics and an irreversible process. This is also the range of assumptions for solute-colloid interactions used in colloid-facilitated transport modelling in recent safety assessments (Appendix 2).

All the modelling teams obtained at least some parameters by inverse modelling of either preliminary field experiments carried out in advance of the main runs, or the main runs themselves. Although agreement between fitted curves and experimental breakthrough curves and plausibility and self-consistency of the fitted parameters provides some test of the applied models, it is certainly not as convincing a test as the ideal situation, where all model parameters are fixed in advance on the basis of independent measurements (see discussion in Pate et al. 1994).

An important point to note is that *at least as much has been learnt from the failure of certain models to predict or fit experimental results as from successful models*. Thus, poor predictions and fits, as well as more successful ones, have been discussed in this report.

The CRR experiment and the modelling work indicate that, in the main experimental run #32 with bentonite colloids added to the injection cocktail:

- Am, Pu and Th are transported principally in association with colloids
- Cs is also transported in part in association with colloids, although the main part of the injected inventory is transported in solution

Furthermore, some radionuclide tracers, namely Am, Pu, and Th (and also Tb and Hf) are transported in colloidal form, even when no bentonite colloids are added to the injection cocktail (run #31). The addition of bentonite colloids, however, increases the recovery of these tracers. Laboratory experiments, however, demonstrated that colloidal species are of minor relevance for Np(V) and U(VI).

The role of colloids in the transport of Np and U in the two main runs was not unambiguously determined.

Modelling results provide evidence for:

- the occurrence of matrix diffusion (and the insignificance of advection/dispersion in the matrix) for tracers transported as solutes
- the exclusion of colloids from the pores of the rock matrix adjacent to shear zone fractures
- the non-Fickian dispersion of colloids (and tracers associated with colloids), and, potentially at least, the non-Fickian dispersion of solutes
- the inapplicability of an equilibrium sorption approach (using sorption parameters based on laboratory experiments) in modelling the association of sorbing tracers with colloids

It is possible that the association of these tracers with colloids is effectively irreversible, or only partly reversible, on the timescale of the experiments.

A problem encountered especially by the PSI and JNC modelling teams was uncertainties, or non-uniqueness, in the fitted model parameters. The JNC team carried out inverse modelling using the code PEST, which estimates these uncertainties. In some cases, the magnitude of the

uncertainties greatly exceeded the magnitude of the best-fit parameter. This problem is related to the sometimes large number of parameters that were calibrated in this way, the lack of constraints from independent observations (e.g. observations that could constrain the way in which shear zone structure is modelled), the subtle or negligible effects that some processes may have had on tracer breakthrough (such as advection in the rock matrix), and the limited duration and accuracy of the experiment.

The suggestion that non-Fickian dispersion may be significant for the transport not only of colloids, but also of aqueous solutes, and the difficulty in separating non-Fickian dispersion effects from the effects of matrix diffusion implies that matrix diffusion and sorption parameters for safety assessment derived by inverse modelling of breakthrough curves using a model based on Fickian dispersion have to be viewed with caution.

All the models applied in CRR are highly simplified representations of reality, and may only be applicable, or "valid", over the spatial and temporal scales of the CRR experiments, and conclusions drawn from the modelling work may not necessarily hold over the far larger spatial and longer temporal scales of interest in repository safety assessment. The results do, however, suggest that the issue of slow sorption/desorption kinetics and the possibility of effective irreversibility of sorption of tracers on colloids deserves further study in longer-term experiments such as CFM.

On the basis of this discussion, the following recommendations are made for future experiments and modelling studies:

- The experience from run #31, where some tracers appear to have been transported in colloidal form even in the absence of bentonite colloids, suggests that, in future studies, more attention should be paid to other ways, in which colloid-facilitated transport can arise, including, for example, the impact of natural groundwater colloids and experimental artefacts.
- The non-uniqueness of fitting encountered in the inverse modelling carried out for CRR suggests that, in future studies, a more formal approach might be needed with perhaps ranges of plausible parameter values discussed and agreed in advance of inverse modelling being carried out - fitted parameters found to lie outside these ranges would indicate either a bias in the estimation of ranges or a problem with the model.
- A greater emphasis should be placed on encouraging "blind predictions" (Pate et al. 1994) in advance of experiments being carried out, using, as far as possible, data from independent experiments to calibrate models.
- Tests covering larger spatial and longer temporal scales would be valuable to assess whether the findings of CRR regarding colloid filtration, for example, remain valid over such scales.

5 References

Alexander W. R., Frieg B., Ota K. & Bossart P. (1996). The RRP Project: Investigating Radionuclide Retardation in the Host Rock. Nagra Bulletin No. 27 (June, 1996), pp43-55.

Alexander W. R., Smith P. A. & McKinley I. G. (2003). Modelling radionuclide transport in the geological environment: a case study from the field of radioactive waste disposal. Ch.5 *in* E.M.Scott (ed.), Modelling Radioactivity in the Environment, Elsevier, Amsterdam, The Netherlands.

ADINA (2001). ADINA (Automatic Dynamic Incremental Nonlinear Analysis) R & D Inc., Report ARD 01-9, Watertown, MA, USA.

Baeyens B., Maes A. & Cremers A. (1985). *In situ* Physico-chemical Characterization of Boom Clay; Radioactive Waste Management and the Nuclear Fuel Cycle; 6, p. 391.

Barten W. (1996). Linear Response Concept Combining Advection and Limited Rock Matrix Diffusion in a Fracture Network Transport Model. Water Resources Research 32(11), pp. 3285-3296.

Barten W. & Robinson P. C. (2001). Contaminant Transport in Fracture Networks with Heterogeneous Rock Matrices: The PICNIC code. PSI Report 01-02, Paul Scherrer Institut, Villigen, Switzerland.

Bathe K. J. (1996). Finite Element Procedures, Prentice-Hall, Englewood Cliffs, NJ, USA.

Berkowitz B., Kosakowski G., Margolin G. & Scher H. (2001). Application of Continuous Time Random Walk theory to Tracer Test Measurements in Fractured and Heterogeneous Porous Media, Ground Water, 39(4), pp. 593-604.

Berkowitz B. & Scher H. (1995). On Characterization of Anomalous Dispersion in Porous and Fractured media, Water Resources Research, 31(6), pp. 1461-1466.

Biggin C., Möri A., Alexander W. R., Ota K., Frieg B., Kickmaier W. & McKinley I. G. (2002). *In situ* Radionuclide Retardation in Groundwater Conducting Systems: Overview of the Research Carried out at Nagra's Grimsel Test site, Central Switzerland. Proceedings 9th International Symposium on Environmental Radiochemical Analysis, September 2002, Kent.

Bossart P. & Mazurek M. (1991). Grimsel Test Site: Structural geology and water flow-paths in the migration shear zone. Nagra Technical Report 91-12, Nagra, Wettingen, Switzerland.

Dierckx A., Put M., De Cannière P., Wang L., Maes N., Aertsens M., Maes A., Vanccluysen J., Verdickt W., Gielen R., Christiaens M., Warwick P., Hall A. & Van der Lee J. (2000). Transport of Radionuclides due to Complexation with Organic Matter in Clay Formations - TRANCOM-Clay. EUR19135EN, Final Report Nuclear Science and Technology, European Commission, Brussells, Belgium.

Dodds J. (1982). La Chromatographie Hydrodynamique. Analysis, Vol. 10, pp. 109-119.

Doherty J. (2002). http://www.epa.gov/ceampubl/mmedia/pest/PESTMAN.PDF.

Fierz Th., Geckeis H., Götz R., Geyer F. W. & Möri A. (ed.) (2001). GTS V/CRR: Tracer tests #1 - #16 (September 1999 – January 2001). Unpublished Nagra Internal Report. Nagra, Wettingen, Switzerland.

Frick U., Alexander W. R., Baeyens B., Bossart P., Bradbury M. H., Bühler Ch., Eikenberg J., Fierz Th., Heer W., Hoehn E., McKinley I. G. & Smith P. A. (1992). Grimsel Test Site – The Radionuclide Migration Experiment: Overview of investigations 1985-1990. Nagra Technical Report NTB 91-04, National Cooperative for the Disposal of Radioactive Waste, Wettingen, Switzerland.

Fisch H. R. (2002). Task 5a: Hydraulic testing in the boreholes BOCR 99.002 and BOCR 00.003. Unpublished Nagra Internal Report, Nagra, Wettingen, Switzerland.

Gardiner M. P., Grindrod P. & Moulin V. (2001). The Role of Colloids in theTransport of Radionuclides from a Radioactive Waste Repository: Implication on Safety Assessment. Final Project Report EUR 19781, European Commission, Brussels, Belgium.

Geckeis H., Hauser W., Geyer F. W., Götz R., Schäfer Th., Fierz Th., Alexander W. R. & Möri A. (eds.) (2003a). GTS V/CRR: Preparatory tracer tests with bentonite colloids, homologues, Br-82 and Sr-85. Unpublished Nagra Internal Report. Nagra, Wettingen, Switzerland.

Geckeis H., Geyer F. W., Hauser W., Marquardt C. M., Schäfer TH., Eikenber J., Fierz Th. & Möri A. (eds.) (2003b). GTS V/CRR: Tracer tests #28 - #35 (January – March 2002); raw data report. Unpublished Nagra Internal Report, Nagra, Wettingen, Switzerland.

Geckeis H., Schäfer T., Hauser W., Rabung Th., Missana T., Degueldre C., Möri A., Eikenberg J., Fierz Th., & Alexander W. R. (2004): Results of the colloid and radionuclide retention experiment (CRR) at the Grimsel Test Site (GTS), Switzerland – impact of reaction kinetics and speciation on radionuclide migration, Radiochim. Acta 92, 765–774.

Guimerà J., Duro L. & Bruno J. (2000). Radionuclide field tests in a single fracture. Proc. Int. Conf. on tracers and modelling in hydrogeology; Liège, Belgium (Dassargues, Ed); IAHS Pub. 262, 309-314.

Hadermann J. (2001). Colloid-related Retention Processes. Conclusions of Working Group 3. In: Radionuclide Retention in Geologic Media, Workshop Proceedings, Oskarshamn, Swden, 7-9 May 2001, OECD/NEA, Paris, France.

Haggerty R. & Gorelick S. M. (1995). Multiple-rate Mass Transfer for Modeling Diffusion and Surface Reactions in Media with Pore-scale Heterogeneity, Water Resour. Res., 31(10), pp. 2383–2400.

Hauser W., Geckeis H., Kim J.I. & Fierz Th. (2002). A Mobile Laser-induced Breakdown Detection System and its Application for the *in situ* Monitoring of Colloid Migration. Colloids and Surfaces A: Physicochemical and Engineering Aspects; 203, pp. 37-45.

Heer W. & Hadermann J. (1996). Modelling Radionuclide Migration Field Experiments. PSI Report 94-13, Paul Scherrer Institut, Villigen, Switzerland, Nagra Technical Report 94-18, Nagra, Wettingen, Switzerland.

Ibaraki M. and Sudicky E. A. (1995a). Colloid-facilitated Contaminant Transport in Discretely Fractured Porous Media 1. Numerical Formulation and Sensitivity Analysis, Water Resour. Res., 31(12), pp. 2945-2960.

Ibaraki M. and Sudicky E. A. (1995b). Colloid-facilitated Contaminant Transport in Discretely Fractured Porous Media 2. Fracture Network Examples, Water Resour. Res., 31(12), pp. 2961-2969.

James S. C. and Chrysikopoulos C. V. (1999). Transport of Polydisperse Colloid Suspensions in a Single Fracture, Water Resources Research, 35(3), pp. 707-718.

JNC (2000). H12 Project to Establish Technical Basis for HLW Disposal in Japan, Project Overview Report and three Supporting Reports. JNC TN1410 2000-001 ~ 004, JAEA, Tokai, Japan.

Kersting A. B., Efurt D. W., Finnegan D. L., Rokop D. J., Smith D. K. & Thompson J. L. (1999). Migration of Plutonium in Groundwater at the Nevada Test Site, Nature, 397: pp. 56-59.

Kolditz O., Habbar D., Kaiser R., Rother T. & Thorenz C. (1999). RockFlow - Theory and Users Manual. Release 3.4, Institut für Strömungsmechanik und Elektr. Rechnen im Bauwesen, University of Hanover, Germany.

Kosakowski G. (2004). Anomalous Transport of Colloids and Solutes in a Shear Zone. Journal of Contaminant Hydrology, 72, 23-46.

Kosakowski G. & Smith P. A. (2004). Modelling the Transport of Solutes and Colloids in a Water Conducting Shear Zone in the Grimsel Test Site. Nagra Technical Report NTB 04-01. Nagra, Wettingen, Switzerland.

Meier P. M. (1999). Estimation of representative groundwater flow and solute transport parameters in heterogeneous formations. Ph.D. dissertation, School of Civil Engineering, Barcelona.

Miller W. M., Alexander W. R., Chapman N. A., McKinley I. G. &Smellie J. A. (2000). Geological Disposal of Radioactive Wastes and Natural Analogues. Waste Management Series, vol. 2, Pergamon, Amsterdam, The Netherlands.

Missana T. & Adel A. (2000). On the Applicability of DLVO Theory to the Prediction of Clay Colloids Stability. J. Coll. Interface Sci., 230, pp. 150-156.

Missana T., Alonso U. & Turrero M. J. (2003a). Generation and Stability of Bentonite Colloids at the Bentonite/Granite Interface of a Deep Geological Radioactive Waste Repository. Journal of Contaminant Hydrology 61 (1-4), 17-31.

Missana T., Garcia-Gutierrez M. & Alonso U. (2003b). Kinetics and Irreversibility of Caesium and Uranium Sorption onto Bentonite Colloids. Applied Clay Science, 26 (2004) pp. 137-150.

Missana T., Garcia-Gutierrez M., Turrero M. J., Alonso U. & Mingarro M. (2003c): The role of colloids in the radionuclide transport in a deep geological repository. Technical Report 05/2003, Enresa (empresa nacional de residuos radiactivos, s.a.), Madrid, Spain (2003).

Missana T. & Geckeis H. (2006) (eds.). The CRR final project report series II: Results of the Supporting Laboratory Programme. Nagra Technical Report NTB 03-02, Nagra, Wettingen, Switzerland

Möri A. (2001). GTS V - CRR Experiment: Scoping calculations, base data set V-3. Unpublished Nagra Internal Note, Nagra, Wettingen, Switzerland.

Möri A. (ed.) (2004). The CRR Final Project Report Series I: Description of the Field Phase-Methodologies and Raw data. Nagra Technical Report NTB 03-01, Nagra, Wettingen, Switzerland.

Möri A., Alexander W. R., Geckeis H., Hauser W., Schäfer Th., Eikenberg J., Fierz Th., Degueldre C. & Missana T. (2002). The Colloid and Radionuclide Retardation experiment (CRR) at the Grimsel Test Site (GTS): influence of bentonite colloids on radionuclide migration in a fractured rock. Colloids and Surfaces A: Physicochemical and Engineering Aspects; 217, pp. 33-47.

Möri A., Alexander W. R., Ota K. & Frieg B. (eds.) (2006). The Nagra-JNC *in situ* study of safety relevant radionuclide retardation in fractured crystalline rock III: the RRP project final report. Nagra Technical Report NTB 00-07 (*in prep*), Nagra, Wettingen, Switzerland.

Neretnieks I. & Ernstsson M.-L. (1997). A Note on Radionuclide Transport by Gas Bubbles. Materials Research Society Symposium Proceedings 467, pp. 855-862.

Pate S. M., McKinley I. G. and Alexander W. R. (1994). Use of natural analogue test cases to evaluate a new performance assessment TDB. CEC Report EUR15176EN, European Commission, Brussels, Belgium.

Prieve D. C. & Hoysan P. M. (1978). Role of Colloidal Forces in Hydrodynamic Chromatography. Journal of Colloid Interface Science, Vol. 64, No. 2, pp. 201-213.

Pudewills A., Hauser W., & Geckeis H. (2002). Numerical Modelling of Flow and Transport Phenomena in Fractured Crystalline Rock. Proceedings of 2nd Biot Conf.on Poromechanics, Grenoble, F, August 26-28, 2002, Eds. J.-L. Auriault et at., A.A. Balkema; pp. 527-532.

Schäfer T., Geckeis H., Bouby M. & Fanghänel T. (2004): U, Th, Eu and colloid mobility in a granite fracture under near-natural flow conditions, Radiochim. Acta 92, 731–737.

Smith P. A., Alexander W. R., Heer W., Fierz Th., Meier P. M., Baeyens B., Bradbury M. H., Mazurek M. & McKinley I. G., (2001). The Nagra-JNC *in situ* Study of Safety Relevant Radionuclide Retardation in Fractured Crystalline Rock I: Radionuclide Migration Experiment – Overview 1990-1996, Nagra Technical Report NTB 00-09, Nagra, Wettingen, Switzerland.

Tsang Y. W. (1995). Study of Alternative Tracer Tests in Characterizing Transport in Fractured Rocks. Geophysical Research Letters, 22(11), pp. 1421-1424.

Wan J. & Wilson J. L. (1994a). Visualization of the Role of the Gas-water Interface on the Fate and Transport of Colloids in Porous Media. Water Resources Research, 30, pp. 11- 23.

Wan J. & Wilson J. L. (1994b). Colloids Transport in Unsaturated Porous Media. Water Resources Research, 30, pp. 857- 864.

Witherspoon P. A., Wang J. S. Y., Iwai K. & Gale J. E. (1980). Validity of cubic law for fluid flow in a deformable rock fracture. Water Resources Research, 16(6), 1016-1024.

Appendix 1

Detailed description of the work of the CRR modelling teams

A1.1 PSI modelling report

Georg Kosakowski (PSI) & Paul Smith (SAM)

A1.1-1 Introduction

A1.1-1.1 Scope and purpose of the present work

The present document provides a summary of modelling work by the Paul Scherrer Institute (PSI) to analyse *in situ* experiments carried out at the Grimsel Test Site (GTS) within the framework of the Colloid and Radionuclide Retardation Project (CRR). A detailed description is given in Kosakowski (2004) and Kosakowski & Smith (2004). The modelling work takes as its starting point earlier modelling carried out by PSI in the context of the Migration Experiment (MI; see Frick et al. 1992, Smith et al. 2001a, b, for details), and develops and modifies the earlier models to take account of the effects of bentonite colloids added to the experimental injection cocktails. A number of alternative modelling approaches have been developed for some aspects of the system. In some cases, it was possible to make model predictions in advance of particular experimental runs in order to check the feasibility of the planned experiments and to test particular modelling hypotheses.

A1.1-1.2 Overview of the present report

Chapter A1.1-2 gives a description of the methodology adopted in the PSI modelling study. It describes three alternative models used to analyse and predict the results of the tracer tests, namely a 1-D advection-dispersion model, a 2-D advection-dispersion model, and a non-Fickian dispersion model: the CTRW (continuous time random walk) model. It describes assumptions and procedures that are common to all the models, as well as the distinguishing features of the three models. It identifies the computer codes that are used and, finally, the procedure used in applying the models to the analysis and prediction of the CRR tracer test results is explained.

Chapter A1.1-3 presents the results obtained using the models described in the previous chapter. It describes the fitting of the breakthrough curves of preliminary tests carried out in advance of the main CRR experimental runs, which shows that the 1-D and 2-D advection-dispersion models with matrix diffusion provide similarly good fits for tracers conveyed as aqueous species. Assuming, however, that colloids do not undergo matrix diffusion, the non-Fickian dispersion model is required in order to provide an adequate fit in the case of colloids. It also describes predictions of breakthrough for the main experimental runs, and suggests reasons for the discrepancies between predictions and measurements.

Chapter A1.1-4 presents a review of the model concepts and parameters used in the analyses and predictions of Chapter A1.1-3, in the light of the measured data from the main runs, and describes some modifications that improve agreement between theoretical and measured breakthrough curves. It describes some general observations that strongly suggest that part at least of the injected inventories migrates in association with colloids. It also discusses the specific influence of bentonite colloids on transport.

Chapter A1.1-5 describes the reasons why advective and hydrodynamic processes, as represented by the non-Fickian dispersion model, are the most likely explanation for the inability of the 1-D and 2-D advection dispersion models to fit colloid breakthrough adequately. Finally, evidence that supports the influence of non-Fickian dispersion on the tailing of colloid breakthrough curves is presented.

Chapter A1.1-6 describes some unresolved problems associated with the CRR experiment and discusses the limitations of the modelling approach as used in the present study. These include, (i), the counter-intuitive correlation between extraction flow rate and peak arrival time, which is currently unexplained, but is probably a result of the heterogeneous characteristics of the shear zone, (ii) the problem of non-uniqueness of the fits, i.e. different sets of parameters could, in some cases, fit particular breakthrough curves equally well, (iii), the filtration of colloids, which is currently not included in the modelling approaches presented here, although some inferences regarding the most likely mechanisms can be made from experimental observations, (iv), the possibility that non-Fickian dispersion may be an important mechanism for the transport of aqueous solutes, as well as colloids, which has implications for the interpretation of tracer transport experiments, and (v), various other artefacts that may have arisen because of the simplified nature of the models.

Finally, Chapter A1.1-7 presents some conclusions and discusses the implication of the present study for safety assessment.

A1.1-2 Methodology

A1.1-2.1 The use of alternative models

In the present study, three different models are used, which will be referred to as:

- the 1-D advection-dispersion (-matrix diffusion) model,
- the 2-D advection-dispersion(-matrix diffusion) model, and
- the non-Fickian dispersion or CTRW model.

The first model is essentially the same as the model used by Hadermann & Heer (1996) who found that they could describe the transport of tracers in the MI *in situ* experiments with a double porosity model. They represented the shear zone as a set of parallel open fractures ("flow porosity") embedded in highly porous fault gouge ("matrix porosity"). Transport was considered to occur by advection and longitudinal dispersion in the fractures along 1-D transport paths, retarded by diffusion into the porous rock matrix and sorption on rock matrix pore surfaces. Dispersion is modelled as a diffusion-like process, described by Fick's Laws (referred to as "Fickian dispersion" in the present study). Hadermann and Heer were able to use this model to fit the experimental breakthrough curves, with parameters consistent with independent information. They were also able to make acceptable predictions for a different dipole flow field.

The 2-D advection-dispersion model differs from the 1-D model only in its representation of the flow field and its inclusion of transverse dispersion. Additionally it allows the inclusion of known artificial structures (e.g. tunnel) and more complicated regional boundary conditions (regional hydraulic gradients). The non-Fickian dispersion model provides a more generally applicable representation of advective and hydrodynamic dispersion processes in highly heterogeneous media.

The application of three alternative models in the present study can be seen as a test of the following hypotheses:

1. that a representative 1-D transport path is adequate to represent the transport of tracers between the injection well and the withdrawal well in the CRR *in situ* tests, and

2. that the process of hydrodynamic dispersion for both aqueous solutes and colloids can be adequately represented as a diffusion-like process, governed by Fick's Laws of diffusion.

The failure of the 1-D advection-dispersion model and success of the 2-D advection-dispersion model to represent or predict one or more of the breakthrough curves would constitute a falsification of the first hypothesis. Similarly, the failure of the 1-D and 2-D advection-dispersion models and success of non-Fickian dispersion model to represent or predict one or more of the breakthrough curves would constitute a falsification of the second hypothesis.

A1.1-2.2 Assumptions and procedures common to all the models

A1.1-2.2.1 Assumptions regarding the structure of the shear zone

To date, several attempts to model transport in the Grimsel shear zone have been based on a structural model described in Heer & Hadermann (1996), and this structural model is also used in the present work. As in Heer & Hadermann (1996), the complex and highly connected network of open and partially filled fractures observed in the actual shear zone is replaced by a set of parallel, open fractures, separated by a homogeneous porous rock matrix, representing the heterogeneous mixture of fault gouge, adjacent rock and dead end pores between the actual fractures.

All transport-relevant properties of the fractures and the rock matrix are assumed to be constant in space and time.

The replacement of heterogeneous geological media with hypothetical homogeneous media (i.e., the fractures and matrix) is carried out in order to formulate tractable equations for flow and transport based on the consideration of mass balance in representative elementary volumes (REVs) (see, e.g. Bear 1972). The success of such an approach is highly dependent on the scale of the problem in relation to the size and structure of the heterogeneities in geological media. In general, if the size of the heterogeneities is much smaller than the model size, the replacement of heterogeneous media by homogeneous media with effective hydraulic and transport properties is justified for modelling purposes. Otherwise heterogeneities have to be included explicitly into a model or model approaches have to be used that, like CTRW, is not based on REVs.

A1.1-2.2.2 Assumptions regarding flow

All three models used in the present study assume that a steady-state dipole flow field exists in the shear zone, controlled by the injection and withdrawal flow rates. The small fluctuations in flow rate that actually occurred in the course of individual tests were assumed to be insignificant. In principle, the computer code used to solve the equations of the 2-D advection-dispersion model would have allowed the fluctuations to have been included, but this would have resulted in much longer computational times.

A1.1-2.2.3 Assumptions regarding transport processes

All three models were originally developed to predict the transport of solutes. In the present study, the following additional assumptions are made in order to model the transport of cocktails of tracers that can include both solutes and colloids.

Firstly, it is assumed that the transport of each component of the cocktails can be calculated independently. This implies the following additional assumptions.

- Tracers in aqueous solution do not interact (chemically) with each other.
- Colloids are stable, and do not interact with each other or with tracers in aqueous solution - radionuclide tracers may be associated with colloids at the time of injection, but no further interaction takes place, i.e. the colloid bound fraction of each tracer remains constant during migration.
- There is no competition for sorbing sites on rock matrix pore surfaces, and sorption coefficients measured on fault gouge material in the laboratory can be applied directly to sorption on rock matrix pore surfaces.

Both solutes and colloids are assumed to be transported by advection and dispersion in the fractures. Advective transport in the rock matrix is assumed to be negligible. Solutes may undergo limited matrix diffusion and sorption on matrix pore surfaces. Sorption is assumed to be a linear, equilibrium process, described by an element-dependent sorption coefficient K_d [m^3 kg^{-1}]. It is assumed, that colloids are excluded from matrix pores as a result of their size and/or charge effects (this assumption is discussed further in Chapter A1.1-5). The non-Fickian dispersion model used in the present study does not as yet include matrix diffusion, and so is only applied to colloid transport and the transport of radionuclide tracers associated with colloids. Neither solutes nor colloids are considered to be subject to immobilisation processes, such as colloid filtration, or interactions of any kind with the fracture walls.

At the injection well, the models assume time dependent aqueous tracer and colloid concentrations that are based on the experimentally measured concentration of uranine at the well, scaled according to injected tracer mass.

Finally, radioactive decay is assumed to be negligible for all the radionuclide tracers over the timescale of the experimental runs. This assumption is easily justified for all tracers apart from ^{85}Sr and ^{131}I, which have half lives of about 1560 and 190 hours, respectively. Even for these tracers, however, the concentration changes due to decay are small.

A1.1-2.2.4 Procedure for the generation of breakthrough curves

Since it is assumed that the transport of each component of the tracer cocktails can be calculated independently, the generation of breakthrough curves for colloids, for radionuclide tracers bound entirely to colloids (i.e. a 100 % colloid bound fraction) and for radionuclides tracers that are transported entirely in the aqueous phase (i.e. a 0 % colloid bound fraction) is straight-forward. In the case of radionuclides tracers that are transported entirely in the aqueous phase, the models are simply run for each individual tracer and the calculated concentration at the withdrawal well as a function of time gives the breakthrough curve. In the case of colloids and colloid-bound radionuclides, the fact that colloid filtration is not included in the models means that the calculated breakthrough curves must be multiplied by the observed or expected colloid recovery, or the experimentally measured data must be normalised to 100 % recovery.

In the case of tracers that are partially associated with colloids and are partially transported in the aqueous phase, separate model runs are carried for the colloid bound fraction and the aqueous fraction. Since it is assumed that no further sorption on or desorption from colloids takes place during transport, the two resulting breakthrough curves (corrected for recovery in the case of the colloid curve) can then be superimposed to give the overall breakthrough curve for the tracer.

A1.1-2.3 The 1-D advection-dispersion model

The 1-D advection-dispersion model is based on the model developed during the MI experiment and described in detail by Heer & Hadermann (1996) and Hadermann & Heer (1996).

The governing equations for transport in a fractured porous medium are given, for example, in Heer & Hadermann (1996) and are not reproduced here. These equations are solved numerically in order to generate the model breakthrough curves for the 1-D advection-diffusion model in the present study.

A1.1-2.4 The 2-D advection-dispersion model

In the 2-D advection-dispersion model, flow and transport in the shear zone were evaluated using a finite element approach, thus avoiding the approximations associated with the discretisation of the flow field into stream tubes and transport paths that are a feature of the 1-D model.

Initially the fracture plane is meshed 2-D with a few finite elements (the code used is adaptive, so this discretisation changes with time). At the start of each model run, the mesh is refined around the injection and withdrawal wells in order to represent the flow field adequately in areas where velocity gradients are highest. The dimensions of the model fracture are 40 meters by 40 meters. A constant head boundary condition is applied at the outer boundaries. The finite dimensions of the injection and withdrawal wells are not considered in the model and two single nodes spaced 2.5 meter apart in the centre of the model are chosen to represent the injection and withdrawal wells. The chosen model dimensions and the boundary conditions ensure that the flow field near the wells mimics the theoretical dipole field for an infinite plane as closely as possible.

The porous rock matrix is represented by parallel layers of 3D elements on top of the 2-D elements in the fracture plane (the symmetry of the modelled system means that the region below the fracture plane does not need to be explicitly represented).

For modelling transport, a free outflow boundary condition for both, flow and transport, is applied to the outer model boundaries, although the large distance between the model boundaries and the dipole flow field means that the boundary condition has a negligible impact on the results. The concentrations of tracers at the withdrawal well are calculated as functions of time to obtain breakthrough curves.

A1.1-2.5 The non-Fickian dispersion (CTRW) model

One possible approach for dealing with non-Fickian transport is the continuous time random walk (CTRW) approach, a robust and easily applicable method introduced by Berkowitz & Scher (1995). The formalism of the CTRW approach is well documented and described in Berkowitz et al. (2001). Only the important points relating directly to the following analyses are summarised below. The justification for considering this model as an alternative to the more commonly used Fickian model of dispersion is discussed in Chapter A1.1-5 in Kosakowski (2004) and in Kosakowski & Smith (2004).

Tracer transport in heterogeneous geological media with strongly varying groundwater flow fields can be envisioned as particles moving along different paths with spatially varying velocities. Different paths are traversed by different numbers of particles. This can be described by a joint probability density function, $\psi(s,t)$, which gives the probability for a particle displacement, s, with a difference of arrival times, t. The challenge is to map the important

aspects of the particle motion onto $\psi(s,t)$. Identification of $\psi(s,t)$ lies at the heart of the CTRW model. It can be shown that the principal characteristics of tracer movements are dominated by the behaviour of $\psi(s,t)$ at large (or asymptotic) times. As discussed by, for example Berkowitz et al. (2001), non-Fickian transport arises in cases where the large time behaviour of $\psi(s,t)$ is a power law, i.e. $\psi(s,t) \sim t^{-1-\beta}$, with the constant exponent $\beta > 0$.

As in the present study, tracer test measurements often consist of breakthrough curves; i.e. tracer concentrations as functions of time t at a given distance from the tracer source. In the context of the CTRW model, the breakthrough curve corresponds to a First Passage Time Distribution (FPTD) of particles through a plane within the medium. The FPTD is defined as the probability per time unit for a tracer particle to reach a location s at a specific time t for the first time.[14]

The shape of the FPTD functions (and hence the tracer breakthrough curves), including the time of occurrence of the peak, varies strongly as a function of β (Berkowitz et al. 2001). For $0 < \beta < 1$, dispersion is highly non-Fickian, and the concentration peak moves much more slowly than the average fluid velocity, with a longer forward advance of particles. For $1 < \beta < 2$, the mean particle plume moves with the average fluid velocity (as in the case of Fickian dispersion), but the tails remain broader ("heavier") than those of the Fickian case. For $\beta > 2$, the dispersion becomes Fickian.

The FPTD solution for $0 < \beta < 1$ requires the specification of two parameters: β, which characterises the dispersive process, and x_{shift}, which characterises the effective tracer velocity at a given distance. By contrast, the FPTD solution for $1 < \beta < 2$ involves three parameters: β, t_{mean} and b_β. The mean fluid velocity can be calculated from t_{mean} by dividing by the transport distance L. For the case of $\beta = 2$, it can be shown that the solution is equivalent to the 1-D advection-dispersion solution and that b_β is directly related to the longitudinal dispersion length, a_L, in the Fickian representation of dispersion: $b_\beta = a_L v/L$, where v is the fluid velocity in a Fickian advection-dispersion model.

As discussed in Kosakowski et al. (2001), convolution of the FPTD solutions can be used to deal with experimental systems in which either the input boundary condition is something other than pulse or step input, or transport occurs through regions with distinctly different properties.

A1.1-2.6 Computer codes

The governing equations of the three models used in the present study can be solved using the computer code PICNIC (PSI/Quantisci Interactive Code for Networks of Interconnected Channels), in the case of the 1-D advection-dispersion model, RockFlow, in the case of the 2-D advection-dispersion model, and GRACE, in the case of the non-Fickian dispersion (or CTRW) model. It should be noted that, in the case of PICNIC and RockFlow, only small subsets of the features of the codes were required for the present study.

The PICNIC code can be used to calculate transport in fracture networks (or one or more parallel fractures, as in the present application), with one- or two-dimensional matrix diffusion in a homogeneous or heterogeneous rock matrix. A detailed description the code can be found in Barten (1996) and Barten & Robinson (2001).

---

[14] This concept is identical to the concept of the 1-D advection-dispersion model. The "injection" or source plane is the surface of the injection borehole and the exiting plane is essentially the surface of the extraction borehole. Transport between both planes (surfaces) is treated as one-dimensional. Dispersion in the measurement equipement is assumed to be negligible.

RockFlow is based on the finite element method (FEM) in a hybrid approach, in which a 3-D model domain can contain a mix of 1-D, 2-D and 3-D structural elements. Thus, it is possible to simulate fractures as 2-D elements embedded in a matrix of 3-D elements. A detailed description the code can be found in Kolditz et al. (1999).

GRACE is a graphical analysis package that can access external functions present in either system or third-party shared libraries or modules specially compiled for use with GRACE. The CTRW-software library for use with GRACE can be downloaded from the CTRW homepage[15]. The capabilities of the library are described in Berkowitz et al. (2001). The library includes not only the CTRW solutions for different parameters, but also convolution functions that enable arbitrary injection functions to be taken into account. GRACE itself can also be downloaded[16].

A1.1-2.7 Application of the models

A1.1-2.7.1 Strategy

The strategy for applying the 1-D and 2-D advection-dispersion models was:

(i) to fit the models to the breakthrough curves from the preliminary experiments carried out prior to the main runs (#31 and #32) by adjusting the model parameters until as good a fit as possible is obtained,

(ii) to use fitted parameters describing the material and transport properties of the dipole, together with laboratory sorption data and data on injection concentrations, to make predictions of the breakthrough curves for the main runs, in advance of the runs being carried out, and

(iii) to modify the models or their parameter values as necessary in the light of the comparison between model predictions and experimental predictions.

In addition to providing parameters for step (ii), step (i) provides a first test of the applicability of the advection-dispersion models. This is achieved by examining the quality of the fits and assessing the plausibility of the values of the free parameters that are adjusted in the fitting procedure - e.g. by comparing with independently derived data and parameter values obtained from MI. Step (ii) was intended to assist in the planning of the main runs by indicating whether it would be possible to detect the breakthrough of the different radionuclides with the combination of planned input concentrations and given detection limits. It was also intended to provide a rigorous test of the models by comparing the actual breakthrough data with the predicted curves.

The non-Fickian dispersion model (CTRW) was used where steps (i) or (iii), above, suggested that the advection-dispersion models are inadequate. This was found to be the case for colloid breakthrough, as discussed in Chapter A1.1-3 (see in particular, the upper left part of Fig. A1.1-3.1).

A1.1-2.7.2 Fitting the models to the breakthrough curves

It is assumed that colloids are excluded from matrix pores, and are thus not subject to the retardation processes of matrix diffusion and sorption. Thus, to model colloid breakthrough, parameters associated with matrix diffusion and sorption can be set to zero, and breakthrough

---

[15] http://www.weizmann.ac.il/ESER/People/Brian/CTRW/

[16] http://plasma-gate.weizmann.ac.il/Grace/

curves can be fitted by adjusting parameters associated only with advection and dispersion. If it is assumed that these parameters are also applicable to conservative tracers, then, for a given dipole flow field, the breakthrough curves for these tracers can be fitted by adjusting parameters associated with matrix diffusion, but using the parameters associated with advection and dispersion that were obtained from the colloid breakthrough curves. Similarly, the breakthrough curves for sorbing tracers can be fitted by adjusting parameters associated with sorption, while using the parameters associated with advection, dispersion and matrix diffusion that were obtained from the colloid and conservative tracer breakthrough curves.

A1.1-2.7.3 Predictive modelling for run #31

Main run #31 involved a cocktail of conservative and sorbing tracers. Fitted parameters describing the material and transport properties of dipole 1, together with laboratory sorption data and data on injection concentrations, were used to make predictions of the breakthrough curves for thus run with the 1-D advection-dispersion model, in advance of the run being carried out. Laboratory sorption data and data on injection concentrations for the tracers used cocktail for runs #31 are given in Table A1.1-2.1.

This procedure assumes that it is appropriate to use the same material and transport parameters for all tracers in dipole 1, with the exception of the sorption coefficient[17]. It was also initially assumed that *all radionuclides tracers are transported only in solution*, and there is no production of colloids due, e.g. to oversaturation or precipitation (see e.g. Kosakowski & Baeyens 2001), and the effects of natural groundwater colloids are negligible - i.e. all radionuclide tracers are subject to matrix diffusion and (in the case of sorbing tracers) sorption on matrix pore surfaces. This final assumption had to be revisited after the tests had been carried out, as described in Chapter A1.1-3.

A1.1-2.7.4 Predictive modelling for run #32

Main run #32 involved bentonite colloids, in addition to a cocktail of conservative and sorbing tracers. Fitted parameters describing the material and transport properties of dipole 1, together with laboratory sorption data and data on injection concentrations and colloid bound fractions, were used to make predictions of the breakthrough curves for this run, again in advance of the run being carried out. As mentioned above and discussed further in Chapter A1.1-3, however, it was found necessary to use the non-Fickian dispersion model (CTRW) for colloid transport and the transport of radionuclides associated with colloids.

Laboratory sorption data and colloid bound fractions for the tracers used cocktail for runs #32 are given in Table A1.1-2.1.

For modelling this run, it was assumed that the tracers are distributed between the aqueous phase and the colloid bound fraction according to the data given in Table A1.1-2.1 at the time of injection, and the colloid bound fraction remains constant during migration - i.e. there is no further sorption of radionuclides to (or desorption from) colloids. It is assumed to be appropriate to use the same material and transport parameters for all tracers in dipole 1, with the exception of the sorption coefficient and the colloid bound fraction. In the case of Cs, it is known that sorption is, in reality, non-linear and thus, in principle, the natural background Cs concentration in the Grimsel groundwater, which is comparable to that of the tracer solution, should be taken

[17] In principle, radionuclides show different effective diffusivities, but the difference is moderate and sorption in the porous rock matrix is the main process for sorbing radionuclides.

into account. For simplicity, however, the non-linearity of the sorption isotherm and the background concentration of Cs were not considered in the predictive modelling.

The colloid experiments in dipole 3 gave a recovery of the injected mass of about 55 % (LIBD detected concentration for run #6a, see Fierz et al. 2001). For predictive modelling of run #32 in dipole 1, it is assumed that colloids show the same bulk recovery. The fraction of the radionuclides sorbed on the colloids is also assumed to have also a recovery of 55 %. Effects due to a preferred filtration of larger colloids, as measured by Degueldre & Laube (2000) and their effect on associated radionuclides are not considered in the calculations.

Tab. A1.1-2.1: Laboratory sorption data and data on injection concentrations and colloid bound fractions for the tracers used cocktail for runs #31 and #32, together with their detection limits

The sorption coefficients were measured by FZK and CIEMAT and are summarised in Möri (2001a). The colloid bound fraction of the tracers is based on Geckeis (2001)

Run #31 tracers	***Kd* (fracture filling material)** $m^3\ kg^{-1}$	**Run #32 tracers**	**Colloid bound fraction** %	***Kd* (fracture filling material** $m^3\ kg^{-1}$
^{243}Am	46×10^{-3}	^{241}Am	97.7	46×10^{-3}
^{242}Pu	8×10^{-3}	^{244}Pu	72.2	8×10^{-3}
^{238}Pu	8×10^{-3}	^{238}Pu	72.2	8×10^{-3}
^{237}Np	10^{-3}	^{137}Cs	14.9	596×10^{-3}
^{238}U	5.6×10^{-3}	^{237}Np	9.1	1×10^{-3}
^{232}Th	not known	^{233}U	1.6	5.6×10^{-3}
^{85}Sr	8×10^{-3}	^{99}Tc	0.7	11.5×10^{-3}
^{131}I	0	^{232}Th	97.6	not known
		^{85}Sr	0	8×10^{-3}
		^{131}I	0	0

A1.1-3 Results

A1.1-3.1 Breakthrough curve fitting

A1.1-3.1.1 The advection-dispersion models

The 1-D and 2-D advection-dispersion models were used to fit breakthrough curves from experimental results carried out in dipole 1 using:

- colloids - or, more specifically, Th, Tb and Hf, which are believed to be transported in colloidal form, even without the addition of bentonite colloids to the injection cocktail[18] (see below),
- uranine: a conservative tracer, and
- Sr: a moderately sorbing tracer.

Tab. A1.1-3-1 shows the experimental runs that were fitted using the 1-D and 2-D advection-dispersion models and summarises key modelling assumptions.

As explained in Chapter A1.1-2, free parameters that are adjusted to fit colloid breakthrough are used to fix some of the parameters required to model conservative tracer breakthrough. Similarly, the remaining free parameters that are adjusted to fit conservative tracer breakthrough are used to fix some of the parameters required to model sorbing tracer breakthrough.

Tab. A1.1-3.1: Tracer breakthroughs that were fitted using the 1-D and 2-D advection-dispersion model and key modelling assumptions

Tracer	Experimental runs	Models fitted	Key assumptions
Th, Tb, Hf	#14	2-D advection dispersion	Th, Tb and Hf transported in colloidal form, no matrix diffusion
Uranine	#13, #21	1-D advection dispersion	Limited matrix diffusion; no uranine sorption
			Unlimited matrix diffusion; no uranine sorption
	#21	2-D advection dispersion	Unlimited matrix diffusion; no uranine sorption
Sr	#21	1-D and 2-D advection dispersion	Unlimited matrix diffusion; linear, equilibrium Sr sorption

Table A1.1-3.2 shows the fitted parameters values, and compares these values with those obtained by Heer & Hadermann (1996) by fitting MI data, and also the values from other independent sources quoted by Heer & Hadermann (1996). The third and the fourth columns give the parameters for the 1-D and 2-D models assuming a single fracture representation of the shear zone. The parameters are nearly identical, as expected from the narrowness of the dipole flow field. Only the fluid velocities and the dispersion parameters are slightly different.

[18] In the case of dipole 1, no experiments were conducted in advance of the main runs #31 and #'32 that specifically addressed colloiod transport

Longitudinal dispersion in particular has to be increased with respect to the 2-D model in order to account for spreading due to effects not included in the 1-D model, namely the finite width of the dipole flow field and the effects of transverse dispersion. The fifth column gives parameters for the 2-D model assuming four parallel fractures (as in Heer & Hadermann 1996). This gives rise to some differences in the fitted matrix properties. Nevertheless, with the exception of retardation factor and sorption coefficient for Sr (discussed further, below), the fitted material and transport parameters for the three model variants fall into the ranges specified by Heer & Hadermann (1996) for the earlier MI experiment. The case with four fractures in particular gives parameter values that are very close to the values estimated during MI.

(i) Fitting Th, Tb and Hf breakthrough

Figure A1.1-3.1 (upper left) shows the Th, Tb and Hf breakthrough data from runs #14. Th, Tb and Hf are sorbing tracers. Nevertheless, comparing the breakthrough of these tracers with that of non-sorbing uranine (Fig. A1.1-3.1, upper right and lower row), all show a maximum breakthrough at a little over 1 hour, suggesting that sorption does not retard the breakthrough of Th, Tb and Hf. In fact, the maximum breakthrough for Th, Tb and Hf occurs slightly before that of uranine, which is the behaviour observed for injected colloids in the case of dipole 3 (see Section A1.1-4, Fig. A1.1-4.1). This strongly suggests that Th, Tb and Hf are transported in colloidal form (even in the absence of bentonite colloids in the injection cocktail) and that these colloids, while they can be filtered to some extent during transport, are not retarded by, for example, matrix diffusion or reversible attachment to fracture walls.

On the basis of this hypothesis, the 1-D and 2-D advection-dispersion models without matrix diffusion were fitted to the breakthrough data, as also shown in Figure A1.1-3.1. Flow in the shear zone was, in this case, assumed to be confined to a single fracture. The fracture aperture in the models was adjusted to match the peak arrival time for the tracers. For the chosen boundary conditions (fixed injection/withdrawal flow rates), the magnitude of the velocity field depends only on the aperture of the fracture and therefore the time of the breakthrough maximum also depends only on the fracture aperture. The longitudinal dispersion length is used to fit the width of the breakthrough curve. In the case of the 2-D model, the transversal dispersion length was arbitrarily fixed to a value of 0.001 m.

The fit is not entirely satisfactory. In particular, it was not possible to fit both the early concentrations and the late concentrations with one dispersion length. It appears that either a process is not represented by the model, or the processes that are represented and not correctly. These discrepancies provided the motivation for applying the non-Fickian dispersion (CTRW) model to colloid breakthrough curves (see Section A1.1-3.2). Nevertheless, the aperture and dispersion parameters obtained from the fits were employed as fixed parameters in modelling uranine and strontium breakthrough.

(ii) Fitting uranine breakthrough

Figure A1.1-3.1 (upper right) shows the uranine breakthrough data from runs #13 and #21, and fits of these data using the 1-D advection-dispersion model. Uranine was assumed to be non-sorbing and flow in the shear zone was again, in this case, assumed to be confined to a single fracture.

The breakthrough data shows a maximum at a little over 1 hour after injection and a prolonged tail. On the bases of previous modelling studies, it is assumed that the later part of the tail is attributable to matrix diffusion (see e.g. Heer & Hadermann 1996). If the depth of the diffusion-accessible rock matrix is modelled as being unlimited (i.e. the matrix extends without limit normal to the fracture surfaces), then the later part of the tail displays a $t^{-3/2}$ slope. Limited

matrix diffusion gives rise to a so-called "tail-end perturbation" - i.e. a reduction in this slope. In Figure A1.1-3.1 fits of the data assuming both unlimited matrix diffusion and limited matrix diffusion with different matrix depths (*d*) is shown. Unfortunately, the scatter in the data[19] is such that a unique value for the matrix depth cannot be extracted from the fits, although a lower bounding value of about 3 mm is suggested. Nevertheless, the 1-D advection-dispersion model with matrix diffusion provides a good fit to the uranine breakthrough curves, confirming the findings of the earlier MI modelling studies.

Figure A1.1-3.1 shows the breakthrough data from run #21, and fits of these data using both the 1-D and 2-D advection-dispersion models, with unlimited matrix diffusion. Similarly good fits can be obtained using either model. It was also observed that good fits could be obtained assuming that the flow in the shear zone is distributed between four parallel fractures, as had been assumed in the modelling of MI, rather than assuming a single fracture.

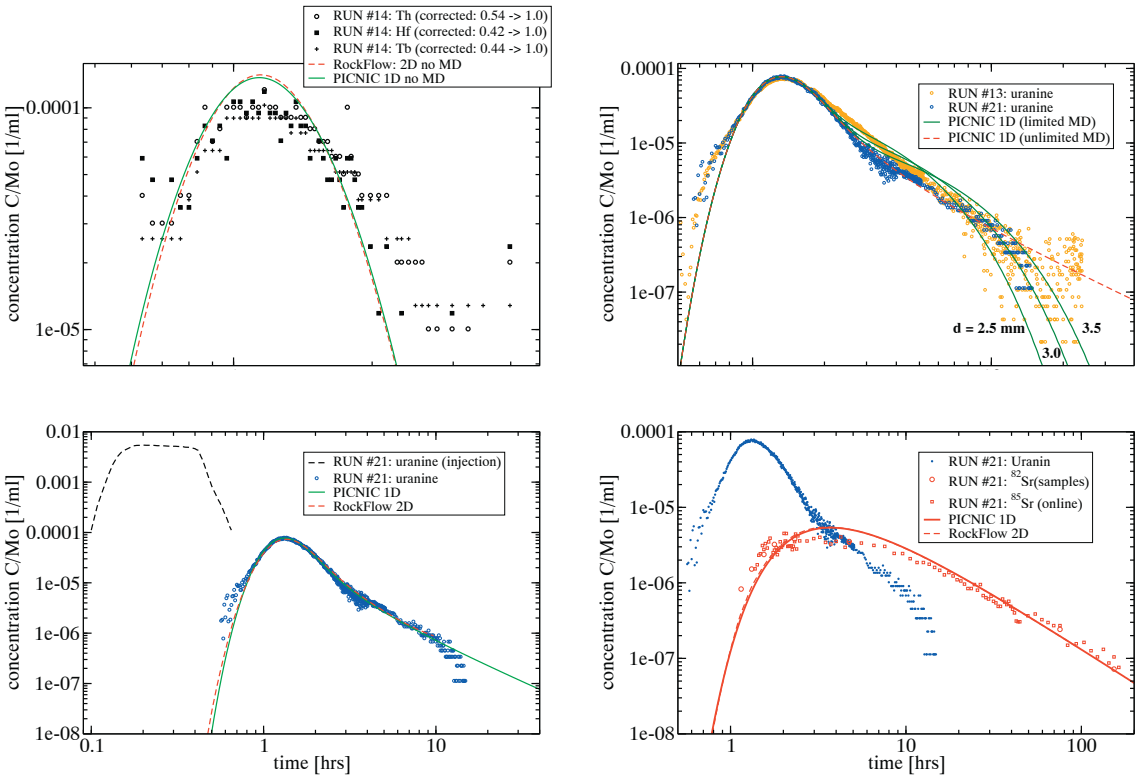

Fig. A1.1-3.1: Breakthrough data from run #21

Upper left: The breakthrough data for Th, Hf and Tb from run #14, and fits of these data using the 1-D and 2-D advection-dispersion models, assuming that the tracers are transported in colloidal form with no matrix diffusion. The breakthrough data are normalised to 100 % recovery. Upper right: The breakthrough data for uranine from runs #13 and #21, and fits of these data using the 1-D advection-dispersion model, with limited and unlimited matrix diffusion. Lower left: The breakthrough data for uranine from runs #21, and fits of these data using the 1-D and 2-D advection-dispersion models, with unlimited matrix diffusion. Lower right: The breakthrough data for uranine and Sr from run #21, and fits of the Sr data using the 1-D and 2-D advection-dispersion models, with unlimited matrix diffusion.

[19] The detection limit for uranine is about 10^{-6} mL^{-1}

Tab. A1.1-3.2: Summary of parameters extracted by fitting breakthrough curves with the 1-D and 2-D advection-dispersion models with single and multiple fractures and comparison with values used in modelling the MI-experiment

Parameters derived from combinations of other model parameters are shown in parentheses

Symbol	Description	CRR modelling study			Heer & Hadermann (1996)	
		Single fracture representation of shear zone		Multiple fracture represen-tation of shear zone		
		1-D	2-D	2-D	MI modelling	Other sources
Fixed-value parameters						
N [-]	Number of fractures	1	1	4	4	
L_0 [m]	Distance between injection and withdrawal wells	2.5	2.5	2.5	4.9	-
α_T [m]	trans. dispersion	-	0.001	0.001	-	-
ρ_p [kg m^{-3}]	bulk matrix density	2670	2670	2670	2670 (±200)	2670
Parameter values fixed by modelling colloid breakthrough (i.e. Th, Tb and Hf)						
2b [m]	fracture aperture	0.55×10^{-3}	0.55×10^{-3}	0.14×10^{-3}	0.093 $(+0.046 -0.03) \times 10^{-3}$	-
(v [m s^{-1}])	fluid velocity	7.05×10^{-4}	variable	variable	5.51×10^{-4}	-
α_L [m]	long. dispersion	0.1	0.075	0.075	0.25 (+0.05 -0.04)	-
(Pe) [-])	Peclet number	25	variable	variable	19.6	-
Parameter values fixed by modelling conservative-tracer breakthrough						
ε_p [-]	matrix porosity	0.3	0.3	0.15	0.062 (+0.068 -0.032)	0.15 (+0.12 - 0.07)
D_p [m2 s^{-1}]	diffusion constant in rock matrix	7.4×10^{-11}	7.4×10^{-11}	1.85×10^{-11}	2.5 $(+11 -2) \times 10^{-11}$	5.5 $(+1.9 -0.9) \times 10^{-11}$
D_e [m2 s^{-1}]	effective diffusion constant in rock matrix	2.2×10^{-11}	2.2×10^{-11}	0.28×10^{-11}	$0.2 \cdot 10^{-11}$	0.83×10^{-11}
d [m]	effective matrix thickness	$>3 \times 10^{-3}$	$>3 \times 10^{-3}$	$>3 \times 10^{-3}$	6.2 $(+7.4 -3.4) \times 10^{-3}$	-
Parameter values fixed by modelling reactive-tracer (Sr) breakthrough						
R_p for Sr [-]	retardation factor due to sorption in matrix (equation 5)	72	72	72	905	136 - 731
(K_d for Sr [m^3 kg^{-1}])	mass specific sorption coefficient	8×10^{-3}	8×10^{-3}	16×10^{-3}	21 $(+38 - 14) \cdot \times 10^{-3}$	$7.6 - 41 \times 10^{-3}$

(iii) Fitting Sr breakthrough

Figure A1.1-3.1 (lower right) shows the uranine and Sr breakthrough data from run #21, and the fit of the Sr data that can be obtained using both the 1-D and 2-D advection-dispersion models. Flow in the shear zone was again assumed to be confined to a single fracture, although the case of four fractures was also considered and gave a similarly good fit.

The retardation factor R_p (which was fixed at value $R_p = 1$ for modelling uranine breakthrough) was adjusted until an optimal fit was achieved. The value obtained was 72, which is significantly smaller than the value of 905 obtained by Heer & Hadermann (1996). The retardation factor can be used to obtain a sorption coefficient (K_d) using the matrix porosity given in Table A1.1-3.2 and assuming a bulk matrix density of 2670 kg m^{-3}, as in Heer & Hadermann. This gives $K_d = 8 \times 10^{-3}$ m^3 kg^{-1} for the single-fracture models and 16×10^{-3} m^3 kg^{-1} for the 4-fracture models, which is within the range obtained by Heer and Hadermann from the evaluation of Sr breakthrough in MI - i.e. 21 (+38 or -14) $\times 10^{-3}$ m^3 kg^{-1} - and is within the range quoted by Heer and Hadermann from independent sources - i.e. 7.6×10^{-3} to 41×10^{-3} m^3 kg^{-1}.

Finally, it was found that the quality of the fit could be improved by adjusting both the longitudinal dispersion length (or equivalently the Peclet Number, Pe = L/a_L) and the retardation factor (or sorption coefficient K_d) simultaneously, rather than the retardation factor alone. The best fit was obtained using a lower Peclet number than in Table A1.1-3.2 (a Peclet number of 12 rather than 25), and a higher value of R_m (a K_d of 14×10^{-3} m^3 kg^{-1} rather than 8×10^{-3} m^3 kg^{-1}). One of the findings of Heer & Hadermann (1996) was that, in MI, the longitudinal dispersion length did not depend on the sorption properties of the tracer under consideration. The suggestion of such a dependency in the present study is, however, consistent with the theoretical work of Gelhar (1987), which examined the influence of sorption on dispersion in a heterogeneous fractured medium.

A1.1-3.1.2 The non-Fickian dispersion model

Given that the fit of the advection-dispersion models to the breakthrough data for Th, Tb and Hf was not entirely satisfactory, and given the evidence (especially from dipole 3) that these tracers are transport as colloids that are not retarded by matrix diffusion and sorption (see Chapter A1.1-5), it seems reasonable to suggest that it is an inappropriate representation of advection and dispersion that gives rise to the discrepancies. Thus, the non-Fickian dispersion (CTRW) model was applied to the breakthrough curves to see whether an improved fit was obtained.

The uncertainty in the breakthrough data for Th, Tb and Hf in the case of dipole 1 is relatively large, and it is not possible to obtain unique parameters for the CTRW model from these data by curve fitting. If, however, it is assumed that the CTRW dispersion parameter β is the same for bentonite colloids in dipole 3 as for Th, Tb and Hf in colloidal form in dipole 1, then fitting the colloid breakthrough data from dipole 3, and transferring the result to dipole 1 can determine this parameter. This reduces the number of free parameters needed to fit of the CTRW model to the breakthrough data for Th, Tb and Hf in dipole 1, and a good fit can be obtained, as shown in Fig. A1.1-3.2.

The mean particle velocity of the CTRW fit is lower than that of the 1-D advection dispersion model fit (2.2×10^{-4} m s^{-1} in Fig. A1.1-3.2 compared to 7.5×10^{-4} m s^{-1} in Tab. A1.1-3.2). This is due to the fact that the stream tube approach matches the velocity for the breakthrough peak, whereas the CTRW approach yields the velocity of the centre of mass of the particle plume.

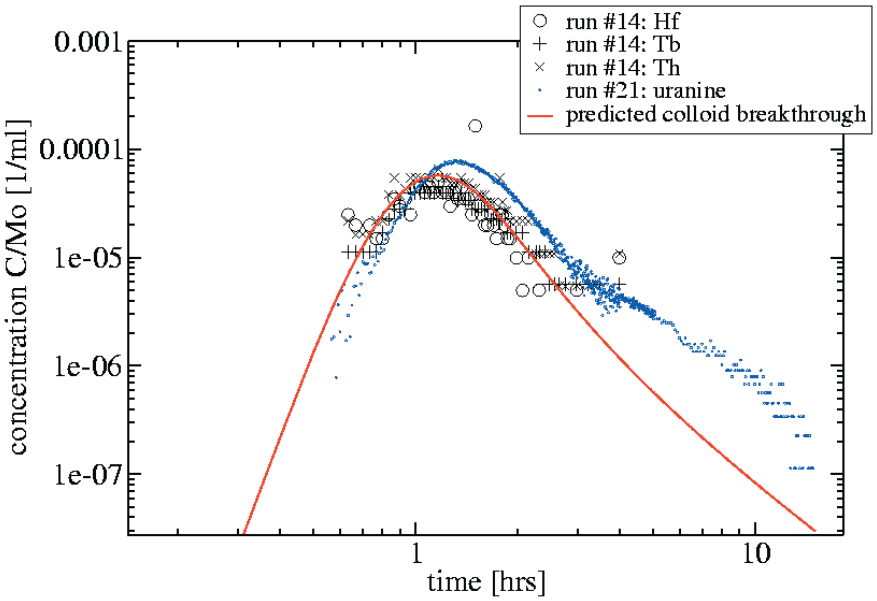

Fig. A1.1-3.2: The breakthrough data for Th, Tb and Hf from run #14, and uranine from run #21, and fits of the Th, Tb and Hf data using the non-Fickian dispersion (CTRW) model

CRTW parameters are $\beta = 1.2$, $t_{mean} = 2.0$ hours and $b_\beta = 0.335$. The calculated mean particle velocity is 2.2×10^{-4} m s^{-1}

For fitting the colloid breakthrough data from dipole 3 with the CTRW model, the colloid injection functions[20] for relevant experimental runs were repeatedly convoluted with FPTD solutions for particular combinations of the CRTW parameters, and the parameters were adjusted until optimal fits were obtained. Fits for run #6a (bentonite colloids) and run #7a (bentonite colloids, together with Th, Tb and Hf) are shown in Figures A1.1-3.3 and A1.1-3.4, respectively. In each case, a combination of automated non-linear curve fitting and manual selection of fitting parameters was used.

[20] The injection functions for colloids were not directly available. Rather, the normalised measured uranine concentrations in the injection borehole were used, on the assumptions that these were identical to the injection functions for colloids.

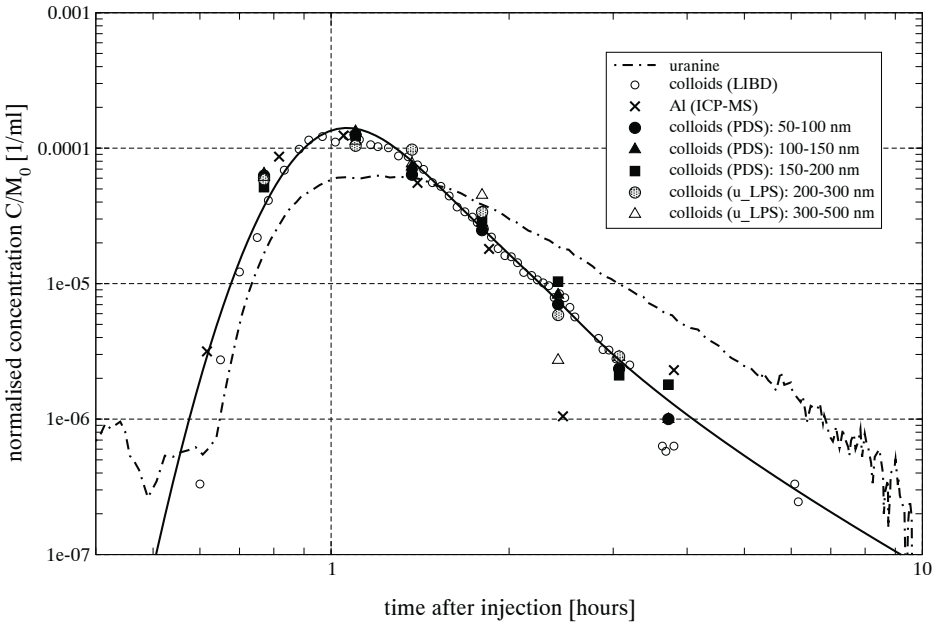

Fig. A1.1-3.3: The breakthrough data for bentonite colloids from run #6a, and uranine from run #6, and fits of the bentonite colloid data using the non-Fickian dispersion (CTRW) model

CRTW parameters are $\beta = 1.2$, $t_{mean} = 1.42$ hours and $b_\beta = 0.25$. The calculated mean particle velocity is 9.8×10^{-4} m s^{-1}. Colloid recovery for each size fraction is normalised to 100 %

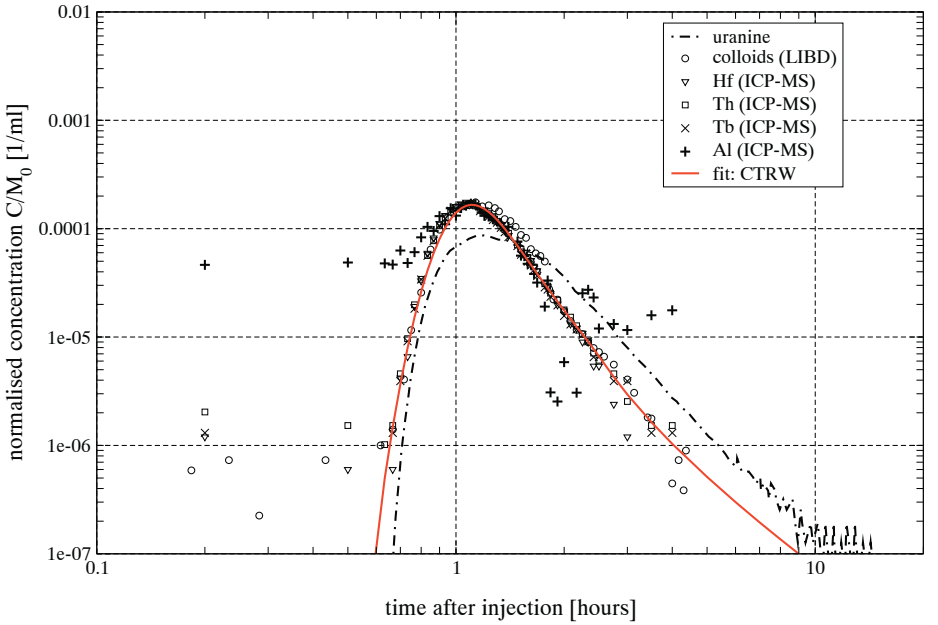

Fig. A1.1-3.4: The breakthrough data for bentonite colloids and Th, Tb and Hf from run #7a, and uranine from run #7, and fits of the bentonite and Th, Tb and Hf colloid data using the non-Fickian dispersion (CTRW) model

CRTW parameters are $\beta = 1.2$, $t_{mean} = 1.40$ hours and $b_\beta = 0.25$. The calculated mean particle velocity is 9.9×10^{-4} m s^{-1}. Recovery in each case is normalised to 100 %

A1.1-3.2 Predictive modelling

A1.1-3.2.1 Models used

Given the good agreement between the results of the 1-D and 2-D advection-dispersion models as shown in the previous section, predictive modelling of aqueous tracer transport for the main runs #31 and #32 was carried out using the 1-D advection-dispersion model only. The non-Fickian dispersion model was used for predictions of colloid transport.

A1.1-3.2.2 Use of predictive modelling for the planning of runs #31 and #32

An evaluation of the predictions made for runs #31 and #32 in advance of the runs being carried out showed that, for the planned injection concentrations, the breakthrough curves would exceed detection limits and, in nearly all cases, it should be possible to measure the full breakthrough in 10 days (240 hours), the planned duration of the experiment. Only for Cs in run #32 was it predicted that the decline of the breakthrough concentration for Cs in solution in would not be seen, and this was confirmed on carrying out the run (see below). The modelling study thus provided a useful planning tool for the experiments.

A1.1-3.2.3 Predictions and measurements of Am breakthrough

Figure A1.1-3.5 shows the model predictions and measured data for Am breakthrough in runs #31 and #32. There is a marked difference between the predictions for the two runs, due to (i), the relatively high sorption of Am on rock matrix pores, leading to a retardation of the migration of Am in solution in run #31, and (ii), the high colloid-bound fraction assumed for Am in run #31, which is not subject to retardation by matrix diffusion and sorption (see Tab. A1.1-2.1). The amount of Am predicted to be transported in solution in run #32 is very small and is only visible in the change of the slope for the late time breakthrough curve. For long times, the slopes of the curves for both runs are identical.

The experimental data for run #31 and run #32 coincide closely with each other. This contradicts the model prediction that breakthrough for run #31 should be significantly more retarded than that for run #32. The prediction for run #32 matches the experimental data for both runs well (although the measured tailing is somewhat more pronounced than in the predictions). This strongly suggests that the assumption of the model of run #31 than Am migrates as an aqueous solute is incorrect, and that it in fact migrates predominantly as colloids, even in the absence of bentonite colloids in the injection cocktail.

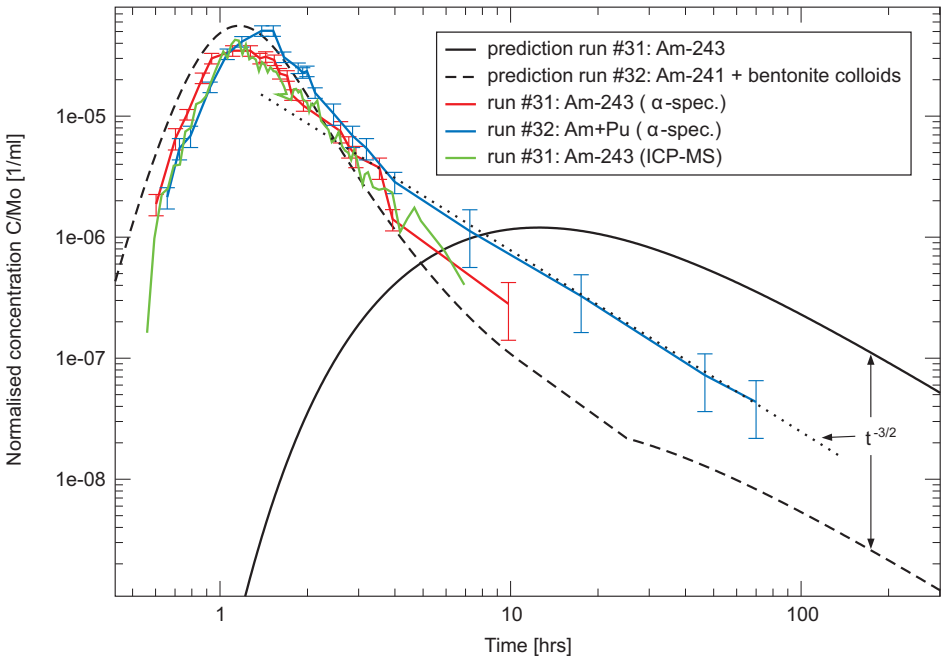

Fig. A1.1-3.5: The predictions (black full and dashed lines) and measured data (coloured lines) for Am breakthrough in runs #31 and #32

Although the α-spectroscopy measurements are based on the combined activity measurements of ^{241}Am and ^{238}Pu, it is reasonable to assume that the behaviour of ^{241}Am is dominating the normalised curve since the injected activity of ^{241}Am is about 2.8 times higher than the injected activity of ^{238}Pu

A1.1-3.2.4 Predictions and measurements of Pu breakthrough

Figure A1.1-3.6 shows the predictions and measured data for Pu breakthrough in runs #31 and #32. Similar observations are made here as in the case of Am. The comparison of predictions with experimental data strongly suggests that the assumption of the model for run #31 that Pu migrates as an aqueous solute is incorrect, and that it in fact migrates predominantly as colloids, even in the absence of bentonite colloids from the injection cocktail.

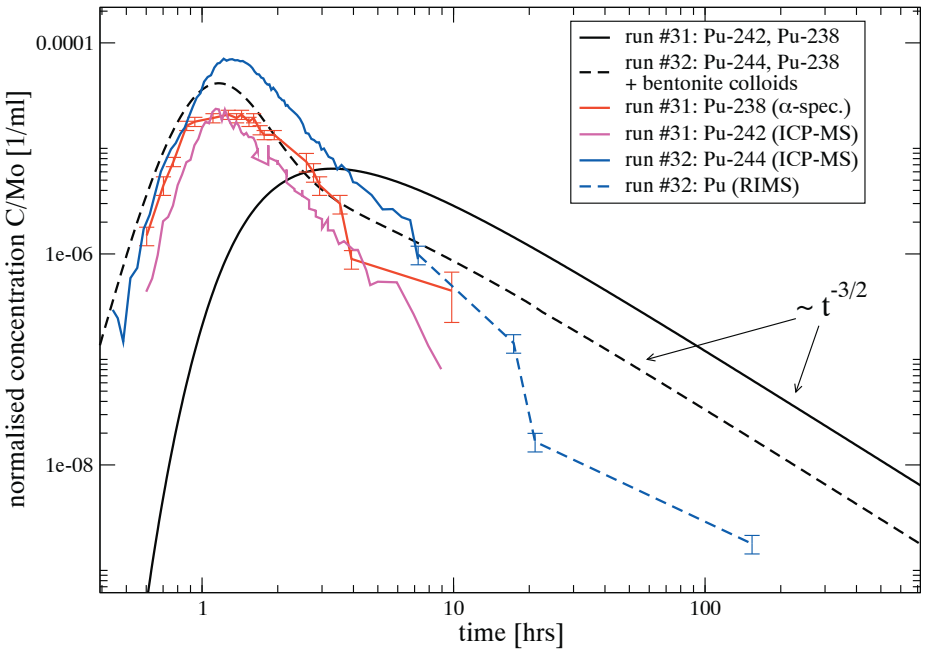

Fig. A1.1-3.6: The predictions (black full and dashed lines) and measured data (coloured lines) for Pu breakthrough in runs #31 and #32

A1.1-3.2.5 Predictions and measurements of Np breakthrough

Figure A1.1-3.7 shows the predictions and measured data for Np breakthrough in runs #31 and #32. The predictions for the two runs are similar, due the low colloid-bound fraction assumed for Np in run #31. Np is thus predicted to be transported predominantly as an aqueous solute in both runs. The effects of colloids are evident only in the higher predicted breakthrough concentrations at early times in the case of run #32, and these have only a minor influence on overall Np recovery.

The experimental data for run #31 and run #32 coincide closely with each other and with the predictions. The early time breakthrough is not sufficiently resolved in order to identify the effects of colloids.

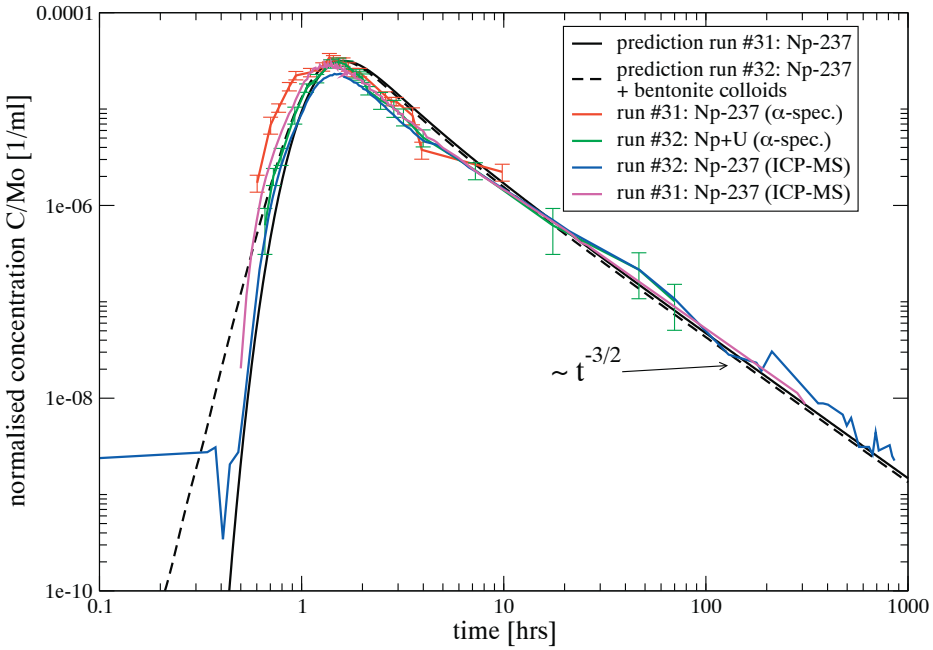

Fig. A1.1-3.7: The predictions (black full and dashed lines) and measured data (coloured lines) for Np breakthrough in runs #31 and #32

A1.1-3.2.6 Predictions and measurements of U breakthrough

Figure A1.1-3.8 shows the predictions and measured data for U breakthrough in runs #31 and #32. As in the case of Np, the predictions for run #31 and run #32 are similar, due the fact that U is transported predominantly as an aqueous solute in both runs.

The experimental data for run #31 and run #32 coincide closely with each other (again, as in the case of Np), but differ significantly from the predictions. In particular, the peak in the measured data is higher and earlier that that of the predictions. It appears that the sorption of U on the matrix pore surfaces has been overestimated using the sorption coefficients given in Table A1.1-2.1. Possible reasons for this are discussed in detail in Moeri (2004) and Missana & Geckeis (2006) [21].

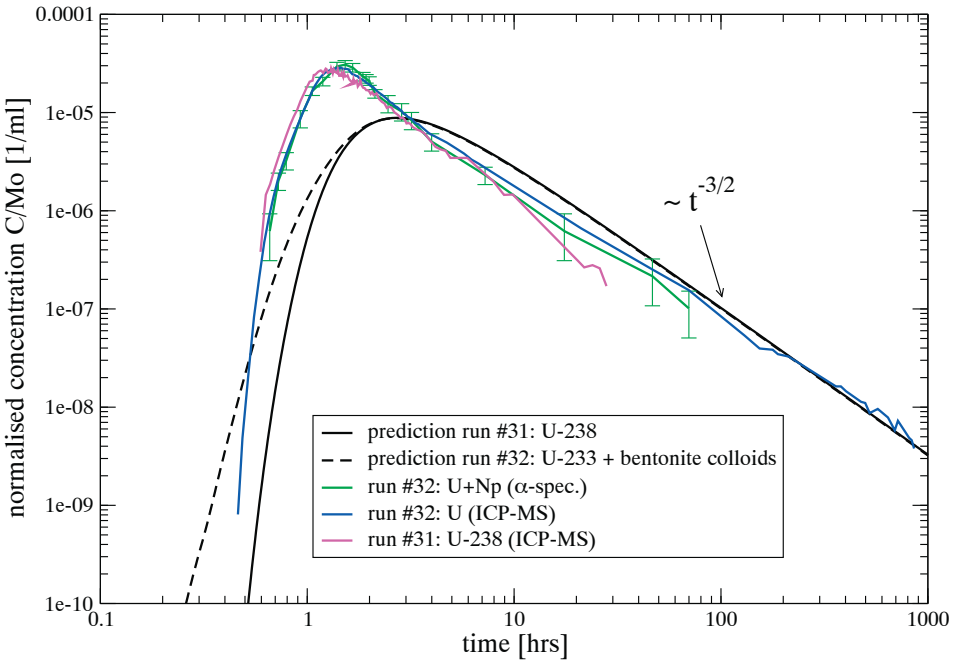

Fig. A1.1-3.8: The predictions (black full and dashed lines) and measured data (coloured lines) for U breakthrough in runs #31 and #32

[21] Another possible reason, as discussed in Bradbury & Baeyens (2003), is that scaling effects, experimental procedures or mineralogical variability can lead to sorption coefficients measured in laboratory experiments differing by a factors of about 5 from those applicable *in situ*, although it is unclear why this should be a difficulty in the case of U, but not, say, in the case of Np in the present study.

A1.1-3.2.7 Predictions and measurements of Cs breakthrough

Figure A1.1-3.9 shows the predictions and measured data for Cs breakthrough in run #32; Cs was not used in the injection cocktail for run #31. Cs has a colloid bound fraction (about 15 %) that is intermediate between the high values (98 % and 72 %) for Am and Pu on the one hand, and the much lower values for Np (9 %) and U (2 %) on the other. Both colloidal and aqueous phase transport are significant and, since sorption of Cs on matrix pore surfaces is relatively strong, the aqueous component is significantly retarded. This gives rise to two peaks in the breakthrough curves. The first corresponds to the breakthrough of Cs sorbed on bentonite colloids. The second corresponds to the breakthrough of Cs transported in aqueous solution and delayed by matrix diffusion and sorption on the porous rock matrix.

Both prediction and experimental results show two peaks and there is reasonable agreement in their times of occurrence. There are, however, discrepancies in the magnitudes of the peaks, which may be attributed, at least in part, to inaccuracy in assumed colloid bound fraction (see ChapterA1.1-4). In the case of the second peak, additional factors contributing to the discrepancy between prediction and experiment could include neglecting of the possibility of sorption disequilibrium[22], and neglecting non-linear sorption and the natural background concentration of Cs in the predictions.

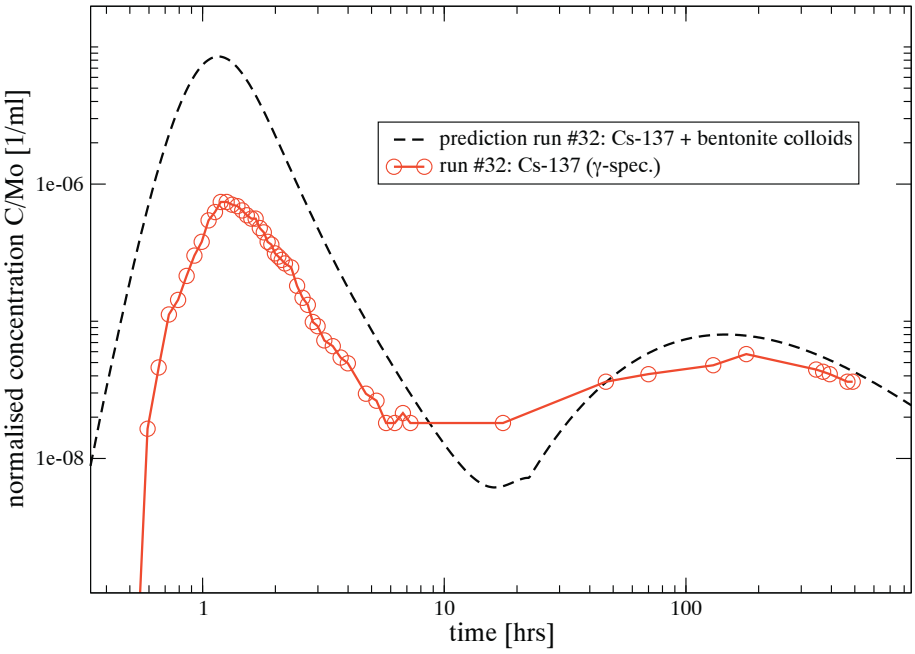

Fig. A1.1-3.9: The predictions (black dashed line) and measured data (coloured line) for Cs breakthrough in run #32

[22] As discussed in Geckeis et al. (2004), references therein and also in the present report, it has been observed that radionuclide sorption to Grimsel fracture infill minerals is dependent on contact time

A1.1-4 Review and modification of model concepts and parameters in the light of the measured data and the comparison between predictions and measurements

A1.1-4.1 General observations

As noted in the previous sections, the measured breakthrough data for runs #31 and #32 showed clear evidence for the association of a number of radionuclide tracers with colloids. In the case of run #32, Figure A1.1-4.1 shows the breakthrough data for colloids, as well as for Am, Pu, Th and Cs. All are normalised to 100 % recovery, and, in the case of breakthrough curves measured using colloid detection techniques (LIBD, PDS, PCS and ICP-MS[23]), the background concentration of natural groundwater colloids from the measured colloid concentrations has been subtracted off.

It can be seen that the breakthrough curves for colloids coincides closely with those of Am, Cs, Pu, Th, and also with that of the conservative tracer iodine, although the conservative tracer peaks slightly later and, as noted previously, Cs displays a second peak at a much later time. These observations support the model assumption that a part of the inventory of these radionuclides is transported in association with colloids. The discrepancies between some measured breakthrough data and the predictions, however, call into question the assumptions regarding the proportions of some tracers that are associated with colloids, as well as the parameters describing the non-Fickian dispersion of colloids, as discussed in the following sections.

The estimated recoveries for the colloids confirm in principle the results from the preliminary runs in dipole 3. The small colloid size classes show a nearly complete recovery as indicated by the breakthrough measured with the LIBD and the PDS. The recovery is decreasing with increasing colloid size. The bulk mass recovery extracted from the normalisation of the breakthrough curves in Figure A1.1-4.1 for all size classes is therefore lower: between 57 % (measured with PCS) and 70 % (Al content measured with ICP-MS). The bulk mass recoveries are indeed not comparable between both dipoles, because the size distributions of the injected bentonite colloids are different. There are much less bigger colloids injected in run #32 and the effect of filtration of the bigger colloids does not decrease the mass recovery as much as in the runs in dipole 3.

[23] Aluminium concentrations at the withdrawal well were measured with inductively coupled plasma mass spectrometry (ICP-MS). Aluminium has been taken as an alimental indicator for clay colloids.

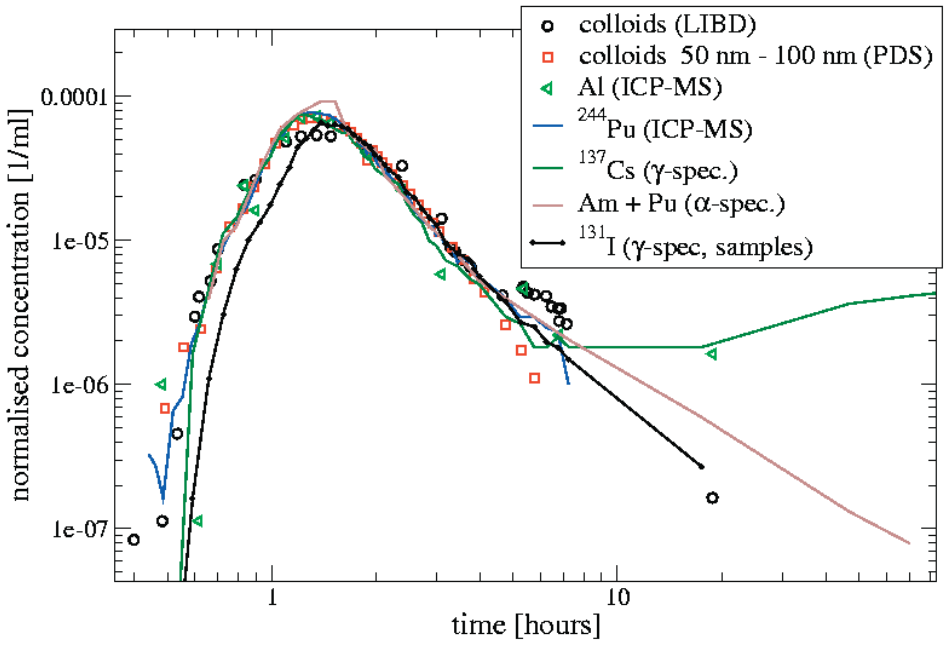

Fig. A1.1-4.1: The breakthrough data for colloids and tracers conveyed almost entirely (Am and Pu) or in part (Cs) on colloids from run #32

A1.1-4.2 The association of radionuclides with colloids

A1.1-4.2.1 The influence of bentonite colloids on transport

At first sight, the results in Chapter A1.1-3 appear to suggest that the presence of bentonite colloids significantly affected transport only in the case of Cs. U and Np were transported predominantly as aqueous species. Am, Pu, Th, Tb and Hf were transported in colloidal form, even when no bentonite colloids were added to the injection cocktail. The addition of bentonite colloids does, however, significantly affect the *recovery* of these tracers.

A comparison of the recoveries of Th, Tb and Hf, without and with bentonite colloids, clearly indicates that the presence of bentonite colloids substantially increases recovery (Möri 2001a). This suggests that, without the addition of bentonite colloids, a significant fraction of the injected inventories of these tracers enters the dipole as aqueous solutes. These solutes are then retarded to such an extent that they do not breakthrough over the timescale of the experiments. With the addition of bentonite colloids, greater proportions of the injected inventories enter the dipole in association with colloids, and thus experience little or no retardation during transport, increasing recovery.

A1.1.-4.2.2 Characterisation of the colloid bound fractions in the injection cocktails

The injection cocktails for run #31 and #32 were not completely characterised at the time the predictions were calculated. Although the fraction associated with bentonite colloids can be estimated on the basis of batch experiments (Tab. A1.1-2.1), it was not clear if, and to what extent, elements form or become associated with other types of colloids e.g. by the precipitation

of hydroxide/oxide colloids and/or sorption on natural groundwater colloids[24]. The proportion of any given tracer transported on colloids (or in colloidal form) was therefore uncertain and, especially in the case of Am and Pu, led to significant discrepancies between predictions and measurements in the case of run #31.

After the predictions had been made, the injection cocktail was analysed, allowing the mass of each element in solution and the mass bound to colloids to be determined directly. The mass bound to colloids in the case of run #32 was found to be generally similar to that assumed for predictive modelling, as shown in Table A1.1-4.1. It was, however, confirmed that some tracers, most notably Th, Pu and Am, were injected and transported in colloidal state even in run #31 in the absence of bentonite colloids. An extensive discussion on these findings and possible reasons for them can be found in Moeri (2004) and Missana & Geckeis (2006).

Tab. A1.1-4.1: Comparison of the colloid bound fraction used for predictive modelling of run #32 (see Tab. A1.1-2.1)

The measured colloidal fraction in the injection cocktail and the fraction extracted from the normalisation of the colloid breakthrough curves

Tracer	**Calculated fraction sorbed on bentonite colloids [%]**	**Colloidal fraction measured in the injection cocktail [%]** (see Moeri 2003)	**Fraction associated to colloids calculated from normalisation of the measured breakthrough curves [%]** (compare Fig. A1.1- 4.1)
Am-241	97.7	99	55 (Am + Pu, α-spec. by PSI)
Pu-244	72.2	84	90 (ICP-MS by FZK)
Pu-238	72.2	84	
Cs-137	14.8	8	1
Np-237	9.1	0-1	
U-233	1.6	6	
Tc-99	0.7	12	
Th-232	97.6	94	70
Sr-85	not known	0	
I-131	0	0	

With this information it was then possible to recalculate the breakthrough curves by correcting the relative amount of radionuclides transported as colloids and the amount transported in solution. The result was a reasonable fit of all the measured breakthrough curves. There remains, however, a systematic time difference of a few minutes between predicted and measured breakthrough curves, a possible reason for which is suggested in Chapter A1.1-6, as well as a discrepancy between predicted and modelled tailing of colloid breakthrough curves, which required a further modification of the non-Fickian dispersion parameters, as discussed below.

[24] There is, however, some evidence that the impact of natural groundwater colloids is negligible (see, e.g. Kosakowski & Baeyens 2001)

A1.1-4.3 Dispersion of colloids

Figures A1.1-3.5 and A1.1-3.6 show a change in slope (at about 3-4 hours after injection in the experimental data in the former case) that occurs as the dominant transport meachanism changes from colloid facilitated transport to solute transport with matrix diffusion (the slope of the breakthrough curve beyond this change is proportional to $t^{-3/2}$, which is a signature of matrix diffusion). At earlier times, Figure A1.1-3.5 in particular indicates that the slope of the experimental breathrough curves is somewhat shallower than the predictions, which were made using the non-Fickian dispersion (CTRW) model. This observation suggests the main fitting parameter of the model responsible for tailing (β) needs to be revised.

Figure A1.1-4.2 shows the good fit than can be obtained to the measured data for colloids, as well as tracers conveyed almost entirely (Am and Pu) or in part (Cs) on colloids, if β is decreased from 1.2 to 1.1. The lower value for β for dipole 1 than the one derived for dipole 3 indicates a stronger heterogeneity of the underlying flow field (see e.g. Kosakowski et al. 2001; Berkowitz et al. 2001).

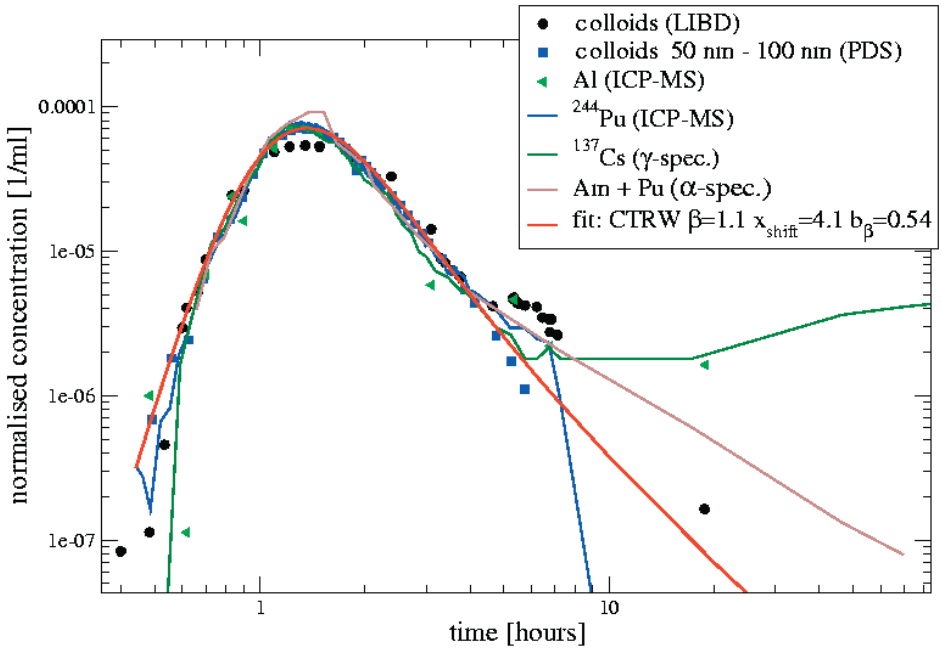

Fig. A1.1-4.2: The breakthrough data for colloids and tracers conveyed almost entirely (Am and Pu) or in part (Cs) on colloids from run #32, and a fit using the non-Fickian dispersion (CTRW) model

CRTW parameters are β = 1.1, t_{mean} = 4.1 hours and b_β = 0.45. The calculated mean particle velocity is 1.7×10^{-4} m s^{-1}

A1.1-5 Justification for the use of the non-Fickian dispersion model for colloid transport

A1.1-5.1 Possible factors affecting the tailing of colloid breakthrough curves

It was shown in Chapter A1.1-3 that fit of the 1-D and 2-D advection-dispersion models without matrix diffusion to the breakthrough data for colloids, or radionuclides associated with colloids, was not entirely satisfactory. In particular, it was not possible to fit both the early concentrations and the late concentrations with one dispersion length (Fig. A1.1-3.1). The non-Fickian dispersion (CTRW) model, which provides a more generally applicable representation of advective and hydrodynamic dispersion processes in highly heterogeneous media, gave a considerably improved fit. As discussed in Kosakowski (2004) and Kosakowski & Smith (2004), this is in accordance with increasing evidence of non-Fickian dispersion reported in the literature. Such non-Fickian dispersion gives rise to a scale-dependent spreading of contaminant plumes, as well as earlier breakthrough times or longer late time tails in breakthrough curves, compared with the predictions of a Fickian representation of dispersion.

The similarity of the measured breakthrough data for conservative tracers and colloids (see, e.g. Fig. A1.1-4.1), however, raises the question as to whether matrix diffusion of colloids, rather than non-Fickian dispersion of colloids, could provide an equally satisfactory explanation of the tailing behaviour of the colloid breakthrough data. This possibility is considered in Section A1.1-5.2. A number of other explanations have also been proposed for the tailing of solute and colloid breakthrough curves in fractured geological media (Becker & Shapiro 2000), including that it is an artefact of the tracer injection process, the result of the finite width of the dipole flow field, or the result of the interactions with the fracture walls. These possibilities are considered in Kosakowski (2004) and it was found, that there is no evidence that such processes influence the transport.

A1.1-5.2 Evidence for the influence of non-Fickian dispersion on the tailing of colloid breakthrough curves

The observation that the fit of the 1-D and 2-D advection-dispersion models to the breakthrough data for colloids is not entirely satisfactory is consistent with previous experimental studies on both solutes and colloids (e.g. Hatano & Hatano 1998; Sidle et al. 1998; Becker & Shapiro 2000). These show that advective processes in heterogeneous media can cause tailing of breakthrough curves that is not adequately described using advection-dispersion models based on a Fickian representation of dispersion. There are also more general reasons for questioning the adequacy of the Fickian representation of the dispersion. For example, studies of the breakthrough of solutes transported through geological media, interpreted using the Fickian representation of dispersion, indicate that the longitudinal dispersion length increases with the scale of the system under consideration (see, e.g., Gelhar et al. 1992). This suggests that, while such a model may, to some approximation at least, represent the shapes of breakthrough curves, the spatial distribution of the solutes within the media will be in error. A more detailed study on this topic can be found in Berkowitz & Scher (1995).

The CTRW model used in the present study represents a general, physically based approach to the quantification of non-Fickian dispersion. Berkowitz & Scher (1998) conducted numerical experiments for particle transport in 2-D networks of fractures. They could show that non-Fickian dispersion does indeed occur, resulting from subtle features of the steady flow-field distribution through the network, and there is good quantitative agreement between their simulations and the CTRW approach. Park et al. (2003) extended this approach to the investigation of particle transport in 3-D fracture networks. Transport simulations at fracture

intersections showed that local flow circulations can arise from variability within the hydraulic head distribution along fracture intersections and from the internal no flow condition along fracture boundaries. They found that local flow cells act as an effective mechanism to enhance the non-Fickian breakthrough tailing in discrete fracture networks. It was also shown that transport in such systems can be modelled by considering advection in the complex flow field using the CTRW approach. Applications of this approach to experimental systems are reported, for example, by Berkowitz et al. (2000) for laboratory flow cells containing heterogeneous porous media, and by Kosakowski et al. (2001) for a medium-scale field experiment in a fractured till.

The Excavation Experiment (EP) described in Ota et al. (2002) and Möri et al. (2006) focused on the detailed investigation of the shear-zone structure. It was already known that the shear zone is highly heterogeneous, and the main result of the EP core analyses was to show that open channels in water conducting features or fractures within the shear zone control tracer migration to a very high degree. Tracers were found in dead-end channels, short cuts between adjacent channels and merging and bifurcations of pathways occurred on the meter and centimetre scale. In the case of CRR, hydraulic tomography and inverse modelling also showed that the shear zone is highly heterogeneous, especially the area around dipole 1.

In natural fracture networks, dead-end channels are not really "dead" in terms of fluid flow. Small pressure differences will set up local flow cells and particles can advectively enter such flow cells and will be delayed compared to particles not entering such low velocity zones. In general, the occurrence of low velocity regions will cause a delay of some particles. From structural geological investigations, it is known that the flow channels are partially filled with non-cohesive fault gouge material and water flow is also possible in the highly porous fault gouge material (Smith et al. 2001b; Möri et al. 2006). Flow and transport processes in the open parts of the shear zone will differ completely from the ones in the fault gouge filled parts (Lunati et al. 2003). It can be expected that the fluid velocities, and therefore the particle velocities, are higher in the open channels than in the filled parts of the fracture. Particles entering the filled fractures are delayed. Furthermore, in the fault gouge filled parts, transport behaviour is likely to be much smoother, with tracer fronts moving much more regularly than in open rough fractures.

By comparing the findings of the EP project (Möri et al. 2006) and other tests on the CRR shear zone with the numerical investigations of Park et al. (2003), it can be inferred that the occurrence of an interconnected network of open channels in conjunction with low velocity regions (e.g. in dead-end channels) is one possible reason for the observed non-Fickian tailing of colloid breakthrough curves.

A1.1-6 Remaining problems and limitations of the current modelling approach

A1.1-6.1 Fluctuations in the experimental extraction and injection flowrates and the heterogeneous characteristics of the shear zone

As noted in Chapter A1.1-4.2, there is a systematic time difference of a few minutes between predicted and measured breakthrough curves. This time shift can be attributed to small changes in the experimental extraction and injection rates between the runs. For example, Figure A1.1-6.1 shows how the extraction flow rates and the injection flow rates are related to the differences between the peak arrival time for uranine in dipole 1 and the peak of the injection function. The late arrival times for runs #1, #2 and #3 are strongly (and inversely) correlated to the injection flow rate. Peak arrival times for the other runs show a less systematic relationship to the injection flow rate, but there is an indication that, counter-intuitively, increased extraction flow rates cause later peak arrival times. This behaviour is contrary to the behaviour one would expect for an ideal dipole flow field in a homogeneous aquifer. Similar findings are also described in Guimerà & Carrera (2000). Possible explanations are related to the spatial heterogeneity of the shear zone (see also Chapter A1.1-5) or the influence of the hydraulic boundary conditions (e.g. flow field around the tunnel, regional hydraulic gradients).

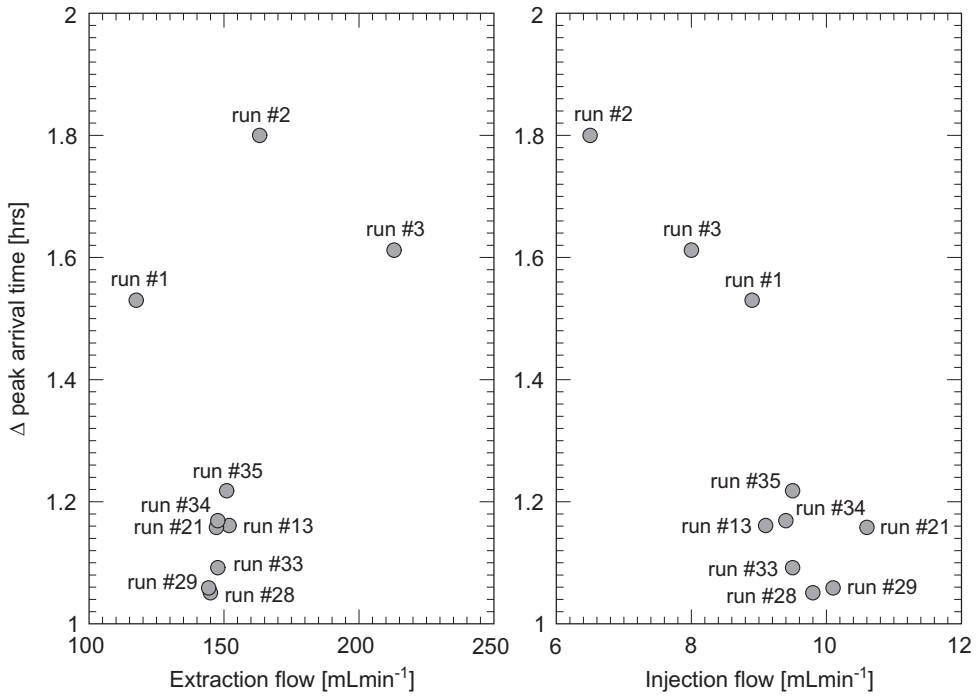

Fig. A1.1-6.1: Correlation between extraction flow rate, injection flow rate and peak arrival time for uranine in dipole 1

A1.1-6.2 Non-uniqueness of the fitted model parameters

The model parameters were set, to some extent, using information from the experimental set-up (e.g. the dipole length, the injection concentrations) and information from independent sources (e.g. sorption parameters). It was not, however, possible to make model predictions purely on the basis of such information. The models had to be calibrated against preliminary tests using curve-fitting procedures. Due, however, to the number of parameters to be calibrated, the

limited duration and accuracy of the experiments and the fact that the models provide a highly simplified representation of the actual shear zone system, not all parameters could be uniquely determined in this way. Different sets of parameters could, in some cases, fit particular breakthrough curves equally well. Thus, for example, it was possible to set only a lower bound to the effective matrix thickness and the single fracture representation of the shear zone, and multiple (four) fracture representations were equally successful in fitting the breakthrough curves.

The latter observation may be understood by considering that, in the absence of retardation processes, the main parameter influencing advective transport is the (mean) fluid velocity. In the case of the dipole experiments the volume flow rates through the system is fixed by the injection and extraction flow rates. For such experimental conditions the fluid velocity in the idealised shear zone depends only on the sum of the fracture apertures. The velocity field in a single fracture of aperture $2b$ is identical with the velocity field in a system of four fractures with the apertures $2b/4$. Matrix diffusion is a more effective retardation process for a system of four narrower fractures, compared to a single broad fracture. It is, however, relatively easy to adjust the value of the porosity of the matrix rock or the diffusion coefficient to compensate the change in the fracture aperture without changing the fit. Eventually changes of the matrix porosity induce changes in the (fitted) sorption coefficients. Of course not all combinations of porosity, diffusivity and fracture aperture are possible. All parameters should be reasonable and in the range defined by additional information.

The transmissivity of the system of four narrower fractures is different to that of a single broader fracture. For a given flowrate, this will lead to a different pressure difference between in inlet in the two conceptualisations. In principle, the measurement of the actual pressure difference could be used to discriminate between the conceptualisations. In practice, however, such discrimination would require a reliable theoretical relationship between transmissivity and aperture. For flow between parallel plates, the so-called "cubic law" can be used (Witherspoon et al. 1980), but this relationship generally fails to hold for the heterogeneous fractures found in geological systems. It was shown by Meier et al. (2001) that the shear zone used in CRR is hydraulically highly heterogeneous and that it is not possible to uniquely model the hydraulic behaviour of the shear zone (and hence the aperture and number of fractures appropriate for the transport modelling) based on current hydraulic information.

A1.1-6.3 Filtration of colloids

The models used in the present study did not address the issue of colloid immobilisation or filtration during transport. There are, however, clear indications that that filtration of larger colloids took place in the CRR *in situ* tests. Figure A1.1-6.2 shows the breakthrough data for colloids of different size fractions, as well as for uranine, indicating the recovery for each size fraction.

The recoveries for the different colloid size classes in Figure A1.1-6.2 decrease systematically with increasing size. PDS measurements for the two smallest colloid size classes yield recoveries of more than 90 %, whereas particles in bigger size classes (not shown in Fig. A1.1-4.2) yield very low recoveries.

Immobilisation of colloids can occur as a result of mechanical filtration, sedimentation (gravitational settling), and electrochemical filtration such as electrostatic attraction or chemical adsorption. Electrochemical filtration does not explain the observation that it is the larger particles that are immobilised to the greatest extent; James & Chrysikopoulos (1999, 2000) showed that this mechanism would lead to the smallest particles being preferentially deposited

onto the fracture walls. Furthermore, at the high pH-value of the Grimsel groundwater (pH~9.6), bentonite colloids, as well as the natural groundwater colloids and the rock surface, possess a negative surface charge and the attachment of colloids to the rock surface is not favoured (Degueldre et al. 1996a, b). The short mean residence time of the bentonite colloids in the shear zone due to the high fluid velocities during the tracer tests also minimises the probability of an interaction between colloids and fracture surfaces. Gravitational settling and/or mechanical filtration are, however, both possible immobilisation mechanisms.

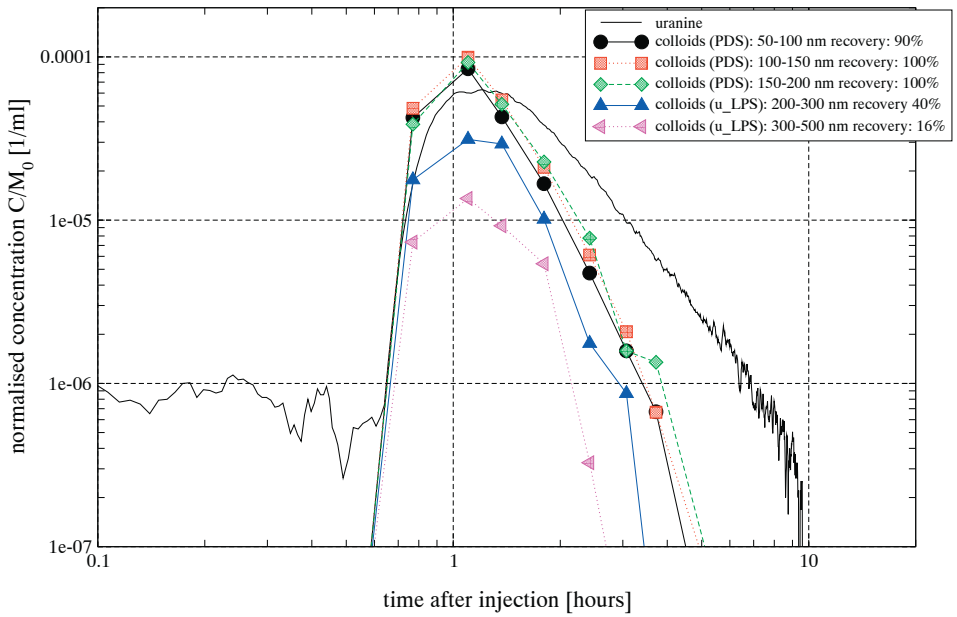

Fig. A1.1-6.2: The breakthrough data for bentonite colloids from run #6a, and uranine from run #6 (without normalisation to 100 % recovery)

A1.1-6.4 The possibility of non-Fickian dispersion of solutes

As shown in Chapter A1.1-3, it was possible to fit the breakthrough curves of both conservative and sorbing tracers that are transported in the aqueous phase very successfully with the advection-dispersion-matrix diffusion conceptual model developed during MI. Nevertheless, given the evidence for non-Fickian dispersion of colloids (Section A1.1-5.2), it seems reasonable to suppose that tracers in the aqueous phase may also undergo a degree of non-Fickian dispersion. Non-Fickian dispersion is unlikely to account fully for the form of all the breakthrough curves; the breakthrough data for Sr in Figure A1.1-4.1 shows the typical behaviour normally associated with matrix diffusion, namely the $t^{-3/2}$ slope of the tail (see e.g. Tsang 1995; Hadermann & Heer 1996; Jakob 1997). Some impact of non-Fickian dispersion cannot, however, be discounted, although the breakthrough curves of sorbing and non-sorbing aqueous-phase tracers were not fitted using the CTRW model, because matrix diffusion effects have not, as yet, been incorporated. Indeed, the fact that the tailing of the breakthrough curves for colloids and conservative tracers is so similar suggests that matrix diffusion is not an important contributory process to the tailing of either, at least over the duration of the experiments.

A1.1-6.5 Artefacts associated with model simplifications

The sorption coefficient for Sr has been obtained by fitting the advection-dispersion models to the breakthrough curves for run #21 (see Tab. A1.1-3.2). If part of the tailing attributed in these fits to matrix diffusion is in fact caused by non-Fickian dispersion, then the sorption coefficient may have been underestimated - i.e., in reality, there may have been less matrix diffusion, but higher sorption in the porous rock matrix.

The overestimation of matrix diffusion (and the associated underestimation of sorption) is a possible partial explanation[25] for the differences between distribution coefficients measured in the laboratory and distribution coefficients extracted from the field experiments. For example, values of sorption coefficients K_d for sorption of Sr on fault gouge material measured in the laboratory with batch experiments do not correspond to those found by fitting the *in situ* experiments. Furthermore, the present modelling has assumed equilibrium sorption. However, as discussed in Geckeis et al. (2004), references therein and also in the present report, it is has been observed that radionuclide sorption to Grimsel fracture infill minerals can depend on contact time.

A related model artefact associated with the modelling of a complex heterogeneous system as a set of parallel fractures is that the effective fracture surface available for matrix diffusion might be underestimated. In a fracture network, the available surface is much larger than in a set of parallel fractures with the same hydraulic transmissivity. In local flow cells, the fluid velocity is smaller and any solutes entering such slow velocity zones have more time to diffuse into the matrix.

All of these effects, i.e. non-Fickian dispersion, different time constants characterising matrix diffusion in slow velocity regions, possible non-equilibrium sorption, and a possible underestimation of the available surface area for matrix diffusion, have to be compensated by an appropriate choice of values for the fitting parameters (fracture aperture/effective surface area, fluid velocity, matrix porosity, pore diffusion coefficient for matrix diffusion and sorption coefficients in the matrix) when fitting the breakthrough curves with a matrix diffusion model utilising the parallel plate representation of a fracture.

A1.1-7 Conclusions

A1.1-7.1 General

This document has described modelling work by PSI to analyse *in situ* experiments carried out at the GTS within the framework of the CRR project. The modelling work took as its starting point earlier modelling carried out by PSI in the context of the Migration Experiment (MI), and developed and modified the earlier models to take account of the effects of bentonite colloids added to the experimental injection cocktails. A number of alternative modelling approaches were developed for some aspects of the system. In some cases, it was possible to make model predictions in advance of particular experimental runs in order to check the feasibility of the planned experiments. The fitting of models to the experimental breakthrough data and the prediction of experimental breakthrough in advance of the main experimental runs enabled modelling hypotheses to be tested and improvements in the models to be made. The work has certain implications for safety assessment as discussed at the end of this chapter.

---

[25] In addition, Bradbury & Baeyens (2003) showed that sorption coefficients measured in laboratory experiments can differ by factors of about 5 from those applicable *in situ* due to scaling effects, experimental procedures or mineralogical variability.

A1.1-7.2 Aqueous phase transport

The modelling work described in this report showed that it is possible to fit the breakthrough curves of both conservative and sorbing tracers that are transported in the aqueous phase very successfully with the advection-dispersion-matrix diffusion conceptual model developed during MI.

A1.1-7.3 Colloid-facilitated radionuclide transport

The CRR experiment and the modelling work described in this report show that, in the *in situ* tests:

- Am, Pu, Th are transported principally in association with colloids, and
- Cs is also transported in small parts in association with colloids, although the main part of the injected inventory is transported in solution.

Furthermore, some radionuclide tracers, namely Am, Pu, and Th (and also Tb and Hf) are transported in colloidal form, even when no bentonite colloids are added to the injection cocktail. The addition of bentonite colloids, however, increases the recovery of these tracers.

Colloids showed little or no retardation during transport - there was a marked similarity between the breakthrough of colloids and that of a conservative tracer, and indeed the peak breakthrough for colloids occurred slightly earlier. Hydrodynamic chromatography, the retardation of colloids according to their size, could not be observed. Some colloids were, however, filtered during transport. The dependence of the degree of filtration on colloid size suggests that gravitational settling and/or mechanical filtration are the most likely immobilisation mechanisms.

A1.1-7.4 1-D vs. 2-D modelling of the breakthrough curves

The 1-D and 2-D advection-dispersion models with matrix diffusion provided similarly good fits to the breakthrough curves of tracers conveyed as aqueous solutes. This is because the experiments were conducted in a "weak" or narrow dipole, with a nearly radial convergent flow field around the withdrawal well and most of the injected tracer following a nearly direct line from the injection to the withdrawal well. In such a flow field, the effect of the width of the flow field is minimised, and a single, 1-D transport path adequately described the system.

A1.1-7.5 Non-Fickian dispersion

The experiments showed a significant tailing in the breakthrough of colloids, as well as conservative and sorbing tracers. The tailing of the breakthrough curves of tracers transported as aqueous species is generally attributed to a mixture of hydrodynamic dispersion and matrix diffusion. In the case of colloids, an advection-dispersion model with matrix diffusion, where dispersion was modelled as a Fickian process, could reproduce the shape of the observed breakthrough curves, but not with a consistent set of parameters. A number of other possible explanations for the tailing of the breakthrough data for colloids have been reviewed, and it was shown that non-Fickian dispersion is the most likely cause. In the case of solutes, the possibility of non-Fickian dispersion also exists, but, in the present study, it has not been possible to discriminate between the impact of non-Fickian dispersion of solutes and matrix diffusion effects on the shape of the breakthrough curves. The topic of non-Fickian dispersion is currently under further investigation at PSI (Kosakowski 2004).

A1.1-7.6 Implications for safety assessment

The models applied to modelling the CRR *in situ* tests are highly simplified, and may well only be applicable, or "valid", over the spatial and temporal scales of the CRR experiments. The main limitation lies in the assumption that the fraction of a tracer that is bound to colloids remains constant during migration - i.e. there is no further sorption of radionuclides to (or desorption from) colloids. For the relatively short transport times of the colloids in these experiments, it may be reasonable to assume that sorption and/or desorption on bentonite colloids is sufficiently slow to be neglected. For repository safety assessment, on the other hand, the relevant transport times are much longer and this assumption may not hold.

The modelling approach used in the present study may therefore not be directly applicable to safety assessment problems and the direct implications for the results of this study for safety assessment are limited. It can, however, be said that the study has demonstrated the high degree of mobility of bentonite and other colloids in a system that is at least in some ways comparable to those of interest in safety assessment, and has shown that bentonite colloids can *at least potentially* affect the transport of some safety relevant radionuclides over longer time and space than those addressed here. It has also shown that parameters for safety assessment (and especially sorption coefficients) derived by fitting field tracer transport experiments using advection-dispersion models based on Fickian dispersion with matrix diffusion need to be viewed with caution.

A1.1-8 Acknowledgements

The authors thank Res Möri (GI) for many helpful discussions, and Andreas Jakob and Ralph Mettier (PSI) for useful comments and various corrections.

The CRR project is conducted in the frame of Phase V of the Grimsel Test Site and the project partners are NAGRA (Switzerland), ENRESA (Spain), ANDRA (France), JNC (Japan), SNL (USA) and FZK-INE (Germany). The partners are thanked for kindly provided the data from the CRR experiments. This work was partially funded by NAGRA.

A1.1-9 References

Barten W. (1996). Linear response concept combining advection and limited rock matrix diffusion in a fracture network transport model. Water Resour. Res. 32 (11), 3285-3296.

Barten W. & Robinson P. C. (2001). Contaminant transport in fracture networks with heterogeneous rock matrices: The PICNIC code. PSI Report 01-02, Paul Scherrer Institute, Villigen, Switzerland.

Bear J. (1972). Dynamics of fluids in porous media, Elsevier, New York.

Becker M. W. & Shapiro A. M. (2000). Tracer transport in fractured crystalline rock: Evidence of nondiffusive breakthrough tailing, Water Resour. Res., 36 (7), 1677-1686.

Berkowitz B. & Scher H. (1995). On characterization of anomalous dispersion in porous and fractured media, Water Resour. Res., 31(6), 1461-1466.

Berkowitz B. & Scher H. (1998). Theory of anomalous chemical transport in fracture networks, Phys. Rev. E, 57(5), 5858-5869.

Berkowitz B., Scher H. & Silliman S. E. (2000). Anomalous transport in laboratory-scale, heterogeneous porous media, On characterization of anomalous dispersion in porous and fractured media, Water Resour. Res., 36 (1), 149-158, (with a minor correction, published in Water Resour. Res., 36 (5), 1371).

Berkowitz B., Kosakowski G., Margolin G. & Scher H. (2001). Application of Continuous Time Random Walk theory to tracer test measurements in fractured and heterogeneous porous media, Ground Water, 39 (4), 593-604.

Bradbury M. & Baeyens B. (2003). Near-field sorption data bases for compacted MX-80 bentonite for performance assessment of a high-level radioactive waste repository in Opalinus Clay host rock. Nagra Technical Report NTB 02-18. Nagra, Wettingen, Switzerland.

Degueldre C. & Laube A. (2000). Bentonite colloid migration in a granitic fracture at the Grimsel Test Site. Technical Report TM-44-00-07, Paul Scherrer Institute, Villigen, Switzerland.

Degueldre C., Grauer R., Laube A., Oess A. & Silby H. (1996a). Colloid properties in granitic groundwater systems. II: Stability and transport study, Applied Geochemistry, 11, 697-710.

Degueldre C., Pfeiffer H.-R., Alexander W. R., Wernli B. & Brütsch R. (1996b). Colloid properties in granittic groundwater systems – I: sampling and characterization. Applied Geochemistry, 11, 677-695.

Fierz Th., Geckeis H., Goetz R. & Geyer F. W. (2001). GTS V / CRR: Tracer Tests #1-#16 (September 1999-January 2001). Unpubl. Nagra Internal Report, Nagra, Wettingen, Switzerland.

Frick U., Alexander W. R., Baeyens B., Bossart P., Bradbury M. H., Bühler Ch., Eikenberg J., Fierz Th., Heer W., Hoehn E., McKinley I. G. & Smith P. A. (1992). Grimsel Test Site – The Radionuclide Migration Experiment: Overview of investigations 1985-1990. Nagra Technical Report NTB 91-04, Nagra, Wettingen, Switzerland.

Geckeis H. (2001). Reply to the note AN-44-01-19: G. Kosakowski, B. Baeyens, Sorption capacity of natural colloids in Grimsel water. Unpubl. short note, Institut für Nukleare Entsorgung, Forschungszentrum Karlsruhe, Karlsruhe, Germany.

Geckeis H., Schäfer T., Hauser W., Rabung Th., Missana T., Degueldre C., Möri A., Eikenberg J., Fierz Th.& Alexander W.R. (2004): Results of the Colloid and Radionuclide Retention experiment (CRR) at the Grimsel Test Site (GTS), Switzerland - Impact of Reaction Kinetics and Speciation on Radionuclide Migration. Radiochim. Acta 92, 765-774.

Gelhar L. W. (1987). Applications of stochastic models to solute transport in fractured rocks. SKB Technical Report 87-05, SKB, Stockholm, Sweden.

Gelhar L. W., Welty C. & Rehefeldt K. R. (1992). A Critical Review of Data on Field-Scale Dispersion in Aquifers; Water Resources Research, Vol. 28 (7), 1955-1974.

Guimerà J. & Carrera J. (2000). A comparison of hydraulic and transport parameters measured in low-permeability fractured media. Journal of Contaminant Hydrology, 41, 261-281.

Hadermann J. & Heer W. (1996). The Grimsel (Switzerland) migration experiment: integrating field experiments, laboratory investigations and modelling. Journal of Contaminant Hydrology, 21, 87-100.

Hatano Y. & Hatano N. (1998). Dispersive transport of ions in column experiments: An explanation of long-tailed profiles, Water Resour. Res., 34(5), 1027-1033.

Heer W. & Hadermann J. (1996). Modelling Radionuclide Migration Field Experiments. Nagra Technical Report 94-18, Nagra, Wettingen, Switzerland.

Jakob A. (1997). Modelling solute transport using the double porous medium approach. In: Grenthe, I. & Puigdomenech, I. (eds.), Modelling in Aquatic Chemistry. OECD/NEA, Paris, France.

James S. C. & Chrysikopoulos C. V. (1999). Transport of polydisperse colloid suspensions in a single fracture, Water Resour. Res., 35 (3), 707-718.

James S. C. and Chrysikopoulos C. V. (2000). Transport of polydisperse colloids in a saturated fracture with spatially variable aperture, Water Resour. Res., 36 (6), 1457-1465.

Kolditz O., Habbar D., Kaiser R., Rother T. & Thorenz C. (1999). RockFlow - Theory and Users Manual. Release 3.4, Institut für Strömungsmechanik und Elektr. Rechnen im Bauwesen, Universität Hannover.

Kosakowski G. (2004). Anomalous transport of colloids and solutes in a shear zone. Journal of Contaminant Hydrology, 72, 23-46.

Kosakowski G. & Baeyens B. (2001). Sorption capacity of FEBEX bentonite and natural groundwater colloids. Unpubl. PSI Internal Report AN-44-01-19, Paul Scherrer Institute, Villigen, Switzerland.

Kosakowski G. & Smith P. A. (2004). Modelling of transport in the Grimsel Migration shear zone. Nagra Technical Report NTB 04-01. Nagra, Wettingen, Switzerland.

Kosakowski G., Berkowitz B. & Scher H. (2001). Analysis of field observations of anomalous transport in a fractured till. Journal of Contaminant Hydrology, 47, 29-51.

Lunati I., Kinzelbach W. & Sørensen I. (2003). Effects of pore volume-transmissivity correlation on transport phenomena, J. Cont. Hydrol. 67, p.195-217.

Meier P. M., Medina A. & Carrera J. (2001). Geostatistical inversion of cross-hole pumping tests for identifying preferential flow channels within a shear zone, Groundwater, 39 (1), 10-17.

Missana T. & Geckeis H. (eds.) (2006). The CRR final project report series II: Results of the Supporting Laboratory Programme. Nagra Technical Report NTB 03-02. Nagra, Wettingen, Switzerland.

Möri A. (2001). GTS V - CRR Experiment: Scoping calculations, base data set V-3 (actualised May 2001). Unpublished Nagra Internal Note, Nagra, Wettingen, Switzerland.

A. Möri (ed.) (2004). The CRR final project report series I: - Description of the Field Phase - Methodologies and Raw Data. Nagra Technical Report NTB 03-01. Nagra, Wettingen, Switzerland.

Möri A., Alexander W. R., Ota K. & Frieg B. (2006) (eds.). The Nagra-JNC *in situ* study of safety relevant radionuclide retardation in fractured crystalline rock III: the RRP project final report. Nagra Technical Report NTB 00-07 (*in press*), Nagra, Wettingen, Switzerland.

Ota K., Alexander W. R., Smith P. A., Möri A., Frieg B., Frick U., Umeki H., Amano K., Cowper M. M. & Berry J. A. (2002). Building confidence in radionuclide transport models for fractured Rock: The Nagra/JNC Radionuclide Retardation Programme, Mat. Res. Soc. Symp. Proc., 633, 1033-1041.

Park Y.-J., Lee K.-K., Kosakowski G. & Berkowitz B. (2003). Transport behavior in three-dimensional fracture intersections. Water Resour. Res., 39(8), 1215.

Sidle C. R., Nilsson B., Hansen M. & Fredericia J. (1998). Spatially varying hydraulic and solute transport characteristics of a fractured till determined by field tracer tests, Funen, Denmark, Water Resour. Res., 34(10), 2515-2527.

Smith P. A., Alexander W. R., Kickmaier W., Ota K., Frieg B. & McKinley I. G. (2001a). Development and Testing of Radionuclide Transport Models for Fractured Rock: Examples from the Nagra/JNC Radionuclide Migration Programme in the Grimsel Test Site, Switzerland, Journal of Contaminant Hydrology, 47, 335-348.

Smith P. A., Alexander W. R., Heer W., Fierz Th., Meier P. M., Baeyens B., Bradbury M. H., Mazurek M. & McKinley I. G. (2001b). The Nagra-JNC *in situ* study of safety relevant radionuclide retardation in fractured crystalline rock I: Radionuclide Migration Experiment – Overview 1990-1996, Nagra Technical Report NTB 00-09, Nagra, Wettingen, Switzerland.

Tsang Y. W. (1995). Study of alternative tracer tests in characterizing transport in fractured rocks. Geophys. Res. Let., 22 (11), 1421-1424.

Witherspoon P. A., Wang J. S. Y., Iwai K. & Gale J. E. (1980). Validity of cubic law for fluid flow in a deformable rock fracture. Water Resources Research, 16(6), 1016-1024.

A1.2 The FZK modelling report

Numerical Modelling of Flow and Transport Phenomenain the CRR-Experiment

Alexandra Pudewills (FZK-INE) - April 2003

A1.2-1 Background and Objectives

In the past decade, crystalline rocks have been extensively investigated as a potential waste disposal medium. Such rocks like granite are nearly impermeable, the groundwater flows only through fractures or joints. In a worst-case scenario the fractures provide the primary pathway for the migration of radionuclides from the underground repository to the biosphere. In order to predict the movement of radionuclides, the processes involved must be understood and quantified. For this purpose, laboratory tests, field experiments, and the use of adequate numerical models are needed.

The **C**olloid and **R**adionuclide **R**etardation Experiment (CRR) is carried out in the frame of an international cooperation agreement. The aim of this international, multidisciplinary project is to study the migration of radionuclides and colloids through a fractured shear-zone of crystalline rock under *in situ* conditions in the underground facility at the Grimsel Test Site (Switzerland) (Möri 2001, Fierz et al. 2001). This experiment was accompanied by a series of tracer tests to determine the hydraulic and transport properties of the fracture zone and to study the colloid migration at the experiment location. In the final field tests a tracer cocktail containing representative radionuclides in absence and presence of bentonite colloids was injected in the Grimsel groundwater and the migration through the shear zone was observed. The flow fields and transport processes in these tests were investigated by model calculations performed by different teams.

The present paper focuses on the numerical simulation of the flow fields and transport processes in two different dipole experiments with a distance of about 5 m and 2.2 m between injection/extraction holes, respectively. Figure A1.2-1.1 shows the location of the access gallery and the boreholes within the shear zone plane. For the numerical simulation it is assumed that the shear zone at the experiment location is plane which allows a two dimensional (2D) analysis. The investigations were performed with the ADINA-F finite element code (Adina 2001). The mathematical model is based on the Darcy's law for groundwater flow and the advection-dispersion equation for solute transport with a linear sorption of radionuclides in the fracture material.

The objectives of these numerical analyses are: (1) to describe the groundwater flow in the dipole experiments, (2) to calibrate the model and determine its parameters from a series of conservative tracer tests, (3) to validate the model with respect to the migration of bentonite colloids and (4) to illustrate the practical application of the calibrated model for the simulation of the radionuclides migration in the presence of bentonite colloids. This modelling marks a milestone in our model development effort in the CRR project.

The comparison of calculation results and experimental data is presented as breakthrough curves. The agreement between the modeled and measured curves is quite good for conservative tracers, bentonite colloids and radionuclides with the exception of cesium. Furthermore, the numerical results provide an overview of the present state of the art of the numerical code and help to improve our understanding of flow and solute transport through a fractured shear zone of crystalline rock.

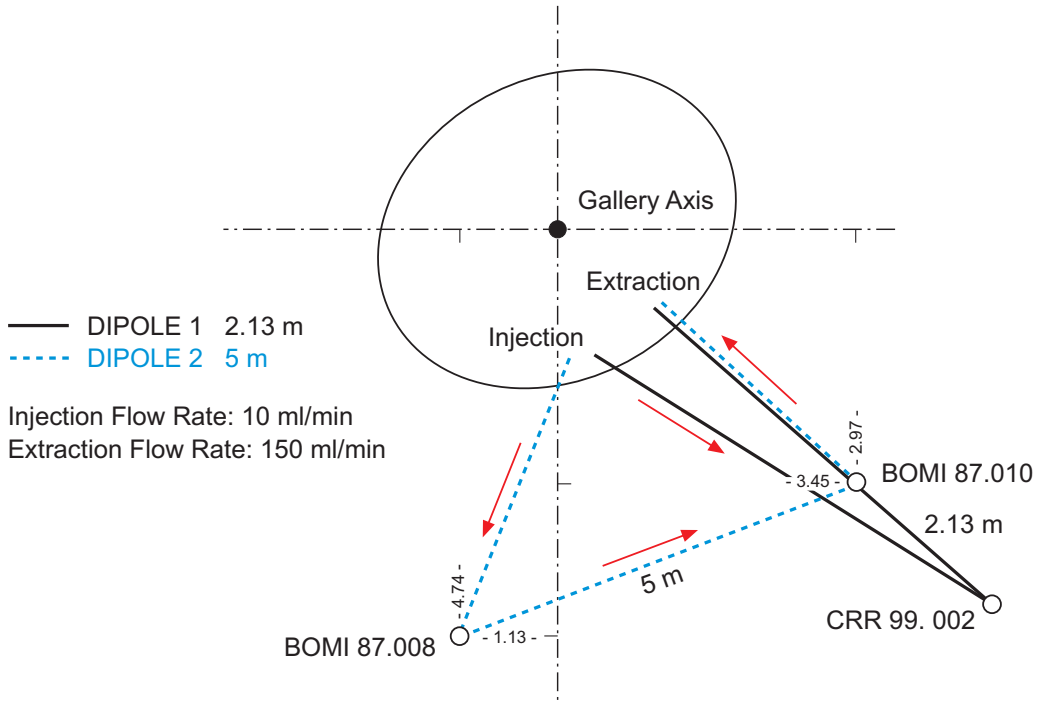

Fig. A1.2-1.1: Location of the dipole tests in the shear zone at the Grimsel Test Site

A1.2-2 Methodology

A1.2-2.1 Geometry and boundary conditions

Figure A1.2-2.1 shows the schematic setup of the experiment in the plane of the fracture and the dimension of the model with the boundary conditions used. The problem studied is symmetric about the y-axis at the mid-plane. Therefore, a simplified half domain (i. e. the shadow domain in Fig. A1.2-2.1) was discretized in the numerical simulation. This water-conducting zone with a thickness of 1 cm was treated as a saturated porous medium with anisotropic permeability. The laboratory gallery was not considered.

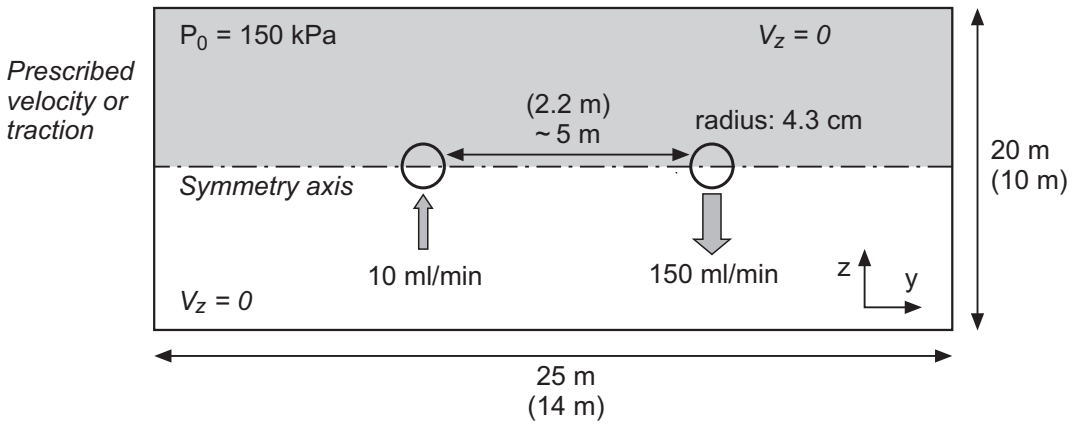

Fig. A1.2-2.1: Schematic diagram for the 2D model of the dipole tests; the dimensions of the dipole 1 test field are given in the parenthesis

The hydraulic boundary conditions consist of an impermeable top and bottom and a regional water flow from left to right with the velocity of 10 m/year. In the dipole tests the groundwater was injected with a rate of 10ml/min and extracted with a rate of 150 ml/min. After the steady-state flow conditions were established, the injection of about 20 mg/l uranine solution was performed. The uranine concentration was measured on line in order to determine the input function. In the Dipole 3, the volume of the injected colloids dispersion was about 101 ml, corresponding to a total amount of 2.02 mg. In the final field test, run #31, a tracer cocktail containing relevant radionuclides of high-level radioactive waste such Am, Np, Pu, U, Sr and I are injected in Grimsel groundwater and the migration through the shear zone was observed. In the second test, run #32, nearly the same tracer cocktail together with a dispersion of 20 mg/l bentonite colloids was injected.

A1.2-2.2 Flow and Transport equations

Assuming that the fluid flow in the fracture is laminar and isothermal, the momentum balance equation of the fluid flow can be simplified to the well known Darcy's law (Bear 1979). For the 2D incompressible flow in a porous media the governing equation is defined by

$$\mathbf{V} = - 1/\mu\, \mathbf{K} \cdot \nabla p \qquad (1)$$

where $\mathbf{V} = [Vy, Vz]^T$ is the vector of the components of averaged groundwater velocity in the *y, z* directions, μ is the viscosity coefficient, **K** the absolute permeability tensor and ∇p a prescribed pressure gradient. The equation of the mass transport of a single species in the *y - z* plane of the porous media is given by

$$\partial c / \partial t = 1 / R \, [\, (D\nabla) \, \nabla c - V \cdot \nabla c \,] \qquad (2)$$

where *c* is the concentration of the species in the pore fluid and R is the retardation factor for linear sorption in the porous material. **D** is the tensor of hydrodynamic dispersion. The coefficients of hydrodynamic dispersion are evaluated using the equation:

$$Dkl = (Do + \alpha T \, V) \, \delta kl + (\alpha L - \alpha T) \, (Vk \, Vl) / V \qquad (3)$$

where D_o *is* the coefficient of molecular diffusion, α_L, α_T are the longitudinal and transverse dispersivities, δ_k is Kronecker's delta, V_k, V_l are the components of the average groundwater velocity, *V* is the magnitude of the average groundwater velocity and the set (*k, l*) range over the index *y, z*. The retardation in the porous materials, when it is assumed to occur by linear reversible sorption can be calculated as:

$$R = 1 + (\rho / n) \, Kd \qquad (4)$$

with ρ the dry density of the material, *n* is its porosity and K_d is the mass specific sorption coefficient.

A1.2-2.3 Hydraulic and transport parameters

The flow and transport properties of the fracture material obtained from model fitting to experimental breakthrough curves of conservative tracers such the uranine are summarized in Table A1.2-2.1. These parameters with some minor changes are then used in the analyses of the final experiment. The diffusion coefficients of both uranine and colloids were determined in the laboratory.

Tab. A1.2-2.1: Flow and transport parameters used for model calculations

Parameters	Description	Dipole 3	Dipole 1
		Uranine test 7 & 8	**Uranine test 26 & 34**
n [%]	Porosity	12.5	8.5 - 8.25
κ_y [m^2]	Permeability (horiz.)	$3.5 \cdot 10^{-11}$	8.5×10^{-12}
κ_z [m^2]	Permeability (vertical)	7.0×10^{-11}	7.0×10^{-12}
α_L [m]	Long. dispersion length	0.08	0.04
α_T [m]	Trans. dispersion length	0.04	0.02
D_0 [m^2/s]	Diffusion coefficient	2×10^{-11}	2×10^{-11}

A1.2-3 Modelling

A1.2-3.1 Numerical tool

The numerical analysis was performed with the ADINA-F finite element code which is a general purpose code with a wide range of capabilities. In our study ADINA-F was used for calculation of fluid flow coupled with the mass transport in a saturated, porous media. Both iterative and direct solution procedures can be used. Details of this computer code and the numerical algorithm used may be found in (Bathe 1996 and Adina 2001).

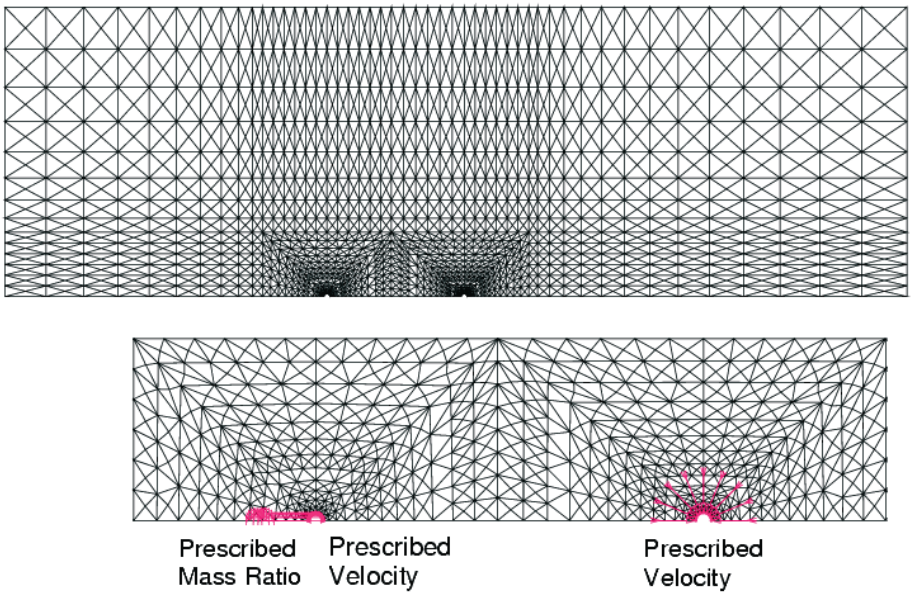

Fig. A1.2-3.1: Finite element mesh and detail discretisation near the boreholes

A1.2-3.2 Numerical model

The computational domain of 14 m × 5 m for the dipole 1 and 25 m × 10 m for dipole 3, respectively, is sufficiently large to guarantee a proper definition of the boundary conditions. The 2D-finite element calculations were performed using a model which was discretized by 3564 three-node planar elements corresponding to 1867 nodes. The boreholes are explicitly modelled. The entire mesh and a detail of the mesh near the walls are shown in the Figure A1.2-3.1. The groundwater was injected at one borehole and extracted from the second at rates of 10 ml/min and 150 ml/min, respectively.

A1.2-4 Calculation Results

The numerical analysis starts with the modelling of the steady-state groundwater flow field in the dipole experiments. In Figure A1.2-4.1 the distribution of the fluid velocity vectors around the boreholes, the stream lines and the pore-water pressure for the uranine run #29, (dipole 1) are illustrated. From the velocity vectors and the stream-lines plots can be seen that the flow field is mainly influenced by the high water extraction rate compared to the injection rate (i.e. the ratio between extraction and injection rates was about 15). The pressure gradient around the extraction wall is also induced by these high rates.

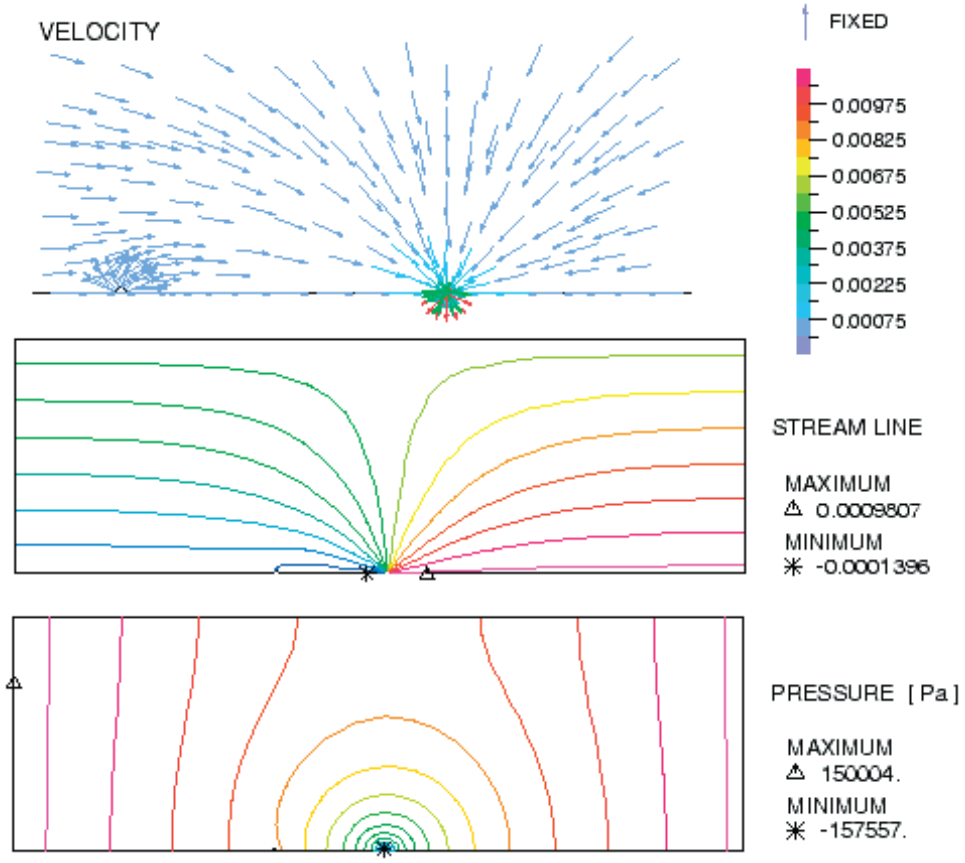

Fig. A1.2-4.1: Distribution of the velocity vectors, the stream lines and the pore pressure in the shear zone plane

A1.2-4.1 Uranine breakthrough curves

Simulation of the uranine run #7 and #8 have been used for the calibration of the numerical models for the dipole 3 and the uranine run #29, #34 and iodine (run #31) for the dipole 1, respectively. To obtain a reliable calibration of the models the following strategy was applied: The parameters fitted to the first runs series (i.e. #7 and #29, respectively) have been then tuned by modelling of the second runs series. Figure A1.2-4.2 shows the measured uranine input function used in the calculations for the dipole 3.

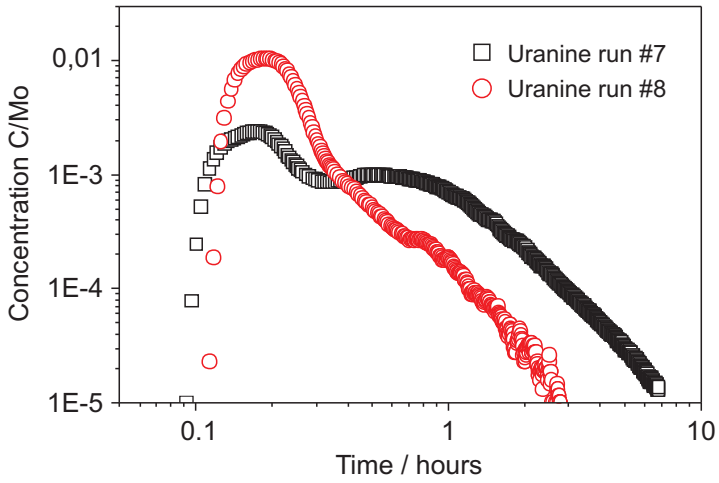

Fig. A1.2-4.2: Measured uranine concentrations at the injection hole, dipole 3

A comparison of the numerical results and experimental data is presented as breakthrough curves where the uranine concentration is plotted versus time (Fig. A1.2-4.3). As can be seen from this figure, the simulation results match the experimental data fairly well. The peak concentration is positioned slightly later than the field data but the shape of tailing is reproduced smoothly. Nevertheless, the overall agreement of model and experiment is reasonable. The recovery of the uranine was about 95 %.

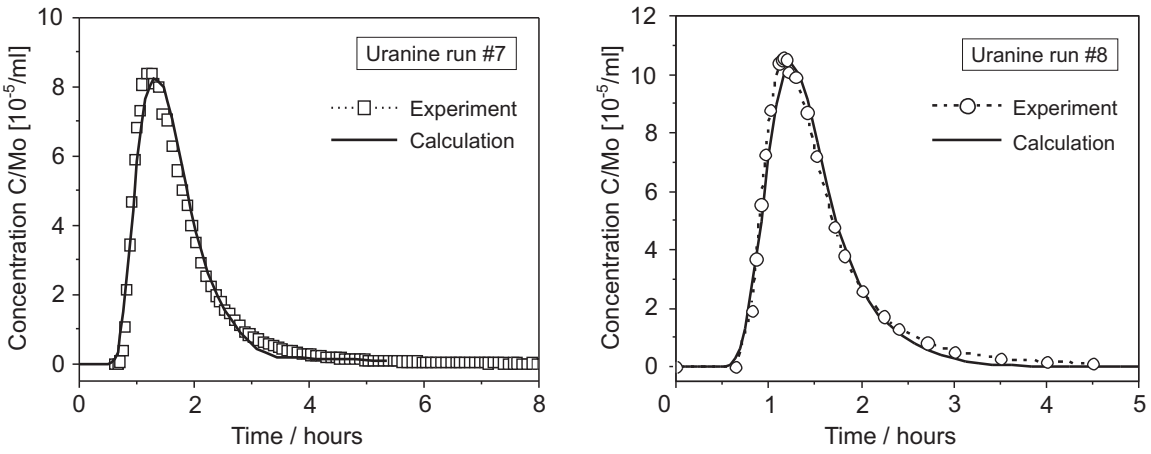

Fig. A1.2-4.3: Comparison of measured and calculated uranine breakthrough curves in run #7 and #8, dipole 3

In dipole 1, many tracer runs with uranine and iodine (^{131}I) were performed. In this calculation the uranine runs #29 were considered, and #34. The measured uranine input functions for run #29 and #34 are drawn in Figure A1.2-4.4.

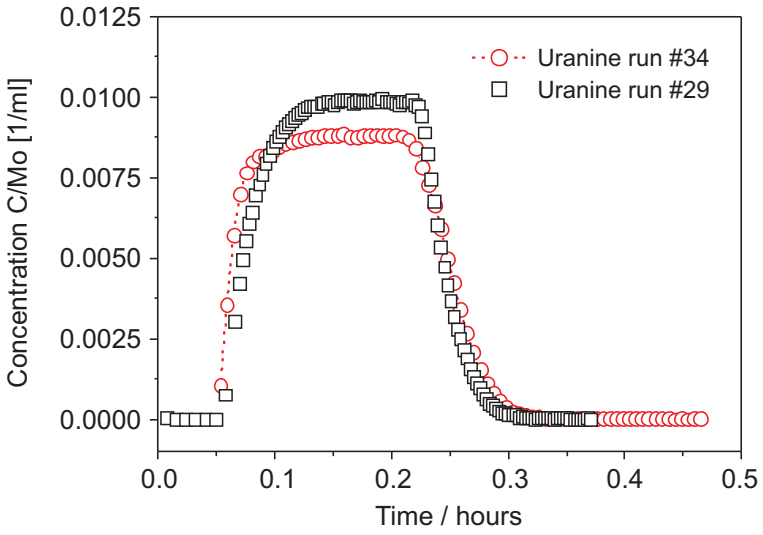

Fig. A1.2-4.4: Measured uranine concentrations at the injection hole, dipole 3

The calculated evolution of the uranine concentrations at the extraction borehole for both tests together with the field data are shown in Figures A1.2-4.5 and A1.2-4.6. As can be observed the agreement is in general satisfactory. However, the comparison of calculation results for run #34 and ^{131}I in the tailing part shows some differences.

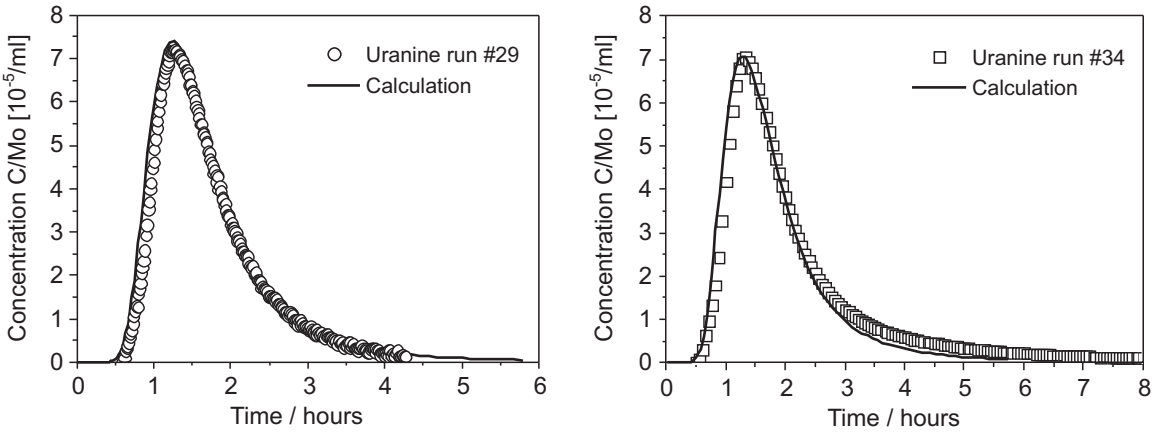

Fig. A1.2-4.5: Comparison of measured and calculated uranine breaktrough curves in run #29 and #34, dipole 1

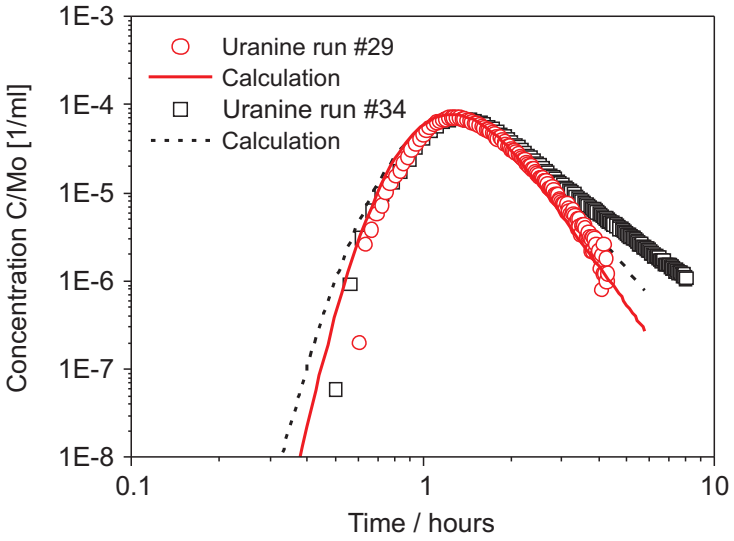

Fig. A1.2-4.6: Comparison of measured and calculated uranine breakthrough curves in run #29 and #34 (logarithmic presentation)

A1.2-4.2 Bentonite colloids migration

This section presents a brief example of the used calibrated model by simulation of conservative tracers in order to study the migration of bentonite colloids suspension in test 1 and 2, dipole 3. A suspension of bentonite colloids with a concentration of about 20 mg/l was injected. From the results of the colloid characterization by the on line Laser-Induced Breakdown Detection (LIBD) (Hauser et al. 2002), it appears that larger particles are filtered out during the passage through the fracture. Consequently, the input functions for colloids were approximated from those of uranine tests considering that the particles with a diameter larger than 110 nm are filtered in the host rock (Fig. A1.2-4.7). Furthermore, it was assumed that the longitudinal and transversal dispersion lengths are smaller for the colloids than for the conservative tracers. In this case, α_L and α_T are taken 0.01 and 0.001 m, respectively. The estimated flow end transport parameters for colloid migration are given in Table A1.2-4.1.

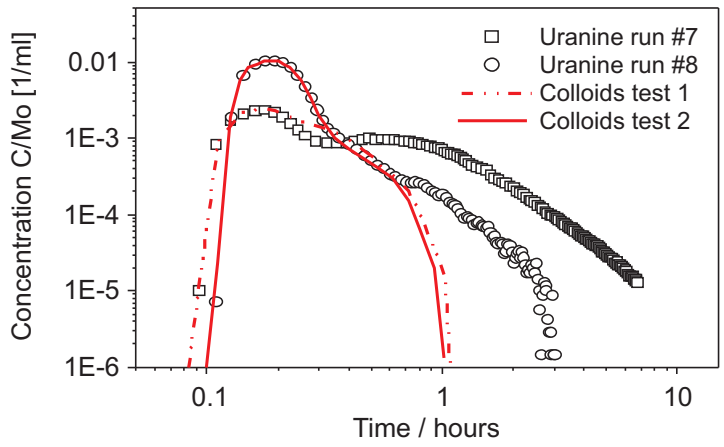

Fig. A1.2-4.7: Measured uranine concentrations at the injection wall and the approximated input functions for the colloid tests modelling

The calculated and the experimental breakthrough curves for both tests with bentonite colloids are presented in Figure A1.2-4.8. They show that the model approximates large parts of the tail and also the peak position quite well. For the colloid size-class (50 – 100 nm) the recovery curves was up to 98 % (Degueldre & Laube 2000).

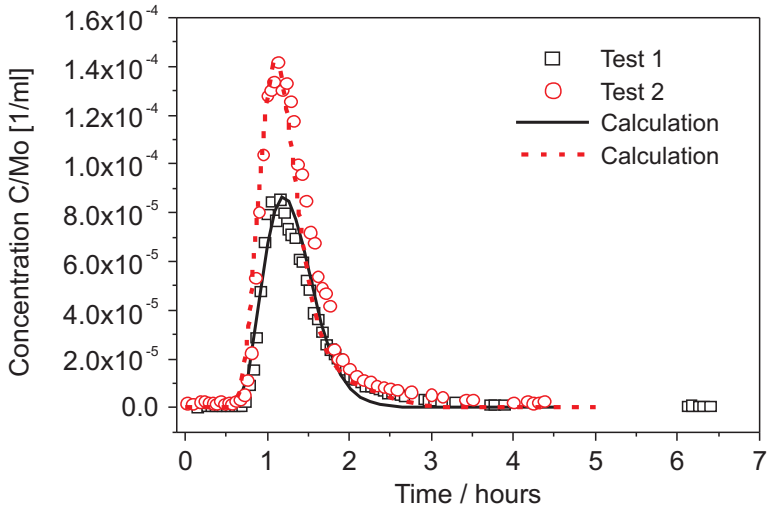

Fig. A1.2-4.8: Comparison between *in situ* measured and modelled colloid breakthrough curves for test 1 and 2, dipole 3

Tab. A1.2-4.1: Flow and transport parameters used for model calculations (dipole 3)

Parameters	**Description**	**Uranine test 7 & 8**	**Colloids test 1& 2**
n [%]	Porosity	12.5	12.5
κ [m^2]	Permeability (horiz.)	3.5×10^{-11}	$5\text{-}3.5 \times 10^{-11}$
κ_z [m^2]	Permeability (vertical)	7.0×10^{-11}	7.0×10^{-11}
a_L [m]	Long. dispersion length	0.08	0.01
a_T [m]	Trans. dispersion length	0.04	0.001
D_0 [m^2/s]	Diffusion coefficient	2×10^{-11}	3×10^{-11}

Figure A1.2-4.9 presents the comparison between the calculated uranine (run #7) and colloid breakthrough curves in test 1. The bentonite colloids are passing about 10 min before the uranine and the peak is much smaller.

The breakthrough curve of the bentonite colloids in dipole 1, run #34 was not modelled in this work because the experimental breakthrough evolution is similar to the conservative tracer.

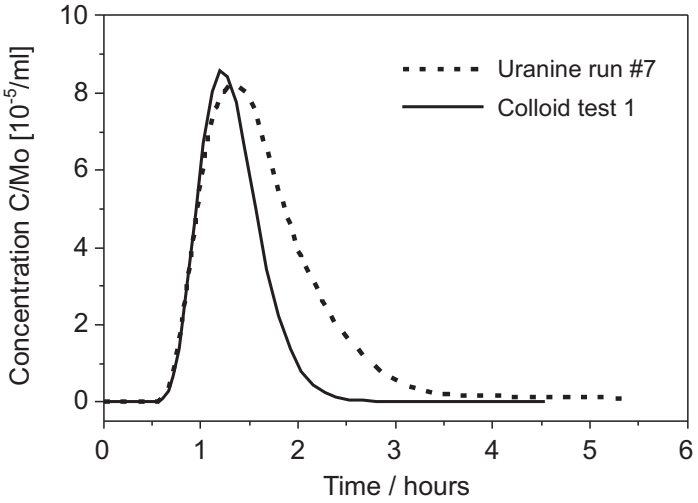

Fig. A1.2-4.9: Comparison of calculated colloids and uranine breakthrough curves

A1.2-4.3 Radionuclide migration

In run #31 a cocktail containing Am, Np, Pu, U, Sr and I was injected in the Grimsel groundwater and the concentration breakthrough was studied. In the following test (i.e. run #32) bentonite colloids were added.

This chapter presents the preliminary results of the numerical modelling of the same radionuclides. In our modelling the migration of ^{237}Np and ^{233}U are of main interest because of the particular shape of the breakthrough curves. The observed concentration peak-time corresponds to the conservative tracer curves (i. e. about 90 min) but the tailing suggests that a part of the nuclides is retarded in the same manner as Sr. Taking into account this fact, it was assumed that 50 % of the injected solution was transport like uranine and the other 50 % is retarded in the shear zone with a retardation factor R of 6 (i.e. a K_d -value of about 0.21×10^{-3} m^3/kg if the density of the porous medium is 2000 kg/m^3 and the porosity of 8.5 %). A comparison of calculated and measured breakthrough concentration of ^{233}U in run #32 is given in Figure A1.2-4.10.

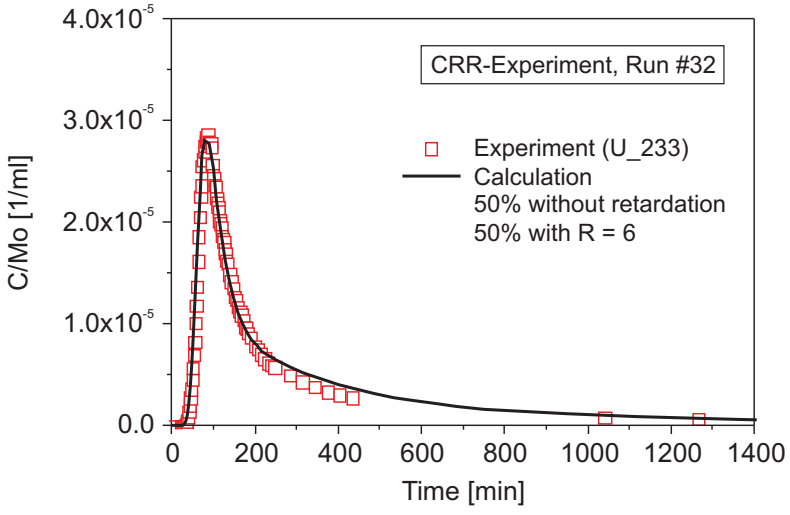

Fig. A1.2-4.10: Simulated and measured breakthrough curves for ^{233}U

A logarithmic plot of these results together with the measured ^{237}Np breakthrough curve is given in Figure A1.2-4.11.

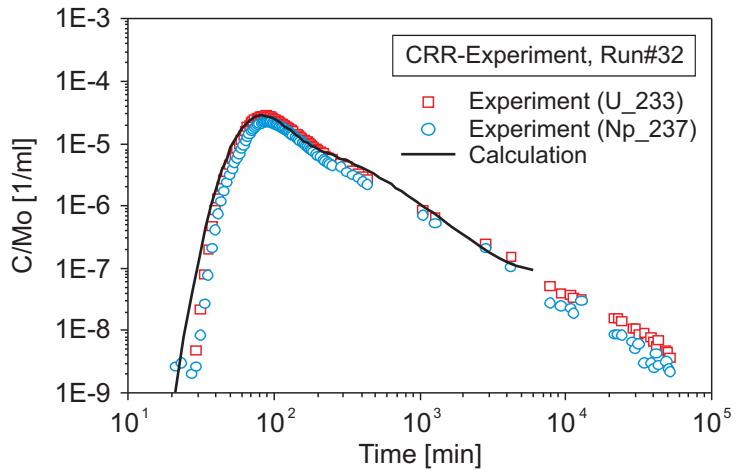

Fig. A1.2-4.11: Comparison between the experimental and calculated data

As can be seen from both figures, the agreement between the calculated and observed curves is satisfactory, the shape of the curves is quite well reproduced.

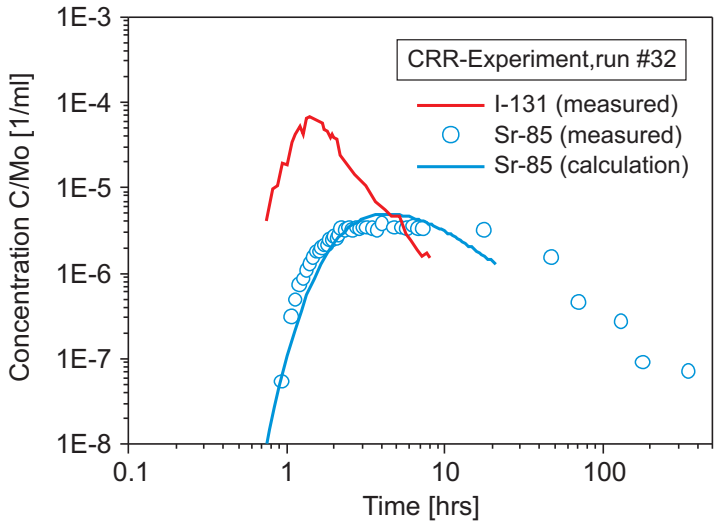

Fig. A1.2-4.12: Comparison between the experimental and calculated data

In the next step, the simulation of the strontium breakthrough curve has been performed using a retardation factor of 10. The results are drawn in Figure A1.2-4.12 together with the breakthrough curves of uranine and iodine. Although, the modelled and observed concentration curves show a relatively good correlation, a final qualification of this result is not possible because the assumed retardation factor for Sr is not yet supported by laboratory experiments. Finally, the trial to simulate the evolution of the cesium concentration failed. Further investigation of Cs migration will be continued in the next work.

A1.2-5 Conclusions

The numerical modelling of the dipole experiments presented in this paper demonstrates that the migration of the conservative tracers and bentonite colloids through a fractured shear zone of crystalline rock can be successfully simulated with the ADINA-F code. Furthermore, the results show that the transport parameters can be estimated on the basis of measured breakthrough curves of conservative tracers. Finally, this model was applied to simulate the migration of selected radionuclides in the final experiment in presence of the bentonite colloids. This preliminary modelling of the radionuclide breakthrough curves shows the limitation of the transport model used. Further development of the model will be done to include the matrix diffusion and the discrete fractures effects. Laboratory and field data are currently collected which should allow the refinement of the model.

A1.2-6 References

ADINA (2001). ADINA (Automatic Dynamic Incremental Nonlinear Analysis), Report ARD 01-9, Watertown, MA, US. See also *http:*//www.adina.com.

Bathe K. J. (1996). Finite Element Procedures, Prentice-Hall, Englewood Cliffs, NJ, USA.

Bear J. (1979). *Hydraulics of groundwater*, McGraw-Hill, New York, USA.

Degueldre C. & Laube A. (2000). Bentonite colloid migration in a granitic fracture at Grimsel Test Site. Unpubl. PSI Internal Report, TM-44-00-07, PSI, Villigen, Switzerland.

Fierz Th., Geckeis H., Götz R., Geyer F. W. & Möri A. (2001). GTS V/ CRR Tracer Tests #1-#16 (Sep. 1999 - Jan. 2001). Unpubl. Nagra Internal Report, Wettingen, Switzerland.

Hauser W., Geckeis H., Kim J. I. & Fierz Th. (2002). A mobile laser-induced breakdown detection system and its application for the *in situ*-monitoring of colloid migration. *Colloids and Surfaces*, 203: 37-47.

Möri A. (2001). CRR Experiment Phase 1. Unpubl. Nagra Internal Report, Wettingen, Switzerland.

A1.3 The JNC modelling report

Modelling the CRR Experiments Using STAMMT–L and COLFRAC (March, 2003)

Scott C. JAMES[1], Motomu IBARAKI[2], Susan J. ALTMAN[1], Susumu KUROSAWA[3], Kazuki IIJIMA[3] and Mikazu YUI[3]

[1]Sandia National Laboratories (SNL)
[2]Ohio State University (OSU)
[3]Japanese Nuclear Fuel Cycle Development Corporation (JNC)

A1.3-1 Introduction

A1.3-1.1 Objectives and expected outcomes

When assessing repository performance, one must account for the potential failure of the engineered barrier system (EBS). With the EBS failure, there is a potential for the release of radionuclides to the geological environment. In addition, if bentonite is used as a part of the EBS design, bentonite colloids could be released. Radionuclides could sorb onto bentonite and naturally occurring colloids, which could facilitate radionuclide transport in the geosphere. Therefore, the effect of colloid enhanced transport of strongly sorbing radionuclides is an important topic that must be addressed. In January of 2002, a series of Colloid and Radionuclide Retardation (CRR) experiments were conducted at the Grimsel Test Site in Switzerland.

The primary objective of JNC is to shed light on processes affecting colloid-facilitated radionuclide transport in discretely fractured media and to assess the relative importance of various phenomenological coefficients that come into play. In order to reach this objective, numerical techniques will be used to solve the governing equations in two dimensions. The numerical model incorporates advective-dispersive aqueous phase solute transport in the fractures and the rock matrix, colloid transport in the fractures, and sorption of the solute. Filtration of the colloidal particles is accounted for, and the solute is allowed to sorb on both the mobile and filtered colloids. The numerical formulation allows for either equilibrium or kinetic sorption reactions onto the fracture walls, the matrix solids, and the mobile and filtered colloids according to either a Langmuir or a Freundlich isotherm.

A1.3-1.2 Structure of the document

In this study, two distinct models of STAMMT-L and COLFRAC adjusted PEST are used to estimate the parameters affecting radionuclide transport in the CRR experiments. STAMMT-L is a one-dimensional model that simulates solute transport only (subject to advection, dispersion, and reaction/mass transfer with the double porosity conceptualization). COLFRAC is a two-dimensional model that simulates colloid and solute co-transport in a discretely fractured porous medium. PEST is used to adjust COLFRAC input parameters such that the discrepancies between the model-generated output concentrations and the corresponding CRR measurements are reduced to a minimum.

STAMMT-L was first used to estimate transport parameters for the non-reactive tracer, I^{131}. From this analysis, the estimated flow velocity and ϕ_{im}/ϕ_m were fixed from the analyses of run#31. STAMMT-L was not used to evaluate the breakthrough curves for run#32 because, the model does not account for any of the competing processes with enhanced colloid transport.

Once the geometry of the system was defined, COLFRAC and PEST were used to fit the I^{131} data by estimating transport parameters (effective diffusion coefficient, hydraulic conductivity, matrix and fracture dispersivity, etc.) for the conservative solute. Once these parameters were estimated, they were set as constant and the transport parameters (forward and backward kinetic reaction rates and matrix retardation coefficient) for the reactive tracers without colloids were estimated. Finally, these reactive transport parameters were set as constant and the enhanced colloid migration parameters (colloid dispersivity, colloid/radionuclide forward and backward kinetic reaction rates, and colloid filtration coefficient) were estimated using the breakthrough curve data from run#32.

A1.3-2 Methodology

A1.3-2.1 Understanding of the features and processes

A1.3-2.1.1 Geochemical structure

(1) Hydrogeochemical overview

The CRR *in situ* experiments were carried out at Nagra's Grimsel Test Site, which is located 1730 m above sea level under approximately 450 m of crystalline rock. The host rock of the test shear zone is Grimsel granodiorite that has partially metamorphosed into gneiss. It is medium to coarse grained and transected by a series of shear zones. The granodiorite consists primarily of 23 % quartz, 23 % plagioclase, 20 % potassium feldspar, and 25 % sheet silicates by volume (Möri et al. 2003). The shear zone is filled with gouge with increased (45 %) sheet silicate content. The increase in sheet silicates and relatively large porosity of 30 – 40 % are responsible for the preferential retardation of radionuclides in this material. The thickness of the shear zone varies between 0.15 and 0.9 m. Evaluation of previous borehole outflow tests revealed transmissivities near 10^{-6} m^2/s. The test site groundwater has a pH of 9.6 and an Eh of –300 mV. The electrical conductivity is 103 µS/cm with ionic strength 0.0012 M. The natural colloid background of the test site groundwater was found to be about 10^{10} colloids/L with sizes between 40 and 1,000 nm (Möri et al. 2003). The CRR test shear zone is characterized as a WSW-ENE striking, steeply dipping (to the SSE) cleavage parallel shear plane.

(2) Experimental setup and system conceptualization

A dipole flow field configuration was instrumented with specially designed triple packer systems to ensure a tight borehole seal. Injection and withdrawal wells were installed 2.5 m apart within the fractured zone. The CRR experiments modeled here are of two separate convergent pumping tests from the CRR experiments are modeled here. In the first experiment (run #31), a 10-minute pulse of a tracer and various radionuclides was injected into one well in the fractured zone, and upon withdrawal from a second well, radionuclide concentrations were measured. In the next experiment (run #32), in addition to radionuclides, 20 mg/ml of bentonite colloids were simultaneously injected into the fracture zone and radionuclide concentrations at the withdrawal well were monitored. Injection rates averaged 10 ml/min and withdrawal rates were approximately 150 ml/min. The withdrawal well was monitored for 216 hours during run#31 and for 858 hours during run #32. Radionuclide breakthrough curves and total recovery in the presence and absence of colloids were compared. Table A1.3-2.1 lists the radionuclides used in each experiment that were modeled for this study. In addition, distribution coefficients for the radionuclides modeled in this report are presented in Table A1.3-2.2 (Möri & Alexander 2001).

Tab. A1.3-2.1: Radionuclide tracers used in each of the two CRR experiments that are analyzed in this study

Run #31: No added colloids	Run #32: 20 mg/ml bentonite colloids
I^{131} (conservative tracer)	U^{233}
Np^{237}	Np^{237}
Am^{243}	Am^{241}

Tab. A1.3-2.2: Distribution coefficients (K_d) for radionuclides modeled in this report (Möri & Alexander 2001)

Radionuclide	Granodiorite	Fracture gouge	Bentonite colloids
Am^{243}	12 ± 4 ml/g	46 ±5 ml/g	$2.1 \pm 0.1 \times 10^6$ ml/g
Np^{237}	< 1 ml/g	< 1 ml/g	$< 5 \times 10^3$ ml/g
U^{233}	12.2 ± 0.2 ml/g	5.6 ± 0.5 ml/g	824 ± 50 ml/g

Several parameters describing the system of saturated flow in the fractured granodiorite zone were measured before conducting the experiment. Table A1.3-2.3 describes the fracture aperture and spacing with the granodiorite matrix as well as the diffusivity of colloids and I^{131} (Heer & Hadermann 1996). Additionally, between the injection (~10 ml/min) and withdrawal (~150 ml/min) wells, the solute velocity 7.05×10^{-4} m/s (Kosakowski 2002).

Tab. A1.3-2.3: Tracer, colloid, and matrix parameters

Parameter	Units	Symbol	Range of values
Matrix porosity	–	ϕ_{im}	0.005–0.03
Fracture aperture	m	$2b$	1×10^{-4}–6×10^{-4}
Fracture spacing	m	2B	$> 6 \times 10^{-3}$
Effective diffusion coefficient (I^{131})	m^2/s	$D_e = \tau D_{aq}$	2×10^{-12}–3×10^{-11}
Aqueous diffusion coefficient (I^{131})	m^2/s	D_{aq}	2.1×10^{-9}
300 nm colloid diffusion coefficient	m^2/s	D_{dm}	1.5×10^{-12}
Bulk density	g/ml	ρ_b	2.67

A1.3-2.1.2 Fundamental processes

Numerous geochemical and hydrological processes are occurring in the CRR experiments. Processes affecting solutes included in this modelling effort are advection, molecular diffusion, mechanical dispersion, sorption (both equilibrium and kinetic) onto the fracture fill and onto the gouge infill, diffusion into and subsequent sorption onto the granodiorite matrix, and sorption onto both mobile and filtered (attached onto fracture fill) colloids. In all cases, radionuclide

sorption is reversible. Similarly, colloids travel by advection, diffusion, and dispersion and may attach to fracture fill. Colloids are considered too large to penetrate the granodiorite matrix. Radionuclide decay and daughter product formation are neglected in all models. Give the large half-life of the radionuclides used as tracer, with the exception of I^{131}, and the short duration of the tracer tests, neglecting radioactive decay is appropriate. For I^{131}, the measured decrease in concentration could be attributed to mass transfer processes (i.e., diffusion) when it fact radioactive decay is partially responsible. Therefore, numerical modelling might overestimate the effects of the mass transfer processes.

COLFRAC requires an input of initial concentration (kg/m^3), however, initial only initial activity (Bq), was reported. Knowing the half-life of each radionuclide and the injected activity, the initial mass may be calculated. First, the disintegration constant, Λ, is calculated:

$$\Lambda = \frac{\ln(2)}{t_{1/2}}. \tag{1}$$

From the disintegration constant and activity, A, the initial number of atoms, N, is calculated as:

$$N = \frac{A}{\lambda}. \tag{2}$$

Note that the half-lives of the injected radionuclides are high enough that we assume there is not significant decay over the injection period. Once the initial number of atoms is known, the initial mass is calculates as:

$$m_o = N\frac{\mathrm{Z}}{N_A}, \tag{3}$$

where Z is the atomic mass and N_A is Avogadro's number. Finally, the initial concentration, C_o, can be calculated by dividing m_o by the injection volume. Results are presented in Table A1.3-2.4.

Tab. A1.3-2.4: Initial masses and concentrations of each injected radionuclide. Note that 100 ml were injected for each run

Radionuclide	**Input Concentration** C_0 (mol/L)*	**Half-life** $t_{½}$ (s)	**Mass** m_o (kg)**	**Concentration** C_o (kg/m^3)
I^{131} (Run#31)	1.24×10^{-12}	6.92902×10^{5}	1.624×10^{-14}	1.624×10^{-10}
Am^{243} (Run#31)	5.93×10^{-9}	2.32889×10^{11}	1.441×10^{-10}	1.441×10^{-6}
Np^{237} (Run#31)	9.44×10^{-7}	6.75314×10^{13}	2.237×10^{-8}	2.237×10^{-4}
Am^{241} (Run#32)	1.15×10^{-8}	1.36392×10^{10}	2.772×10^{-10}	2.772×10^{-6}
Np^{237} (Run#32)	1.09×10^{-6}	6.75314×10^{13}	2.583×10^{-8}	2.583×10^{-4}
U^{233} (Run#32)	8.69×10^{-7}	5.04908×10^{12}	2.025×10^{-8}	2.025×10^{-4}

* From Möri et al. (2003) and also from Table 2.2

** $m_0 = 10^{-4} C_0 Z$

A1.3-2.2 Approach to model development

A1.3-2.2.1 STAMMT-L

A one-dimensional, dual porosity, semi-analytical, multirate code, STAMMT–L (Haggerty & Gorelick 1995) was used to preliminarily model the tracer breakthrough. STAMMT–L provides a semi-analytical solution to the one-dimensional dual-porosity advective-dispersive transport equation where mass-transfer between the mobile and immobile domains is represented as a multirate process (Haggerty & Reeves 1999). In keeping with the classic double-porosity model, advection occurs only within the mobile zone (fractures) and the immobile zone (matrix) acts as a storage volume. For this system, the mobile zone is conceptualized as the gouge filled fractured shear test zone and the immobile zone is the unaltered granodiorite rock. Mass transfer processes, such as adsorption and diffusion, control the distribution of the solute mass between the two zones. The immobile zone is represented as a domain of prescribed thickness with a distribution of diffusion rate coefficients or first-order mass transfer rates. The distribution of mass transfer rates may be interpreted as variability in the apparent diffusion coefficient and/or matrix block size. However, in the modelling results presented here, single rate diffusion is assumed because of the short path length and residence time. Equilibrium sorption of the radionuclides onto the fracture walls as well as onto the porous matrix is assumed. STAMMT–L may be run in an inverse mode where concentration input and resulting breakthrough curves are used to estimate parameters affecting radionuclide transport.

As mentioned above, STAMMT–L can be used to estimate mass transfer rates. Figure A1.3-2.1 illustrates the STAMMT–L conceptual model, a complete description of which is found in the STAMMT–L *User's Manual* (Haggerty & Reeves 1999), as well as in the work of Haggerty & Gorelick (1995; 1998). Versions of STAMMT–L have been used to model transport at the WIPP site (Meigs et al. 1997; Haggerty et al. 2001; McKenna et al. 2001) and the Äspö TRUE-1 tracer tests (McKenna 1999; 2000a, b). It is important to note that STAMMT–L can only model reactive solutes and cannot account for colloid enhanced transport. It is therefore primarily used to estimate the transport parameters of radionuclides not subject to enhanced transport. The CRR experimental setup has closely spaced injection and withdrawal wells and a high flow velocity between them strongly suggesting that a one-dimensional approximation is reasonable.

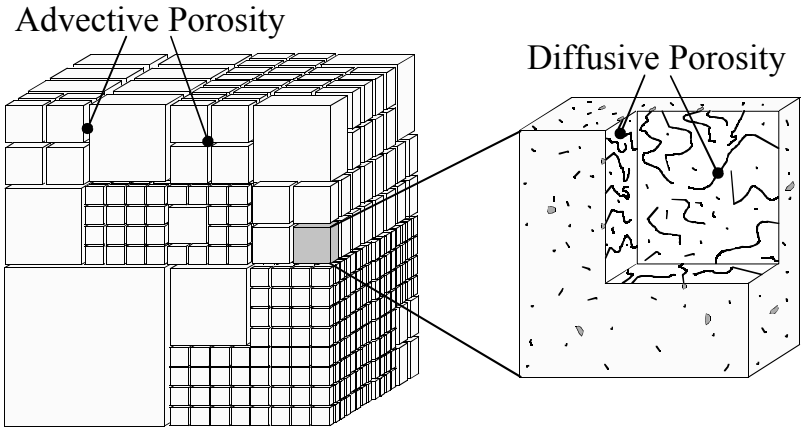

Fig. A1.3-2.1: Conceptual model of diffusion assumed in STAMMT–L model (Meigs et al. 1997)

(1) Governing Equations

Advective-dispersive transport in a one-dimensional system, subject to rate-limited mass transfer can be described mathematically as:

$$\frac{\partial c_m(x,t)}{\partial t} - \Gamma(t) = \frac{\alpha_{Lf} q_f}{R_m} \frac{\partial^2 c_m(x,t)}{\partial x^2} - \frac{q_f}{R_m} \frac{\partial c_m(x,t)}{\partial x}, \tag{4}$$

where c_m [M/L^3] is concentration in the mobile zone; $\Gamma(t)$ [M/L^{3}T] is a time varying source or sink of mass due to rate-limited mass transfer; α_{Lf} [L] is longitudinal dispersivity of the solute in the mobile zone; q_f[L/t] is mobile zone pore-water (solute) velocity; R_m [–] is the retardation factor of the mobile zone; t [t] is time; and x [L] is distance along the flow system from the entry point.

The upstream and downstream boundary conditions on the transport equation are specified flux at the inlet ($x = 0$):

$$c_m(0,t) - \alpha_{Lf} \frac{\partial c_m(0,t)}{\partial x} = c_{inj}(t), \tag{5}$$

and no flux at the end of the system ($x = L_s$)

$$\frac{\partial c_m(L_s,t)}{\partial x} = 0, \tag{6}$$

respectively, where $c_{inj}(t)$ [M/L^3] is the input concentration; and L_s [L] is the total length of the system. STAMMT–L accepts Dirac and square inlet concentration pulses as well as time varying user-specified concentrations. The initial conditions for the system are that the mobile and immobile zone concentrations are in equilibrium. The equilibrium concentration is user defined, $c_m(x,0) \geq 0$.

Although the mass source/sink term due to rate-limited mass transfer into the immobile zone in (4) can be parameterized in a number of ways, in this work, the mass transfer rate is always described as a single value. Mass transfer between the mobile and immobile zones is described as:

$$\Gamma(t) = \beta \frac{\partial \hat{c}_{im}(t;\alpha_d)}{\partial t}, \tag{7}$$

where β is called the capacity coefficient and $\hat{c}_{im}(t;\alpha_d)$ [M/L^3] is the average concentration in the immobile zone subject to α_d [1/t], the diffusion rate coefficient, which is defined as

$$\alpha_d = \frac{D_{aq} \tau \phi_{im}}{(\phi_{im} + K_d \rho_b) \ell^2}. \tag{8}$$

In the preceding equation, D_{aq} [L^2/T] is the aqueous diffusion coefficient; τ [–] is the tortuosity; ℓ [L] is the variable length of the diffusion pathway within the immobile zone or half matrix block length; and the porosity, bulk density, and distribution coefficient of the immobile zone are ϕ_{im} [–], ρ_b [M/L^3],and K_d [L^3/M], respectively. Note that for a non-sorbing tracer, $K_d = 0$, the diffusion rate reduces to $\alpha_d = D_{aq}\tau / \ell^2$.

The immobile zone concentration subject to a specific mass transfer coefficient, α_d, is given by the solution to the diffusion equation:

$$\frac{\partial c_{im}(z,t;\alpha_d)}{\partial t} = D_{aq}\frac{\partial^2 c_{im}(z,t;\alpha_d)}{\partial z^2}, \tag{9}$$

where z [L] is the coordinate along the diffusion pathway and perpendicular to x. As seen in the preceding equation, immobile zones are assumed mathematically one-dimensional. Essentially, each immobile zone is conceptualized as a long, thin, micropore residing within a block or grain aggregate, with one end of the micropore in contact with the mobile zone. All immobile zone pathways are assumed independent with solute concentrations that vary as a function of α_d

The boundary condition at the inlet to each immobile zone is equal to the local mobile zone concentration

$$c_{im}\left(0,t;\alpha_d\right) = c_m\left(x,t\right), \tag{10}$$

and no flux is specified at the end of the immobile zone (matrix block),

$$\frac{\partial c_{im}\left(\ell,t;\alpha_d\right)}{\partial z} = 0. \tag{11}$$

The time derivative of the average solute concentration along a specific diffusion pathway in the immobile zone used in (7) is:

$$\frac{\partial \hat{c}_{im}(t;\alpha_d)}{\partial t} = \frac{1}{\ell}\int_0^{\ell}\frac{\partial c_{im}(z,t;\alpha_d)}{\partial t}\mathrm{d}z. \tag{12}$$

Parameter values are estimated through a least-squares algorithm that minimizes the difference between the observed and modeled data. In the version of STAMMT–L (v1.10) used for this modelling effort, up to seven different parameters may be estimated simultaneously although in this work only the following parameters are of interest.

(2) Parameters

Total capacity – β

The total mass uptake capacity within the aquifer is defined as β:

$$\beta = \frac{R_{im}\phi_{im}}{R_m\phi_m}, \tag{13}$$

where R_{im} [–] is the immobile zone retardation factor and ϕ_m [–] is the porosity of the mobile zone. For a sorbing and diffusing solute at equilibrium, β is the ratio of mobile to immobile zone concentrations and is equal to the ratio of the products of the retardation and porosity of the mobile to immobile zones. For a non-sorbing tracer, the retardation factors are unity and β is simply the ratio of the immobile to mobile zone porosities: ϕ_{im}/ϕ_m.

Mass transfer rate – α_d

The first order mass transfer rate for radionuclides partitioning between the mobile and immobile zones is α_d and is defined in (8). This parameter describes how easily a radionuclide moves from the fractured zone into the granodiorite rock matrix and for a conservative tracer it is proportional to the aqueous diffusion coefficient.

Mobile/immobile zone retardation factors – R_m, R_{im}

The retardation factor for the mobile zone is defined as:

$$R_m = 1 + \left(\frac{1-\phi_m}{\phi_m}\right)\rho_g K_a, \tag{14}$$

where ρ_g [M/L^3] is the grain density of the minerals comprising the surfaces of the fractured rock; and K_a [L/M^3] is the distribution coefficient for sorption onto the fracture walls. The mobile zone retardation factor is assumed equal to one for the conservative tracer (I^{131}) and $K_a = 0$. While R_m is normally defined as ≥ 1, an R_m values less than one is acceptable because of enhanced transport due to sorption onto suspended colloids.

The retardation factor for the immobile zone is defined as:

$$R_{im} = 1 + \frac{\rho_b K_d}{\phi_{im}}. \tag{15}$$

Dilution factor – dilute

The dilution factor is defined as:

$$dilute = \frac{1}{RF}\frac{Q_p}{Q_i} \tag{16}$$

where RF is the fraction of the tracer recovered in the pumping well; and Q_i and Q_p are the injection and pumping volumetric flow rates, respectively. The recovery factor is estimated indirectly in this work through an estimate of *dilute*.

Mobil zone velocity – q_f

The average solute velocity in the mobile zone was provided for the CRR experiments as 7.05×10^{-4} m/s. Although q_f could be one of the parameters estimated from the I^{131} break-through curve, it is always specified in the STAMMT–L input file.

A1.3-2.2.2 COLFRAC

COLFRAC is a two-dimensional finite element code that uses the standard Galerkin scheme to solve the governing equations for both groundwater flow and dissolved solute and colloid transport. Details of the code development may be found in the works of Ibaraki & Sudicky (1995a, b) and Oswald & Ibaraki (2001). In addition, the public domain parameter estimation code, PEST (Doherty 2002) was used in conjunction with COLFRAC to match model results to experimental data as well as to perform an uncertainty and sensitivity analysis on the model input parameters.

(1) Governing equations

Groundwater Flow

Steady-state groundwater flow in discretely fractured porous media can be described by two coupled equations: one for the porous matrix and one for the fractures. It is assumed that the fluid is essentially incompressible, that there is no deformation of the fracture-matrix system, and that isothermal conditions prevail.

For the porous matrix, steady-state groundwater flow is described by (Bear 1972):

$$\frac{\partial}{\partial x_i} K_{ij} \frac{\partial h}{\partial x_j} = 0, \tag{17}$$

where h [L] is the hydraulic head and K_{ij} [L/T] is the hydraulic conductivity. In this model, the hydraulic conductivity tensor is

$$K_{ij} = \begin{bmatrix} K_{11} & 0 \\ 0 & K_{22} \end{bmatrix}. \tag{18}$$

The Darcy flux, q_i [L/T], in the matrix is represented as:

$$q_i = -K_{ij} \frac{\partial h}{\partial x_j}. \tag{19}$$

Assuming a smooth-walled fracture with constant aperture $2b$ [L], steady-state groundwater flow in the fracture is described by (Berkowitz et al. 1988):

$$(2b) K_f \frac{\mathrm{d}^2 h_f}{\mathrm{d}l^2} \pm q_m = 0, \tag{20}$$

where l [L] is the distance along the fracture and h_f [L] is the hydraulic head in the fracture. The term q_m [L/T] is the fluid flux normal to the fracture/matrix boundary and represents fluid leakage between the fracture and the matrix.

The fracture hydraulic conductivity, K_f [L/T] is given by (Bear 1972):

$$K_f = \frac{\rho g (2b)^2}{12\mu}, \tag{21}$$

where g [L/T^2] is gravitational acceleration, and ρ [M/L^3] and μ [M/LT] are the density and the viscosity of the fluid, respectively. The fluid flux, q_f, along the fracture can also be described using the Darcy equation as:

$$q_f = -\frac{\rho g (2b)^2}{12\mu} \frac{\mathrm{d}h_f}{\mathrm{d}l}.$$

Applying the condition that $h = h_f$ along the fracture/matrix interfaces allows coupling of the flow equation for the matrix (17) and for the fracture (20).

Colloid-facilitated Solute Transport

Three main processes are involved in colloid-facilitated solute transport in discretely fractured porous media. These include solute transport in the aqueous phase, colloid transport in the flowing groundwater in the fracture, and sorption of the solute onto the colloids, the fracture surfaces, and the matrix solids. Because it is assumed that the colloids do not migrate in the porous matrix, only a single transport equation describing colloid movement in the fractures is required.

For the dissolved constituent, two transport equations are needed to describe solute movement: one for the fractures and the other for the porous matrix.

Colloid Transport along Fractures

The following governing equations are used in COLFRAC to describe one-dimensional colloid transport in saturated porous media, modified slightly here for the present problem of colloid transport in a fracture (Herzig et al. 1970; Tien et al. 1979; Dieulin 1982):

$$\frac{\partial}{\partial t}\left(n + \frac{\tilde{n}}{b}\right) + q_n \frac{\partial n}{\partial l} - \frac{\partial}{\partial l} D_n \frac{\partial n}{\partial l} = 0, \tag{22}$$

where D_n [L^2/T] is the colloid dispersion coefficient, q_n [L/T] is the colloid velocity in the fracture, and t [T] is time. The quantities n [M/L^3] and $\tilde{n}$ [M/L^2] are the mobile and filtered colloid concentrations, respectively (tildes will be used to denote filtered colloids). Here, n is the mass of suspended colloids in solution per unit volume of solution in the fracture and $\tilde{n}$ is the mass of filtered colloids on the fracture surface per unit area of the fracture surface.

In a fracture, it is known that the velocity profile for a flowing Newtonian fluid takes on a parabolic shape where the maximum velocity occurs at the center of the fracture and the minimum at the wall. When colloids are suspended in the fluid, they are dispersed normal to the

direction of flow by Brownian motion thereby traveling at different velocities across the width of fracture according to the parabolic velocity profile. Larger particles are excluded from the slowest groundwater velocity zone near the fracture wall because of their size, and as a result, tend to move faster than smaller particles. Accordingly, the velocity of colloidal particle flow (q_n) is usually greater than that of water flow (q_f). The ratio of q_n/q_f cannot exceed 1.5 because colloids cannot move faster than the maximum water velocity. The velocity of colloids is reflected not only by the particle sizes but also by the ionic strength of the aqueous phase, which controls physicochemical interactions between colloids and the fracture wall. For example, Small (1974) found that as the ionic strength decreases the ratio of q_n/q_f tends to increase.

The following equation, originally proposed by several researchers for porous media applications, is used to describe the change in the concentration of the filtered colloids over time in a fracture (Herzig et al. 1970; Dieulin 1982):

$$\frac{\partial \tilde{n}}{\partial t} = \lambda q_n n, \tag{23}$$

where λ [–] is the filter coefficient and the rate of mobile colloid filtration is described by λq_n. In (23), remobilization of filtered colloids is neglected. The filter coefficient is an empirically determined coefficient that expresses the efficiency of a medium to filter colloidal particles from suspensions.

The filter coefficient typically varies with colloid size and species (Saltelli et al. 1984); however, in this study a single λ value will be used because a monodisperse colloid system is assumed. To take into account a variable filter coefficient, which is usually observed in a polydisperse colloid system, approaches using the population balance equation have been proposed for porous media applications (Randolph 1964; Avogadro & de Marsily 1984; Travis & Nuttall 1985).

Trajectory analysis, which is one of the approaches used to model the deep bed filtration process, involves explicitly including the forces, which control the filtration mechanisms of colloidal particles. These forces involve hydrodynamic, gravitational, and electrostatic forces.

It has been shown that when a double-layer force between a porous material and a colloidal particle is absent (i.e., a relatively high ionic strength solution), trajectory analysis provides good agreement with experimental data (Payatakes et al. 1974; Guzy et al. 1983). On the other hand, when a double-layer force is significant, predictions based on this approach do not agree with experimental observations even qualitatively (Rajagopalan & Tien 1977; Onorato 1980). Recently, Tien (1993) proposed a patched surface model to improve the prediction capability for analyzing particle deposition in the presence of a repulsive double-layer force.

Solute Transport

The description of solute transport in a discretely fractured porous medium requires governing equations for both the porous matrix and the fractures. The solute may undergo advection, dispersion, sorption onto fracture surfaces and the solid matrix, as well as sorption onto the colloidal particles (radionuclide decay is neglected in this application of COLFRAC). Sorption onto the porous matrix is assumed an equilibrium reaction, whereas sorption onto the fracture surfaces or onto the colloids can be either an equilibrium or kinetic reaction. Because it is assumed that the colloids are too large to diffuse into the matrix, the effects of the colloids on

solute transport in the matrix will not be considered. The appropriate form of the advection-dispersion equation governing solute transport in the matrix is (Bear 1972):

$$\phi_{im} R_{im} \frac{\partial c_{im}}{\partial t} + q_i \frac{\partial c_{im}}{\partial x_i} - \frac{\partial}{\partial x_i} D_{ij} \frac{\partial c_{im}}{\partial x_j} = 0, \tag{24}$$

where D_{ij} [L^2/T] is the matrix dispersion coefficient.

The dispersion coefficient, D_{ij}, is given by (Bear 1972):

$$\phi_{im} D_{ij} = (\alpha_L - \alpha_T) \frac{q_i q_j}{|q|} + \alpha_T |q| \delta_{ij} + \phi_{im} \tau D_{aq} \delta_{ij}, \tag{25}$$

where α_T [L] is the transverse matrix dispersivity and δ_{ij} is the Kronecker delta.

A linear Freundlich sorption isotherm describes equilibrium reversible partitioning of the solute between the aqueous phase and the solid phase comprising the matrix material. As in STAMMT–L, the retardation factor R_{im} can be related to the distribution coefficient, K_d, by (15) (Freeze & Cherry 1979).

In the fracture, the aqueous phase solute is distributed among four phases. These include mass in the mobile fluid, mass on the fracture surfaces, mass on the filtered colloids that are attached onto the fracture surface, and mass on the suspended colloids that are suspended in the groundwater.

Accordingly, the equation that describes aqueous phase solute transport and exchange between each phase can be written as (Ibaraki & Sudicky 1995a):

$$2b\left[\frac{\partial c_m}{\partial t} + q_f \frac{\partial c_m}{\partial l} - \frac{\partial}{\partial l} D_f \frac{\partial c_m}{\partial l} + \frac{\partial}{\partial t} R_{c_m - \tilde{c}_n}\right] + 2\left[\frac{\partial}{\partial t} R_{c_m - \tilde{c}} + \frac{\partial}{\partial t} R_{c_m - \tilde{c}_{\tilde{n}}} \pm q_{fc}\right] = 0, \tag{26}$$

where D_f [L^2/T] is the solute dispersion coefficient defined later. The term q_{fc} [M/L^2T] is a flux representing the advective-dispersive transfer of solute across the fracture/matrix interface. Continuity of solute flux and concentration at the matrix/fracture interface provides a coupling between equations (24) and (26) in a manner similar to the coupling of the matrix and fracture flow equations.

The terms $R_{c_m - \tilde{c}}$ [M/L^2], $R_{c_m - \tilde{c}_n}$ [M/L^3], and $R_{c_m - \tilde{c}_{\tilde{n}}}$ [M/L^2] represent solute mass that is exchanged due to sorption reactions onto the fracture surfaces, the suspended colloids, and the filtered colloids, respectively (tildes will be used to denote sorbed solutes). Accounting for the processes of sorption of the solute onto the fracture surface, $\tilde{c}$ [M/L^2], is described by (Ibaraki & Sudicky 1995a):

$$2b\left[\frac{1}{b}\frac{\partial \tilde{c}}{\partial t} - \frac{1}{b}\frac{\partial}{\partial t} R_{c_m - \tilde{c}}\right] = 0. \tag{27}$$

The solute mass sorbed onto the filtered colloids, $\tilde{c}_{\tilde{n}}$ [M/L^2], is a function of the rate of colloid filtration, λq_n, and the solute concentration on the suspended colloids, $\tilde{c}_n$ [M/L^3], which are

filtered. Accounting for the sorption of solute onto the filtered colloids, $\tilde{c}_{\tilde{n}}$ is described by (Ibaraki & Sudicky 1995a):

$$2b\left[\frac{1}{b}\frac{\partial \tilde{c}_{\tilde{n}}}{\partial t}-\frac{1}{b}\frac{\partial}{\partial t}R_{c_m-\tilde{c}_{\tilde{n}}}-\lambda q_n \tilde{c}_{\tilde{n}}\right]=0. \tag{28}$$

Suspended colloidal particles in the fracture are affected by advective and dispersive processes as well as filtration onto the fracture surfaces. Solute sorbed onto the colloids is therefore affected by the same processes. Taking into account solute sorption onto the suspended colloids and solute lost from suspended colloids in the fracture due to the filtration of colloidal particles onto which the solute is sorbed, the mass balance equation for $\tilde{c}$ is given by (Ibaraki & Sudicky 1995a):

$$2b\left[\frac{\partial \tilde{c}_n}{\partial t}+q_n\frac{\partial \tilde{c}_n}{\partial l}-\frac{\partial}{\partial l}D_n\frac{\partial \tilde{c}_n}{\partial l}-\frac{\partial}{\partial t}R_{c_m-\tilde{c}_n}+\lambda q_n \tilde{c}_n\right]=0. \tag{29}$$

The dispersion coefficients, D_f and D_n, are described in the usual way as:

$$\begin{aligned} D_f &= \alpha_{Lf} q_f + D_{aq}, \\ D_n &= \alpha_{Lc} q_n + D_{dm}, \end{aligned} \tag{30}$$

where α_{Lc} [L] is the longitudinal dispersivity for the colloids.

Solute Sorption Processes

Solute and colloid transport in fractures is coupled by the solute sorption reactions with the colloidal particles. In addition, solute can be sorbed onto the fracture surfaces. It is assumed that kinetic reactions describe the adsorption and desorption processes occurring between the solute, the colloids, and the fracture surfaces. It is also assumed that the sorption reactions follow a linear Freundlich isotherm although COLFRAC can accommodate other sorption models like equilibrium or Langmuir. For kinetic-Freundlich reactions, the following first-order equations identical to the expressions proposed by Lapidus & Amundson (1952) are employed:

$$\begin{aligned} \frac{\partial \tilde{c}}{\partial t} &= \beta_a\left(K_a \rho_g c_m - \tilde{c}\right), \\ \frac{\partial \tilde{c}_n^*}{\partial t} &= \beta_n\left(K_n c_m - \tilde{c}_n^*\right), \\ \frac{\partial \tilde{c}_{\tilde{n}}^*}{\partial t} &= \beta_{\tilde{n}}\left(K_{\tilde{n}} c_m - \tilde{c}_{\tilde{n}}^*\right), \end{aligned} \tag{31}$$

where β_a [1/T], β_n [1/T], and $\beta_{\tilde{n}}$ [1/T] are the kinetic rate constants for the fracture surface, the suspended colloids, and the filtered colloids, respectively, and K_a [M/L^3], K_n [L^3/M], and $K_{\tilde{n}}$ [L^3/M] are the distribution coefficients for the fracture surface, the suspended colloids, and the filtered colloids, respectively. Recall that ρ_g is the grain density of the minerals on the fracture surface. Note that $\beta_n = \beta_{\tilde{n}}$ and $K_n = K_{\tilde{n}}$ in all COLFRAC simulations. The quantities $\tilde{c}_n^*$ [M/M] and $\tilde{c}_{\tilde{n}}^*$ [M/M] represent the mass of solute adsorbed onto the mobile and filtered

colloids, respectively, per unit mass of mobile and filtered colloids. They are related to $\tilde{c}_n$ and $\tilde{c}_{\tilde{n}}$ according to (Ibaraki & Sudicky 1995a):

$$\begin{aligned} \tilde{c}_n &= \tilde{c}_n^* n, \\ \tilde{c}_{\tilde{n}} &= \tilde{c}_{\tilde{n}}^* \tilde{n}. \end{aligned} \tag{32}$$

The use of a Freundlich isotherm, whether or not the sorption process is instantaneous, implies that the colloids and fracture surfaces have an infinite capacity to adsorb the solute. When the reactions are kinetic and the sorbed-phase concentration ($\tilde{c}$, $\tilde{c}_n^*$, and $\tilde{c}_{\tilde{n}}^*$) attains its equilibrium concentration value given by (31), the sorbed-phase concentration will not change unless the aqueous-phase concentration changes.

(2) Parameters

An example COLFRAC input file is supplied in A1.3-A Appendix: Example COLFRAC input file for I131. COLFRAC input files contain numerous variables, logical switches, and output control parameters, that are described in the *User's Manual* (Ibaraki, *personal communication, 2003*). All parameters varied by PEST (see §A1.3-2.2.3) and the corresponding CRR data used for the fitting are listed in Table A1.3-2.5. Because U^{233} was not modeled without colloids, it should be noted that K_a, β_a, and R_{im} had to be additionally estimated in the U^{233} model run with colloids (see Tab. A1.3-2.5). Furthermore, although COLFRAC allows different parameter values to be specified for reaction terms in the horizontal and vertical direction, all such values were held equal. It should be noted that COLFRAC requires a non-zero value for reverse kinetic reaction rates, even when modelling a conservative tracer (zero forward reaction rate). In addition, non-zero colloid concentrations are also required, even for model runs without colloids, therefore these parameters were set to 10^{-15}.

Tab. A1.3-2.5: COLFRAC parameters manipulated through PEST

Parameter	I^{131}	Am^{243} and Np^{237}	Am^{241} +coll.	Np^{237}+coll.	U^{233}+coll.
α_{Lf}	Fit	From I^{131} fit	From I^{131} fit	From I^{131} fit	From I^{131} fit
α_L	Fit	From I^{131} fit	From I^{131} fit	From I^{131} fit	From I^{131} fit
$2b$	Fit	From I^{131} fit	From I^{131} fit	From I^{131} fit	From I^{131} fit
α_T	Fit	From I^{131} fit	From I^{131} fit	From I^{131} fit	From I^{131} fit
K_{ij}	Fit	From I^{131} fit	From I^{131} fit	From I^{131} fit	From I^{131} fit
D_e	Fit	From I^{131} fit	From I^{131} fit	From I^{131} fit	From I^{131} fit
$_{im}$	Fit	From I^{131} fit	From I^{131} fit	From I^{131} fit	From I^{131} fit
$\beta_a K_a \rho_g$	N/A	Fit	From Am^{243} fit	From Np^{243} fit	Fit
β_a	N/A	Fit	From Am^{243} fit	From Np^{243} fit	Fit
R_{im}	N/A	Fit	From Am^{243} fit	From Np^{243} fit	Fit
α_{Lc}	N/A	N/A	Fit	Fit	Fit
$\beta_n K_n$	N/A	N/A	Fit	Fit	Fit
β_n	N/A	N/A	Fit	Fit	Fit
λ	N/A	N/A	Fit	Fit	Fit

A1.3-2.2.3 PEST

The parameter estimation program, PEST, is used to adjust COLFRAC input parameters such that the discrepancies between the model-generated output concentrations and the corresponding CRR measurements are reduced to a minimum. It does this by taking control of the model and running it as many times as is necessary to determine this optimal set of parameters.

COLFRAC is used to relate the results of various experimental runs to parameters that can actually be interpreted (dispersivity, kinetic reaction rates, colloid filtration rates, etc.). Specifically, COLFRAC has several parameters that govern radionuclide and colloid facilitated radionuclide transport. Initial guesses for unknown model parameters are supplied to PEST along with acceptable ranges of these parameters. Then, PEST initiates a series of COLFRAC runs with varied input parameters in an attempt to match model output to experimental data. In the process, PEST performs a sensitivity analysis describing the parameters most influential on model output. Furthermore, a 95 uncertainty range for each parameter is also obtained.

The Gauss-Marquardt-Levenberg algorithm used by PEST is described in detail in the *User's Manual* (Doherty 2002). For nonlinear models such as COLFRAC, parameter estimation is an iterative process. At the beginning of each iteration, the relationship between model parameters and model-generated observations is linearized by formulating it as a Taylor series expansion about the best current parameter set. Therefore, the derivatives of all observations with respect to all parameters must be calculated. This linearized problem is then solved for a better parameter set, and the new parameters tested by running the model again. By comparing parameter changes and objective function improvement achieved through the current iteration with those achieved in previous iterations, PEST can tell whether it is worth undertaking another optimization iteration; if so the whole process is repeated.

A1.3-3 Results

A1.3-3.1 STAMMT–L

STAMMT–L was used for preliminary analyses of the experimental data. While STAMMT–L cannot explicitly account for enhance colloid transport, through examination of calculated retardation coefficients, a qualitative analysis of the effects of the colloids can be conducted. Although STAMMT–L can model multi-rate diffusion, in this model, the single rate option is chosen because of the short residence time and path length of the tracer. STAMMT–L was first used to estimate transport parameters for the nonreactive tracer, I^{131}. From this analysis, the estimated flow velocity and ϕ_{im}/ϕ_m were fixed for the analyses of run#31. STAMMT–L was not used to evaluate the breakthrough curves for run#32 because, the model does not account for any of the competing processes with enhanced colloid transport.

(1) Iodine 131

Table A1.3-3.1 lists the input and resulting estimated parameters used in the STAMMT–L model fit of the I^{131} data. The semi-analytical solution in STAMMT–L specifies a no flux boundary condition at some distance, L. While the straight-line distance between the injection and withdrawal well is 2.5 m (solute concentrations are analyzed here), a system length of 4 m was chosen to prevent the no flux boundary condition at $L = 4$ m from influencing the solution at the withdrawal well ($x = 2.5$ m). Figure A1.3-3.1 illustrates the inverse modelling results. When modelling a conservative tracer with an assumed retardation factor of 1, according to (13) , the capacity of the matrix to store solute, β, is simply the ratio of the porosities in the matrix to

the mobile fractured zone (Tab. A1.3-2.3). Substituting the range of porosities of the matrix, ϕ_{im}, from Table A1.3-2.1 and β = 0.82 into (13) yields a fractured zone porosity of $0.006 < \phi_m < 0.04$. This is consistent with the porosity of a fill or gouge material occupying much of the fractured zone. Furthermore, the dispersivity is α_L = 0.15 m, a reasonable value given L_s = 2.5 m and the fast interstitial velocity $v_x = 7.05 \times 10^{-4}$ m/s. Over the 600-s the established dipole results in a dilution facto of at least 15, which is notably smaller than what was estimated. This higher estimate for the dilution factor is not unreasonable because the withdrawal well is pumping at a continuous rate of approximately 15 times the injection rate and fluid already in the system is diluting the injectant. Finally, the mass transfer rate between the matrix and fractured zone was approximated as $\alpha_d = 7.1 \times 10^{-5}$ 1/s for I^{131}. This number is close to the value of 7.5×10^{-5} 1/s reported by McKenna (1999) for the Äspö STT-1b tracer tests for uranine.

Tab. A1.3-3.1: Parameters used in STAMMT–L to model the conservative tracer, I^{131}

Parameter	**Value**	**Usage**
L (m)	4	specified
R_m (–)	1	specified
v_x (m/s)	$4.25 \pm 0.08 \times 10^{-4}$	estimated
α_d (m/s)	$5.8 \pm 0.6 \times 10^{-5}$	estimated
α_L (m)	0.19 ± 0.02	estimated
β (–)	0.72 ± 0.07	estimated
dilute (–)	$1{,}481 \pm 61$	estimated

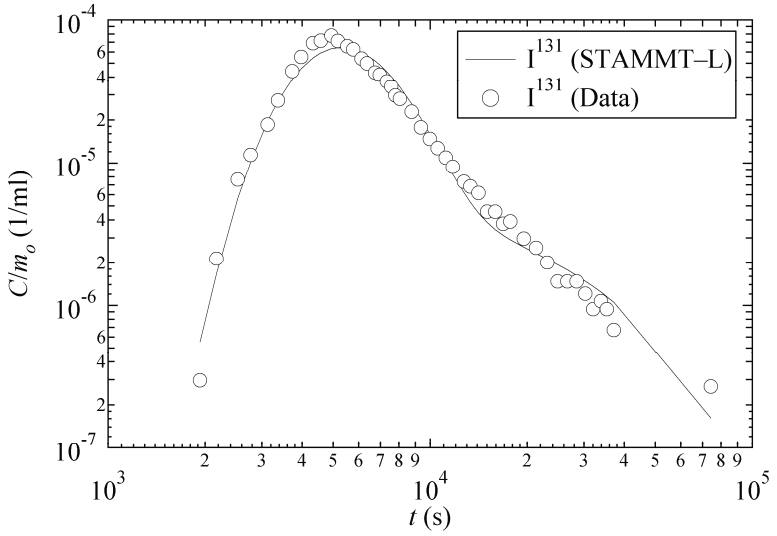

Fig. A1.3-3.1: STAMMT–L fit to I^{131} CRR experimental data

(2) Americium 243 and Neptunium 237 without colloids

Recall that dispersivity and velocity were taken from the I^{131} analysis (see Tab. A1.3-3.1). Considering the high interstitial fluid velocity and short pathlength, the mobile zone retardation is set equal to one. Figure A1.3-3.2 compares the STAMMT–L results with the experimental data for Am^{243} and Np^{237}. The estimated mobile zone dilution factors, capacity coefficients, and mass transfer rates for the reactive solutes not subject to colloid enhanced transport, $Am^{243}$and Np^{237}, are listed in Table A1.3-3.2.

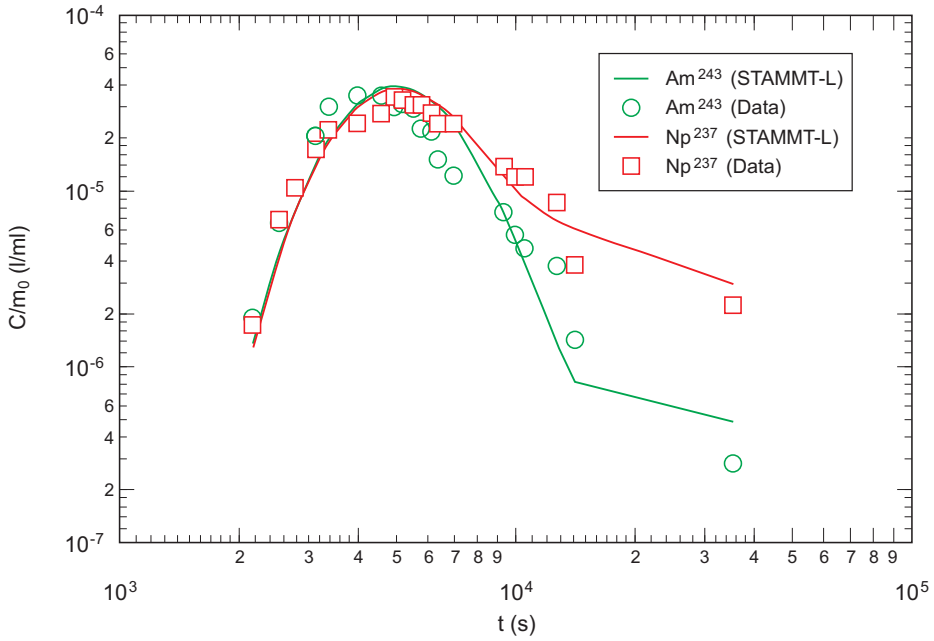

Fig. A1.3-3.2: STAMMT–L fits to Am243 and Np237 without bentonite colloids (run#31)

Tab. A1.3-3.2: STAMMT–L estimated parameters for Am^{243} and Np^{237} transport without bentonite colloids (run#31)

Parameter	**Am^{243}**	**Np^{237}**	**Source**
R_m (–)	1	1	specified
R_{im} (–)	51	4	from (13) and (15)
β (–)	37 ± 24	3 ± 1	estimated
α_d (1/s)	$3.8 \pm 0.9 \times 10^{-6}$	$5.7 \pm 0.9 \times 10^{-5}$	estimated
dilute (–)	1,504 ± 408	1,567 ± 208	estimated
ϕ_{im}/ϕ_m (–)	0.72	0.72	from I^{131} analysis
v_x (m/s)	4.25×10^{-4}	4.25×10^{-4}	from I^{131} analysis

It is not surprising that within confidence limits, the dilution factor is unchanged from I^{131} because all three radionuclides were run in the same experiment. Greater retardation in the immobile zone is calculated for Am^{243} than Np^{237}. This is expected based on the values reported

in Table A1.3-2.2. Furthermore, substituting $\rho_b = 2.67$ g/ml and $\phi_{im} = 0.02$ from Table A1.3-2.3 and R_{im} from Table A1.3-3.2 into (15) yields $K_d = 0.4$ ml/g for Am^{243} and $K_d = 0.02$ ml/g for Np^{237}. The magnitude of these values is different from those shown in Table A1.3-2.2. A partial explanation for this could be sorption disequilibrium, given the short residence time in the experiment. On the other hand, the fact that the K_d for Np^{237} is an order of magnitude lower than that of Am^{243} is consistent with what is reported in Table A1.3-2.2.

A1.3-3.2 COLFRAC

The unknown parameters to be estimated with COLFRAC are grouped into two categories: 1) parameters related to the geometry of the system independent of the tracer tests (fracture number and frequency, fracture length, and fracture aperture; and, 2) parameters related to the tracer tests (reactivities and dispersivities). COLFRAC simulation results are highly dependent upon the first group, and although estimates of some of the parameters are available (Tab. A1.3-2.3), there is significant uncertainty.

The fracture geometry selected is presented in Figure A1.3-3.3. This geometry was determined through trial and error to best match the characteristics and shape of the I^{131} breakthrough curve. Horizontal fractures are spaced 2.5 cm apart and vertical fractures are spaced 10 cm apart. Fracture spacing and length were set as constants in subsequent simulations. Fracture aperture was estimated, but it did not vary greatly.

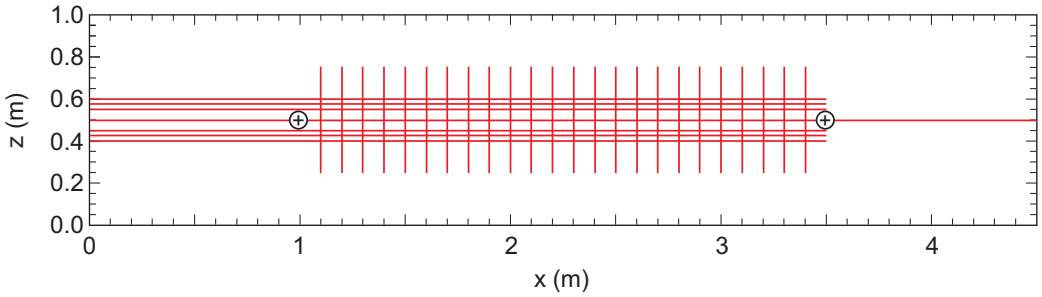

Fig. A1.3-3.3: Geometry of the fracture system used in COLFRAC

Note the injection and withdrawal wells at $x = 1$ and $x = 3.5$ m, respectively

Once the geometry of the system was defined, COLFRAC and PEST were used to fit the I^{131} data by estimating transport parameters (effective diffusion coefficient, hydraulic conductivity, matrix and fracture dispersivity, etc.) for the conservative solute. Once these parameters were estimated, they were set as constant and the transport parameters (forward and backward kinetic reaction rates and matrix retardation coefficient) for the reactive tracers without colloids (Am^{243} and Np^{237}) were estimated. Finally, these reactive transport parameters were set as constant and the enhanced colloid migration parameters (colloid dispersivity, colloid/radionuclide forward and backward kinetic reaction rates, and colloid filtration coefficient) were estimated using the breakthrough curve data from run#32. Because U^{233} without colloids was not modeled, the transport and colloid enhanced migration parameters were all estimated from this radionuclide.

(1) Iodine 131

Initial concentrations of the injected tracers are listed in Table A1.3-2.4. These data had to be converted from normalized concentration to kg/m^3 for use in COLFRAC. Even after this

conversion, the COLFRAC breakthrough curve for I^{131} still required scaling to match the CRR data regardless of the transport parameters selected by PEST. Perhaps this scaling is related to the large dilution factor reported in Table A1.3-3.1. All output concentrations for run#31 were multiplied by 1.2×10^{-2} (Fig. A1.3-3.5). This scaling was performed for all of the radionuclides of run #31 only.

PEST was used to run COLFRAC (47 model calls) to estimate system and transport parameters for I^{131} and in the process perform a sensitivity analysis. Because I^{131} is a conservative tracer, the retardation factor is set to 1 and all matrix and colloid forward reaction parameters are set to 0. Table A1.3-3.3 lists the parameters that were varied by PEST, their estimated values, and corresponding 95 % uncertainty range. Entries are listed in order from the most sensitive parameter to the least sensitive parameter. Thus, it can be seen that the longitudinal and transverse dispersivities in the matrix, α_L and α_T, are least sensitive. The model is thought to be least sensitive to these parameters due to a combination of low immobile zone porosity and low hydraulic conductivity. In addition, note that the uncertainty ranges increase with decreasing sensitivity. This makes sense because as a parameter has less impact on the model output, the range of values that it can assume while still yielding a tractable result increases. Figure A1.3-3.5 illustrates the match between PEST optimized parameters used in COLFRAC, both raw and scaled, and the CRR data.

Estimated values of fracture aperture and immobile zone porosity are consistent with those listed in Table A1.3-2.3. The 95 % uncertainty range for hydraulic conductivity is within the acceptable range for granodiorite. Effective diffusion coefficient estimates, however appear to be too large as compared to Table A1.3-2.3. In fact, estimated D_e is approximately that of free water (although within the 95 % uncertainty range D_e is reasonable). One reason why D_e is high could be due to the assumed model geometry input to COLFRAC. The fewer the fractures, the greater the D_e required to match the spreading of the solute plume. Although it was not investigated, an increase in fracture frequency might result in a lower D_e. The estimated longitudinal dispersivity appears reasonable, approximately and order of magnitude lower than the travel distance.

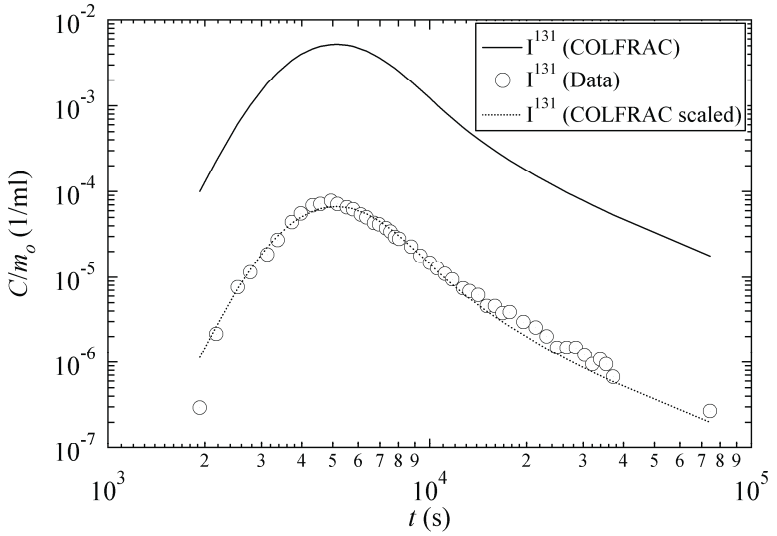

Fig. A1.3-3.4: COLFRAC fit to CRR experimental data with and without output concentration scaling (run#31)

Tab. A1.3-3.3: COLFRAC parameters estimated by PEST for I^{131} listed in order of model sensitivity

The best estimate, along with the 95 % uncertainty range, is also presented (run#31)

Parameter	Estimated value	Uncertainty range
$2b$ (m)	2.0×10^{-4}	$1.9–2.1 \times 10^{-4}$
K_{ij} (m/s)	1.2×10^{-11}	$0–2.8 \times 10^{-9}$
D_e (m^2/s)	3.4×10^{-9}	$0–3.7 \times 10^{-8}$
ϕ_{im} (–)	0.015	0–0.05
α_{Lf} (horizontal) (m)	0.14	0–0.20
α_{Lf} (vertical) (m)	0.07	0–0.41
α_L (m)	0.1	0–35.4
α_T (m)	0.01	0–3.54

(2) Americium 243 and Neptunium 237 without colloids (run#31)

Once parameter baselines have been established (Tab. A1.3-3.3), they are applied to the reactive radionuclides and PEST is used to estimate reactive transport parameters. Figure A1.3-3.5 and Table A1.3-3.4 show the PEST matches of scaled COLFRAC output to CRR data for Am^{243} (25 model calls) and Np^{237} (30 model calls). These values are also listed in order of sensitivity.

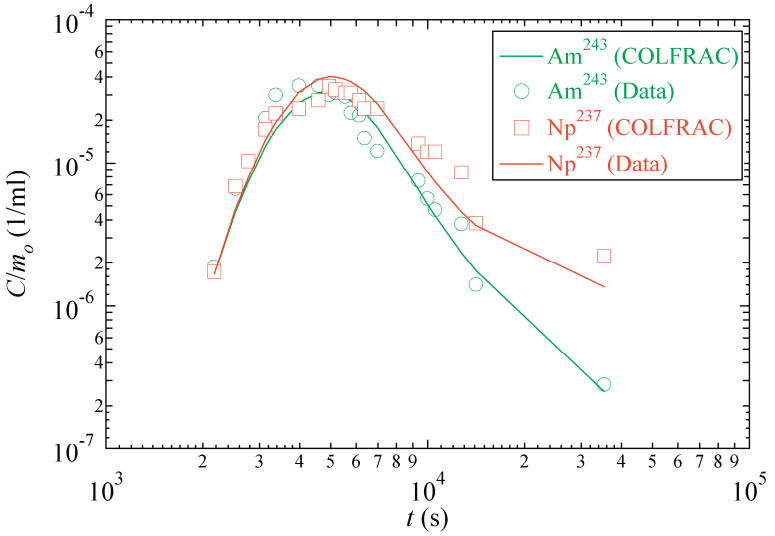

Fig. A1.3-3.5: COLFRAC results compared to CRR experimental data for Am^{243} and Np^{237} (run#31)

Comparison of the forward and reverse reaction rates for Am^{243} and Np^{237} show similar forward reaction rates. However, the reverse rate for Np^{237} is significantly higher than that for Am^{243}, which may correspond to increased tailing in its breakthrough curve. One explanation for this tailing is increased desorption from the fracture walls and matrix for Np^{237}. In addition, for kinetic reactions, a higher desorption rate typically corresponds to a lower K_d.

Both radionuclides show that within the 95 % uncertainty range there is essentially no immobile zone retardation. Recall that the immobile zone retardations for Am^{243} and Np^{237} from STAMMT–L were significantly greater than one. This discrepancy may be explained in the fundamentally different system conceptualizations of each model. Because STAMMT–L is one-dimensional, spreading of the solute plume must arise from the dispersivity term and interaction between the mobile and immobile zones because there is only one flowpath. In COLFRAC, the low porosity and hydraulic conductivity of the immobile zone leave little interaction between the fractures and matrix. In addition to that arising from sorption onto the fracture walls, much of the spreading and tailing seen in COLFRAC can be attributed to solutes assuming different tortuous flowpaths down the two-dimensional network of fractures.

Tab. A1.3-3.4: COLFRAC parameters estimated by PEST for Am^{243} and Np^{237} listed in order of sensitivity (run#31)

Parameter	**Am^{243}**		**Np^{237}**	
	Estimate	**95 % Confidence**	**Estimate**	**95 % Confidence**
$\beta_a K_a \rho_g$ (–)	2.3×10^{-8}	1.4×10^{-9}–4.5×10^{-8}	4.4×10^{-8}	2.4–6.4 × 10^{-8}
R_{im} (–)	1.0	1.0–1.5	1.1	1.0–1.6
β_a (1/s)	1.5×10^{-10}	0–4.2×10^{-5}	6.9×10^{-6}	0–8.4×10^{-5}

(3) Americium 243, Neptunium 237, and Uranium 233 with bentonite colloids

Once parameter baselines have been established (see Tab. A1.3-3.3 and Tab. A1.3-3.4), they are applied to the reactive radionuclides of run#32 and PEST is used to estimate colloid reactive transport parameters. Figure A1.3-3.6 and Table A1.3-3.5 show the PEST matches of COLFRAC output to CRR data for run#32. These values are also listed in order of sensitivity to the Am^{241} run. Table A1.3-3.6 shows the reactive transport parameters for U^{233}.

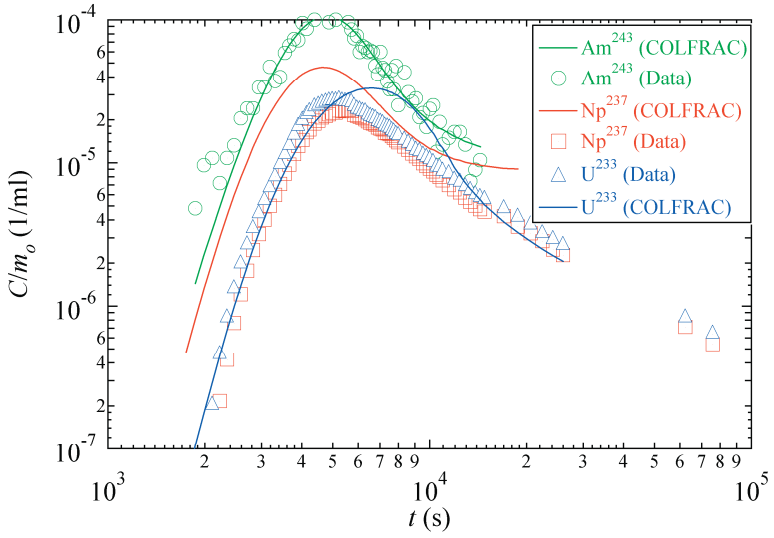

Fig. A1.3-3.6: COLFRAC results compared to CRR experimental data for Am^{241}, Np^{237}, and U^{233} in the presence of bentonite colloids (run#32)

Tab. A1.3-3.5: COLFRAC parameters estimated by PEST for Am^{241}, Np^{237}, and U^{233} with bentonite colloids listed in order of model sensitivity (run#32)

Parameter	**Am^{241}**		**Np^{237}**		**U^{233}**	
	Estimate	**95 % Confidence**	**Estimate**	**95 % Confidence**	**Estimate**	**95 % Confidence**
α_{Lc} (vertical) (m)	0.02	0–1.3	0.02	N/A	0.05	N/A
α_{Lc} (horizontal) (m)	0.13	0.03–0.23	0.13	N/A	0.15	N/A
λ (–)	1.2	0.7–1.8	1,200	N/A	1.0×10^{-12}	N/A
β_n (1/s)	8.1×10^{-6}	0–2.1×10^{-3}	8.1×10^{-6}	N/A	4.2×10^{-14}	N/A
$\beta_n K_n$ (1/s)	7.5×10^{-2}	0–3.1	0.8	N/A	2.3×10^{-2}	N/A

N/A – Not available

Tab. A1.3-3.6: Reactive transport parameters for U^{233} (run#32)

Parameter	**U^{233}**	
	Estimate	**95 % Confidence**
$\beta_a K_a \rho_g$ (1/s)	0	N/A
β_a (1/s)	1.1×10^{-14}	N/A
R_{im} (–)	1.0	N/A

PEST and COLFRAC were able to fit the Am^{241} data well without scaling the output concentrations. Note that the least sensitive parameters are the colloid forward and reverse reaction rates while the colloid dispersivities are the most sensitive. This indicates that the Am^{241} sorbed onto colloids is affecting breakthrough and that fraction of this radionuclide associated with the bentonite is an important process affecting its breakthrough.

PEST was unable to find a good match for either the Np^{237} or U^{233} breakthrough curves for run#32. Because of the significant disparity between the best fit and the experimental data, PEST could not calculate a covariance matrix and therefore a 95 % uncertainty interval is not available. It is unclear why COLFRAC cannot be used to match the experimental data in these cases. When COLFRAC runs for run#32 were scaled by 1.2×10^{-2} (the value used to scale results for run#31), the model was able to match Np^{237} and U^{233} breakthrough, but not Am^{241} data. In addition, as discussed below, while the qualitative experimental results for Am^{241} are expected, perhaps there are processes that the model does not account for that are affecting Np^{237} and U^{233} breakthrough.

A1.3-4 Discussion

Before summarizing the modelling results, a qualitative analysis of the experimental setup and observed data can provide insight into the system. First, consider the experimental setup. Dipole flow is established in the fractured zone (test shear zone) of a granodiorite rock mass with injection and withdrawal wells spaced 2.5 m apart. The velocity established between wells is high, yielding a travel time of approximately 1.7 hours. Such a short residence time and high velocity suggest that:

- an assumption of equilibrium reaction may not be the appropriate way to model radionuclide sorption;
- measured mass transfer is dependent on the length and time scales of the system – with the fast pumping rates and short travel distance of these experiments, only a small portion of the system may interact with the tracers;
- and, that flow and transport between the injection and withdrawal wells can likely be estimated with a one-dimensional model.

Second, the effect of the colloids on radionuclide breakthrough is conceptually difficult to explain based upon known information and the shape of the breakthrough curves. Figure A1.3-3.7 compares the Am^{243} and Np^{237} breakthrough curves both with and without added colloids. Comparing run#31 (open symbols) to run#32 (filled symbols), colloids appear to have enhanced the transport of Americium while not significantly affecting the transport of Np^{237}. Given the distribution coefficients of Am^{243} and Np^{237} to bentonite (Tab. A1.3-2.2), these results are expected as Am^{243} is expected to sorb more strongly onto colloids. Along with this observation, we would also expect greater recovery of Am^{243} when colloids are added to the system as more will sorb onto the colloids than the fracture walls or matrix. This phenomenon was also observed, as the recovery rate of Americium went from 30 % in run#31 to 70 % in run#32 (Möri & Alexander 2001). The experimental results for Np^{237} cannot be analyzed as easily. Data reveal a slight retardation of Np^{237} when bentonite is present without an associated loss of recovery. Total recovery of Neptunium did not change significantly in the presence of colloids (80 % in both runs), indicating that there was not significant sorption of Np^{237} onto the colloids or that such sorption did not significantly affect sorption of Np^{237} to the fracture walls or matrix. However, the breakthrough was delayed and peak concentrations were slightly diminished in the presence of colloids implying that Np^{237} is somehow retarded is increased when colloids are added to the system. One possible explanation is that Np^{237} may be sorbing onto filtered colloids. However, why would colloids with Np^{237} be filtered more than colloids with Am^{243}? These results suggest that there might be some unaccounted for processes affecting the system. Are naturally occurring colloids or some other process affecting the transport of Np^{237}? Without more data (e.g., concentration of natural colloids and associated radionuclides), this question remains open to debate.

Third, note that the tails of the breakthrough curve of Np^{237} and U^{233} in run#32 show approximately a –3/2 slope. Tsang (1995), Heer & Hadermann (1996), and Haggerty et al. (2001) state that the late time behavior of breakthrough curves with a –3/2 slope is indicative of significant matrix diffusion. Thus, the observed –3/2 slope may indicate that colloids have a negligible impact on the transport of these radionuclides and that most of their transport behavior is due to interaction with the fracture gouge and rock matrix.

In general, modelling results are consistent with these qualitative analyses. STAMMT–L provided excellent matches to colloid-free solute transport; however, the equilibrium assumption used in the model is questionable under these experimental conditions. Furthermore, the dilution factor is a difficult parameter to physically quantify and its variations could be due

to changes in fluid collection and/or recovery rates. While COLFRAC's kinetic reaction rates are probably more defensible than equilibrium reactions, the reaction rate parameters, while making intuitive sense with respect to the shapes of the breakthrough curves, may not be fully consistent with the known chemistry of the radionuclides (i.e., high K_d for Americium).

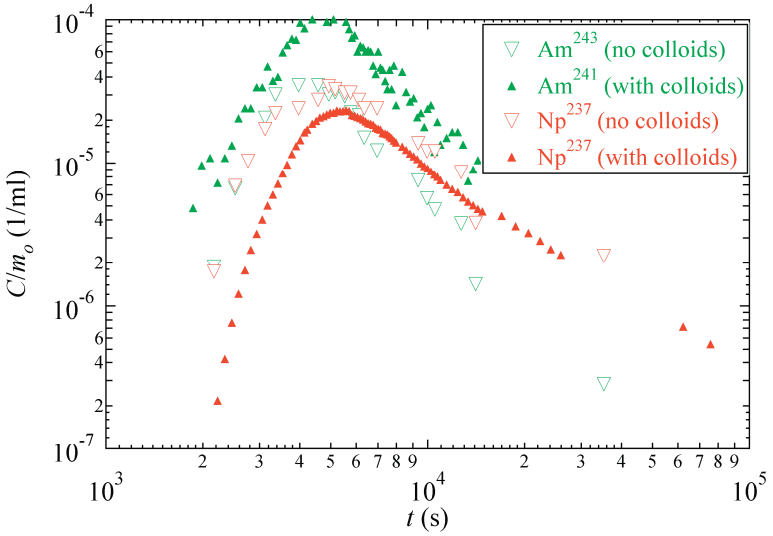

Fig. A1.3-3.7: Breakthrough curves comparing breakthrough for Americium and Neptunium both with and without added colloids

Some shortcomings in these modelling efforts should be noted. First, it must be reiterated that while COLFRAC was able to match the shapes of the breakthrough curves, all output concentrations for run#31 were scaled by 1.2×10^{-2}. Perhaps selection of a different geometry would yield results that did not require scaling, but COLFRAC was particularly sensitive to geometry parameters and did not allow successful interfacing with PEST to select them. On the other hand, this scaling factor may also have been due to the small injection volume in run#31. In addition, COLFRAC could not match the breakthrough curves for Np^{237} or U^{233} in run#32 without scaling even when using non-physical parameters. As mentioned above, it appears that there is some process unaccounted for in our modelling affecting Np^{237} and U^{233} breakthrough.

An improvement in the modelling results is expected if colloid breakthrough curves were accounted for in the inverse modelling with COLFRAC. Ideally, PEST would have been used with COLFRAC to estimate the horizontal and transverse dispersivities of the colloids and the colloid filtration coefficient independently of the radionuclide breakthrough data. That is, COLFRAC could have been run (without radionuclides) to match colloid breakthrough concentrations while estimating α_{Lc} and λ. These values would then have been fixed in the parameter estimation process for run#32 before estimating solute sorption and desorption rates onto colloids, $\beta_n K_n$ and β_n. This might have led to more accurate estimates of colloid reaction rates and better fits to the data. Finally, a one-dimensional kinetic reaction cotransport code may be the best way to analyze these data. This code would need to easily integrate with PEST to estimate reaction parameters for the fractured medium as well as those related to colloid enhanced transport of radionuclides.

In summary, model shortcomings could possibly be overcome by: 1) adjusting the geometry parameters used in COLFRAC; and, 2) using the colloid concentration breakthrough curves in addition to solute breakthrough curves with the inverse modelling with COLFRAC and PEST.

Future fieldwork should consider modification to the experimental setup to facilitate a direct evaluation of colloid facilitated radionuclide transport. The effects of naturally occurring colloids should be studied more carefully. Injecting colloid-free fluid at the same rate as withdrawal could help abate the impact of naturally occurring colloids. Additionally, an attempt should be made to ascertain the fraction of radionuclides associated with colloids in the effluent. Finally, to facilitate a direct comparison of experimental results, identical conditions should be used in each experiment and the same data measured (e.g., injection rate and colloid and radionuclide concentrations).

A1.3-5 Conclusion

Field tests performed as part of the CRR project provide an excellent opportunity to stud *in situ* colloid facilitated radionuclide transport. Analysis results indicate that under the conditions produced in the test shear zone, bentonite colloids influence the retardation behavior of certain radionuclides. For the radionuclides modeled here, only Americium provides the greatest evidence of colloid enhanced transport in the form of greatly increased recovery and slightly decreased transport time. For the radionuclides with much lower distribution coefficients, Np^{237} and U^{233}, the addition of bentonite colloids does not appear to facilitate their travel and may even hinder transport.

Overall, results indicate that colloid enhanced transport may be an important factor in repository performance for strongly sorbing radionuclides, although more experimental data are needed to build a model with better predictive capabilities.

Nomenclature

A	activity, [Bq]
$2b$	(apv, aph) fracture aperture, [L]
$\tilde{c}$	solute mass sorbed onto fracture surfaces, [M/L^2]
$\widehat{c}_{im}$	average concentration in the immobile zone, [M/L^3]
c_{inj}	(cpval) solute injection concentration, [M/L^3]
c_m	mobile zone solute concentration, [M/L^3]
$\tilde{c}_n$	solute concentration sorbed onto suspended colloids, equal to $\tilde{c}_n^* n$ [M/L^3]
$\tilde{c}_n^*$	solute mass sorbed per suspended colloid mass, [M/M]
$\tilde{c}_{\tilde{n}}$	solute concentration sorbed onto filtered colloids, equal to $\tilde{c}_{\tilde{n}}^* \tilde{n}$ [M/L^2]
$\tilde{c}_{\tilde{n}}^*$	solute mass sorbed per filtered colloid mass, [M/M]
C_o	initial concentration of radionuclides, [M/L^3]
dilute	solute dilution factor, [–]
D_{aq}	aqueous diffusion coefficient, [L^2/T]
D_{dm}	colloid diffusion coefficient, [L^2/T]
D_e	(dstar) effective immobile zone solute diffusion coefficient, equal to τD_{aq}, [L^2/T]

D_f mobile zone solute dispersion coefficient, equal to $\alpha_{Lf}q_f+D_{aq}$, [L^2/T]

D_{ij} matrix dispersion tensor, [L^2/T]

D_n colloid dispersion coefficient, equal to $\alpha_{Lc}q_n+D_{dm}$ [L^2/T]

g gravitational acceleration, [L/T^2]

h hydraulic head in the immobile zone, [L]

h_f hydraulic head in the mobile zone, [L]

i subscript implying x-direction, [–]

j subscript implying z-direction, [–]

K_a distribution coefficient for solute sorption onto fracture walls, [L/M^3]

K_d distribution coefficient, [L^3/M]

K_f fracture hydraulic conductivity, [L/M]

K_{ij} (ckxx, ckzz) hydraulic conductivity tensor, [L/T]

K_n distribution coefficient for solute sorption onto suspended colloids, [L/M^3]

$K_{\tilde{n}}$ distribution coefficient for solute sorption onto filtered colloids, equal to K_n[L/M^3]

l distance along a fracture, [L]

ℓ half matrix block length, [L]

L_s total length of the system, equal to 4 m, [L]

m_o initial mass of radionuclides, [M]

n suspended colloid concentration, [M/L^3]

$\tilde{n}$ mass of filtered colloids per unit fracture surface area, [M/L^2]

N number of atoms, [–]

N_A Avogadro's Number, equal to 6.0221367×10^{23} atoms/mole, [–]

q_f fluid flux along a fracture/mobile zone pore water velocity, [L/T]

q_{fc} advective-dispersive solute flux across the fracture/matrix interface, [M/L^2T]

q_i Darcy fluid flux in the matrix, [L/T]

q_m fluid flux normal to the fracture/matrix boundary, [L/T]

q_n colloid velocity in a fracture, [L/T]

Q_i injection well pumping rate, equal to ~10 ml/min, [L^3/T]

Q_p withdrawal well pumping rate, equal to ~150 ml/min, [L^3/T]

$R_{c_m-\tilde{c}}$ solute mass exchanged due to sorption onto fracture surfaces, [M/L^2]

$R_{c_m-\tilde{c}_n}$ solute mass exchanged due to sorption onto suspended colloids, [M/L^3]

$R_{c_m-\tilde{c}_{\tilde{n}}}$ solute mass exchanged due to sorption onto filtered colloids, [M/L^2]

RF recovery factor, [–]

R_{im} (retard) immobile zone retardation, [–]

R_m mobile zone retardation, [–]

t time, [T]

$t_{½}$ half-life, [T]

x horizontal coordinate distance along the flow system, [L]

z vertical coordinate distance perpendicular to the flow system, [L]

Greek Symbols

α_d mass transfer rate between mobile and immobile zones, [1/T]

α_L (`al`) immobile zone longitudinal dispersivity, [L]

α_{Lc} (`alfracmh`, `alfracmv`) colloid fracture (mobile zone) dispersivity, [L]

α_{Lf} solute fracture (mobile zone) dispersivity, [L]

α_T (`at`) immobile zone transverse dispersivity, [L]

β capacity coefficient, equal to $R_{im}\phi_{im}/R_m\phi_m$, [–]

β_a (`betafh`, `betafv`) kinetic rate constant for solutes sorbing onto the fracture surfaces, [1/T]

β_n (`betacfh`, `betacfv`) kinetic rate constant for solutes sorbing onto suspended colloids, [1/T]

$\beta_{\tilde{n}}$ (`betacfh`, `betacfv`) kinetic rate constant for solutes sorbing onto filtered colloids, equal to β_n, [1/T]

Γ mass exchange between mobile and immobile zones, [M/L^{3}T]

δ_{ij} Kronecker delta, [–]

ϕ_{im} (`por`) immobile zone (matrix) porosity, [–]

ϕ_m mobile (fractured) zone porosity, [–]

λ (`ftfrach`, `ftfracv`) colloid filter coefficient, [–]

Λ disintegration constant, [1/T]

μ interstitial fluid viscosity, [M/LT]

ρ interstitial fluid density, [M/L^3]

ρ_b bulk (matrix) density, [M/L^3]

ρ_g grain density of the fracture surfaces, [M/L^3]

τ tortuosity, [–]

A1.3-6 References

Avogadro A. & de Marsily G. (1984).The role of colloids in nuclear waste disposal, *Mat. Res. Soc. Symp. Proc.*}, 26, 495–505.

Bear J. (1972). *Dynamics of fluids in porous media*, Elsevier Science, New York.

Berkowitz B., Bear J. & Braester C. (1988). Continuum models for contaminant transport in fractured porous formations, *Water Resour. Res*., **24**(8), 1225–1236.

Dieulin A., (1982). Filtration de colloides d'actinides par une colonne de sable argileux, LHM/RD/82/23, Centre d'Informatique Géologique de l'Ecole Nationale Supérieure des Mines de Paris.

Doherty J. (2002). http://www.epa.gov/ceampubl/mmedia/pest/PESTMAN.PDF.

Freeze R. A. & Cherry J. A. (1979). *Groundwater*, Prentice-Hall, Inc., Englewood Cliffs, New Jersey.

Guzy C. J., Bonano E. J. & Davis E. J. (1983). The analysis of flow and colloidal particle retention in fibrous porous media, *J. Colloid. Interface Sci*., **95**(2), 523–543.

Haggerty R., Flemming S. W., Meigs L. C. & McKenna S. A. (2001). Tracer tests in a fractured dolomite 2. Analysis of mass transfer in single-well injection-withdrawal tests, *Water Resour. Res*., **37**(5), 1129–1142.

Haggerty R. & Gorelick S. M. (1995). Multiple-rate mass transfer for modeling diffusion and surface reactions in media with pore-scale heterogeneity, *Water Resour. Res*., **31**(10), 2383–2400.

Haggerty R. & Gorelick S. M. (1998). Modeling mass transfer processes in soil columns with pore-scale heterogeneity. *Soil Sci. Soc. Am J*., **62**(1), 62–74.

Haggerty R. & Reeves P. (1999). STAMMT–L: Solute Transport and Multirate Mass Transfer, User's Manual. Sandia National Laboratories, NM.

Heer W. & Haddermann J. (1996). Modelling radionuclide migration field experiments, *Nagra Technical Report* 94–18, Nagra, Switzerland.

Herzig J. P., Leclerc D. M. & Le Goff P. (1970). Flow of suspensions through porous media. Application to deep filtration, *Ind. Eng. Chem*., **62**(5), 8–35.

Ibaraki M. & Sudicky E. A. (1995a). Colloid-facilitated contaminant transport in discretely fractured porous media 1. Numerical formulation and sensitivity analysis, *Water Resour. Res*., **31**(12), 2945–2960.

Ibaraki M. & Sudicky E. A. (1995b). Colloid-facilitated contaminant transport in discretely fractured porous media 2. Fracture network examples, *Water Resour. Res*., **31**(12), 2961–2969.

Kosakowski G. (2002). Evaluation of tracer tests in a shear-zone with a single fracture model, PSI Unpubl. Internal Report TM–44–02–03, PSI, Villigen, Switzerland.

Lapidus L. & Amundson N. R. (1952). Mathematics of adsorption in beds, VI. The effect of longitudinal diffusion in ion exchange and chromatographic columns, *J. Phys. Chem*., **56**, 984–988.

McKenna S. A. (1999). Solute transport modelling of the Äspö STT-1b tracer tests with multiple rates of mass transfer, Task 4E: Äspö Task Force on Modelling of Groundwater Flow and Transport of Solutes, *SKB–ICR–99–02*, Swedish Nuclear Fuel and Waste Management Company.

McKenna S. A. (2000a). Prediction of STT-2 tracer tests: Application of the multirate model, *SAND2000-2190C*, Sandia National Laboratories, NM.

McKenna S.A. (2000b). Solute transport modeling of the Äspö STT-1b tracer test with multiple rates of mass transfer, *SAND2000–2189C*, Sandia National Laboratories, NM.

McKenna S. A., Meigs L. C., & Haggerty R. (2001). Tracer tests in a fractured dolomite 3. Double-porosity, multiple-rate mass transfer processes in convergent flow tracer tests. *Water Resour. Res*., **37**(5), 1143–1154.

Meigs L. C. Beauheim R. L. & Jones T. L. (1997). Interpretations of tracer tests performed in Culebra dolomite at the Waste Isolation Pilot Plant, *SAND97–3109*, Sandia National Laboratories, NM.

Möri A. & Alexander W. R. (2001). The Colloid and Radionuclide Retardation project: Status report of year 2001 activities. Unpubl. Nagra Internal Report, Nagra, Wettingen, Switzerland.

Möri A., Alexander W. R., Geckeis H., Hauser W., Schaefer T., Eikenberg J., Fierz Th., Degueldre C. & Missana T. (2003). The Colloid and Radionuclide Retardation experiment (CRR) at the Grimsel Test Site (GTS): influence of bentonite colloids on radionuclide migration in a fractured rock. Colloids and Surfaces A, 217, 33-47.

Onorato F. J. (1980). The effect of surface interaction on particle deposition, *Chem. Eng. Commun*., **7**, 363–370.

Oswald J. G. & Ibaraki M. (2001). Migration of colloids in discretely fractured porous media: Effect of colloidal matrix diffusion, *J. Contam. Hydrol*., **52**, 213–244.

Payatakes A. C., Tien C. & Turian R. M. (1974). Trajectory calculation of particle deposition in deep bed filters: Part I and II., *AIChE Journal*, **20**, 889–901.

Rajagopalan R. & Tien C. (1977). Trajectory analysis of deep-bed filtration with sphere-in-cell porous media model, *AIChE Journal*, **22**(3), 523–533.

Randolph A. D. (1964). A population balance for countable entities, *Can. J. Chem. Eng*., **42**, 280–281.

Saltelli A., Avogadro A. & Bidoglio G. (1984). Americium filtration in glauconitic sand columns, *Nuclear Tech*., **67**, 245–254.

Small H. (1974). Hydrodynamic Chromatography, A technique for size analysis of colloidal particles, *J. Colloid and Interface Sci*., **48**(1), 147–161.

Tien C. (1993). Particle deposition in porous media in the presence of a repulsive double layer force, *Manipulation of groundwater colloids for environmental restoration*, 21–24, Lewis Publishers, Boca Raton.

Tien C., Turian R. M. & Pendse H. (1979). Simulation of the dynamic behavior of deep bed filters, AIChE Journal, **25**(3), 385–395.

Travis B. J. & Nuttall H. E. (1985). A transport code for radiocolloid migration: With an assessment of an actual low-level waste site, Mat. Res. Soc. Symp. Proc., **44**, 969–976.

A1.3-A Appendix: Example COLFRAC input file for I^{131}

```
crr109 Iodine 131 (conservative tracer)
.false.               ldiff      diffusion only
.true.                lflow      flow solution
.true.                ltrans     transport solution
.true.                kfrac      fractured/porous media
.true.                lpmsh      print mesh data
.true.                lpvel      print Darcy flux data
.true.                lphed      print head data
.true.                ldvel      write Darcy flux data
.true.                ldhed      write head data
.false.               lperm      element/zoned hydraulic conductivity
.false.               lap        element/zoned fracture aperture
.true.                lslice     flux crossing a plane
.false.               lrstrt     restart
.true.                kinec      kinetic reaction solute/colloids
.false.               klangc     Langmuir type reaction solute/colloids
.false.               ksrbst     sorption start before/after colloids in
fracture
.false.               ksrbaf     sorption at source is always equilibrium
reaction
.true.                kinef      kinetic reaction solute/fracture surface
.false.               klangf     Langmuir type reaction solute/fracture
surface
.false.               klist      print concentrations to listing file
.false.               kmslmp     mass lumping form for solution
0.00 4.50             xmin, xmax overall
0.00 1.00             zmin, zmax overall
0.02 0.005            Max element size x and z
-1                    Seed for random number generator
matrix
0.00 4.50             xmin, xmax
0.00 1.00             zmin, zmax
6.000E-5 6.000E-5     ckxx, ckzz hydraulic conductivity
0.0997782 0.0099778   al at
1.134E-4 0.015064 1.0 dstar por retard
done porous media zones
vertical fracture
1.10 3.40             xvfmin, xvfmax  x-range
0.25 0.75             zvfmin, zvfmax  z-range
0.10                  vspace   fracture spacing
0.1306061             alfracv  dispersivity
0.0                   alphafv  forward kinetic react. rate const. solute/frc
0.1                   betafv   bkwd. kinetic react. rate const. solute/frc
1.0                   smaxfv   maximum sorbed concentration solute/frc
1.708E-4              apv      aperture
0.1                   alfracmv dispersivity (colloid)
0.0                   ftfracv  filter coefficient (colloid)
0.0                   alphacfv forward kin. react. rate const. solute/colld
0.1                   betacfv  bkwd. kin. react. rate const. solute/colld
1.0                   smaxcfv  maximum sorbed concentration solute/colld
done vertical fracture zones
0.05                  fxmin    min spacing between rand. vert. frac.
5                     nnxm     min nodes between rand. vert. frac.
done random vertical fractures
main horizontal fracture
0.00 4.50             xhfmin,  xhfmax  x-range
0.50 0.50             zhfmin,  zhfmax  z-range
0.005                 hspace   fracture spacing
0.0899565             alfrach  dispersivity
0.0                   alphafh  forward kinetic react. rate const. solute/frc
0.1                   betafh   bkwd. kinetic react. rate const. solute/frc
1.0                   smaxfh   maximum sorbed concentration solute/frc
```

```
2.002E-4              aph      aperture
0.1                   alfracmh dispersivity (colloid)
0.0                   ftfrach  filter coefficient (colloid)
0.0                   alphacfh forward kin. react. rate const. solute/colld
0.1                   betacfh  bkwd. kin. react. rate const. solute/colld
1.0                   smaxcfh  maximum sorbed concentration solute/colld
horizontal fractures below
0.00 3.50             xhfmin,  xhfmax  x-range
0.40 0.45             zhfmin,  zhfmax  z-range
0.025                 hspace   fracture spacing
0.0899565             alfrach  dispersivity
0.0                   alphafh  forward kinetic react. rate const. solute/frc
0.1                   betafh   bkwd. kinetic react. rate const. solute/frc
1.0                   smaxfh   maximum sorbed concentration solute/frc
2.002E-4              aph      aperture
0.1                   alfracmh dispersivity (colloid)
0.0                   ftfrach  filter coefficient (colloid)
0.0                   alphacfh forward kin. react. rate const. solute/colld
0.1                   betacfh  bakwd. kin. react. rate const. solute/colld
1.0                   smaxcfh  maximum sorbed concentration solute/colld
horizontal fractures above
0.00 3.50             xhfmin,  xhfmax  x-range
0.55 0.60             zhfmin,  zhfmax  z-range
0.025                 hspace   fracture spacing
0.0899565             alfrach  dispersivity
0.0                   alphafh  forward kinetic react. rate const. solute/frc
0.1                   betafh   bakd. kinetic react. rate const. solute/frc
1.0                   smaxfh   maximum sorbed concentration solute/frc
2.002E-4              aph      aperture
0.1                   alfracmh dispersivity (colloid)
0.1                   ftfrach  filter coefficient (colloid)
0.0                   alphacfh forward kin. react. rate const. solute/colld
0.1                   betacfh  bkwd. kin. react. rate const. solute/colld
1.0                   smaxcfh  maximum sorbed concentration solute/colld
done horizontal fracture zones
0.08                  fzmin    min spacing between rand. horiz. frac.
5                     nnzm     min nodes between rand. horiz. frac.
done random horizontal fracture zones
right end of aquifer
0.00 1.00             zmin, zmax
0.86 0.86             hmin, hmax
left end of aquifer
0.00 1.00             zmin, zmax
1.00 1.00             hmin, hmax
done specified head fill segments
done specified head points
done specified fluid flux fill segments
at injection well
1.00 0.50             flux-x,   flux-z coordinate
1.44e-03              flux vel, concentration
at pumping well
3.50 0.50             flux-x,   flux-z coordinate
-2.16e-02             flux vel, concentration
done specified fluid flux points
0.0                   decay_s   specified solute flux nodes
0.0                   decay_1   specified concentration nodes
0.0                   decay_3   third-type rectangle elements
0.0                   decayv3   third-type vfrac elements
0.0                   decayh3   third-type hfrac elements
done specified concentration regions
source at injection well
1.00 0.50             cpx, cpz coordinate
5.5e-09               cpval    concentration
1.0e-30               cpmval   concentration (colloid)
0.0 0.00694444        cpon, cpoff    time on, off
```

```
0.0 0.0               cponm, cpoffm  time on, off (colloid)
done specified concentration points
done third-type concentration fill segments
done third-type concentration fill segments (colloid)
done specified solute flux fill segments
done specified solute flux points
0.0                   cinit   default initial concentration (solute)
done different initial concentration zones (solute)
0.0                   cminit  default initial conc. (colloid)
done different initial concentration zones (colloid)
0.0                   csinit  default initial conc. (filtered colloid)
done different initial concentration zones (filtered colloid)
col
1.8                   xslice  slice column x or row z
1.8144e-04            diffus  free-solution diffusion coefficient
1.296e-07             diffusm free-solution diffusion coefficient (colloid)
1.0                   velfac  ratio of colloid velocity/solute velocity
998.0                 rho     fluid density
8.66592e+1            visc    fluid viscosity
0.0                   clamda  solute first-order decay constant
7.320139776e+10       grav    gravity constant
3                     north   # of orthogonalization
1000                  maxitf  max # of iterations for flow
1                     norderf ordering scheme
3                     levelf  level of preconditioning
.true.                dptolf  switch for drop tolerance
1.0e-4                epsrnf  drop tolerance
1.0e-6                ctolf   absolute convergence criteria
0.0e+0                rrctolf residual reduction convergence criteria
1000                  maxit   max # of iterations for concentration
1                     norder  ordering scheme
8                     level   level of preconditioning
.true.                dptol   switch for drop tolerance
1.e-4                 epsrn   drop tolerance
1.0e-6                ctol    absolute convergence criteria
0.0e+0                rrctol  residual reduction convergence criteria
5                     isymstp perform sym. fac. every isymstp-th step
1                     iacl    acceletation method
0.0001                dt      time step size
0.001                 dtmax   max. time step size
0.10                  cstar   max conc. change
1.0                   tw      time weighting
47                    nts
0.022338
0.025116
0.029282
0.03206
0.036227
0.039005
0.043171
0.046065
0.050116
0.053009
0.057176
0.059838
0.064063
0.06684
0.070949
0.073611
0.078009
0.080729
0.084838
0.087616
0.090394
0.093287
```

```
0.101505
0.108333
0.115625
0.12228
0.129398
0.136111
0.147361
0.154398
0.163657
0.174074
0.184491
0.194907
0.205324
0.226157
0.246991
0.267361
0.288194
0.309028
0.329861
0.350694
0.371528
0.392361
0.409722
0.430556
0.860417
0.001388888888 times
```

A1.4 The Enviros modelling report

J. Guimerà, A. Delos and L. Duro (Enviros)

A1.4-0 Summary

The interpretation of *in situ* tracer tests carried out with ^{131}I as conservative tracer, and cocktails of radionuclides containing strontium, caesium, americium, thorium, plutonium, neptunium, tecnetium and uranium, both with and without bentonite colloids is presented. Hydrodynamic parameters were obtained by automatic calibration of flow and conservative solute transport. The set of parameters resulting from the flow simulation have been fed into a reactive transport model together with Kd and BET values obtained from laboratory experiments. The present document describes the calibration of the model with the conservative tracer tests and the hydrogeochemical conceptual model which assumes that the surface reactions are in equilibrium. The model equations are implemented in a multicomponent reactive transport code, and the results for the RN and colloids are discussed.

A1.4-1 Introduction

The performance assessment (PA) of the storage of radioactive waste in deep geological repositories needs understanding of the detailed processes that can potentially affect the transport of radionuclides (RN) in a real scale. RN transport depends on the nature of the nuclide, the source term, the geological media, the geochemical environment and the interactions of RN with other components of groundwater, such as colloids. Therefore, a proper understanding of the fate and behaviour of RN must take several coupled processes into account.

An accurate study of the main processes occurring in this system requires the performance of detailed experiments. A large amount of experimental effort has been devoted to the understanding of the behaviour of RN but, due to experimental limitations, few of *in situ* experiments used RN with a high specific radioactivity. Thus, relevant tests have been performed making use of RN under field conditions, but none of them used the long lived tracers that can be released from spent nuclear fuel. Another important issue of concern for the transport of RN is the presence of colloids in the medium. Indeed, in several HLMW repository designs one of the engineered barriers to isolate the waste from the geosphere consists of compacted bentonite, a clay with high swelling capacity and able to retain RN through sorption onto its surface. One of the problems that the presence of this bentonite buffer can pose on the system is the generation of colloids at the interface with the host rock, that can be transported with flowing groundwater and that can facilitate the transport of the RN sorbed onto their surface.

The colloid-facilitated transport of RN is well known and has been widely recognised (Kim et al. 1984). Recent findings from the Nevada Test Site increased the interest in these processes (Kersting et al. 1999, DOE 2002). Such interest is evident in a significant number of contributions in laboratory experiments (Artinger et al. 2002, Bunn et al. 2002, Grolimund et al. 1996, Nowack & Stone 1999, Saiers 2002, Vilks & Baik 2001), the development of models for the interaction of colloids and dissolved substances (van de Weerd & Leijnse 1997) and development of models to predict colloid transport in heterogeneous domains. Hence, the presence of colloids is tackled in many PA exercises and R+D programmes undertaken by the agencies responsible for the radwaste management (Contardi et al. 2001).

However, despite all these contributions, the lack of field scale tests with colloids and RN in fractured medium was recognised by Vilks & Bachinski (1996), who undertook a large scale tracer test with colloidal silica in a high transmissivity fracture.

To overcome this lack of fundamental understanding, the CRR project (Colloids and Radionuclide Retardation) focuses on fundamental processes that affect the RN transport. The *in situ* experiment consisted on the injection of a cocktail of RN (^{137}Cs(I), ^{85}Sr(II), ^{241,243}Am(III), ^{99}Tc(IV), ^{232}Th(IV), ^{238,242,244}Pu(IV), ^{237}Np(V), and ^{233,238}U(VI)) at low concentrations in a granitic fracture, similar to the ones existing in a potential repository with and without the presence of bentonite colloids in the injection cocktail. The redox state of the system remained unchanged. Previous studies determined the solubility limits of RN under the conditions of the site and the composition of the RN cocktail took into account this information in order to avoid precipitation of any solid phase of the RN in the fracture. The hydrodynamic parameters were obtained after the interpretation of field tests. These field experiments took place in the MI fracture of the Grimsel Test Site in Switzerland.

The objective of this report is to present a methodology to model the fate and behaviour of RN in field conditions, with and without bentonite colloids and without introducing major disturbances in the natural geochemical state of the system. This work within the CRR project is mainly focused at understanding the behaviour of actinides and elements such as Tc that undergo sorption onto reactive surfaces. Since the understanding of the migration behaviour of actinides and their homologues is, in general, poor, any advance in this regard represents an important breakthrough towards a complete picture of the processe, both, retarding and facilitating the transport of these elements through the geosphere under the conditions expected in an underground repository.

Despite the fact that Sr and Cs have been used in the context of the experiment, the present report concentrates on actinides.

A1.4-2 Background of the experiment

The *in situ* experiments took place in a flow dipole established between two boreholes separated by 2.5 m in a well-characterised granitic shear zone (Bossart & Mazurek 1991; Möri & Adler 2001). The thickness of the shear zone varies between 0.15 and 0.90 m. Reactivation of the shear zone resulted in the formation of fault gouge between the sheared planes. Hydraulic testing showed transmissivities in the order of 10^{-6} m^2s^{-1}.

Several preparatory tracer tests have been carried out with the conservative tracers uranine, ^{82}Br and ^{131}I. The best hydraulic conditions selected in terms of travel times and recoveries of the tracer were 10 ml/min and 150 ml/min for the injection and extraction flow rate respectively. The groundwater flow direction during the experiment is mostly coincident with the natural flow and points towards the tunnel.

The composition of native groundwater and the RN mass injected in the cocktails are presented in Table A1.4-2.1 to A1.4-2.3. ^{131}I was preferred to be added to the actinide cocktails as conservative tracer given that it does not interact with RN, as it is the case for uranine, and it has a half-life longer than ^{82}Br.

The RN cocktails were prepared in laboratory and kept under controlled conditions until they were injected. Native groundwater from the fracture was used for the preparation of the cocktail. The master chemical parameters of the groundwater, Eh and pH, were, as far as possible, kept constant throughout all the experiment at the original values of the native water: Eh = -350mV;

pH = 9.6, although Eh in particular is hard to measure and sensitive to traces of oxygen contamination, so some variation cannot be excluded.

Tab. A1.4-2.1: Chemical composition of the CRR experiment groundwater

Component	Concentration (M)
Na^+	6.9e-4
K^+	5.0e-6
Mg^{2+}	6.2e-7
Ca^{2+}	1.4e-4
Sr^{2+}	2.0e-6
Rb^+	2.5e-8
Cs^+	5.0e-9
SO_4^{2-}	6.1e-5
F^-	6.1e-5
Cl^-	1.6e-4
Br^-	3.8e-7
I^-	1.0e-9
HCO_3^-	2.9e-4
pH	9.6
Eh	-350mV

Tab. A1.4-2.2: Chemical composition of the injected RN cocktail (run 31)

Component	Concentration (M)
I-131 (I)	1.26e-13
Sr-85 (I)	1.30e-12
Am-243 (III)	6.01e-10
Th-232 (IV)	1.14e-09
Pu-242 (IV)	1.01e-09
Np-237 (V)	9.57e-08
U-238 (VI)	9.63e-08
I-131 (I)	1.26e-13
Sr-85 (I)	1.30e-12

Tab. A1.4-2.3: Chemical composition of the injected RN cocktail with bentonite colloids (run 32)

Component	Concentration (M)
^{131}I (I)	9.56e-14
^{85}Sr (I)	1.07e-12
^{137}Cs (II)	1.43e-09
^{241}Am (III)	6.46e-11
^{232}Th (IV)	1.12e-09
$^{238+244}$Pu (IV)	6.89e-10
^{99}Tc (IV)	9.04e-09
^{237}Np (V)	1.09e-07
^{233}U (VI)	7.45e-08
Bentonite colloids (ppm)	2.65e-06

The colloid suspension was prepared with a reference bentonite (FEBEX Bentonite, grain size < 63 μm). In the case of using colloids in the cocktail 20 mg of bentonite per L of aqueous cocktail were added (the proper concentration indicated already in the Table above).

The recovery of the colloids in the extraction borehole was analysed by means of two different methods: The first method, the PCS (Photon Correlation Spectroscopy), analysed the concentration and the size distribution of the colloids. Size analysis revealed a background colloid size in the Grimsel groundwater in the range 300 to 500 nm, and an average bentonite colloid diameter of 211 nm in the injection suspension. Large colloids are transported under the hydraulic conditions of the *in situ* experiment. The mean colloid size decreases to values around 200 nm in the colloid breakthrough. This variation might be due to some errors or to some size exclusion effects, but additional measurements reveal mean diameters of the colloids passing the fracture comparable with those of the injected colloids. The second method used for the colloid detection was the Laser-Induced Breakdown Detection (LIBD). The LIBD results validated the previous observation. The colloid recovery was in the order of 90 %. This indicated that an important fraction of bentonite colloids travelled through the fracture zone without being retained and that filtration *sensu lato* was not very significant.

Breakthrough curves of conservative tracers and RN are presented in Figure A1.4-2.1. Curves indicate that a considerable portion of the RN is not affected by surface interaction with the fracture filling material (FFM). They travel in a similar way to conservative tracers and in fact, the maximum concentration of the breakthrough curve is attained slightly earlier than the conservative tracer. Both observations –the fast travel times and the arrival time of maximum concentration- suggest that this part of the RN is travelling in a colloidal form. To date, no differences have been established between radiocolloids, attachment to naturally occurring colloids or artificially added colloids, in the run 32. Table A1.4-2.4 shows the results of the breakthrough curves of the conservative tracer (^{131}I), colloids and some of the RN present in the cocktail of run 32.

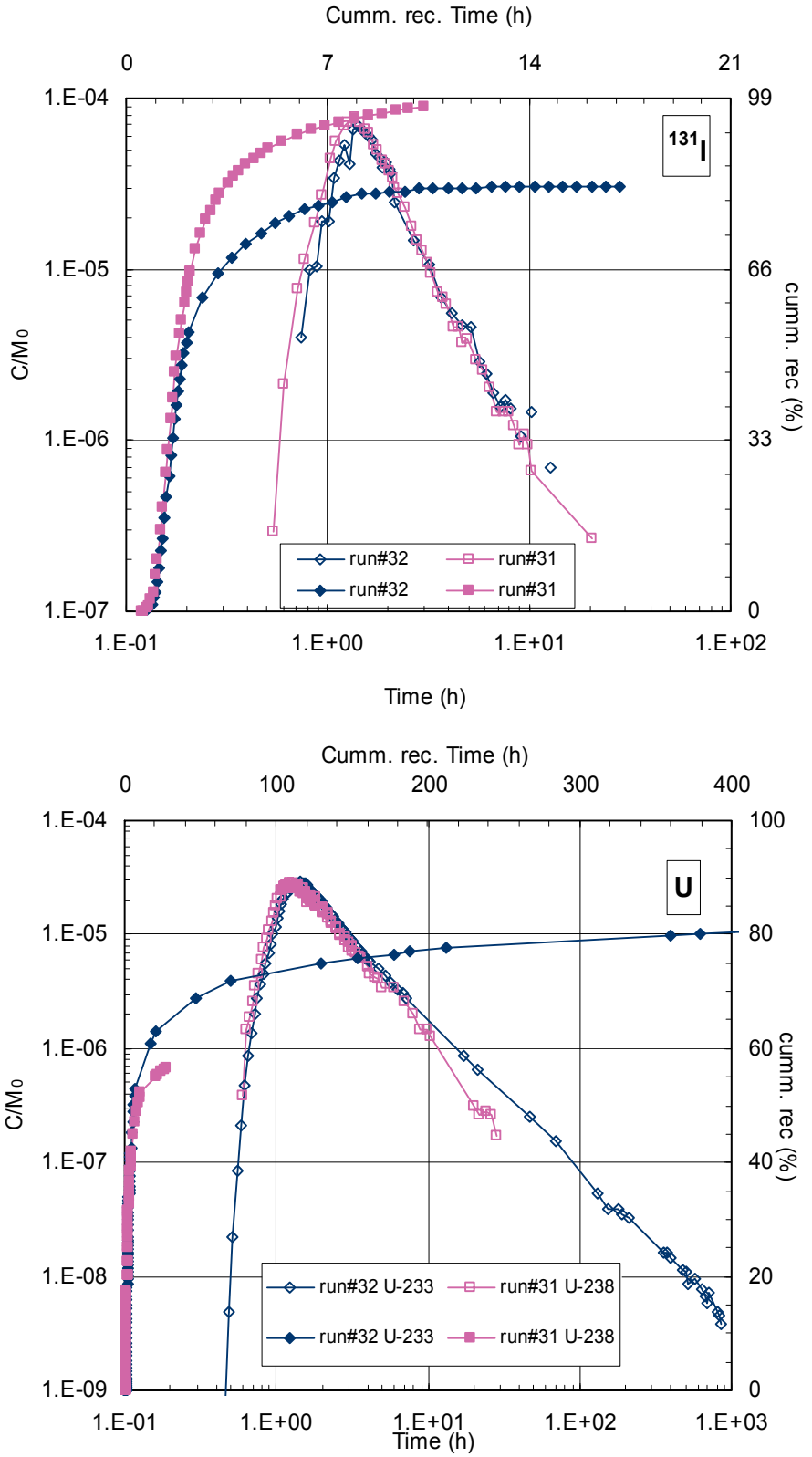

Fig. A1.4-2.1: Measured breakthrough curves (open symbols) and recovery (filled symbols) of the I and RN in runs 31 and 32

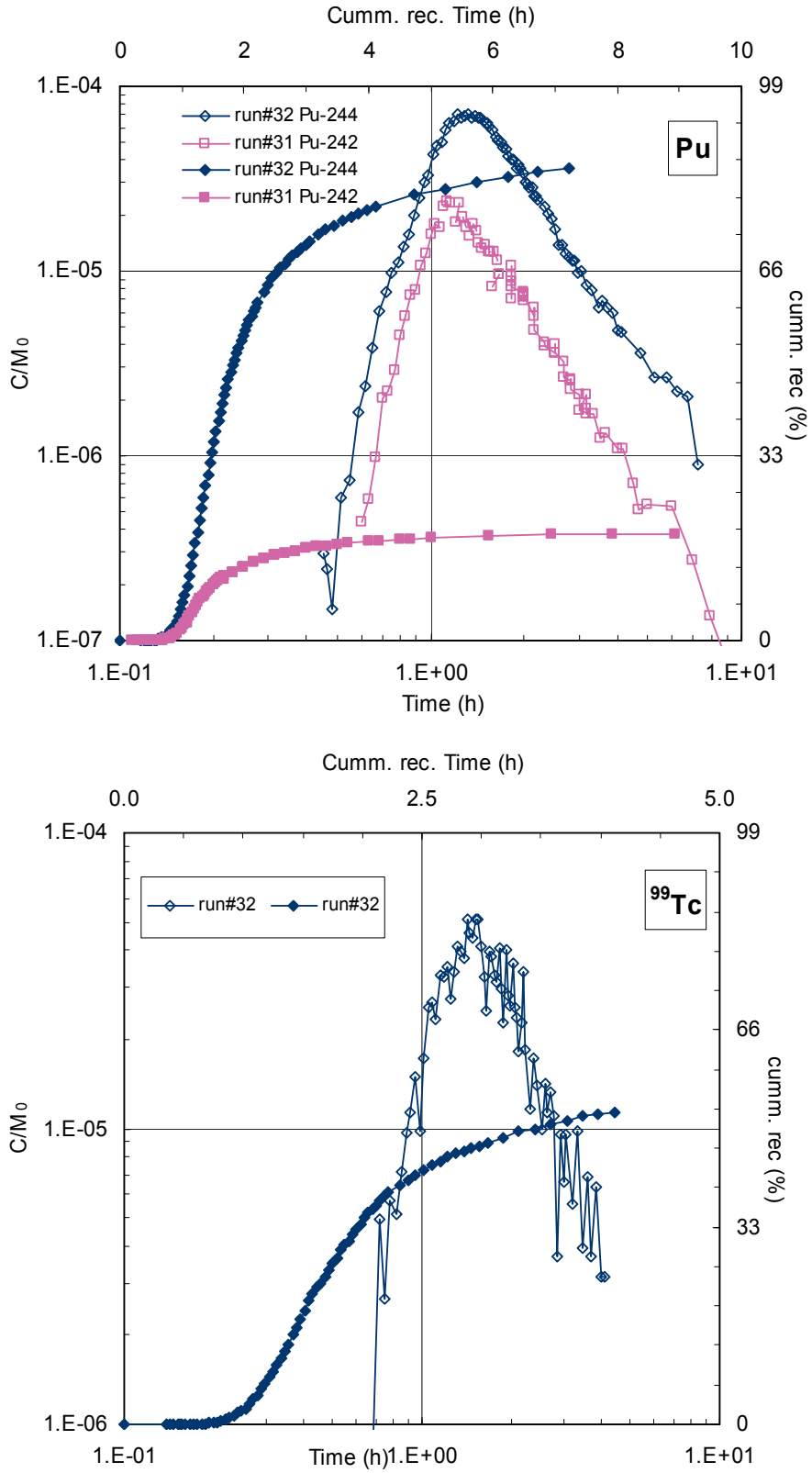

Fig. A1.4-2.1: (cont.) Measured breakthrough curves (open symbols) and recovery (filled symbols) of the I and RN in runs 31 and 32

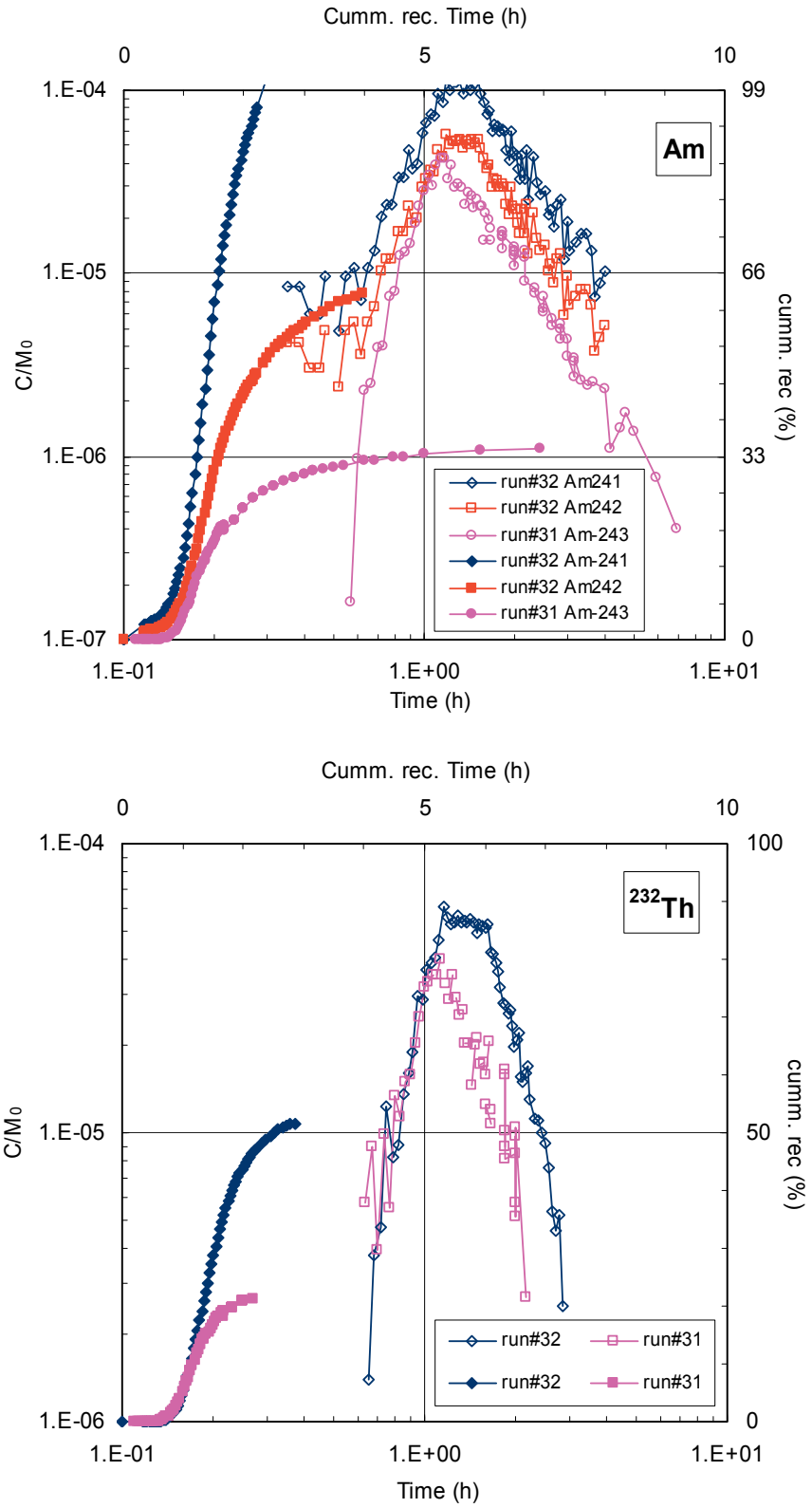

Fig. A1.4-2.1: (cont.) Measured breakthrough curves (open symbols) and recovery (filled symbols) of the I and RN in runs 31 and 32

Tab. A1.4-2.4: Comparison of the peak arrival times (t_m in min) and the recovery of the RN with the conservative tracer and colloids

t_{50} expresses the time at which 50 % of the total recovered mass is achieved. Results refer to run 32

Component	t_m	t_{50}	Rec (%)
^{131}I	85	105	82
^{85}Sr	223	1309	88
^{137}Cs	74	15600	20
Colloids	81	114	90-100
^{241}Am	71	93	86
^{232}Th	69	87	51
$^{244+238}$Pu	79	99	84
^{99}Tc	85	103	52
^{237}Np	87	223	66
^{233}U	87	247	84

Observing Table A1.4-2.4, it is worth noticing that Sr and Cs behave quite differently to the other RNs. Although the recovery of Sr is similar to the conservative tracer recovery, its peak arrival time is strongly delayed, as well as its time median. Similarly, Cs although displaying very poor recovery (only 20 %), it presents an early peak arrival time and a very late time median. Unlike the other tracers, Sr sorbs mainly by cation exchange, and so, in part, does Cs.

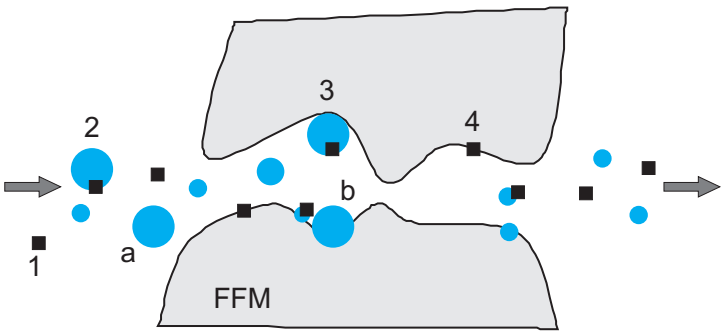

Fig. A1.4-2.2: Conceptual model of the RN and colloids behaviour

Colloids can be mobile (a) or immobile (b). RN are present in the fracture in aqueous form (1) and sorbed either onto the bentonite colloids (2 and 3) or onto the fault gouge (4). Granite is not considered as a reactive surface and all flow and transport and associated processes occur in the FFM

A1.4-2.1 Conceptual model

RN are expected to undergo retardation due to interactions with the FFM. However, they can additionally form colloids, sorb onto the naturally occurring colloids as well as onto the mobile or immobile bentonite colloids (Fig. 1.4-2.2).

Hence we need as many partial differential equations as components considered to describe the transport of RN in this experiment. The advective-dispersive flow will take place as:

$$a\varepsilon_L R_f \frac{\partial c}{\partial t} = \nabla(D\nabla c) - q\nabla c + q_r(c - c') \text{ in } \Omega \quad [1]$$

where ε_L is the flow porosity of the shear zone, a is the shear zone thickness, c is the solute concentration, t is time, q is Darcy's velocity, and R_f is the retardation factor. The last term in the right hand of the equation represents the sink-source term due to the fixed injection and extraction flows, where q_r is the injection or extraction flow rate, and c' the external concentration of the solute, colloid or RN species in the borehole. Ω is the domain over which the equation is solved.

The retardation factor expresses adsorption, as long as it takes place instantaneously and is fully reversible:

$$R_f = 1 + Kd(\rho_b \frac{1-\varepsilon_L}{\varepsilon_L}) \quad [2]$$

where Kd is the distribution coefficient, and ρ_b the density of the solid material.

IK_d is determined experimentally in well known conditions. In the laboratory, flow and chemical conditions can be well controlled, and the physical characteristics of the batch experiment are well defined. Varying one of the fixed parameter has a direct consequence on the Kd value. These conditions are not so well known and controlled in the *in situ* experiment. Above all, the ratio solid to liquid which determines the solid surfaces in contact with the flow water, is not defined for experiments in real scale. This is one of the reasons why in the multi-component reactive transport approach the value of *Kd* measured in laboratory experiments (Missana & Mingarro 2000, Geckeis 2000) is transformed into a thermodynamic constant, which could be upscaled from laboratory experiments to field experiments.

The second and most important motivation is that reactions over colloidal and mineral surfaces can be handled at the same time, thus mimicking the conditions of the experiment.

The process that transforms Kd into K is detailed below.

The general sorption equilibrium is expressed as:

$$> X\text{-}OH + M^{n+} = >XO\text{-}M^{n-1} + H^+ \quad [3]$$

where > X-OH stands for the surface functional groups (surface of the fracture filling material or of the bentonite colloids), M^{n+} represents the predominant aqueous species of the metal M in solution and > $XO\text{-}M^{n-1}$ is the complex formed between the surface of the solid and the metal M.

A surface complexation constant is given by:

$$K = \frac{[> X - O - M^{n-1}][H^+]}{[> X - OH][M^{n+}]} \quad [4]$$

In both cases, for FFM and colloids, if there is sufficient surface available, we can assume that the proportion of surface sites occupied, i.e., the value of [>X-O-Mn-1] is very low in comparison with the total concentration of surface sites [>X-OH]tot, and we can make the following approximation:

$$[>X\text{-}OH]tot \approx [>X\text{-}OH] \quad [5]$$

Under the conditions of the test site groundwater, we can also assume that there is one aqueous species of the metal accounting for more of the 90 % of the total metal in solution:

$$[M]aq\ tot \approx [M^{n+}] \quad [6]$$

Therefore, we can transform the *Kd* values into surface complexation constants by using the following expression:

$$K = \frac{Kd\left(ml/g\right)\frac{S}{L}\left(g/ml\right)[H^+]\left(mol/l\right)}{[> X - OH]\left(mol/l\right)} \quad [7]$$

where S/L stands for the solid to liquid ration used in the experiments where the value of *Kd* was determined.

The surface complexation processes for RN and their associated equilibrium constants are presented in Table A1.4-2.5. It is worth noticing that the RN which interact with FFM or colloids by cation exchange have not been modelled. Migration of alkaline and alkaline-earth elements is normally retarded by cation exchange processes, given the low acidity of these elements and, consequently, their low affinity to co-ordinate water or terminal -OH groups present at the solid surfaces. The migration of these type of metals was studied during the MI experiment and fairly good predictions were accomplished by Heer & Hadermann (1996). This work within the CRR project was mainly focused at understanding the behaviour of actinides and elements such as Tc, that present a much more complicated chemistry than alkaline elements. As a consequence, the understanding of the migration behaviour of actinides and their homologues is, in general, much poorer, and any advance in this regard represents an important breakthrough towards a complete picture of the processes that it has to be considered when trying to assess which are the main processes retarding and facilitating the transport of these elements through the geosphere under the conditions expected in an underground repository.

Tab. A1.4-2.5: Surface complexation processes for both the fracture filling material (FFM) and bentonite colloids for the RN considered in this report

Thermodynamical equation	**$logK_{FFM}$**	**$logK_{colloid}$**
>X-OH +$Am(OH)_2^{2+}$ =>X-O-$Am(OH)^{2+}$ + H^+	-5.80	-0.56
>X-OH +$Pu(OH)_4(aq)$ =>X-O-$Pu(OH)_4^-$ + H^+	-6.58	-1.87
>X-OH +$UO_2(OH)_3^-$ =>X-O-$UO_2(OH)_3^{2-}$ + H^+	-6.73	-2.10
>X-OH +$Th(OH)_4$ =>X-O-$Th(OH)_4^-$ + H^+	-6.58	-1.87
>X-OH +$TcO(OH)_2$=>X-O-$TcO(OH)_2^-$ + H^+	-7.88	-2.37

These chemical equilibria are based upon the study of the speciation of each RN under the conditions of the Grimsel groundwater (pH = 9.5, $\log[HCO_3^-] = -3.54$) and on the determination of the distribution coefficients (*Kd*) in laboratory conditions (Missana & Mingarro 2000) and (Geckeis 2000). Guided by the laboratory results and in contrast to approaches which consider the sorption of RN onto colloids is ruled by two different kinetic reactions (van de Weerd et al. 1997) our approach considers that sorption is instantaneous and fully reversible. In fact, due to the flow imposed in the dipole, the residence time of the tracers in the fracture is quite short. Therefore a kinetic sorption is unlikely to occur according to the laboratory data expressed in Table A1.4-2.6 to Table A1.4-2.8. The peak of the breakthrough curves arrives around 80min and the total extraction lasts about one day. These tables show that the Kd values do not display significant changes that justify kinetic sorption during the field experiment.

Tab. A1.4-2.6: Kd values for all CRR relevant radionuclides in a Grimsel granite / GGW solution under anoxic conditions (Möri 2001)

	Contact Time							
RN c_o in molar concentrations	**1 h ml/g**	**2 h ml/g**	**1 d ml/g**	**14 d ml/g**	**28 d ml/g**	**54 d ml/g**	**84 d ml/g**	**100 d ml/g**
^{237} **Np** ($c_o=3\cdot10^{-5}$)	--	--	--	0.2	---	0.04	---	0.2
^{241} **Am** ($c_o=3\cdot10^{-10}$ M)	--	--	--	110	---	>250	---	>250
^{238} **Pu** ($c_o=6\cdot10^{-9}$ M)	--	--	--	13	---	44	---	78
^{99} **Tc** ($c_o=5.33\ 10^{-7}$M)	0.34	0.18	1.67	150	141	---	122	---
^{75} **Se** ($c_o=1.36\ 10^{-7}$M)	0.8	0.28	0.22	0.5	10	---	38	---
^{137} **Cs** ($c_o=1.10\ 10^{-7}$M)	155	167	206	63	45	---	60	---
^{233} **U** ($c_o=4.04\ 10^{-7}$M)	9.88	12.18	20.25	29	179	---	430	---

Tab. A1.4-2.7: Kd values for all CRR relevant radionuclides in a fracture filling material / GGW solution (Möri 2001)

	Contact Time									
	1 h ml/g	**2 h ml/g**	**24 h ml/g**	**1 w**			**2 w**	**5 w**		
Fraction (µm)			**???**	**<71**	**<300**	**<1160**		**<71**	**<300**	**<1160**
^{237}Np* (c_o=3·10^{-5} M)		<0.5 [<0.5]	1.7 [2.1]	---	---	---	3.6 [4.1]	---	---	---
^{241}Am* (c_o=3·10^{-10} M)		46 [2.2]	233 [9.0]	---	---	---	1223 [38.4]	---	---	---
^{238}Pu* (c_o=6·10^{-9} M)		8 [2.0]	38 [2.4]	---	---	---	306 [9.1]	---	---	---
^{99}Tc (c_o=2.79 10^{-7}M)	0.42	0.48	---	8.71	3.00	0.38		8.12	70 ?	2.50
^{75}Se (c_o=7.1 10^{-8}M)	1.71	1.88	---	7.50	6.60	2.80		---	---	---
^{137}Cs (c_o=7.6 10^{-8}M)	538	610	---	908	724	449		1643	1319	1575
^{233}U (c_o=2.2 10^{-7}M)	5.23	5.97	---	8.05	5.30	1.81		15.40	13.70	10.40

* values in brackets indicate Kd values in the presence of 20 mg/l bentonite colloids; question marks indicate significant uncertainties

Tab. A1.4-2.8: Kd values for granite (size fraction 250 - 800 µm) in the presence of 20 mg/L bentonite colloids (Möri 2001)

(values in brackets stand for the granite fraction without bentonite colloids)

	Contact Time		
	2 hours	**2 days**	**2 weeks**
^{237}Np (c_o = 9·10^{-9} M)	< 1 [<1] (ml/g)	< 1 [<1] (ml/g)	< 1 [<1] (ml/g)
^{243}Am (c_o= 9·10^{-10} M)	1.2 [12] (ml/g)	3.6 [21] (ml/g)	17.3 [130] (ml/g)
^{244}Pu (c_o =3 .5·10^{-11} M)	0.6 [4.8] (ml/g)	2.5 [14] (ml/g)	3.0 [78] (ml/g)

The concentration of surface sites [>X-OH] in the experiments can be calculated by using the experimental parameters and by considering that, according to Davis & Kent (1990) the average density of surface sites of an oxide surface can be taken as 2.31 sites per nm^2:

$$\left[>X-OH\right]_{tot}\left(molsites/l\right)=\frac{\frac{S}{L}\left(g/l\right)*BET\left(m^2/g\right)*2.31.10^{18}\left(sites/m^2\right)}{\mathrm{A}\left(sites/molsites\right)} \quad [8]$$

being BET the surface area measurement per unit mass and A the Avogadro number. This methodology was quite successfully applied in previous works (section A1.4-4.3 in Delos et al. 2002). The differences between the $\log K_{colloid}$ in Table A1.4-2.5 and $\log K_{colloid}$ calculated in previous work is due to the total concentration of colloids considered. In Delos et al. (2002), only 35 % of the colloids were considered in the model, whereas in this work the total amount of bentonite colloids is taken into account. Different values of the surface area measurements per unit mass for the fracture filling material have been published that range from 0.5 to 8 m^2/g (Möri 2001). The effect of reducing the surface area of the material would be to reduce the moles of sites available for the sorption of the RN and therefore the extent of sorption would be reduced as well.

Colloid filtration and/or size exclusion effects are not considered in the conceptual model, since total recoveries are higher than 90 %.

A1.4-2.2 Numerical model

A1.4-2.2.1 Flow calibration

PHAST (Parkhust et al. 2000), a 3-dimensional multicomponent reactive transport code, has been used to model the tracer tests. As a first step, the calibration of the model has been done with the interpretation of the conservative tracer test with ^{131}I (called model 2 in Fig. A1.4-2.4). Because PHAST solves the direct problem, in a first stage the automatic inverse modelling has been carried out with Transin II (Medina et al. 1996). The resulting heads and set of hydraulic parameters have been used to build up the conceptual model with PHAST, whose domain is far more restricted around the dipole of interest (Fig. A1.4-2.3). The simulations are steady state for groundwater flow, in a 2D homogenous domain. The final set of parameters obtained is the transmissivity $T = 8.8 \cdot 10^{-7}$ $m^2 \cdot s^{-1}$, longitudinal and transversal dispersivities, $\alpha_L = 1.5 \cdot 10^{-1}$ m and $\alpha_T = 1.5 \cdot 10^{-2}$ m respectively, $\varepsilon_L = 1.06 \cdot 10^{-2}$, which gently agree with previous studies (Meier et al. 1998) and with the values used for the prediction of these *in situ* experiment (Delos et al. 2002). Dispersion coefficient values are quite uncertain. In our conceptual model, colloids are not size excluded, do not interact with the media and it is assumed that the adsorption of a RN onto the colloid surface does not have any influence on their transport. As a matter of fact, a second hydrodynamic model has been calibrated, making use of the colloid breakthrough curve, and the resulting dispersion values were then increased by a factor of 2. Hence, Figure A1.4-2.4 also displays the simulation with the results of the second model (called model 1 in Fig. A1.4-2.4), that is presented in section A1.4-4.3. We attribute such range of values and the lack of good fits to the simplicity of the model.

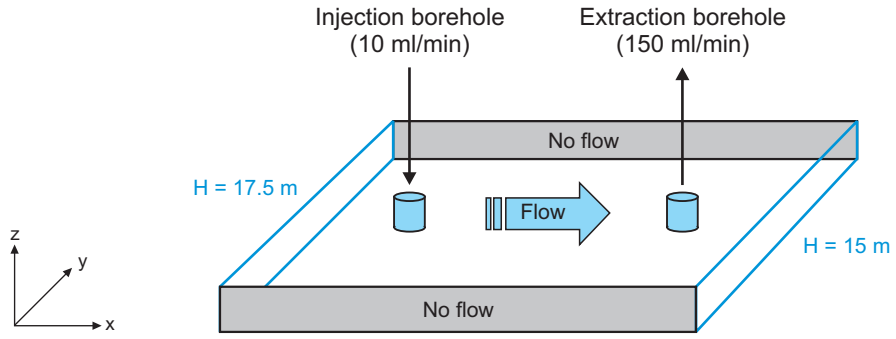

Fig. A1.4-2.3: Model structure used. The boundary conditions are extracted from a larger scale model (see Delos et al. 2002)

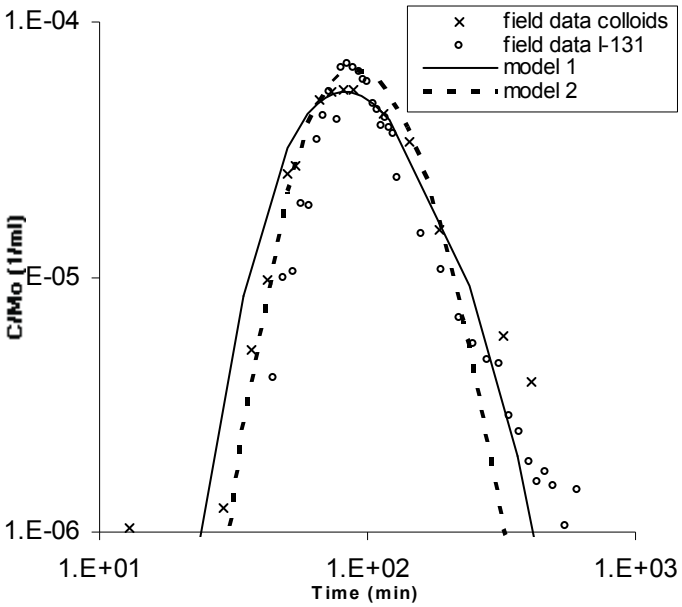

Fig. A1.4-2.4: Breakthrough curve for the conservative tracer using PHAST

Dashed line, model calibrated with the ^{131}I data. Solid line, model reproduced with colloid data

Transport of RN (run 31)

The conceptual model explained in chapter A1.4-3 does not apply for a significant portion of the RN, which travel as conservative, likely in a colloidal form, as described by the results (Fig. A1.4-2.1). Given that such RN travel essentially as conservative in absence of artificially added colloids, the interpretation concentrates on the portion that is affected by retardation in the FFM.

Table A1.4-2.9 shows the mass fraction used for modelling purposes (aqueous form), which is the total amount in the injection cocktail corrected for the observed colloidal fraction before the injection. Figure A1.4-2.5 presents the results obtained for the RN considered. At first glance, all the figures deserve a similar comment, that is, the mass fraction that is not travelling in

colloidal form, does not attain the detection limits. An exception could be made for uranium, which shows maximum calculated aqueous concentrations close to and sligthly above the detection limit. This could explain, in fact, that the tail displayed by the uranium curve is more pronounced than the the rest of RN.

Little else can be concluded from this run, yet the differentiating factor was the absence of artificially added colloids and the results indicate that a considerable fraction of the RN do travel in a colloidal form. The results of the aqueous species are in general agreement with those predicted by Delos et al. (2002), in which most of such species were close to the detection limit. They are not fully comparable with the final results though, since different injection concentrations to those used in the predictions were finally used.

Tab. A1.4-2.9: Run #31: Details of the input concentration for each RN. The input function of conservative tracers matches the distribution

RN	**A: Injected mass in the experiment (moles)**	**B: Colloidal fraction * in the injection cocktail**	**Injected mass in the model (moles) A-(A*B)**
I-131 (I)	1.26e-13	0	1.26e-13
Sr-85 (I)	1.3e-12	0	1.3e-12
Am-243 (III)	6.01e-10	0.58	2.53e-10
Th-232 (IV)	1.14e-9	0.30	7.95e-10
Pu-242 (IV)	1.01e-9	0.58	4.23e-10
Np-237 (V)	9.57e-8	0.10	8.61e-8
U-238 (VI)	9.63e-8	0.12	8.48e-8

* Defined in NTB 03-01, Möri (2004). There are significant uncertainties and, in NTB 03-01, colloidal fractions are given as ranges

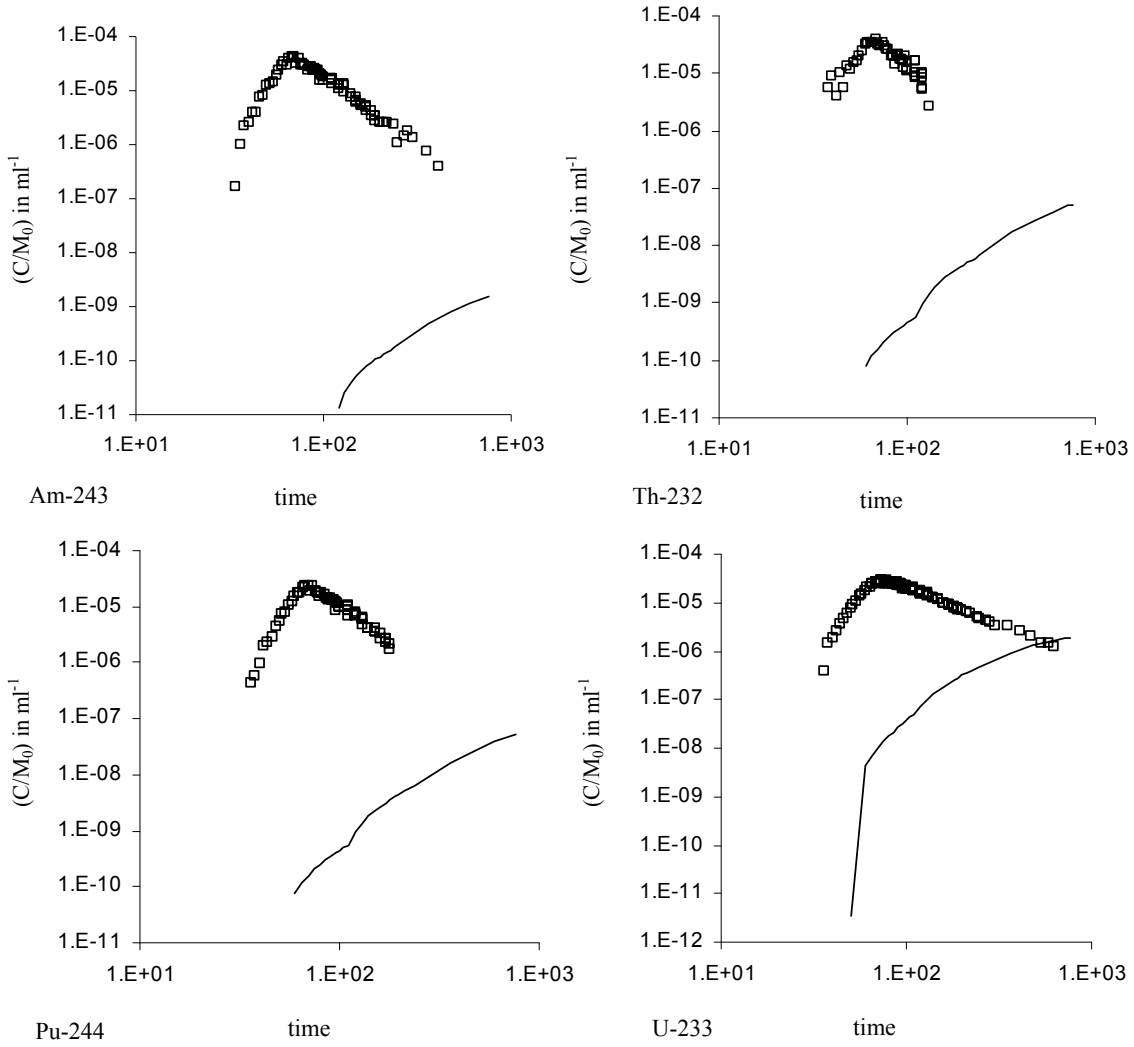

Fig. A1.4-2.5: Results of the Run 31 modelling

Open symbols are the field data. The retarded part, not the colloidal part, has been modelled (line). Concentrations are normalised to injected mass (C/M_0)

Transport of RN and bentonite colloids (run 32)

Figure A1.4-2.6 shows the modelled breakthrough curves against the field data for bentonite colloids and selected radionuclides. Note that contrarily to the Figure A1.4-2.4, the model calibrated with colloid data reproduces better the high concentrations of colloids than the model calibrated with ^{131}I data (model_2, coll_2 in the legend of the upper left hand graph). They are compared in the plot for consistency, and it will be based on the flow field obtained with the colloid breakthrough curves within the rest of the section.

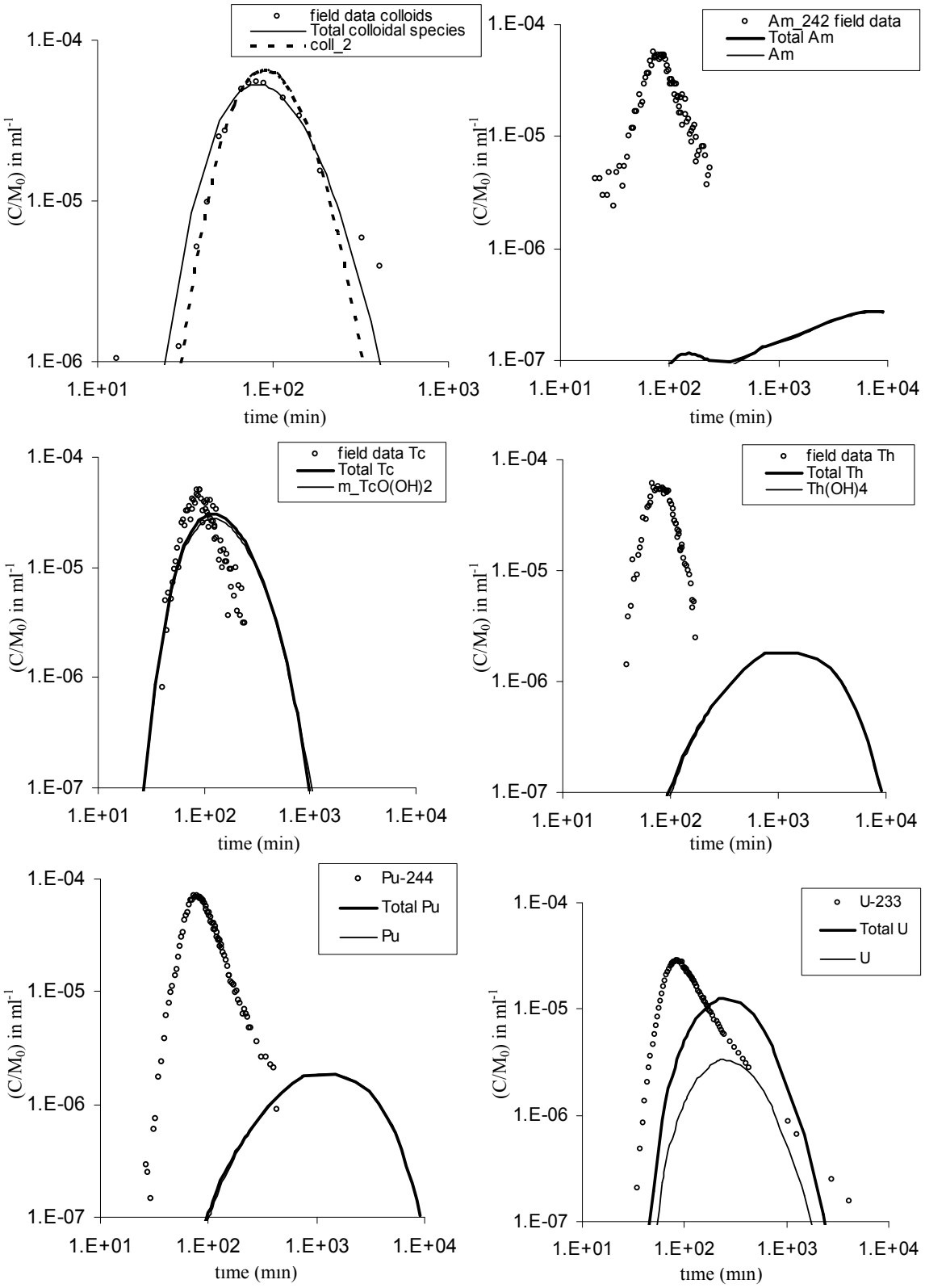

Fig. A1.4-2.6: Results of the field tests (dots) and model simulations with lab parameters

Thick and thin solid lines stand for the total (colloidal and aqueous form) and aqueous phase respectively. Concentrations are normalised to injected mass (C/M_0)

Simulations depicted in Figure A1.4-2.6 have been carried out with data from laboratory measurements. No parameter values set by curve fitting. Thermodynamical constants are those given in Table A1.4-2.5 for both, colloids and FFM and the BET is 0.5 m^2/g. While the simulations are in reasonable agreement with the field experiment in the case of Tc, the rest of the RN are consistently wrong. In general terms, the transport of the RN attached to the bentonite colloids is poorly reproduced. That is, the reactivity of the FFM predominates. This prompted us to vary the BET and the Kcoll to test the sensitivity of the model by varying the values of BET and $Kd_{colloids}$ and to check the range of validity of the laboratory experimental results in the field tests.

The reason to vary the BET of the FFM is that it is the most uncertain parameter, because it defines the number of sites available for the sorption of the RN into the fracture. It has not been defined explicitely for the purposes of CRR project. In general terms, it is in agreement with the general observations that laboratory measurements need a proper upscaling technique before they are used in the interpretation of field tests.

Tab. A1.4-2.10: Comparison between the colloidal form and the aqueous form calculated by the model for each RN

RN	**Peak concentration of colloidal and aqueous form** (1/ml)	**Peak concentration of colloidal form** (1/ml)	**Peak concentration of aqueous form** (1/ml)
Am	4.5e-5	3.1e-5	1.4e-5
Tc	5.3e-5	0.3e-5	5e-5
Pu	4.7e-5	0.6e-5	4.1e-5
Th	4.7e-5	0.6e-5	4.1e-5
U	5e-5	3.5e-5	1.5e-5

Figure A1.4-2.7 shows the results varying the BET value from 0.5 to 0.005 m^2/g. Reducing the BET reduces the number of available sites (like a reduction of the Kd as shown in Fig. A1.4-2.8 below), since they are directly proportional - recall equation 8 - and hence, the role of the colloids should become more evident. The results show effectively that the model is very sensitive to this parameter. The colloidal breakthrough curve is at least captured for all the RN, despite the fact that the simulations are far from actually reproducing the observed behaviour.

It is worth noticing that even in this case, the dominant form of RN is still aqueous except for americium and uranium where there are differences of one order of magnitude in the maximum concentrations detected (see Tab. A1.4-2.10). We contend that this is due to the fact that the RN adsorbed to the colloids are in equilibrium with those in aqueous phase and since the FFM plays a small role in this case, they are essentially moving by advection and dispersion.

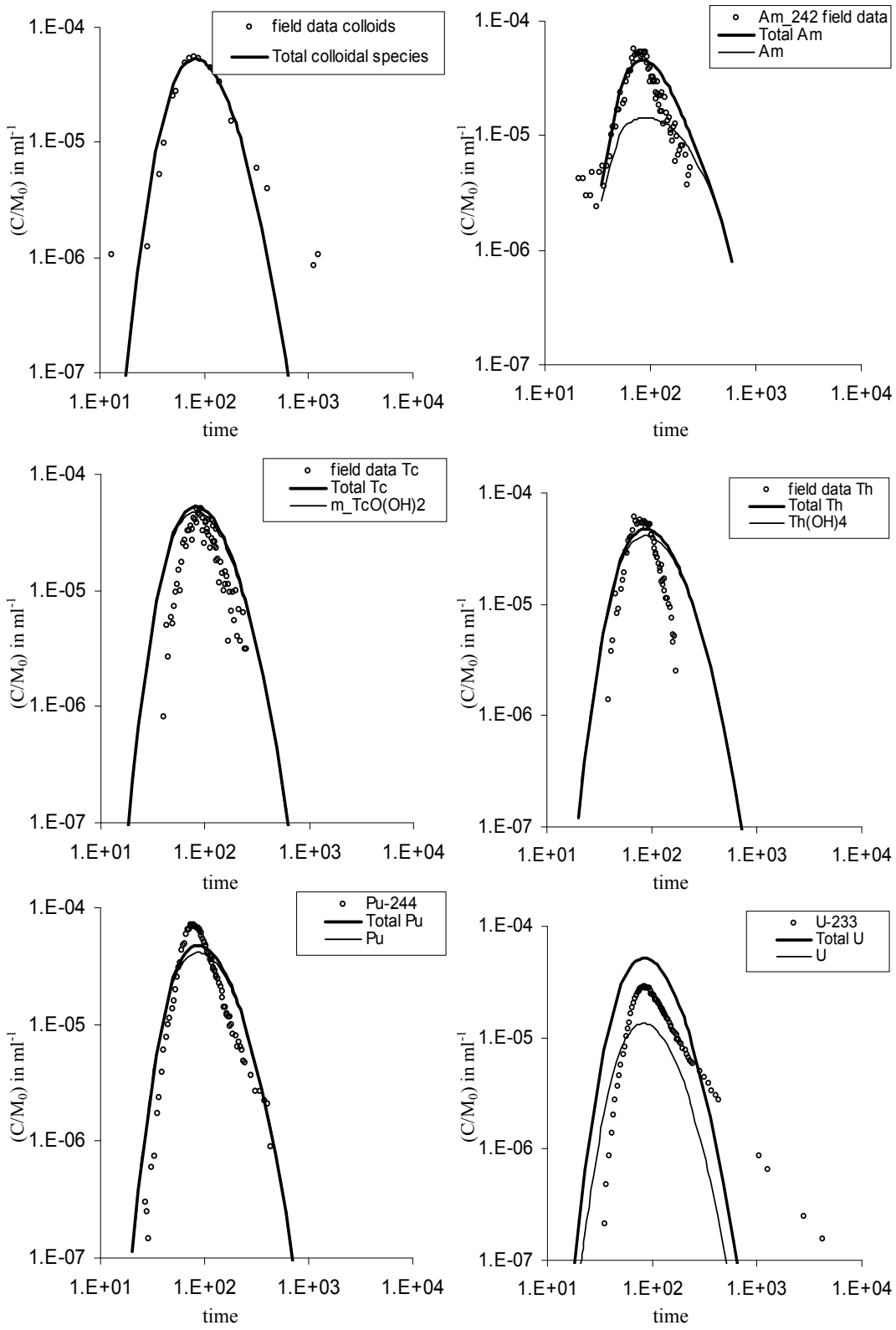

Fig. A1.4-2.7: Results of the field tests (dots) and model simulations with experimental K and with $BET_{FFM} = 0.005\ m^2/g$

Concentrations are normalised to injected mass (C/M_0)

It can be contended, however, that the reduction of the BET_{FFM} in two orders of magnitude is excessive and somehow ambiguous. Hence, we have opted for keeping such BET value to its experimental determination (0.5 m^2/g) and varying the thermodynamical constant that rules the surface reaction between colloids and RN. The results are shown in Figure A1.4-2.8 and the values used for simulation indicated in Table A1.4-2.11 and compared with the experimental ones.

The results of these simulations are much improved in terms of capturing the shape of the breakthrough curves, which is significant for americium and uranium. Understandingly enough, the model reacts to the fundamental parameters of the governing equations.

Tab. A1.4-2.11: Comparison of experimental and calibrated values of logKcoll for the curves depicted in Figure A1.4-2.8

Reaction (sorption of RN onto colloids surface)	**laboratory**	**model**	**ΔlogKcoll**
$>X\text{-}OH + Am(OH)_2^{2+} => X\text{-}O\text{-}Am(OH)^{2+} + H^+$	-0.56	1.5	2.06
$>X\text{-}OH + Pu(OH)_4(aq) => X\text{-}O\text{-}Pu(OH)_4^- + H^+$	-1.87	1.6	3.47
$>X\text{-}OH + UO2(OH)_3^- => X\text{-}O\text{-}UO2(OH)_3^{2-} + H^+$	-2.10	-0.3	2.07
$>X\text{-}OH + Th(OH)_4 => X\text{-}O\text{-}Th(OH)_4^- + H+$	-1.87	1	2.87
$>X\text{-}OH + TcO(OH)_2 => X\text{-}O\text{-}TcO(OH)_2^- + H^+$	-2.37	-1.45	0.92

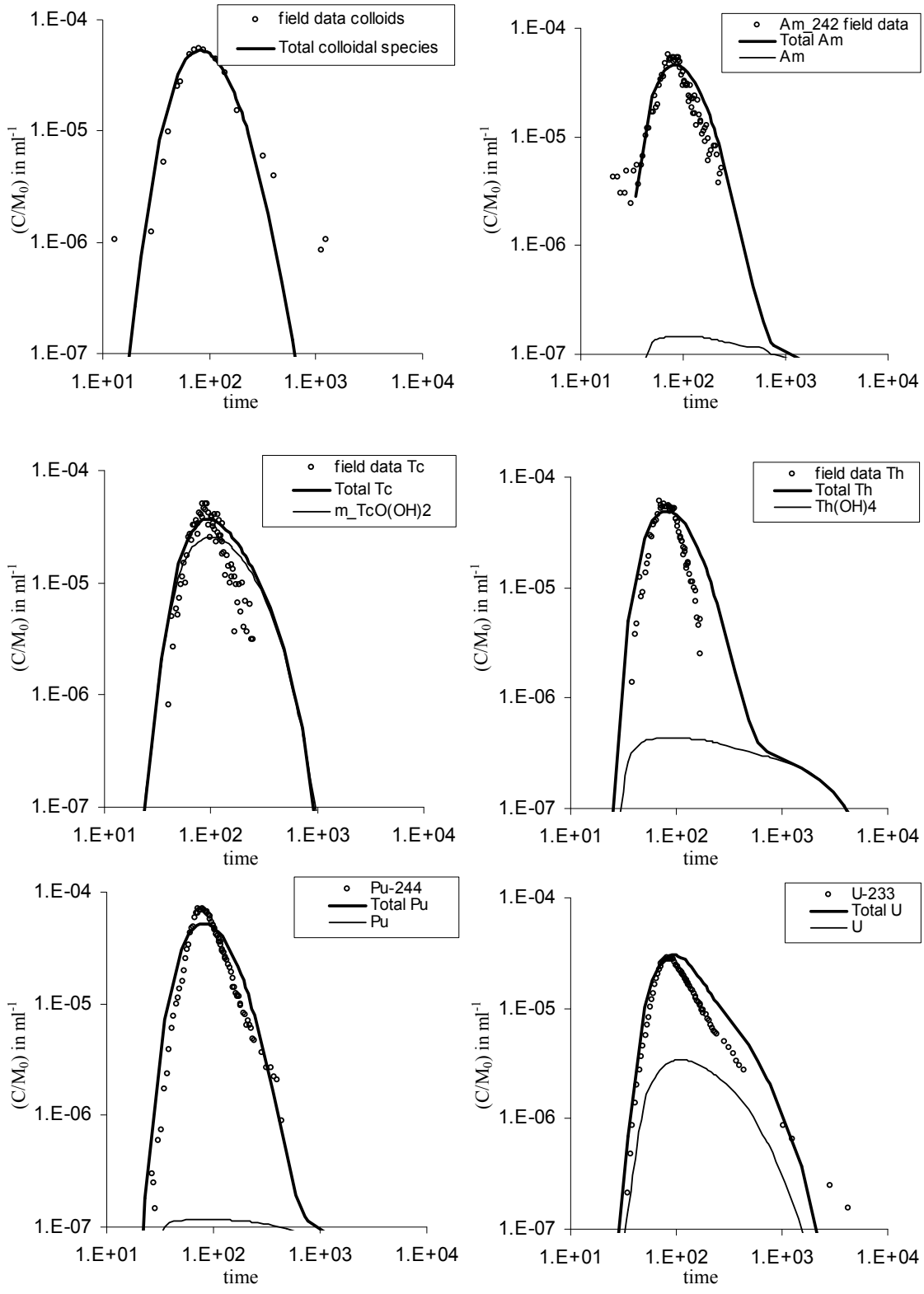

Fig. A1.4-2.8: Results of the field tests (dots) and model simulations with experimental BET (0.5 m^2/g) and callibrating the Kcoll (values indicated in Tab. A1.4-2.11)

Concentrations are normalised to injected mass (C/M_0)

A1.4-3 Conclusions

A first step towards the modelling of an *in situ* tracer test with long lived RN and bentonite colloids has been carried out making use of multicomponent reactive transport approach. The results of the test appear to be conditioned by the heterogeneity of the medium, which has not been considered in this report. Rather, a homogeneous approach is adopted, which has shown some limitations at reproducing the tailings of the tracers.

Based on laboratory experiments, the conceptual model assumes that the surface reactions are in equilibrium (Am and Pu completely almost stick to the colloids and remain there in the time scale of the *in situ* experiment), which results in all species arriving at the extraction borehole at the same time.

Despite these two limitations, the results obtained are rather promising, since the model is capable of predicting the arrival of the RN without ambiguous manual calibration.

The model responds correctly to the fundamental parameters contained in the equations. Hence, as long as they can be properly characterised, it serves for predictive purposes. In fact, its predictive capabilities were used to help at designing the field experiment, which has not been shown here, since constitutes a document on its own.

A problem not tackled during the project and deserves more investigaton is the lack of techniques to upscale properly the parameters determined in lab conditions to be applied in field experiments. It is widely known and recognised, for instance, that batch experiments, by nature, tend to maximise the available surface for reaction, while surfac reaction is very limited in field conditions, especially in heterogeneous media (i.e. channelled flow). Model calibration permits to bound the uncertainty, but certainly more accurate techniques are required.

In general terms, however, the results although limited, are of applicability in performance assessment exercises since, on the one hand, the model captures both, the arrival of RN in solution and sorbed onto colloids. We can anticipate then, that the more realistic the experimental values we use, the more useful will be the outputs of the model for performance assessment. Hence, it is clear that experiments lasting comparable times to lab experiments are required.

A1.4-4 Acknowledgements

Authors wished to thank all individuals and participants of the project that have made this paper possible. In particular, we appreciate the free use of TRANSIN II (Medina et al. 1996) and PHAST (Parkhust et al 2000). They wished to thank also the CRR Project Partners, ENRESA, JNC, Nagra, ANDRA and Sandia/USDOE.

A1.4-5 References

Artinger R., Schlussler W., Schaefer T. & Kim J. I. (2002). A kinetic study of Am(III/Humic colloid inetractions. Environ. Sci. Technol, 36, 4358-4363.

Bossart P. & Mazurek M. (1991). Grimsel Test Site: Structural geology and water flow-paths in the migration shear zone. Nagra Technical Report 91-12, Nagra, Wettingen, Switzerland.

Bunn R. A., Magelky R. D., Ryan J. N. & Elimelech M. (2002). Mobilization of natural colloids from Iron oxide-coated sand aquifer: effect of pH and Ionic strengh. Environ. Sci. Technol., 36, 314-322.

Contardi J. S.; Turner D. R. & Ahn T. M. (2001). Modeling colloid transport for performance assessment, Journal of Contaminant Hydrology vol. 47 n. 2-4 p. 323-333.

Davis J. A. & Kent D. B. (1990). Surface complexation modeling in aqueous geochemistry. In Review in Mineralogy:Mineral Water Interface Geochemistry (ed. M.F. Hochella Jr and A.F. White), pp. 177-248. The Mineralogical Society of America.

Delos A., Duro L., Guimerà J. & Bruno J. (2002). CRR project. Transport modelling for the field test. Unpubl. Nagra Internal Report, Nagra, Villigen, Switzerland.

DOE (2002). Colloid Formation and the Potential Effects on Radionuclide Transport in a Geologic Repository for Spent Nuclear Fuel, DOE/SNF/REP-070. USDOE, Washington, USA.

Geckeis H. (2000). Tentative nuclide composition of injection solutions for the CRR experiment. Unpubl. FZK Internal Note, FZK-INE, Karlsruhe, Germany.

Grolimund D., Borkovec M., Barmettler K. & Sticher H. (1996). Colloid-facilitated transport of strongly sorbing contaminants in natural porous media: A laboratory column study. Environ. Sci. Technol., 30: 3118-3123.

Heer W. & Hadermann J. (1996). Grimsel Test Site, Modelling Radionuclide Migration Field Experiments, Technical Report 94-18, PSI, Würenlingen and Villingen, Switzerland.

Kersting A. B., Efurd D. W., Finnegan D. L., Rokop D. J., Smith D. K. & Thompson J. L. (1999). "Migration of Plutonium in Ground water at the Nevada Test Site", Nature (London), vol. 396, Nº 6714, pp. 56-59.

Kim J. I., Buckau G., Baumgartner F., Moon H. C. & Lux D. (1984). Colloid generation and the actinide migration in groundwaters. Scientific Basis for Nuclear Waste Management 7,31.

Medina A., Galarza G. & Carrera J. (1996). TRANSIN II. Fortran code for solving the coupled flow and transport inverse problem in saturated conditions. El Berrocal Project, Volume IV Hydrogeological modelling and code development, Topical Report 16, ENRESA,217-422, Enresa, Madrid, Spain.

Meier P., Carrera J. & Sánchez-Vila X. (1998). An evaluation of Jacob's method for the interpretation of pumping tests in heterogeneous formations. Water Resources Research, 34, 1011-1025.

Missana T. & Mingarro M. (2000). Summary of the results of sorption experiments for CRR Project. Unpubl. CIEMAT Technical Report CIEMAT/DIAE/54221/4/00, CIEMAT, Madrid, Spain.

Möri A. & Adler M. (2001). GTS, Excavation project (EP): The Nagra-JNC *in situ* study of safety relevant radionuclide retardation in fractured crystalline rock: Structural description and conceptual model of flow paths and radionuclide retardation sites. Unpubl. Nagra Internal Report, Nagra, Wettingen, Switzerland.

Möri A. (ed.) (2004). The CRR final project report series I: Description of the Field Phase– Methodologies and Raw Data. Nagra Technical Report NTB 03-01, Nagra, Wettingen, Switzerland.

Möri A. (2001). GTS V - CRR Experiment: Scoping calculations, base data set V-3 (actualised May 2001). Unpublished Nagra Internal Note, Nagra, Wettingen, Switzerland.

Nowack B. & Stone A. T. (1999). Phosphonate adsorption in the absence and presence of metal ions. Interfacial and colloidal phenomena in aquatic environments symposia. Chemical Processes at the Solid Water Interface. Anaheim, CA, USA, March 21-25 1999.

Parkhurst D. L., Kipp K. L. & Engesgaard P. (2000). PHAST. A Program for Simulating Ground-Water Flow and Multicomponent Geochemical Reactions. User's guide. USGS, 154 pp.

Saiers J. E. (2002). Laboratory observations and mathematical modeling of colloid-facilitated contaminant transport in chemichally heterogenous systems. Water Resources Research 38 n4. 1029/2001.

van de Weerd H. & Leijnse A. (1997). Assessment of the effect of kinetics on colloid facilitated radionuclide transport in porous media. Journal of Contaminant Hydrology, 26, 245-256.

Vilks P. & Baik M. H. (2001). Laboratory migration experiments with RN and natural colloids in a granite fracture. Journal of Contaminant Hydrology Vol 47 pp 197-210.

Vilks P. & Bachinski D. B. (1996). Colloid and suspended particle migration experiments in a granite fracture. Journal of Contaminant Hydrology 21, 269-279.

Appendix 2

Models of colloid facilitated transport used in safety assessments

A2.1 Overview

All models used to date to treat colloid facilitated transport in safety assessments do so in a highly simplified manner, and are to a large degree phenomenological. This is due to the limited available experimental data and limited understanding of relevant processes. Parameters such as colloid concentration and sorption parameters are selected or "calibrated" for a given set of physical and chemical conditions. The models themselves cannot be used to predict how colloid facilitated transport changes if these conditions are altered, although more mechanistic models that do account for such changes can be used to select parameters for the conditions of interest (see, e.g. Contardi et al. 2001). Phenomenological models do, however, enable the effects of colloids to be at least scoped or bounded.

The development of mechanistic models has so far been hampered by limitations in the fundamental understanding of relevant processes. Some more mechanistic models do exist and have been used for the interpretation of field observations and field and laboratory experiments, as described, for example, by Gardiner et al. (2001) in the context of the European Commission CARESS Project and by Van der Lee et al. (1997). Such models have not, however, been applied in safety assessments, mainly because of their high data requirements.

The geosphere transport models used in the Swiss Kristallin-I safety assessment (Nagra 1994), the Japanese H-12 safety assessment (JNC 2000) and the UK Nirex 97 safety assessment (Nirex 1997) to evaluate the effects of colloids embody very similar conceptual assumptions, including the assumption of equilibrium, linear sorption on colloids, although there are some minor differences mainly in terminology and notation. The key assumptions used in these models are outlined in Section A2.2, below. Other models that include sorption kinetics and irreversible sorption are discussed briefly in Sections A2.3 and A2.4, respectively.

A2.2 Models assuming equilibrium linear sorption on colloids

The geosphere transport models used in the Kristallin-I, H-12 and Nirex 97 safety assessments and the safety assessment undertaken by the US DOE as part of its evaluation of a proposed repository at Yucca Mountain (USDOE 2000) consider transport along one or more thin planar fractures surrounded by a porous, saturated rock matrix. In Nirex 97, colloid facilitated transport in media where groundwater flows predominantly through the rock matrix is also considered, although this model variant is not discussed further here.

The models consider only natural groundwater colloids. These are assumed to have concentrations in the fractures that are constant in space and time. The generation of colloids within or around the repository is not included in the models. The assumption of constant colloid concentration in space and time implies a local equilibrium between colloid loss (e.g. by filtration, dissolution, coagulation) and colloid generation or the remobilisation of filtered colloids. Furthermore, colloids are conservatively assumed not to diffuse into matrix pores due to their size and/or electrical charge effects. This is a key assumption. The effects of colloids in enhancing transport due to their velocities being higher than the average groundwater velocity in a fracture, as well as other effects related, for example, to hydrodynamic dispersion and the effects of channelling, are generally trivial compared to the reduction in transport times that arises if colloids suppress retardation by matrix diffusion and sorption on matrix pore surfaces.

Radionuclides enter the geosphere in the aqueous phase and are thereafter distributed between the following states (see also 3.3) in the main report:

1. Aqueous solution within the fractures
2. Aqueous solution within the (matrix) pore space
3. Directly sorbed on fracture walls
4. Sorbed on mobile colloids within the fractures
5. Sorbed on immobile colloids within the fractures - i.e. colloids attached to fracture walls
6. Sorbed to the rock matrix pores.

Exchange takes place between state (1) and states (2), (3), (4), and (5) and between (2) and (6). Another key assumption, as mentioned before, is that radionuclide sorption on colloids and matrix pore surfaces can be described as a linear, equilibrium process (the safety assessment undertaken by the USDOE as part of its evaluation of a proposed repository at Yucca Mountain also considered an "irreversible model", see Section A2.4, below). A fixed ratio, K_a [m], is assumed between the surface concentration of colloids reversibly attached to the fracture walls and the volume concentration of mobile colloids present in the flowing water in the fractures. These assumptions result in transport equations identical in form to those for solute transport, but with modified parameter definitions.

In the absence of colloids, the governing equation for the evolution of aqueous radionuclide concentration, C_n [M], in a fracture conveying water in the x-direction is:

$$\frac{\partial C_n}{\partial t} = -\frac{u}{R_n}\frac{\partial C_n}{\partial x} + \frac{a_L u}{R_n}\frac{\partial^2 C_n}{\partial x^2} - \lambda_n C_n + \lambda_{n-1} C_{n-1} + \frac{\mathrm{M}(x,t)}{R_n}, \qquad \text{(A2-1)}$$

where u [m a^{-1}] is the advection velocity, a_L [m] is the longitudinal dispersion length, λ_n [a^{-1}] is the radioactive decay rate of radionuclide n, M(x,t) is a term that accounts for matrix diffusion and R_n is a retardation factor that accounts for radionuclide-wallrock interactions.

In order to take into account the presence of colloids, the advection velocity is replaced by an "effective velocity" u' [m a^{-1}] defined by:

$$\frac{u'}{u} = 1 + \frac{u_c}{u}\chi K_{nc}\,. \qquad \text{(A2-2)}$$

Here, χ is the colloid concentration (kg of colloidal material per m^3 of groundwater) and K_{nc} [m^3 kg^{-1}] is the distribution coefficient for the sorption of radionuclide n on colloids. u_c is the advection velocity of the colloids which, as noted earlier, may be somewhat larger than the mean velocity of the flowing water. In addition, the retardation factor R_n is replaced by R_{nc}, defined by:

$$\frac{R_{nc}}{R_n} = 1 + \chi K_{nc}\left(1 + \frac{K_a}{b}\right), \qquad \text{(A2-3)}$$

where $2b$ [m] is the fracture aperture.

In most applications of such models in safety assessments, the sorption of colloids on fracture surfaces is generally conservatively neglected (i.e. K_a is set to zero in Eq. A2-3), due to lack of data and/or doubts as to whether colloid/wallrock interaction is adequately represented as a linear, equilibrium process. u_c is generally set equal to u. Again, this is a conservative simplification, which is made due to lack of data to support a higher colloid advection velocity. With these simplifications, it can be seen from Eq. A2-2 and A2-3 that the condition for negligible impact of colloids is:

$$\chi K_{nc} << 1, \qquad \text{(A2-4)}$$

The approach outlined above is not directly applicable to the modelling of colloid facilitated transport in the CRR *in situ* migration experiments; bentonite colloids are introduced as a pulse of limited duration and thus the assumption that colloid concentration is constant in space and time does not hold. The assumption of equilibrium radionuclide sorption on colloids is, however, adopted by the Enviros modelling team.

A2.3 Models incorporating non-linear sorption and sorption kinetics

The representation of sorption described in the previous section does not provide an adequate quantitative framework for interpreting field observations and laboratory experiments involving colloid facilitated transport in which there are indications that sorption is non-linear, and/or only slowly reversible or irreversible. It may also be inadequate (non-conservative) for use in safety assessments in these circumstances, although it should be noted that a process that appears to be slowly reversible or even irreversible over experimental timescales may still be adequately described by an equilibrium model when the timescales of interest are orders of magnitude longer.

Models have thus been developed that explicitly include non-linear sorption, as well as the kinetics of radionuclide sorption and desorption on colloids and the kinetics of colloid attachment to and detachment from fracture walls. For example, as part of ongoing research on colloids in SKI's programme, the COLLAGE II model for radionuclide transport has been developed (Grindrod & Cooper 1993), in which exchange of radionuclides between dissolved, mobile sorbed, and immobile sorbed phases, is governed by first-order reaction rate constants. This is the main tool used by SKI for quantitative assessment of the potential impact of colloids in the Swedish KBS-3 disposal concept (Klos et al. 2002). The computer code TRAPIC (**Tr**ansport of **P**ollutants **I**nfluenced by **C**olloids) models colloid facilitated transport through porous media, and considers non-linear sorption and sorption kinetics (Lührmann et al. 1998). This code includes a colloid source term, rather than an assumption of constant colloid concentration in space and time. The interaction of contaminants with colloids is governed by Langmuir isotherms and kinetic Langmuir equation, and the interaction of colloids with the pore surfaces is described by first-order kinetics. Corapcioglu et al. (1999) & JNC (the present study) have also developed kinetic models.

A first-order kinetic model of radionuclide sorption on colloids, which is incorporated in the COLFRAC code, has been applied in modelling colloid facilitated transport in the CRR *in situ* migration experiments by the JNC modelling team.

A2.4 Models incorporating the assumption of irreversible sorption

The studies undertaken by the USDOE as part of its evaluation of a proposed repository at Yucca Mountain (USDOE 2000) are unique among safety assessments in that they include both reversible and irreversible sorption of radionuclides on colloids in their geosphere transport modelling. In the "irreversible model", radionuclides bound irreversibly to colloids are transported through fractures by advection-dispersion only. Interaction with the aqueous phase and immobile rock is neglected. The partitioning of radionuclides between the colloids and the aqueous phase based on observations from the Nevada Test Site, but is assigned a wide range of parameter uncertainty.

Lindgren & Cvetkovic (2001) presented a model in which radionuclides are irreversibly bound to bentonite colloids released from a repository, and the colloids interact reversibly with fracture walls. A similar approach (although with no interaction between colloids and fracture walls) is applied to modelling colloid facilitated transport in the CRR *in situ* migration experiments by the FZK and PSI modelling teams.

A2.5 References

Contardi J. S., Turner D. R. & Ahn T. M. (2001). Modeling Colloid Transport for Performance Assessment. J. Cont. Hydrology, 47, pp. 323 - 333.

Corapcioglu M. Y., Jiang S. & Kim S.-H. (1999). Comparison of Kinetic and Hybrid-Equilibrium Models for Simulating Colloid-facilitated Radionuclide Transport in Porous Media. Transport in Porous Media, 36, pp. 373 - 390.

Gardiner M. P., Grindrod P. & Moulin V. (2001). The Role of Colloids in the Transport of Radionuclides from a Radioactive Waste Repository: Implication on Safety Assessment. Final Project Report EUR 19781, European Commission, Brussels, Belgium.

Grindrod P. & Cooper N. (1993). COLLAGE II: A Numerical Code for Radionuclide Migration through a Fractured Geosphere in Aqueous and Colloidal Phases. SKI Report 93:45, Swedish Nuclear Power Inspectorate, Stockholm, Sweden.

JNC (2000). H12 Project to Establish Technical Basis for HLW Disposal in Japan, Project Overview Report and three Supporting Reports. JNC TN1410 2000-001 ~ 004, JAEA, Tokai, Japan.

Klos R. A., White M. J., Wickham S. M., Bennett D. G. & Hicks T. W. (2002). Quantitative Assessment of the Potential Significance of Colloids to the KBS-3 Disposal Concept. SKI Report 02:34, Swedish Nuclear Power Inspectorate, Stockholm, Sweden.

Lindgren G. A. & Cvetkovic V. (2001). Colloid Retention in Äspö Crystalline Rock: a Generic Computational Assessment. In: Radionuclide Retention in Geologic Media, Workshop Proceedings, Oskarshamn, Sweden, 7-9 May 2001, OECD/NEA, Paris, France.

Lührmann L., Noseck U. & Tix C. (1998). Model of Contaminant Transport in Porous Media in the Presence of Colloids Applied to Actinide Migration in Column Experiments. Water Resources Research, 34, No. 3, pp. 421 - 426.

NAGRA (1994). Kristallin-I: Safety Assessment Report. Nagra Technical Report 93-22, Nagra, Wettingen, Switzerland.

NIREX (1997). Nirex 97, An Assessment of the Post-Closure Performance of a Deep Waste Repository at Sellafield. Nirex Science Report S/97/012, 5 volumes, Nirex, UK.

Parkhurst D. L., Kipp K. L. & Engesgaard P. (2000). PHAST. A Program for Simulating Ground-Water Flow and Multicomponent Geochemical Reactions. User's guide. USGS, 154 pp.

USDOE (2000). Total System Performance Assessment for the Site Recommendation. Technical Report TDF-WIS-PA-00001 Rev 00. Prepared for the U.S. Department of Energy. Prepared by Civilian Radioactive Waste management System Management and Operating Contractor.

Van der Lee J., Ledoux E., de Marsily G., Vinsot A., Van de Weerd H., Leijnse A., Harmand B., Rodier E., Sardin M., Dodds J. & Hernandez A. (1997). Development of a Model for Radionuclide Transport by Colloids in the Geosphere. Nuclear Science and Technology EUR 17480 EN, European Commission.